Dynamic culture of a new genetically modified liver-derived cell line as a model of bioartificial liver

Hodowla dynamiczna nowej genetycznie zmodyfikowanej linii komórkowej pochodzenia wątrobowego jako model biosztucznej wątroby

Małgorzata Jakubowska

Doctoral thesis

Laboratory of Tissue Engineering, Department of Hybrid and Analytical Microbiosystems,

Nalecz Institute of Biocybernetics and Biomedical Engineering, Polish Academy of Sciences

Supervisor: Prof. Dorota G. Pijanowska, PhD, DSc Eng.

Auxiliary supervisor: Krzysztof D. Pluta, PhD

Warsaw, 2024

Pragnę serdecznie podziękować Promotorom
Prof. dr hab. inż. Dorocie Pijanowskiej oraz Dr Krzysztofowi Plucie
za wsparcie merytoryczne, cenne uwagi i okazaną życzliwość.

Dziękuję również moim niezastąpionym Koleżankom z zespołu
za wszelką pomoc i wsparcie, bezcenne wskazówki,
a także za stworzenie miłej atmosfery w pracy.

Dziękuję mojej Rodzinie, a w szczególności Mężowi,
za cierpliwość, motywowanie i wspieranie w trudnych chwilach,
a przede wszystkim za wiarę, że uda mi się dojść do celu.

Contents

Abbreviations

3D – Three dimensional space

A1AT – Alpha-1-antitrypsin

AALD – Alcohol-associated liver disease

ACLF – Acute on chronic liver failure

ALF – Acute liver failure

ALSS – Artificial liver support systems

APS – Ammonium persulfate

AQP9 – Aquaporin-9

ARG1 – Arginase 1

ARG2 – Arginase 2

ASL - Argininosuccinate lyase

ASS - Arginosuccinate synthetase

ATCC – American type culture collection

BAL – Bioartificial liver

BCA – Bicinchoninic acid

BLSS - Bioartificial liver support systems

bp – base pair

BSA – Bovine serum albumin

CD54 – Cluster of differentiation 54

cDNA – Complementary deoxyribonucleic acid

C/EBPA - CCAAT/enhancer-binding protein alpha

CLF – Chronic liver failure

CMV – Cytomegalovirus

CPS1 - Carbamoyl phosphate synthetase 1

CYP3A4/CYP3A7 – Cytochrome P450 isoforms 3A4/3A7

DAPI - 4',6-diamidino-2-phenylindole

DILI – Drug-induced liver injury

DMEM – Dulbecco's modified Eagle's medium

DMSO – Dimethyl sulfoxide

DNA – Deoxyribonucleic acid

dNTPs – Deoxynucleotide triphosphates

DsRed/DsRed2 – *Discosoma* sp. red fluorescent protein

ECL – Enhanced chemiluminescence

ECM – Extracellular matrix

EDTA – Ethylenediamine tetra acetic acid

ELISA - Enzyme-linked immunosorbent assay

ESCs – Embryonic stem cells

FACS - Fluorescence activated cell sorting

FBS - Fetal bovine serum

FDA – Food and drug administration

FITC - Fluorescein isothiocyanate

FOXA3 – Forkhead box A3

FSC – Forward scatter

GAPDH - Glyceraldehyde-3-phosphate dehydrogenase

GS – Glutamine synthetase

HCC – Hepatocellular carcinoma

HGF – Hepatocyte growth factor

HIV-1 – Human immunodeficiency virus-1

HNF1A – Hepatocyte nuclear factor 1 alpha

HNF4A – Hepatocyte nuclear factor 4 alpha

HPCs – Hepatic progenitor cells

HPV – Human papillomavirus

HRP – Horseradish peroxidase

hTERT - Human telomerase reverse transcriptase

HSCs – Hepatic stellate cells

HSPA1A – Heat shock protein 70 family A (Hsp70) member 1A

HUVECs - Human umbilical vein endothelial cells

IMAC-1 - Intercellular adhesion molecule-1

IF – Immunofluorescence

iPSCs - Induced pluripotent stem cells

kDa – kiloDalton

LB – Lysogeny broth/Luria-Bertani broth

LF – Liver failure

LP3000 – Lipofectamine 3000

LSECs – Liver sinusoidal endothelial cells

LSS – Liver support systems

LV – Lentivirus

MEM NEAA - Eagle non-essential amino acids solution

mRNA – Messenger ribonucleic acid

MSCs – Mesenchymal stem cells

MTT - 3-(4,5-dimethylthiazol-2-yl)-2,5-diphenyl tetrazolium bromide

NAFLD – Nonalcoholic fatty liver disease

NAG - *N*-acetylglutamate

NAGS - *N*-acetylglutamate synthase

NASH – Nonalcoholic steatohepatitis

NFKB – Nuclear factor kappa B

ORC1 - Ornithine carrier 1

ORFs – Open reading frames

OTC – Ornithine transcarbamylase

P2A – "Self-cleaving" 2A peptide from porcine teschovirus-1

PBS – Phosphate-buffered saline

PCR – Polymerase chain reaction

PE – Phycoerythrin

PERV – Porcine endogenous retrovirus

PI – Propidium iodide

PNF – Primary graft nonfunction

PVDF - Polyvinylidene fluoride

RCF – Relative centrifugal force

RIPA - Radioimmunoprecipitation assay buffer

RNA – Ribonucleic acid

RPL13A – Ribosomal protein L13a

RPM – Rotation per minute

RT – Room temperature

RT-qPCR – Real-time quantitative polymerase chain reaction

SDS – Sodium dodecyl sulfate

SDS-PAGE - Sodium dodecyl sulfate-polyacrylamide gel electrophoresis

SEM – Scanning electron microscopy

SSC – Side scatter

SV40 TAg - Simian virus 40 large T antigen

TAE - Tris-acetate-EDTA buffer

TBST – Tris-buffered saline with Tween-20

TCA – Trichloroacetic acid

TEMED - Tetramethylethylenediamine

TMB - 3,3',5,5'-tetramethylbenzidine

UT-A – Urea transporter type A

UT-B – Urea transporter type B

UV – Ultraviolet

VSV-G - Vesicular stomatitis virus glycoprotein

Abbreviations connected to Liver Support Systems

ADVOS - ADVanced Organ Support

AMC-BAL - Academic Medical Center – Bioartificial Liver

BLSS - Bioartificial Liver Support System

ELAD - Extracorporeal Liver Assist Device

HBAL - Hybrid Bioartificial Liver

HepatAssist - HepatAssist Liver Support System

hiHep-BAL – human induced hepatocytes - Bioartificial Liver

MARS - Molecular Adsorbent Recirculating System

MELS - Modular Extracorporeal Liver Support

Prometheus - Fractionated Plasma Separation and Adsorption system (Prometheus system)

RFB - Radial Flow Bioreactor

SEPET - Selective Plasma Filtration Therapy system

SPAD - Single-Pass Albumin Dialysis system

TECA-HALSS - TECA-Hybrid Artificial Liver Support System

Summary

Liver diseases are one of the most frequent causes of death worldwide. Their mortality rate reaches 2 million deaths yearly, and thus, they are regarded as a global public health problem. Liver diseases without appropriate treatment may lead to organ failure. Under such conditions, the only effective medical solution is orthotopic liver transplantation. Unfortunately, the chronic shortage of organ donors constitutes a great limitation to this therapy. As a result, approximately 10% of patients die each year while waiting for a transplant. Therefore, scientists have paid much attention to developing other methods for the treatment of liver failure. The proposed experimental therapies include the transplantation of hepatocytes, the use of artificial or bioartificial liver support systems, and utilization of techniques, which base on tissue engineering tools (i.e., decellularized liver, 3D bioprinted liver, organoids, etc.). Nonetheless, bioartificial liver support systems seem to be the most promising. Such hybrid devices constitute a bridging therapy for patients and support liver failure until transplantation or regeneration. The main advantage of bioartificial systems is the presence of biological component, which performs metabolic, biosynthetic and regulatory liver-related functions, whereas artificial devices are designed to fulfill only detoxification tasks.

The best source of cells to be used as a biological component is human hepatocytes, which are regarded as the gold standard for such applications. However, their utilization is limited because they quickly dedifferentiate *ex vivo*, resulting in the loss of their ability to perform liver-specific functions. Thus, alternative sources of cells, which could constitute a model of human hepatocytes, have been searched. One of the proposed models is the C3A cell line derived from human hepatocellular carcinoma. These cancer cells exhibit similar phenotype and some physiological functions (e.g., albumin secretion) to liver parenchymal cells. Moreover, C3A cells are characterized by rapid proliferation (unlimited availability), high genetic stability, strong contact inhibition, and low culture requirements. Additionally, no ethical concerns have been raised regarding its clinical utilization. Currently, the C3A cell line is widely used in research concerning the evaluation of xenobiotic toxicity or the development of new drugs. Importantly, C3A is the only tumor-derived cell line that is utilized as a biological component in ELAD, the most advanced device among bioartificial liver support systems, which entered the third phase of clinical trials. However, these cells are characterized by some metabolic deficiencies. The most essential factor is the inability to eliminate toxic ammonia. It results from the nonfunctional urea cycle caused by the lack or low expression of arginase 1 (*ARG1*) and ornithine transcarbamylase (*OTC*) genes, which encode the enzymes involved in

this metabolic process. In fact, an unfunctional urea cycle could be a reason for the failure of clinical trials utilizing the ELAD system, as effective ammonia detoxification is vital for the successful treatment of liver diseases.

Therefore, the aim of my doctoral study was to establish a new genetically modified hepatocellular carcinoma cell line with a restored urea cycle, which could constitute a better source of cells for use in bioartificial liver devices. Genetic modification was performed with the use of self-constructed lentiviral vectors. Introduced changes (transfer plasmid bearing both additional genes under the control of a strong promoter; antibiotic selection) allowed the establishment of a population consisting of nearly 100% *ARG1*- and *OTC*-expressing cells named the C3A_AO_P2A cell line. The success of genetic modification was confirmed at both the DNA (integration of transgenes into the cell genome) and protein levels using PCR, RT-qPCR, and Western blot techniques. Compared with the unmodified C3A cells, C3A_AO_P2A cell line exhibited significant overexpression of h*ARG1* and h*OTC* genes as well as corresponding proteins. Moreover, no negative effect of the conducted genetic modification on cell morphology and viability was observed. Therefore, the overall performance of C3A_AO_P2A cells in monolayer static and dynamic 3D conditions was analyzed and compared with that of parental C3A cells and the previous generation of genetically modified cells (C3A_AO_III), which constitute a mixed population of unmodified cells, cells expressing a single transgene or, in minority, cells transduced with both missing genes.

Research conducted in static culture confirmed that the newly established C3A_AO_P2A cell line synthetized a similar amount of albumin, the main liver protein product, to their parental C3A cells. However, an increase in the secretion of this protein to the same extent as in the case of C3A_AO_III cells has not been confirmed. Additionally, the toxic impact of ammonia on cell viability and metabolic activity was investigated because often in bioartificial liver devices, which have contact with patient serum, nonphysiological concentrations of this substance occur. Thus, the resistance to different concentrations of ammonia was verified. The obtained results showed that both genetically modified cell lines were characterized by greater cell viability and metabolic activity than their parental C3A cells, indicating that they are less prone to ammonia-induced oxidative/nitrosative stress. The most essential result concerns the functionality of the urea cycle. Previously, urea formation was measured only in cell lysates. However, knowing that urea is efficiently transported outside the cell, its content in post-culture medium was also checked. The conducted experiments revealed that the highest urea content in post-culture medium was observed for the new C3A_AO_P2A

cells. In turn, in the case of cell lysates, the greatest amount of urea was produced by C3A_AO_III cells, indicating that this metabolite accumulates inside the cell and that the process of active urea transport might be disrupted. Nonetheless, the conducted research showed that the C3A_AO_P2A cell line produces urea more effectively than the other analyzed cell lines. Moreover, the obtained results proved that genetic modification of C3A cells with self-prepared lentiviral vectors was successful and allowed for the restoration of the urea cycle.

A comparison of cell performance under flow conditions was conducted using a self-constructed system for dynamic cell culture, which consists inter alia of a self-prepared hollow fiber bioreactor (culture module). The performed experiments showed that all analyzed cell lines were characterized by higher albumin secretion than the corresponding static controls. The obtained results indicated that dynamic culture constitutes a more efficient type of culture and ensures better conditions for cell growth. Moreover, the newly established C3A_AO_P2A cells were characterized by the best cell performance under flow conditions among all analyzed cell lines, especially in terms of albumin secretion, indicating that they could be considered a valuable source of cells for use in bioartificial liver devices.

In summary, genetic modification of C3A cells performed with the use of self-prepared lentiviral vectors, ensured the stable integration of additional copies of the h*ARG1* and h*OTC* genes into their genome and allowed the establishment of a new cell line named C3A_AO_P2A. Compared with their parental C3A cells, the newly developed cell line exhibits improved cell performance (e.g., albumin synthesis) under both static and dynamic culture conditions. Moreover, they are characterized by increased resistance to higher concentrations of ammonia. Nevertheless, the most essential achievement concerns the increased ability of C3A_AO_P2A cells to produce urea. It is worth emphasizing the importance of the conducted research because, in my opinion, the aforementioned features allow for considering the utilization of the newly established C3A_AO_P2A cell line as a biological component in improved bioartificial liver devices. Their potential application in such devices might improve the effectiveness of supporting liver failure and, as a result, be beneficial for patients, increasing their chance of survival.

Streszczenie

Choroby wątroby stanowią obecnie jedną z najczęstszych przyczyn zgonów na świecie. Ich śmiertelność szacuje się na 2 miliony zgonów rocznie, w związku z powyższym uznawane są za globalny problem zdrowia publicznego. Choroby wątroby, bez podjęcia odpowiedniego leczenia, mogą prowadzić do niewydolności tego organu. Wówczas, jedyną skuteczną terapią jest przeszczep narządu. Niestety, największym ograniczeniem stosowania tego rodzaju leczenia jest chroniczny niedobór odpowiednich dawców. W rezultacie rocznie umiera około 10% pacjentów oczekujących na transplantację wątroby. Mając to na uwadze, naukowcy rozpoczęli prace nad poszukiwaniem nowych eksperymentalnych metod leczenia lub wspomagania funkcjonowania niewydolnego narządu. Można pośród nich wyróżnić: przeszczep hepatocytów, sztuczne lub biosztuczne systemy wspomagania wątroby oraz wykorzystanie technik opartych na narzędziach inżynierii tkankowej (np. decelularyzowana wątroba, 3D biodruk, organoidy itp.). Niemniej jednak, biosztuczne systemy wspomagania wątroby wydają się być najbardziej obiecujące. Te hybrydowe urządzenia stanowią terapię pomostową dla pacjentów, polegającą na wspomaganiu pracy niewydolnego organu do czasu jego przeszczepienia lub regeneracji. Przewagą biosztucznych systemów wspomagania jest obecność komponentu biologicznego, którego zadaniem jest pełnienie metabolicznych, biosyntetycznych i regulacyjnych funkcji wątrobowych, podczas gdy sztuczne systemy są zdolne jedynie do wspomagania procesów detoksykacyjnych.

Najlepsze źródło komórek do zastosowania jako biologiczny komponent w biosztucznych systemach wspomagania stanowią ludzkie hepatocyty. Pomimo tego, że są uznawane za złoty standard, ich wykorzystanie wiąże się jednak z pewnymi ograniczeniami. Hepatocyty, komórki wysoce zróżnicowane i pełniące specyficzne funkcje wątrobowe, w warunkach *ex vivo* szybko ulegają odróżnicowaniu, co skutkuje utratą zdolności do pełnienia tych funkcji. W związku z powyższym, rozpoczęto poszukiwania alternatywnych źródeł komórek, które mogłyby stanowić model ludzkich hepatocytów. Jednym z proponowanych modeli jest linia komórkowa C3A wyprowadzona z ludzkiego raka wątrobowokomórkowego. Badania pokazują, że te nowotworowe komórki wykazują podobny fenotyp i pełnią niektóre funkcje fizjologiczne (np. wydzielanie albuminy) parenchymalnych komórek wątrobowych. Ponadto komórki linii C3A charakteryzują się szybką proliferacją (nieograniczoną dostępnością), dużą stabilnością genetyczną, silną inhibicją kontaktową i małymi wymaganiami hodowlanymi. Co istotne, nie zgłoszono żadnych zastrzeżeń etycznych w związku z ich wykorzystaniem klinicznym. Obecnie, linia komórkowa C3A jest powszechnie

stosowana w badaniach dotyczących oceny toksyczności ksenobiotyków czy opracowywaniu nowych leków. Co więcej, linia komórkowa C3A, jako jedyna linia nowotworowa, została wykorzystana jako biologiczny komponent w systemie ELAD, najbardziej zaawansowanym urządzeniu wśród biosztucznych systemów wspomagania wątroby, który dotarł do trzeciej fazy badań klinicznych. Komórki linii C3A charakteryzują się jednak pewnymi metabolicznymi dysfunkcjami, z czego najbardziej istotna jest ograniczona zdolność do eliminacji toksycznego amoniaku. Wynika to z niefunkcjonalnego cyklu mocznikowego, co spowodowane jest brakiem lub niską ekspresją genów arginazy 1 (*ARG1*) i transkarbamylazy ornitynowej (*OTC*), kodujących enzymy zaangażowane w ten proces. Biorąc to wszystko pod uwagę, można przypuszczać, iż dysfunkcja cyklu mocznikowego w linii C3A mogła stanowić przyczynę niepowodzenia badań klinicznych z wykorzystaniem systemu ELAD, ponieważ skuteczna detoksykacja amoniaku jest kluczowym elementem w terapiach chorób wątroby.

W związku z powyższym, celem mojej pracy doktorskiej było opracowanie nowej genetycznie zmodyfikowanej linii komórkowej raka wątrobowokomórkowego z przywróconym cyklem mocznikowym, która mogłaby stanowić lepsze źródło komórek do zastosowania w biosztucznych systemach wspomagania wątroby. Modyfikację genetyczną przeprowadzono z wykorzystaniem samodzielnie skonstruowanych wektorów lentiwirusowych. Wprowadzone zmiany (plazmid transferowy niosący oba dodatkowe geny pod kontrolą silnego promotora, selekcja antybiotykowa) pozwoliły na otrzymanie nowej linii komórkowej, nazwanej C3A_AO_P2A, składającej się z prawie 100% komórek zmodyfikowanych genetycznie. Skuteczność przeprowadzonej modyfikacji genetycznej potwierdzono zarówno na poziomie DNA (integracja transgenów do genomu komórki), jak i białkowym, stosując techniki PCR, RT-qPCR i Western blot. Badania wykazały znaczącą nadekspresję genów h*ARG1* i h*OTC* oraz odpowiadających im białek w komórkach linii C3A_AO_P2A w porównaniu z ich niezmodyfikowanymi genetycznie odpowiednikami. Ponadto nie zaobserwowano negatywnego wpływu przeprowadzonej modyfikacji genetycznej na morfologię i żywotność komórek. Dalszą charakterystykę funkcjonalną nowej linii komórkowej C3A_AO_P2A przeprowadzono w warunkach hodowli płaskich statycznych i dynamicznych 3D, zaś uzyskane rezultaty porównywano z wynikami otrzymanymi dla wyjściowej linii komórkowej C3A i poprzedniej generacji komórek genetycznie zmodyfikowanych – C3A_AO_III, która stanowi mieszaną populację komórek niezmodyfikowanych, komórek wykazujących ekspresję pojedynczego transgenu lub komórek stransdukowanych obydwoma brakującymi genami.

Badania przeprowadzone w hodowli statycznej potwierdziły, że nowo utworzona linia komórkowa C3A_AO_P2A syntetyzuje albuminę, główne białko produkowane przez wątrobę, na poziomie podobnym do swoich niemodyfikowanych genetycznie odpowiedników. Nie potwierdzono jednak wzrostu wydzielania tego białka w takim samym stopniu jak w przypadku komórek linii C3A_AO_III. Dodatkowo, zbadano toksyczny wpływ amoniaku na żywotność komórek i ich aktywność metaboliczną, ponieważ bardzo często w biosztucznych urządzeniach wątrobowych, mających kontakt z surowicą pacjenta, występują niefizjologiczne stężenia tej substancji. W związku z powyższym, sprawdzono odporność komórek na różne stężenia amoniaku. Uzyskane wyniki wykazały, że obie genetycznie zmodyfikowane linie komórkowe charakteryzowały się wyższą żywotnością i aktywnością metaboliczną w porównaniu z komórkami wyjściowej linii C3A, co wskazuje, że są one mniej podatne na stres oksydacyjny/nitrozacyjny indukowany amoniakiem. Najważniejszy wynik niniejszej rozprawy doktorskiej dotyczy oceny funkcjonalności cyklu mocznikowego. Dotychczas, ilość wyprodukowanego mocznika mierzono tylko w lizatach komórkowych. Mając jednak na uwadze, że mocznik jest aktywnie transportowany na zewnątrz komórki, ilość tego metabolitu była również mierzona w pożywce pohodowlanej. Przeprowadzone doświadczenia wykazały, że największą zawartością mocznika w pożywce hodowlanej charakteryzowały się komórki linii C3A_AO_P2A. Z kolei, w przypadku lizatów komórkowych, największa ilość mocznika została wykryta w linii C3A_AO_III, co wskazuje, że metabolit ten kumuluje się wewnątrz komórek. Może to być spowodowane zakłóconym procesem aktywnego transportu mocznika. Niemniej jednak, przeprowadzone badania wykazały, że linia komórkowa C3A_AO_P2A produkuje mocznik bardziej efektywnie niż pozostałe linie komórkowe. Zatem, uzyskane wyniki potwierdzają, że przeprowadzona modyfikacja genetyczna komórek linii C3A samodzielnie przygotowanymi wektorami lentiwirusowymi zakończyła się sukcesem i pozwoliła na przywrócenie im funkcjonalnego cyklu mocznikowego.

Ocena funkcjonalności nowej linii komórkowej w warunkach przepływowych została przeprowadzona przy użyciu samodzielnie skonstruowanego systemu do hodowli dynamicznej, na który składa się między innymi samodzielnie przygotowywany bioreaktor z membranami kapilarnymi (moduł hodowlany). Przeprowadzone eksperymenty wykazały, że wszystkie analizowane linie komórkowe charakteryzowały się zwiększoną sekrecją albuminy w porównaniu z odpowiednią kontrolą statyczną. Uzyskane wyniki potwierdzają, że hodowla dynamiczna 3D stanowi bardziej wydajny typ hodowli i zapewnia lepsze warunki do wzrostu komórek. Stwierdzono również, że nowo opracowana linia komórkowa C3A_AO_P2A charakteryzowała się najlepszą funkcjonalnością w warunkach przepływowych spośród

wszystkich analizowanych linii komórkowych, zwłaszcza w wydzielaniu albuminy, co wskazuje, że można ją uznać za cenne alternatywne źródło komórek do zastosowania w urządzeniach typu biosztuczna wątroba.

Podsumowując, modyfikacja genetyczna komórek linii C3A przeprowadzona przy użyciu samodzielnie przygotowanych wektorów lentiwirusowych zapewniła stabilną integrację dodatkowych kopii genów h*ARG1* i h*OTC* do ich genomu i pozwoliła na utworzenie nowej linii komórkowej o nazwie C3A_AO_P2A. Nowo opracowana linia komórkowa charakteryzuje się lepszą funkcjonalnością (np. synteza albuminy) w obydwu analizowanych warunkach hodowlanych, hodowli płaskiej statycznej i 3D w przepływie medium, w porównaniu z wyjściową linią C3A. Komórki linii C3A_AO_P2A wykazują również zwiększoną odporność na wysokie stężenia amoniaku. Niemniej jednak, najważniejszym osiągnięciem niniejszej rozprawy doktorskiej było opracowanie nowej linii komórkowej o zwiększonej zdolności do produkcji mocznika. Warto podkreślić zasadność przeprowadzonych badań, gdyż moim zdaniem powyższe cechy pozwalają na rozważenie wykorzystania nowo powstałej linii komórkowej C3A_AO_P2A jako komponentu biologicznego w biosztucznych systemach wspomagania wątroby. Jej potencjalne zastosowanie w tego typu urządzeniach może poprawić skuteczność wspomagania pracy niewydolnego narządu, a w efekcie przynieść korzyści pacjentom, zwiększając ich szanse na przeżycie.

1. Literature review

1.1 Liver anatomy and physiology

The liver is an essential organ with a remarkable ability to regenerate. The liver is responsible for performing more than 500 vital functions, such as detoxification of xenobiotics, neutralization of toxins, and regulation of the immune response. It also participates in maintaining homeostasis, regulating blood pH and the synthesis and release of hormones. The liver is called the metabolic center because it is involved in the storage of energy and nutrients (glycogen, vitamins, iron); the metabolism of lipids, amino acids and carbohydrates; the synthesis of proteins; and the formation of bile and urea (Kmieć, 2001; Mulaikal and Emond, 2012). The majority of these functions are performed by parenchymal cells – hepatocytes. These cells constitute 60% of all liver cells and 80% of the total liver mass. The remaining 40% are nonparenchymal cells, which include the following cell types: hepatic stellate cells (HSCs), liver sinusoidal endothelial cells (LSECs), cholangiocytes (biliary epithelial cells), macrophages (Kupffer cells), immune cells (natural killer cells, lymphocytes, monocytes, neutrophils) or progenitors. The presence of nonparenchymal cells is vital because they cooperate with hepatocytes and regulate each other directly (heterotypic interactions) or indirectly (through cytokine/growth factor secretion). For example, they are engaged in selective transport between blood and parenchymal cells (LSECs) or endocytosis/phagocytosis (Kupffer cells) (Damm *et al.*, 2013; Godoy *et al.*, 2013).

The liver is located in the superior right quadrant of the abdomen. It consists of two main lobes (right and left), which are divided into eight segments. The basic anatomical unit is a hexagonally shaped structure called the lobule. It is characterized by the presence of a central vein in the middle of the unit and portal triads located at the corners. Each portal triad comprises the bile duct, hepatic artery, and portal vein. Moreover, the structure of the lobule includes sinusoids, which are fenestrated capillaries enabling contact between hepatocytes and the blood. Interestingly, the whole liver is composed of approximately one million lobules (Abdel-Misih and Bloomston, 2010; Mahadevan, 2020). A schematic view of the liver architecture is presented below (Figure 1).

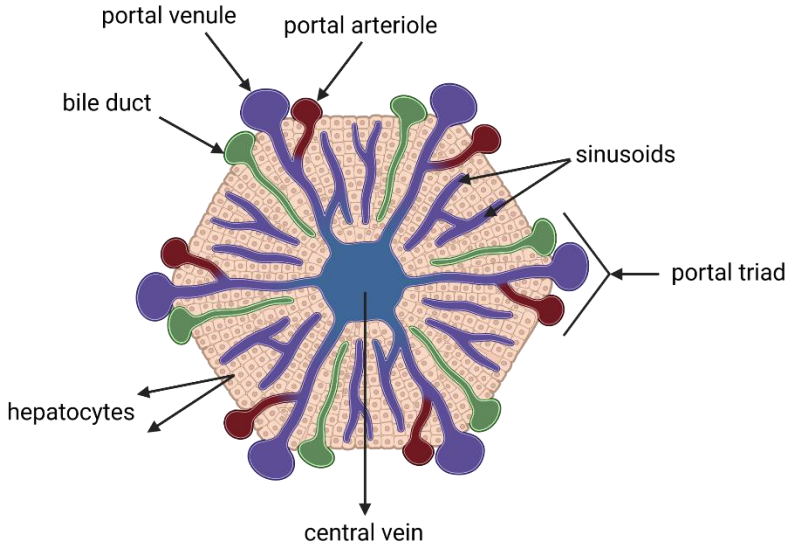

Figure 1. Liver structure – schematic view of the liver lobule. Created with BioRender.com.

The acinus, which represents the smallest functional unit of the liver, constitutes the area of parenchymal cells distributed along the radial axis of the lobule and supplied by afferent blood vessels from the portal triad. Blood from the hepatic artery, which is rich in oxygen, flows toward the central vein, the space with the poorest oxygenation. Thus, different concentrations of oxygen within the acinus are observed. This phenomenon is termed liver zonation. Depending on the oxygen supply, the acinus is divided into three zones, namely, the periportal, mid-lobular, and pericentral zones, where different metabolic functions occur. For example, hepatocytes in the periportal zone (the best oxygenated zone) are responsible for energetically demanding processes such as gluconeogenesis, urea synthesis and protein secretion. In turn, parenchymal cells in the pericentral zone (the poorest oxygenated zone) participate in xenobiotic detoxification, glycolysis or bile acid formation (Cunningham and Porat-Shliom, 2021; Manco and Itzkovitz, 2021). A schematic view of liver zonation is presented below (Figure 2).

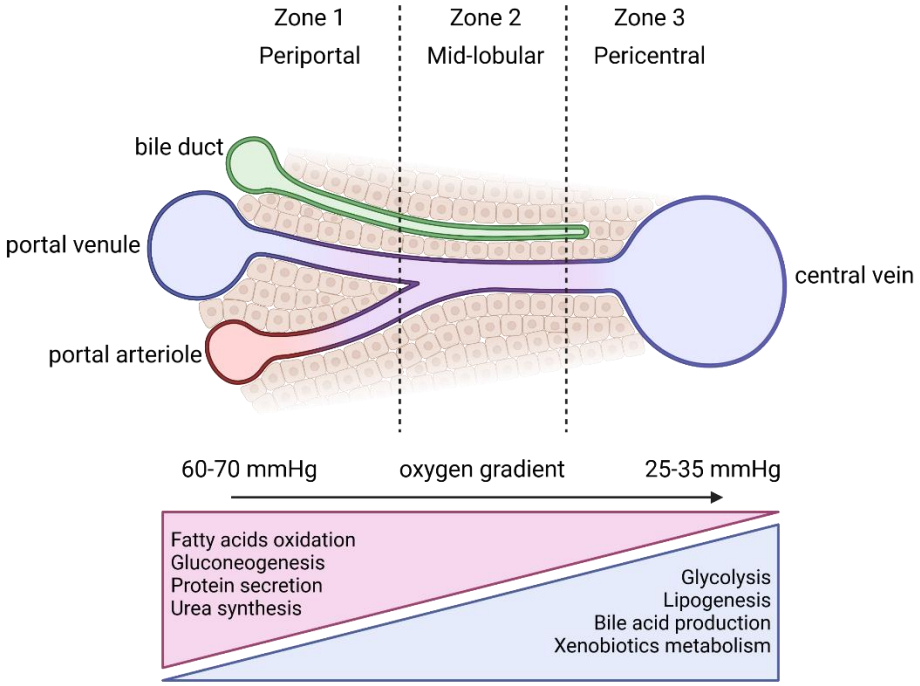

Figure 2. Liver zonation. The scheme presents three different zones in the liver acinus with various oxygen concentrations. Depending on the oxygen tension, different liver-specific functions are performed. Created with BioRender.com.

The elimination of ammonia, which is formed during the metabolism of amino acids and other nitrogenous compounds, is one of the most important liver-specific functions. Because ammonia at higher concentrations is toxic, it should be successively removed from the body. Persistently high concentrations of this compound in the blood (hyperammonemia), especially during liver diseases, can lead to hepatic encephalopathy (impairment of the central nervous system) and ultimately death. Ammonia detoxification occurs through two different pathways. At first, the hepatocytes in the periportal zone convert ammonia into urea (through multiple enzymatic reactions), which is then eliminated in the urine. This process is known as the urea cycle. In turn, uncaptured ammonia compounds are metabolized to glutamine by hepatocytes in the pericentral zone. The urea cycle consists of two mitochondrial and three cytosolic enzymatic reactions. The conversion of ammonia and bicarbonate into carbamoyl phosphate is the first step of this cycle and is catalyzed by carbamoyl phosphate synthetase 1 (CPS1). Then, carbamoyl phosphate and ornithine are transformed into citrulline in the presence of ornithine transcarbamylase (OTC). Subsequently, citrulline is transported to the cytoplasm, and with aspartate is converted into arginosuccinate by arginosuccinate synthetase (ASS). Further, arginosuccinate is transformed into arginine and fumarate in the presence of argininosuccinate lyase (ASL). The last step of the urea cycle is catalyzed by arginase 1 (ARG1) and during this process arginine is converted into urea and ornithine (Wright *et al.*, 2011;

Braissant, McLin and Cudalbu, 2013). The schematic picture of the urea cycle is presented below (Figure 3).

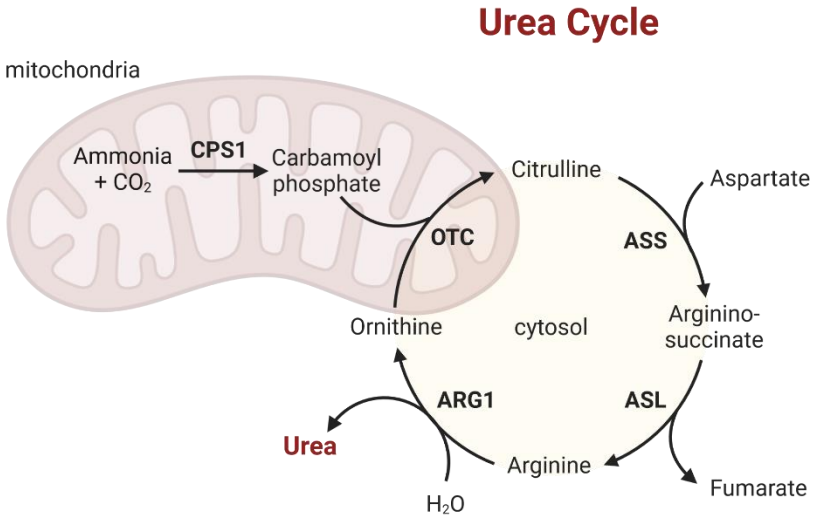

Figure 3. The scheme of the urea cycle. Created with BioRender.com. Abbreviations: ARG1 – arginase 1; ASL - argininosuccinate lyase; ASS - arginosuccinate synthetase; CPS1 - carbamoyl phosphate synthetase 1; OTC - ornithine transcarbamylase.

1.2 Liver diseases and their causes

The main causes and risk factors for liver diseases are viral infections, obesity, excessive consumption of drugs (e.g., acetaminophen) or alcohol (or a combination of both), poisoning with toxic substances (e.g., phallotoxins), and metabolic or autoimmune disorders (Blachier *et al.*, 2013; Melaram, 2021). Among the most common liver diseases are cirrhosis, liver cancer (especially human hepatocellular carcinoma, HCC), alcohol-associated liver disease (AALD), nonalcoholic fatty liver disease (NAFLD), nonalcoholic steatohepatitis (NASH), autoimmune or viral hepatitis (A, B, C, D, E), and drug-induced liver injury (DILI). According to the literature, liver cirrhosis and hepatocellular carcinoma are characterized by the highest global mortality, which makes these diseases the 11th and 16th most common causes of death, respectively (Asrani *et al.*, 2019). Notably, the newest report revealed that liver chronic disease and cirrhosis jumped into 9th place in this ranking in the USA (Xu *et al.*, 2022).

The aforementioned diseases lead to liver impairment, which can occur as acute liver disease or chronic liver disease. Currently, viral hepatitis is the major factor responsible for the morbidity of acute liver disease. In the case of chronic liver disease, the main causes are excessive consumption of alcohol and viral hepatitis (Asrani *et al.*, 2019). Worryingly, in 2016, the prevalence of chronic liver diseases in Europe was approximately 84 million (Pimpin *et al.*, 2018). In turn, the latest report shows that the number of cases of chronic liver disease

worldwide was estimated at 1.5 billion (Moon, Singal and Tapper, 2020). It is worth emphasizing that chronic liver diseases represent a major global public health problem causing approximately 2 million deaths annually (Marcellin and Kutala, 2018).

Without proper treatment, further pathological changes in the liver may occur (e.g., reorganization of the cellular structure), which can ultimately lead to the development of acute liver failure (ALF) or chronic liver failure (CLF). These processes are accompanied by different pathological liver stages, such as fatty liver, liver fibrosis, liver cirrhosis or cancer (e.g., hepatocellular carcinoma) (Ferrell, 2000). The pathology of the liver is presented below (Figure 4).

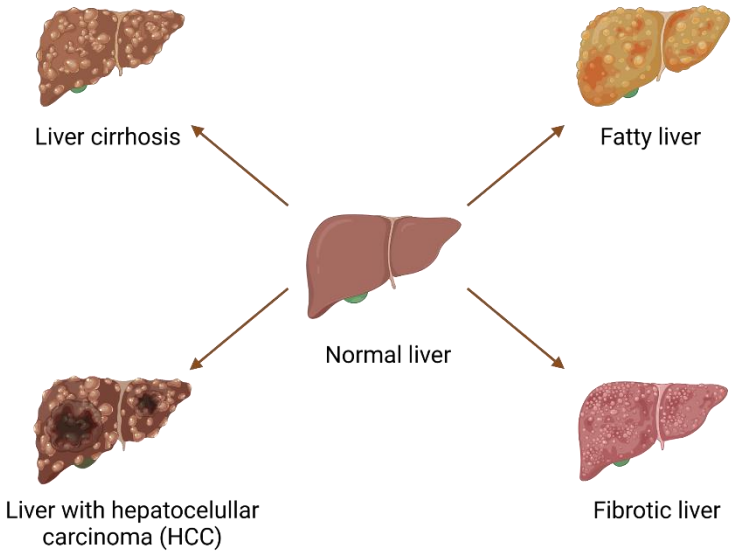

Figure 4. Liver pathology. The different stages of liver pathology: fatty liver, fibrotic liver, liver with hepatocellular carcinoma (HCC), and liver cirrhosis. Created with BioRender.com.

When liver failure (LF) occurs, this organ is not able to perform its functions properly. Depending on the cause, this process can develop slowly or rapidly (resulting in CLF and ALF, respectively). ALF occurs rarely and without the previous presence of any liver disease. It usually results from acetaminophen overdosing, viral hepatitis, poisoning (toxin from mushrooms) or certain metabolic disorders (e.g., Wilson's disease). ALF develops very quickly, with a mortality rate greater than 50%. In some cases, treatment with medications is possible; however, patients often need urgent liver transplantation (Bernal and Wendon, 2013). CLF, the most common type of liver failure, progresses over months or years. CLF is often the result of cirrhosis, which may be caused by hepatitis infection, heavy alcohol intake or obesity. Due to the presence of these damaging factors, scar tissue is formed, which replaces healthy liver tissue. This process is known as fibrosis, and it has developed very slowly for many years. Finally, when the whole liver is scared, it shrinks and hardens, which is called cirrhosis.

Unfortunately, this process is irreversible. CLF is regarded as an end-stage liver disease, which is the final stage of liver failure. In this case, the only effective treatment is liver transplantation (Heidelbaugh and Bruderly, 2006). Sometimes, patients suffering from CLF may experience sudden worsening of liver function. This rapid progression of liver failure is called acute-on-chronic liver failure (ACLF), and it usually results from complications of cirrhosis due to unexpected infections or alcoholic hepatitis. ACLF is characterized by single or multiple organ failure and intense systemic inflammation. Its mortality rate reaches over 15%, and again, only liver transplantation could be beneficial for patient recovery (Kumar, Mehta and Jalan, 2020).

1.3 Methods for the treatment of impaired liver

1.3.1 Liver transplantation

The first successful orthotropic liver transplantation was conducted in 1967, and currently, it is the only long-term cure for patients suffering from liver failure (Starzl *et al.*, 1968). Despite the fact that many obstacles concerning the whole procedure have been overcome over the years, there are still some challenges that scientists have to address. Liver transplantation is an expensive therapy that requires life-long immunosuppressive therapy. Unfortunately, patients often struggle with the side effects of taking immunosuppressive drugs for a long time. Moreover, organ rejection and the risk of postoperative complications are possible. Scientists have also been confronted with issues concerning the development of appropriate donor-recipient matching systems and organ preservation techniques, which ensure their good quality (Davies and Bañares, 2015; Dutkowski *et al.*, 2015; Meirelles Júnior *et al.*, 2015). Interestingly, instead of organ preservation using the static cold storage method, the utilization of dynamic strategies, i.e., liver perfusion machines, has recently gained much attention. The advantages of these methods over standard technique are as follows: the ability to assess organ viability, amelioration of organ ischemic injury during procurement, prolonged storage time, and minimization of the risk of injury during storage. Currently, two liver perfusion machines (OrganOx metra System; OCS liver system) have been approved for clinical use by the Food and Drug Administration (FDA) (Nasralla *et al.*, 2018; Schlegel *et al.*, 2023).

However, the main limitation of liver transplantation is the insufficient number of organ donors compared to the increasing number of patients on the waiting list. According to the US Organ Procurement and Transplantation Network in 2020, more than 12 500 patients were waiting for liver transplantation, while the number of conducted transplants was only 8 782.

Notwithstanding, almost 2 000 patients from the waiting list died, which constitutes approximately 10% of candidates from the waiting list (Kwong *et al.*, 2022). Considering the problems associated with liver donor shortages, several promising therapies aimed at bridging the time until organ transplantation or regeneration have been developed in recent years.

1.3.2 Experimental strategies for supporting liver failure

As mentioned above, orthotropic liver transplantation is currently the only effective medical solution for the treatment of end-stage liver diseases. Nevertheless, the great limitation, which is insufficient organ availability, has encouraged scientists to search for new experimental therapies aimed at supporting liver failure. Among them the most promising are liver support systems (LSS) and cell therapy (hepatocyte transplantation). Apart from these well-known techniques, strategies connected with tissue engineering technologies (3D bioprinting, organ decellularization) are still being developed (Struecker, Raschzok and Sauer, 2014; Pluta *et al.*, 2021). A literature review concerning experimental strategies for supporting liver failure is presented in the sections below.

1.3.2.1 Cell therapy – hepatocyte transplantation

Human hepatocyte transplantation was conducted for the first time in 1992 in Japan (Mito, Kusano and Kawaura, 1992). The whole procedure is simple, less expensive and less invasive than orthotropic liver transplantation. Human hepatocytes are usually isolated from livers rejected for transplantation or from resected liver fragments. Importantly, to ensure a therapeutic effect, they should not be transplanted later than 24 hours after isolation, and the number of transplanted cells should replace 5-15% of the total liver mass. Transplantation occurs by infusion into the liver via the portal vein. Cells can also be injected into the spleen or peritoneal cavity, from which they migrate to the liver. The main advantage of hepatocyte transplantation is that even partial cell replacement is beneficial for the restoration of liver functionality. Moreover, if needed, multiple transplantations from one donor can occur. Additionally, isolated cells can be cryopreserved until their use is necessary. The great limitations of this method are related to the lack of appropriate donors, rapid *in vitro* dedifferentiation of human parenchymal cells, and risk of rejection of transplanted cells. Moreover, cryopreservation can affect cell viability, and the optimal immunosuppressive therapy has not yet been established (Dhawan *et al.*, 2010; Fox, 2014; Forbes, Gupta and Dhawan, 2015; Ibars *et al.*, 2016). According to the literature, clinical trials have shown that hepatocyte transplantation is beneficial for the treatment of various metabolic liver disorders,

especially urea cycle defects. Unfortunately, clinical investigations of patients suffering from acute liver failure or chronic liver disease have not yielded satisfactory results (Iansante *et al.*, 2018; Miki, 2019).

1.3.2.2 Bioengineered liver – utilization of tissue engineering techniques

Recently, to fulfill the unmet need for good-quality liver donors, the concept of creating bioengineered organs has gained much interest. The two most promising approaches to design liver grafts are based on 3D bioprinting and organ decellularization/recellularization techniques. The state-of-the-art of the development of bioengineered liver using the aforementioned methods is described below.

Organ decellularization and recellularization

Whole organ decellularization aims to obtain an acellular scaffold with retained native vascular networks and extracellular matrix (ECM) composition. The preservation of native ECM integrity (protein content, 3D structure, biochemical and biophysical properties) is essential for further cell attachment, survival and proliferation. In turn, retained vascular networks supply seeded cells with oxygen and nutrients (Hillebrandt *et al.*, 2019). The decellularization process is usually carried out with the use of three different types of agents, which are classified as chemical (e.g., acids/bases; detergents; hypotonic/hypertonic solutions), biological (e.g., enzymes; chelating agents), or physical (e.g., temperature – freezing and thawing). To improve the success of decellularization procedure, scientists frequently combine the aforementioned agents. The perfusion of biological and chemical agents is typically performed via the portal vein (antegrade perfusion) or hepatic artery (retrograde perfusion) (Gilbert, Sellaro and Badylak, 2006).

To evaluate the effectiveness of the decellularization process, analysis of residual cellular material must be performed. Because this procedure does not allow for eliminating all cell material, the criteria for minimal residual cell content were established. Thus, to avoid adverse host responses and problems with *in vitro* cytocompatibility, such decellularized ECM should have no visible nuclear components, contain less than 50 ng of DNA/mg of tissue, and DNA fragments should not be longer than 200 base pair (bp). Moreover, the preservation of the appropriate ECM composition and architecture (structural and vascular) also indicates successful decellularization. These aforementioned parameters are usually evaluated using microscopic techniques. Before implantation (or *in vitro* usage), such decellularized ECM must be sterilized to remove endotoxins and viral and bacterial DNA. The most common procedures

are based on incubation with chemical substances (e.g., acids and solvents), exposure to ethylene oxide, and gamma or electron beam irradiation (Crapo, Gilbert and Badylak, 2011). Some successful protocols for whole liver decellularization have been reported in the literature. For example, Soto-Gutierrez et al. successfully decellularized whole rat liver by retrograde perfusion using a combination of physical (freezing-thawing step), biological (enzymes), and chemical (detergents) agents (Soto-Gutierrez *et al.*, 2011). In turn, Baptista et al. achieved the decellularization of whole livers obtained from several animals (mouse, rat, ferret, rabbit, and pig). In general, they perfused organs through the portal vein using only chemical agents, but in some cases, they adjusted the protocol to the size of the liver of the analyzed species (Baptista *et al.*, 2011). Interestingly, Mazza et al. reported successful decellularization of whole human liver. The procedure was conducted by retrograde perfusion with the combination of the three types of aforementioned agents. Decellularization of the whole human liver was achieved within six weeks (Mazza *et al.*, 2015). Each protocol ensured the preservation of intact vascular and structural liver architecture and a lack of visible nuclear content.

The recellularization process aims to repopulate decellularized ECM scaffolds with liver-specific cell types or stem cells to obtain functional liver grafts. This procedure usually occurs via the portal vein or hepatic artery (Wang *et al.*, 2017). Several studies have reported successful repopulation with parenchymal liver cells (e.g., primary hepatocytes, hepatocyte-like cells) and endothelial cells, which are necessary for recapitulating the vascular network (Park *et al.*, 2016; Zhou *et al.*, 2016; Kojima *et al.*, 2018). For example, Robertson et al. achieved successful liver recellularization, which specific functions (e.g., drug detoxification and albumin secretion) were maintained *in vitro* for 28 days (Robertson *et al.*, 2018). In turn, Yang et al. reported the implantation of repopulated liver grafts, which survived for 40 days. Although promising results have been obtained, reconstitution of the functionality of the biliary system remains the greatest challenge in liver bioengineering (Yang *et al.*, 2018).

3D bioprinting

The 3D bioprinting technique is regarded as a very promising tool for organ fabrication. It utilizes 3D inkjet printers, which precisely, in a layer-by-layer manner, manufacture functional liver scaffolds composed of bioinks, which in turn are made of live cells, biomaterials, and biochemicals (i.e., growth factors). Using bioinks and computer-aided models of liver structure, there is a high possibility of creating organs that are identical to those that occur naturally. Moreover, 3D bioprinting enables the control of various mechanical and biological parameters (e.g., size, porosity, strength) (Kryou *et al.*, 2019). However, the

fabrication of liver vascular networks is still very challenging (Lewis and Shah, 2016). 3D bioprinting utilizes one of the following technologies: laser-assisted bioprinting, inkjet-based bioprinting, extrusion-based bioprinting, stereolithography or microvalve-based bioprinting. All of the aforementioned methods have advantages and drawbacks, but extrusion-based techniques have been widely used, especially for fabricating scaffolds with living cells. During this process, multiple biomaterials with different cell types can be used, which enables the creation of heterogeneous scaffolds with the simultaneous preservation of high cell viability (Liu *et al.*, 2018).

The choice of bioink is an essential aspect of 3D bioprinting. As mentioned above, it is composed of living cells and surrounding hydrogel biomaterial. Ideally, the bioink should contain a source of parenchymal liver cells, nonparenchymal liver cells and endothelial cells necessary for building the vascular network. To date, several attempts with the following cell types or their combinations have been reported: parenchymal cells: primary human, rat and mouse hepatocytes, hepatocyte-like cells or human hepatocellular cell lines (i.e., C3A, HepG2, HepaRG, Huh7); nonparenchymal cells: hepatic stellate cells, fibroblasts or Kupffer cells; and component of vascular tree - human umbilical vein endothelial cells (HUVECs). The main role of hydrogel biomaterials is to ensure an appropriate environment for cells. It is vital for hydrogels to have good mechanical properties, especially stiffness, which is responsible for maintaining the whole structure. Moreover, the chosen hydrogel should be biocompatible with cells to ensure their proper functionality. Among the most commonly used hydrogels are alginate, collagen, gelatin, and decellularized ECM. Very rarely synthetic polymers (e.g., polyethylene glycol) are utilized. According to the literature, better results were obtained when a combination of different hydrogels was used (Ma *et al.*, 2020; Gupta and Bit, 2022).

To date, many scientists have reported studies concerning 3D bioprinting of liver tissue using different types of cells, hydrogels, and printing techniques. For example, Nguyen et al. created a mini liver tissue utilizing human hepatocytes, hepatic stellate cells, and HUVECs using the extrusion-based bioprinting method. Moreover, they used as a component of the bioink NovoGel 2.0 hydrogel manufactured by Organovo. Cell viability up to 4 weeks was achieved. Moreover, during this time, higher albumin synthesis and cytochrome P450 activity were observed compared to the monolayer control (Nguyen *et al.*, 2016; Norona *et al.*, 2016). In turn, the Mazzocchi group developed a bioink composed of human hepatocytes, hepatic stellate cells, and a hydrogel made of methacrylated collagen type I and thiolated hyaluronic acid. After printing using the extrusion-based method, the obtained liver tissue remained viable for more than two weeks. Additionally, during this time, cells performed their specific functions

– albumin and urea secretion and drug detoxification (Mazzocchi *et al.*, 2018). Interestingly, Lee et al. proposed a hydrogel made of porcine decellularized ECM with the addition of a synthetic polymer (i.e., polycaprolactone), which supported the maintenance of the 3D structure. As cellular components, the HepG2 cell line and mesenchymal stem cells derived from human bone marrow were utilized. For the creation of the liver tissue model, an extrusion-based printing technique was used. The obtained liver tissue was characterized by increased expression of liver-related genes and higher albumin and urea synthesis compared to the control liver tissue created with collagen bioink (Lee *et al.*, 2017).

Currently, 3D bioprinted liver tissue models are widely applied in drug screening studies, liver disease modeling and microfluidics liver-on-chip platforms. Microfluidic platforms are very useful tools because they enable the mimicking of dynamic and native cellular environment. Thus, liver-on-a-chip platforms can provide information about tissue responses after exposure to various conditions and hence could be widely used in drug development. However, some challenges (e.g., vascularization issues and the composition of the biomaterial) must be overcome before obtaining a brioprinted functional liver (Heydari *et al.*, 2022).

1.3.2.3 Liver Support Systems (LSS)

Another substitutive treatment for patients suffering from liver failure is the use of liver support systems. These hybrid devices are regarded as bridging therapy for patients waiting for liver transplantation (bridge-to-transplant) or until regeneration (bridge-to-recovery). They were divided into two groups: artificial liver support systems (ALSS) and bioartificial liver support systems (BLSS). Both systems utilize filtration, dialysis, perfusion, and adsorption techniques to remove toxins from the patient's blood. However, the only liver function that ALSS replace is detoxification, while BLSS are able to support additionally metabolic and synthetic processes due to the presence of biological component inside the bioreactor (Laleman *et al.*, 2006; García Martínez and Bendjelid, 2018). The characterization of these extracorporeal devices, their clinical application, and the challenges associated with their utilization are described in the section below.

1.3.2.3.1 Artificial Liver Support Systems (ALSS)

The mechanism of action of ALSS is based on the capacity of albumin to bind toxins. The detoxification process occurs through albumin dialysis or plasma separation and filtration. These methods enable the removal of toxins bound to albumin and substances soluble in water

(urea, ammonia, creatinine, cytokines). According to the literature, ALSS are used as bridging therapies for patients suffering from acute liver failure (ALF) or acute-on-chronic liver failure (ACLF). Moreover, these devices are also utilized after liver transplantation as a treatment for liver failure occurred due to the lack or poor functionality of liver grafts. Many clinical studies indicate that ALSS are beneficial because they have an impact on the improvement of hepatic encephalopathy, jaundice, and hemodynamic instability and the reduction of portal hypertension and intracranial pressure. Nonetheless, improvements in patient survival after therapy with ALSS devices have not been documented (Nevens and Laleman, 2012). Among ALSS, we can highlight the following devices: the Molecular Adsorbent Recirculating System (MARS) (Stange *et al.*, 1993), the Fractionated Plasma Separation and Adsorption system (FPSA; Prometheus system) (Falkenhagen *et al.*, 1999), the Single-Pass Albumin Dialysis system (SPAD) (Seige *et al.*, 1999), the Selective Plasma Filtration Therapy (SEPET) (Rozga *et al.*, 2006), and the ADVanced Organ Support (ADVOS) (Al-Chalabi *et al.*, 2013). The principle of action and clinical trials concerning the abovementioned system are described below.

Molecular Adsorbent Recirculating System (MARS)

MARS, which is the most extensively studied device among artificial liver support systems, was developed by Stange et al. in 1993 (Stange *et al.*, 1993). It consists of three compartments – a blood circuit, an albumin circuit, and a dialysate circuit. First, the patient's blood passes through the hollow fiber module named the MARS Flux dialyzer. The module contains polysulfone capillary membranes (with a pore size of 50 kDa), which are coated with albumin. Therefore, the membranes can transiently absorb toxins from the patient's blood. The elimination of toxins bound to fibers occurs through diffusion. Then, they are successively collected by dialysate fluid enriched in high concentrations of human albumin. After that, the solution rich in toxins passes through the dialysate circuit, where the clearance of substances soluble in water occurs. Finally, the albumin-bound toxins are removed while passing through the adsorber columns with anion-exchange resin and activated charcoal. In this way, regeneration of albumin occurs, which is then able to bind the next portion of toxins from the patient's blood (Stange *et al.*, 1999; Mitzner *et al.*, 2001; Mitzner, 2011). The scheme of the MARS principle of action is presented in the figure below (Figure 5).

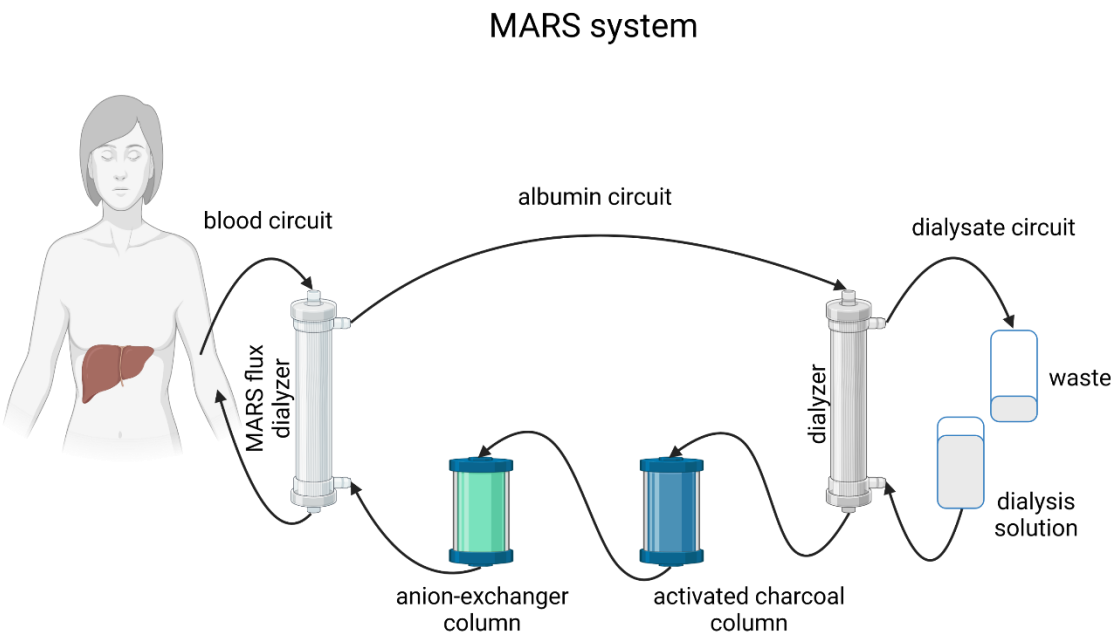

Figure 5. Scheme of the Molecular Adsorbent Recirculating System (MARS). Created with BioRender.com.

MARS is the most widely studied device among artificial liver support systems. To date, many case studies and reports about controlled/uncontrolled, prospective/retrospective, randomized and/or multicenter clinical trials have been published. In this literature review, the description of studies concerning the safety and efficacy of MARS device will be restricted to reports from controlled, randomized, multicenter, and prospective clinical trials. In the case of patients suffering from acute liver failure (ALF), only one clinical trial that met the abovementioned conditions was found. The study included 102 participants from 16 different transplantation centers in France. The patients with ALF were divided into two groups: 49 patients underwent only standard medical therapy (defined as a standard procedure applicable for a given disease entity), while 53 patients were treated additionally with the MARS device (usually 1 session with MARS, which the median duration was 7.5 hours). Moreover, the patients were stratified according to whether ALF was induced by acetaminophen. The results of the clinical trial showed no significant regression of hepatic encephalopathy after bridging therapy with MARS. Moreover, the primary endpoint of the study, i.e., the 6-month overall survival rate, was not significantly improved compared to standard medical therapy (84.9% versus 75.5%). Unfortunately, no definitive conclusions concerning the safety and efficacy of the MARS system could be drawn because of the very short time between randomization and liver transplantation. For example, 14 patients from the group treated with MARS underwent orthotropic transplantation without any session or after

only a short session. Therefore, the authors concluded that the conducted clinical trial did not provide information on whether MARS treatment was truly beneficial for patients (Saliba *et al.*, 2013). Another clinical trial involved 149 participants suffering from acute-on-chronic liver failure (ACLF). Eighty two patients received standard medical therapy, whereas the remaining 67 patients additionally underwent treatment with the MARS device. Despite the fact that the 3-year survival rate increased after treatment with the MARS device (compared to the control group), the patient randomization was inadequate; thus, appropriate conclusions could not be drawn. Moreover, no comparison between biochemical parameters was made. Instead, the authors paid more attention to assessing the cost-effectiveness of MARS therapy (Hessel *et al.*, 2010). To date, the largest controlled, randomized, prospective, and multicenter clinical trial on patients suffering from ACLF has been performed by the Bañares group (the RELIEF trial). A total of 156 participants from different centers in Europe were divided into two groups. Eighty five patients underwent standard medical therapy, while 71 patients were treated additionally with the MARS device (a maximum of 10 sessions for 6-8 hours but not fewer than three sessions). Unfortunately, the outcome of the conducted clinical trial was not satisfactory. Although the safety and effectiveness of albumin dialysis were confirmed, compared to standard medical treatment, a primary endpoint of the study, i.e., a significantly improved 28-day transplant-free survival rate, was not achieved (Bañares *et al.*, 2013).

Fractionated Plasma Separation and Adsorption system (FPSA; Prometheus system)

The Prometheus system, first introduced by the Falkenhagen group, is based on combining adsorption and fractionated plasma separation techniques; thus, the detoxification process occurs in different ways (Falkenhagen *et al.*, 1999). First, the patient's blood passes through an AlbuFlow filter, which consists of polysulfone capillary membranes. Because their cutoff point is 250 kDa, hollow fiber membranes are permeable to the patient's albumin and thus to toxins bound to this protein. Therefore, there is no need to use costly exogenous albumin, as is done in the MARS system. Then, the permeate fraction (containing the patient's albumin-bound toxins) passes through two adsorbers – Prometh01 (a column with neutral resin) and Prometh02 (a column with anion-exchange resin). After toxin elimination, the reactivated albumin returns to the AlbuFlow filter. Finally, to remove water-soluble substances, the patient's blood passes through a high-flux dialyzer (Tandon and Froghi, 2021). The scheme of the Prometheus mechanism of action is presented in the figure below (Figure 6).

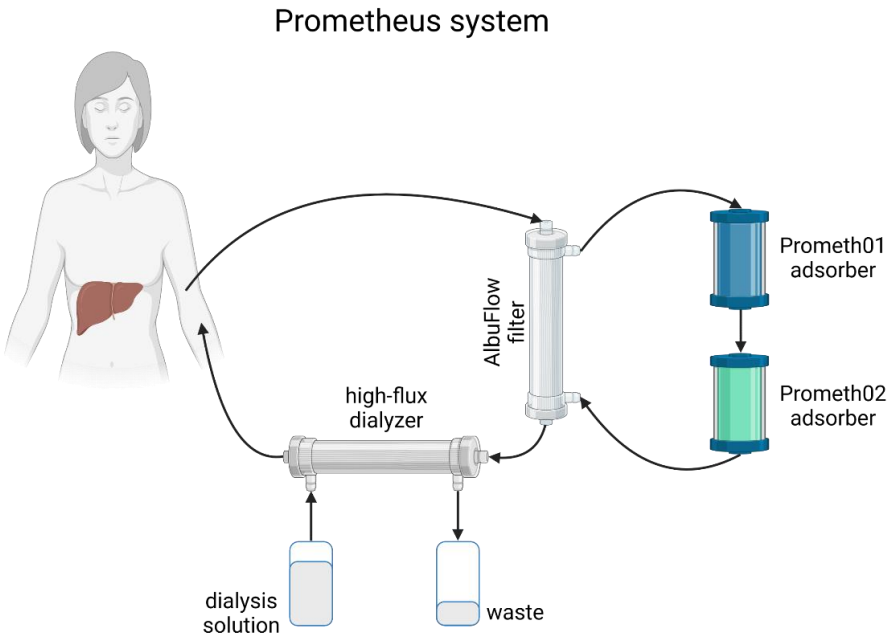

Figure 6. Scheme of the Fractionated Plasma Separation and Adsorption system (Prometheus). Created with BioRender.com.

Among artificial liver support systems, the Prometheus device is the second most studied system. For example, an uncontrolled clinical trial conducted by Rifai et al. was performed on 11 patients suffering from ACLF. The two subsequent treatment sessions lasted more than 4 hours. The safety of the Prometheus system and improvements in biochemical parameters (e.g., bilirubin and bile acid levels) were confirmed (Rifai *et al.*, 2003). In turn, another uncontrolled clinical study performed on 52 patients suffering from ALF, who usually underwent three sessions with the Prometheus device for 6-8 hours, showed a significant decrease in ammonia accumulation. Moreover, improvements in the levels of bilirubin, urea, and creatinine were observed. The outcome of presented study was as follows: 33 patients after treatment with Prometheus device underwent liver transplantation, and the survival rate in this group was 66%. In turn, the remaining 19 patients (also after treatment with Prometheus device) did not receive a graft, resulting in a survival rate of 32% (Grodzicki *et al.*, 2009). To date, Kribben et al. performed the largest multicenter, prospective, randomized, and controlled clinical trial. The aim of this study was to evaluate the effect of treatment with the Prometheus device on patient survival rate. A total of 145 participants suffering from ACLF were divided into two groups. Sixty eight patients underwent standard medical therapy, while the remaining 77 patients were additionally treated with the Prometheus system. Patients usually underwent 8-11 sessions, which lasted a minimum of 4 hours. Among all analyzed biochemical parameters, only a significant difference in the bilirubin level was observed – the value of bilirubin

decreased after the sessions with the Prometheus device. Unfortunately, compared to standard medical therapy, no beneficial effect on the survival rate was confirmed as the primary endpoint of the study; i.e., a significantly improved 28-day transplant-free survival rate, was not achieved (Kribben *et al.*, 2012).

Single-Pass Albumin Dialysis system (SPAD)

The SPAD system, which is commonly regarded as the simplest version of the MARS device, was developed by Seige et al. in 1999 (Seige *et al.*, 1999). The patient's blood is detoxified using the same hollow fiber dialyzer as in the MARS system. The dialysate fluid, containing human albumin, binds toxic substances and is then discarded. Due to the lack of an albumin regeneration process, absorption columns are not needed. The advantages of such a solution are the simplicity of the device and the fact that a lower concentration of human albumin in the dialysate fluid is needed. On the other hand, treatment with the SPAD system is more expensive because without recirculation of the dialysate fluid, high amounts of human albumin are utilized (Kortgen *et al.*, 2009). The scheme of the SPAD device and its principle of action are presented in the figure below (Figure 7).

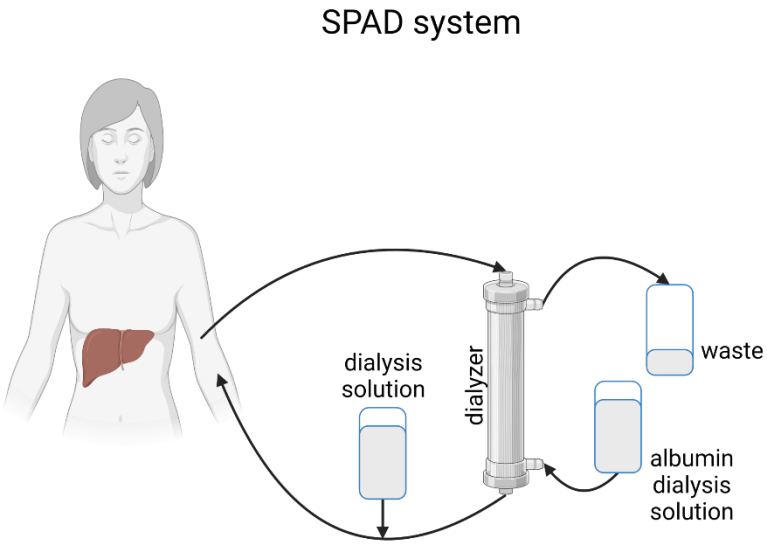

Figure 7. Scheme of the Single-Pass Albumin Dialysis system (SPAD). Created with BioRender.com.

Several studies assessing the safety of bridging therapy with SPAD system have been conducted. For example, Ringe et al. performed an uncontrolled retrospective study on 9 children suffering from ALF. The majority of these patients were bridged to liver transplantation. Moreover, the regression of hepatic encephalopathy was observed in 6 patients (Ringe *et al.*, 2011). Another uncontrolled retrospective study, however, performed on a larger

group of participants, aimed at evaluating the safety of the SPAD system in patients suffering from severe liver dysfunction (Piechota and Piechota, 2016). Unfortunately, no conclusions about its clinical usefulness could be drawn. Recently, the results of two randomized clinical trials that compared MARS and SPAD systems during the treatment of patients with liver failure were published. Both trials confirmed that MARS and SPAD were beneficial for reducing bilirubin levels. However, both groups achieved different results in terms of bile acid, urea, and creatinine levels. The Sponholz group showed that only MARS affected the aforementioned parameters, while the Wallon group revealed no significant differences between the two systems. Unfortunately, no information about the survival rate was available (Sponholz *et al.*, 2016; Wallon *et al.*, 2022).

Selective Plasma Filtration Therapy (SEPET)

The SEPET device was presented by a group led by Rozga. It is based on the technological solutions applied in both Prometheus and SPAD systems. First, the patient's blood enters the single-use hollow fiber bioreactor with a cutoff point of 100 kDa. The plasma fraction containing albumin-bound toxins passes through the porous membranes and is discarded. To replace the lost fluid, fresh frozen plasma, human albumin solution, electrolyte solution or their combination is added to the detoxified patient's blood (Rozga and Malkowski, 2010). The scheme of the SEPET system and its principle of action are presented in the figure below (Figure 8).

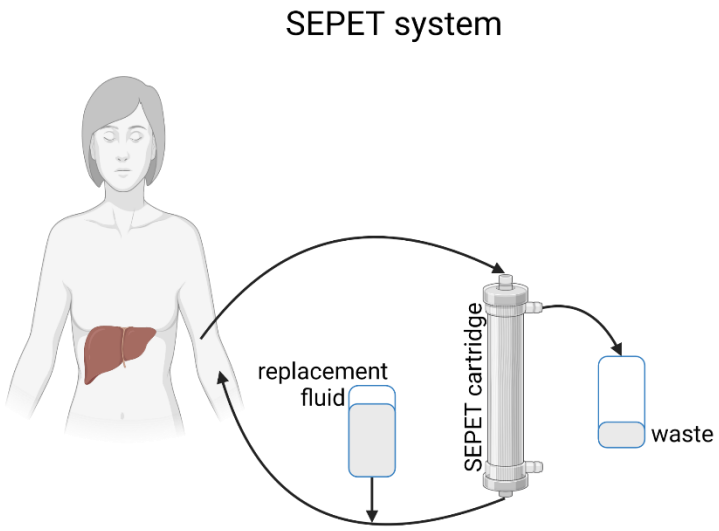

Figure 8. Scheme of the Selective Plasma Filtration Therapy (SEPET). Created with BioRender.com.

Preclinical trials performed on pigs with induced ALF confirmed the safety of the SEPET system (Rozga *et al.*, 2006). Hence, a phase I controlled clinical trial involving patients, who experience the deterioration of liver cirrhosis was conducted. After treatment with the SEPET system, general improvements and the disappearance of hepatic encephalopathy were observed. Despite the fact that continuation of clinical trials (phase II and III randomized controlled multicenter studies) was approved by the Food and Drug Administration (FDA), they did not begin because of a lack of funding (Rozga and Malkowski, 2010).

ADVOS (ADVanced Organ Support)

Recently, a new artificial support system has been introduced. It is called ADVOS, and its prototype is the HepaWash device. The system consists of three compartments: a blood circuit, a dialysate circuit and an ADVOS multicircuit, in which albumin regeneration occurs. The novelty of this device is the method of removing toxins bound to albumin. Briefly, instead of using columns with different adsorbers, physical and biochemical changes are provided to modify the binding abilities of albumin. Dialysate with albumin-bound toxins from the patient's blood is divided into two parts. Then, to each part, acid or base is added (to change the pH), and an appropriate temperature is applied, which enables albumin recovery. Wastes are removed using hollow fiber filters, and cleaned albumin enters the dialysate circuit (Al-Chalabi *et al.*, 2013). The scheme of the ADVOS system is presented in the figure below (Figure 9).

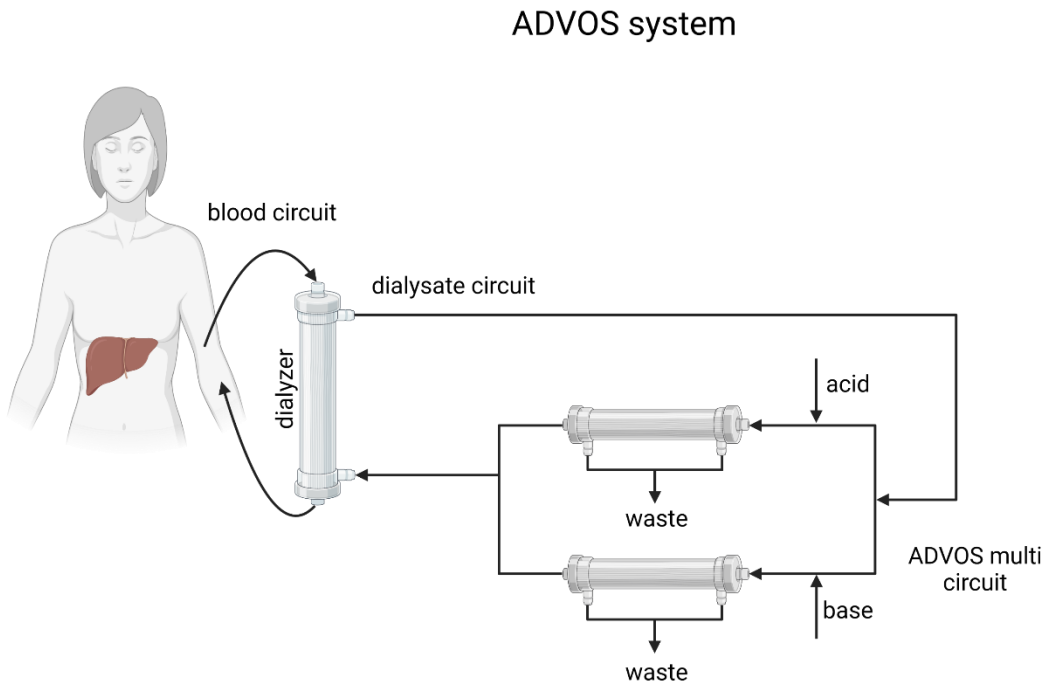

Figure 9. Scheme of the ADVanced Organ Support (ADVOS). Created with BioRender.com.

To date, several clinical trials have been reported. The ADVOS device has been recently used in the treatment of patients suffering from ALF or ACLF (Huber *et al.*, 2017; Kaps *et al.*, 2021). Moreover, it has also been tested for the treatment of multiorgan failure (liver, kidney, and lung) (Fuhrmann *et al.*, 2020). Despite promising results, only uncontrolled clinical trials with small patient groups have been conducted. Therefore, larger and randomized studies must be undertaken to determine the efficacy of therapy with the ADVOS device (Acharya, Berger and Popov, 2022).

1.3.2.3.2 Bioartificial Liver Support Systems (BLSS)

Bioartificial liver support systems, also called bioartificial liver (BAL) devices, are designed to support not only detoxification liver functions but also synthetic and metabolic processes. This resulted from the presence of the biological component inside the bioreactor. In ideal situation, the most preferable source of cells for usefor in BAL devices is human hepatocytes. However, according to the literature, for effective therapy, 10^{10} cells should be utilized, which constitutes approximately 10% of the total number of cells in the liver (Morsiani *et al.*, 2002). Considering the insufficient number of donors from whom the appropriate amount of liver parenchymal cells could be obtained and the rapid deterioration of specific liver functions, the use of human hepatocytes in BAL devices is strongly limited (Nicolas *et al.*, 2017). The problems concerning the availability and *in vitro* preservation of the functionality of human hepatocytes, and hence alternative sources of cells for use in BAL devices, will be widely discussed in the next sections. To date, in BLSS approved for clinical trials, freshly isolated or frozen porcine hepatocytes and the tumor-derived cell line C3A have been utilized (Van De Kerkhove *et al.*, 2004; Pluta *et al.*, 2021). Recently, the use of hepatocyte-like cells obtained from stem cells in the BAL system has been reported (Shi *et al.*, 2016; Wang *et al.*, 2023).

The main role of the bioreactor is to provide effective bidirectional mass transfer and an adequate environment for biological components, so the design of this element is essential. The most commonly used, especially in devices tested in clinical trials, are bioreactors made of bundles of hollow fiber semipermeable membranes. Their main advantages are a large growth surface area, the protection of cells from shear stress and the possibility of immunological isolation due to the presence of a membrane. In general, cells are seeded on the extracapillary surface, while the patient's blood/plasma passes through the hollow fiber lumen (Hui, Rozga and Demetriou, 2001; Legallais *et al.*, 2018; Morelli *et al.*, 2022; Jakubowska *et al.*, 2024). In contrast, the Nyberg group proposed the inoculation of cells entrapped in collagen gel into the

intracapillary space. However, this seeding method enables the placement of too few cells per bioreactor (Nyberg *et al.*, 1993). Interestingly, to resemble the liver structure, the Gerlach group designed a bioreactor in which three different bundles of hollow fibers are arranged in a 3D woven network. Through the first bundle, the culture medium/plasma enters the cells seeded on the outer surface of the fibers, while through the second bundle, it exits. The third bundle supplies the cells with oxygen. The advantages of such a design are more efficient mass exchange and constant, decentralized cell oxygenation (Gerlach *et al.*, 1994).

The main concerns of using hollow fiber bioreactors are connected to uneven cell distribution in capillary spaces and the restriction of effective diffusion caused by the membrane barrier between the biological component and the patient's blood/plasma. To overcome these issues, other types of bioreactors that utilize flat plate membranes, direct perfusion systems or microencapsulation-based systems have been developed (Allen, Hassanein and Bhatia, 2001). Each type has its strengths and weaknesses. For example, flat membranes ensure uniform cell distribution but create problems concerning low surface area, cell exposure to shear stress and difficulties in scaling-up such systems (De Bartolo *et al.*, 2000). In the case of perfused systems, despite resembling 3D structures, they are characterized by nonuniform perfusion, problems with clogging and cell damage due to the subjection to high shear forces (Yanagi, Miyoshi and Ohshima, 1998). In turn, microencapsulated-based systems, even though they provide a uniform microenvironment and are easy to scale up, have faced the following obstacles: cell instability due to damage to the used microcapsules, limited mass transfer due to encapsulation, and cell exposure to shear stress (Harm *et al.*, 2009).

It is also worth paying attention to the material, of which the semipermeable membrane is made, and its porosity. Obviously, the used material should be biocompatible. Moreover, it should be hydrophilic and electrically charged, which promotes cell adhesion. According to the literature, the most suitable are polysulfone-based membranes. Importantly, to enhance cell adhesion, capillary membranes can be coated with collagen or fibronectin; however, such solutions are not used in BAL systems, which were tested clinically (Legallais, David and Doré, 2001; Wung *et al.*, 2014). During the construction of bioreactors, two types of membranes are considered: ultrafiltration or microporous membranes. The first one has 70 kDa as the maximal cutoff point and thus serves as an immunological barrier to prevent an immune response while using porcine hepatocytes as the biological component (Gleißner *et al.*, 1997). The second type has larger pores, with a mean size of approximately 0.2 μm. This allows for the transfer of more proteins (cytokines, etc.) and hence induces the immune system. However, it has been shown

that microporous membranes enable more efficient mass exchange and are more beneficial for use in BAL devices (Watanabe *et al.*, 1997).

The first clinical trial with the use of a BAL device was reported in 1987 by the Matsumura group (Matsumura *et al.*, 1987). Since then, many new systems have been developed and clinically tested. Among them, we can highlight the following devices: the Extracorporeal Liver Assist Device (ELAD) (Sussman *et al.*, 1992), the HepatAssist Liver Support System (HepatAssist) (Demetriou *et al.*, 1995), the Academic Medical Center – Bioartificial Liver (AMC-BAL) (Flendrig *et al.*, 1999), the Modular Extracorporeal Liver Support (MELS) (Sauer and Gerlach, 2002), the Bioartificial Liver Support System (BLSS) (Patzer *et al.*, 1999), the TECA-Hybrid Artificial Liver Support System (TECA-HALSS) (Xue *et al.*, 2001), the Radial Flow Bioreactor (RFB) (Morsiani *et al.*, 2001), and the Hybrid Bioartificial Liver (HBAL) (Ding *et al.*, 2003). The principle of action and clinical trials concerning chosen systems are discussed below.

Extracorporeal Liver Assist Device (ELAD)

The ELAD system, introduced by the Sussman group, has been the only device to date that utilizes the C3A cell line (a subclone of HepG2 cells derived from hepatocellular carcinoma) as the biological component. Originally, the heart of the system consisted of a hollow fiber module made of semipermeable cellulose acetate membranes with a 70 kDa cutoff point. The C3A cells (200 g) were seeded on the extracapillary space of capillaries. Importantly, the patient's blood was not separated into plasma and blood cells but was circulated through a hollow fiber bioreactor with a flow rate of 150-200 mL/min (Kelly *et al.*, 1992; Sussman *et al.*, 1992, 1994; Gislason *et al.*, 1994). However, because the first clinical trials were unsatisfactory, several changes have been incorporated into the system (Ellis *et al.*, 1996). First, the number of hollow fiber modules was increased to four cartridges (for children only two), and for each bioreactor, up to 100 g of C3A cells were loaded (400 g in total). Second, the cutoff point was increased to 120 kDa, and the membrane material was changed to polysulfone. Finally, the flow rate was increased to 500 mL/min, and the plasmapheresis device was added. After these modifications, the ELAD device works as follows: the patient's blood is separated into plasma and blood cellular components, and then the patient's plasma flows into the ELAD chamber, where the four hollow fiber cartridges containing biological components are located. In the ELAD chamber, the temperature is maintained at 37 °C. The use of glucose and oxygen is constantly monitored and successively added to the plasma circuit to assess the metabolic activity of cells. After purification, the plasma passes through a cell filter to prevent tumor cell

transfer to the patient. Finally, it is mixed with blood cells and returned to the bloodstream (Millis *et al.*, 2002; Stevens *et al.*, 2014; Duan *et al.*, 2018). The scheme of the ELAD system and its principle of action are presented in the figure below (Figure 10).

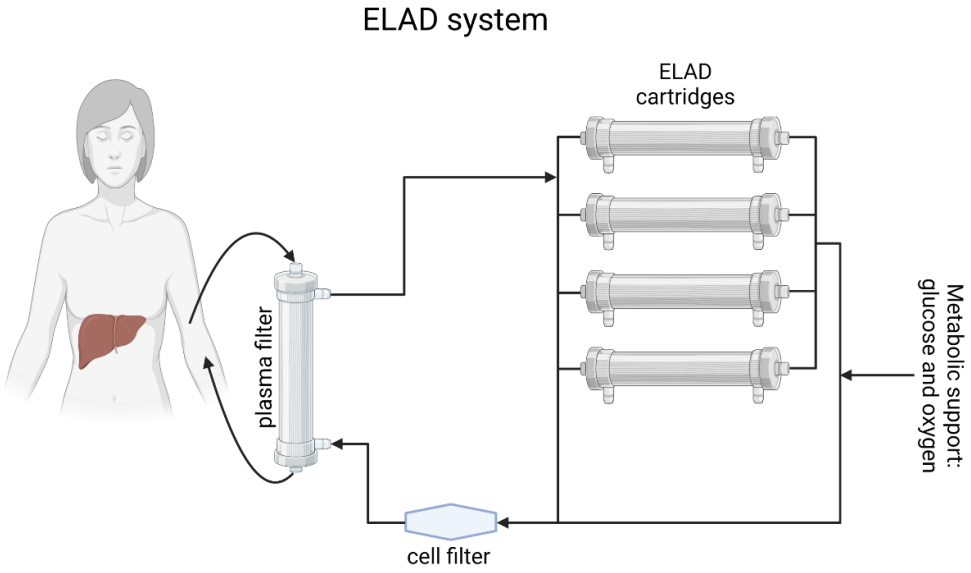

Figure 10. Scheme of the Extracorporeal Assist Liver Device (ELAD). Created with BioRender.com.

The ELAD system, regarded as the most advanced BAL device, has undergone extensive studies and entered phase III clinical trials. As mentioned above, due to the unsatisfactory outcome of initial clinical studies, the ELAD device was modified. After these changes, its safety was evaluated during a pilot clinical trial conducted on a small group of 5 patients suffering from ALF. The duration of treatment was different for each patient and lasted between 12-107 hours. All patients were successfully bridged to liver transplantation. The primary endpoint of this study, i.e., the 30-day survival rate after organ transplantation, was satisfactory and equaled 80% (Millis *et al.*, 2002). Thus, the efficacy of the ELAD device was then evaluated during the II/III phase of a randomized, multicenter, prospective, and controlled clinical trial (VTI-208; NCT01471028). The studies were performed on a large group of patients – 107 patients received standard medical therapy, while 96 patients were additionally subjected to treatment with the ELAD device, which lasted continuously for 120 hours. All patients suffered from severe alcoholic hepatitis. Unfortunately, the endpoints of this study, i.e., 28-day and 91-day transplant-free survival rates, were not satisfactory. No significant differences between the groups were observed. For example, the 28-day survival rate for the control group was 80.4%, whereas for patients treated additionally with the ELAD device, it was only 76%. According to the authors, the reason for this was the choice of a group of patients, which was too heterogeneous (Thompson *et al.*, 2018). Therefore, these conclusions

were investigated during phase III of a randomized, multicenter, prospective, and controlled clinical trial conducted on younger (below 50 years) and healthier participants. The study was performed on 151 patients with severe alcoholic hepatitis. Unfortunately, despite the less heterogeneous group, the results after treatment with the ELAD device were still unsatisfactory (there was no significant improvement in the survival rate). Therefore, the study was terminated in 2018 (VTL-308; NCT02612428). The future of the ELAD system remains unclear.

HepatAssist Liver Support System (HepatAssist)

The HepatAssist device was developed by the Demetriou group (Demetriou *et al.*, 1995). The heart of the system is the hollow fiber bioreactor, which was originally made of cellulose acetate membrane with a pore size of 0.2 µm, and then replaced with a polysulfone membrane with 0.15 µm pores. As a biological component, $5\text{-}7 \cdot 10^9$ cryopreserved porcine hepatocytes are utilized. Before seeding at the outer space of the capillary membrane, the cells are attached to microcarriers made of collagen-coated dextran. The mechanism of action of the HepatAssist device is as follows: the patient's blood is separated into plasma and blood cells, and then the plasma passes through the activated cellulose-coated charcoal column (to reduce its toxicity). Before entering the bioreactor, the plasma is heated and oxygenated and subsequently passes through the hollow fiber module. The flow rate of plasma circulation through the bioreactor is 400 mL/min. After purification, patient plasma is reconstituted with blood cells and returned to the bloodstream (Demetriou *et al.*, 1995; Watanabe *et al.*, 1997). The scheme of the HepatAssist system and its principle of action are presented in the figure below (Figure 11).

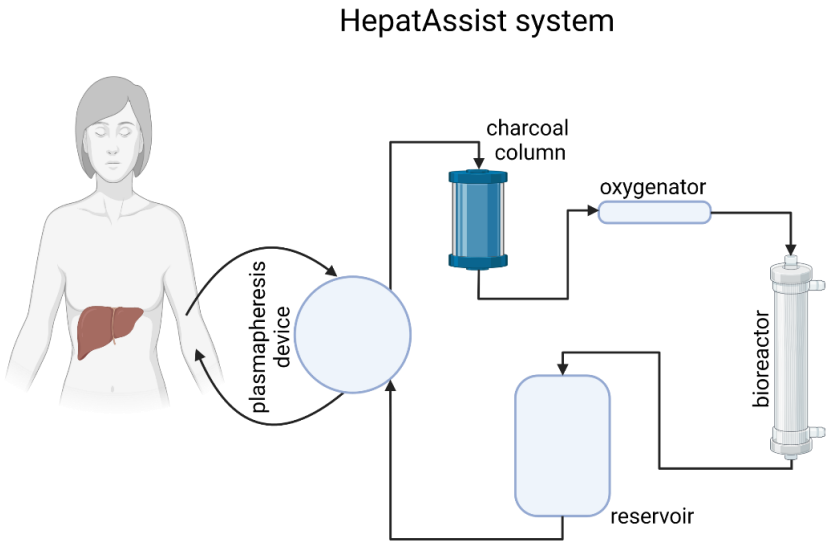

Figure 11. Scheme of the HepatAssist Liver Support System (HepatAssist). Created with BioRender.com.

The HepatAssist device, similar to the aforementioned ELAD, entered III phase of clinical trials. However, its safety was first confirmed during phase I clinical studies. Seven patients suffering from ALF underwent up to three sessions of treatment with HepatAssist device, which lasted 6-7 hours. The obtained results showed no medical complications after therapy, an increase in ammonia elimination and hence a decrease in the progression of hepatic encephalopathy. Moreover, all patients were successfully bridged to liver transplantation and all of them survived the surgery. Unfortunately, the long-term survival rate was not investigated (Rozga *et al.*, 1994). Another phase I uncontrolled multicenter clinical trial was performed on a larger group. Thirty nine patients suffering from ALF (26), ACLF (10) or primary graft nonfunction (PNF; 3) underwent bridging therapy with the HepatAssist device. The number of sessions ranged from one to five and each session lasted 6 hours. The outcome of this trial was as follows: 6 patients recovered from the disease, while 32 patients were successfully bridged to liver transplantation. The endpoint of this study, i.e., the 30-day overall survival rate, equaled 90% (Mullon and Pitkin, 1999). With these promising results, a phase II/III controlled, randomized, multicenter, prospective clinical trial was initiated. The studies included 171 patients suffering from fulminant/subfulminant hepatic failure and PNF. Eighty six patients underwent standard medical treatment, while the remaining 85 patients were treated additionally with the HepatAssist device. The number of sessions with the HepatAssist device reached 14, and each session lasted 6 hours. Bridging therapy with the HepatAssist confirmed the safety of this device. However, compared to standard treatment, this study failed to demonstrate a significant improvement in the primary endpoint, i.e., the 30-day overall survival rate (62% versus 71%) (Demetriou *et al.*, 2004).

Academic Medical Center – Bioartificial Liver (AMC-BAL)

The AMC-BAL device, developed by the Chamuleau group, has a quite different bioreactor design (Flendrig *et al.*, 1999). The bioreactor is made of polysulfone housing and inside it consists of a hydrophilic polyester nonwoven matrix, which is spirally wound around the massive core. Hollow fibers (polypropylene; 0.2 μm pores) in the longitudinal direction are incorporated between the layers of the matrix to supply oxygen and remove CO_2. A total of 10^{10} cells (originally freshly isolated porcine hepatocytes) are seeded in the polyester matrix. The novelty of this bioreactor is direct contact between biological components and patient plasma, which enables optimal mass transfer. The AMC-BAL device works as follows: the patient's blood is separated using a plasmapheresis system. Subsequently, the patient's plasma is heated to 37 °C, then passes through the bioreactor at a flow rate of 150 mL/min and contacts directly

with liver cells. Before reaching the plasmapheresis device, purified plasma enters the leukocyte filter and 0.47 μm filter to reduce the risk of getting through nonattached liver cells or their larger fragments into the patient's blood. Finally, plasma is reconstituted with blood cells and returns to the bloodstream (Flendrig *et al.*, 1997; Sosef *et al.*, 2002). The scheme of the AMC-BAL device is presented in the figure below (Figure 12).

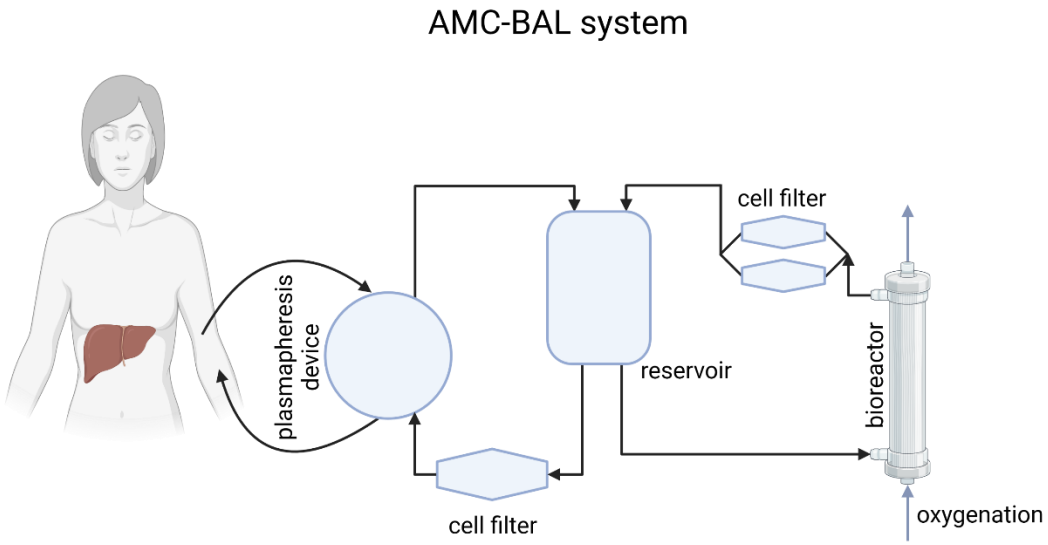

Figure 12. The scheme of the Academic Medical Center – Bioartificial Liver (AMC-BAL). Created with BioRender.com.

The safety of the AMC-BAL system was evaluated in phase I clinical trials involving 7 patients suffering from ALF. Treatment with the AMC-BAL device lasted 8-35 hours, and as a result, 6 patients were successfully bridged to the liver transplant. In turn, one patient (after serial therapy with two different BAL devices) recovered from the disease and did not need surgery. Although four of six patients died within two weeks after orthotropic transplantation, clinical trials confirmed that bridging therapy with AMC-BAL was safe and beneficial (Van De Kerkhove *et al.*, 2002). However, taking into account that the patient's plasma is directly perfused with biological components and thus that xenotransplantation-related risk may occur, scientists have focused on the utilization of the HepaRG cell line (derived from hepatocellular carcinoma) in AMC-BAL instead of porcine hepatocytes. A preliminary study with a rat model of ALF demonstrated the safety and efficacy of the analyzed device. The survival time after therapy with AMC-BAL increased compared to that after treatment with the device without a biological component. Moreover, an increase in the elimination of ammonia and thus regression of hepatic encephalopathy was observed. The obtained results showed that HepaRG cells could be used as a biological component in further clinical trials with the AMC-BAL device (Nibourg *et al.*, 2012).

Modular Extracorporeal Liver Support (MELS)

The MELS system, developed by the Sauer team, consists of three compartments: CellModule, DetoxModule, and DialysisModule. DetoxModule is responsible for the elimination of toxins bound to albumin, while DialysisModule, if needed, can additionally perform hemofiltration. The CellModule part constitutes a special bioreactor in which human/porcine hepatocytes are inoculated. The concept of bioreactor design is based on the research of the Gerlach group. As previously mentioned, the bioreactor consists of three different interwoven bundles of hollow fibers. Two bundles, which are used for plasma perfusion, are made of hydrophilic polyethersulfone membranes (0.5 μm pores). The third bundle (made of hydrophobic multilaminate) supplies the cells with oxygen and removes CO_2. In the MELS system, up to 600 g of biological component is seeded at the extracapillary surface of hollow fiber membranes. The principle of action is as follows: the patient's blood passes through the dialyzer, where albumin dialysis occurs (see description of the SPAD system). Then, the plasma is separated from the patient's blood and enters the CellModule. Finally, the purified plasma is mixed with blood cells and returned to the bloodstream (Gerlach *et al.*, 1994; Sauer and Gerlach, 2002). The scheme of the MELS system and its mechanism of action are presented in the figure below (Figure 13).

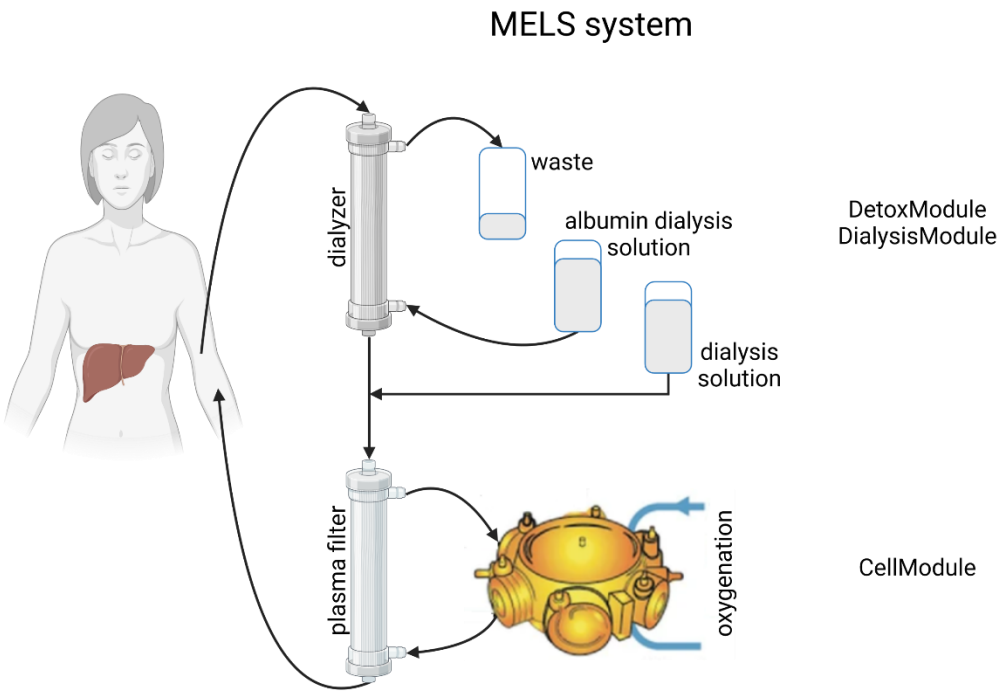

Figure 13. Scheme of the Modular Extracorporeal Liver Support (MELS). Created with BioRender.com.

A phase I nonrandomized clinical trial was conducted on 8 patients suffering from ALF. Treatment with the MELS system lasted for 8-46 hours, and porcine hepatocytes were used as a biological component. All patients were bridged to liver transplantation without any complications, and no infection with porcine endogenous retrovirus (PERV) was observed (Sauer, Kardassis, *et al.*, 2003). In the case of utilizing human hepatocytes in the MELS system, only two preliminary studies were published. Patients who suffered from ALF, ACLF or PNF were treated with the MELS device for 7-144 hours. Both studies confirmed the safety of the tested system (Sauer *et al.*, 2002; Sauer, Zeilinger, *et al.*, 2003).

The newest studies with BAL devices

New BAL devices are still being developed. Among them, the Spheroid Reservoir Bioartificial Liver (SRBAL) system deserves attention because of promising results obtained during studies on animal models. The novelty of this system is the utilization of porcine hepatocytes spheroids or spheroids made of two types of cells: porcine hepatocytes and human umbilical vein endothelial cells (HUVECs). Moreover, liver spheroids are cultured in separate reservoir, unlike in the systems discussed above. The mechanism of action is as follows: the patient's blood enters the polysulfone hollow fiber bioreactor, where albumin-bound toxins pass through the membrane into the dialysate fluid. These fractions are then directed to the reservoir, in which toxic substances are metabolized by liver spheroids. After that, the dialysate fluid containing purified albumin and waste products from metabolic reactions passes through the second hollow fiber bioreactor, where the elimination of wastes occurs, and then the cleaned albumin is recirculated to the bloodstream (Felgendreff *et al.*, 2022). The scheme of the SRBAL system and its principle of action are presented in the figure below (Figure 14).

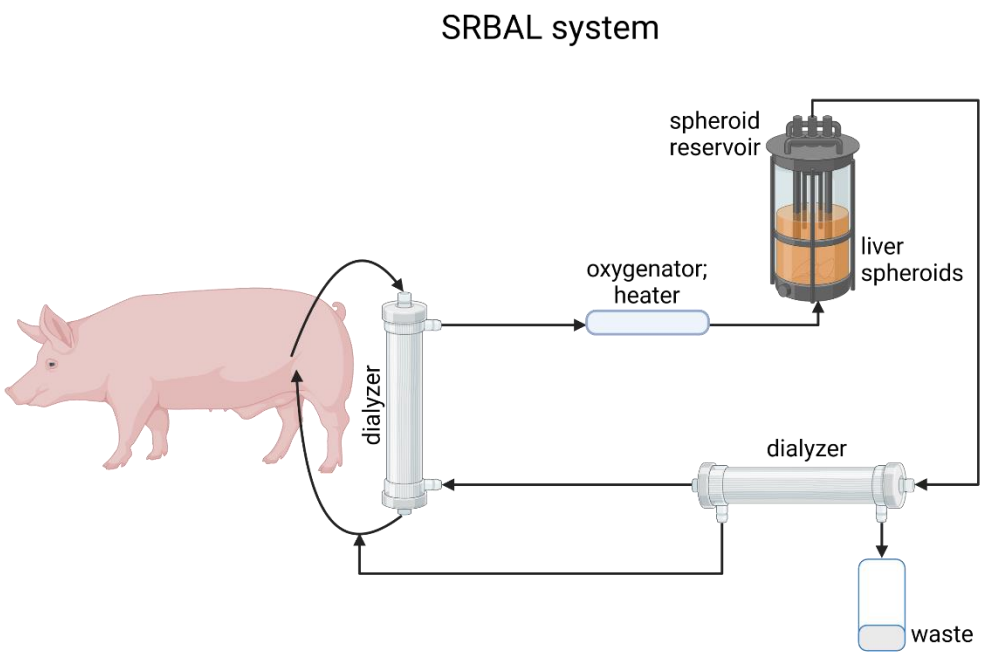

Figure 14. Scheme of the Spheroid Reservoir Bioartificial Liver (SRBAL). Created with BioRender.com.

To date, three preclinical trials on animal models (pigs or monkeys) with induced ALF (surgical or drug) have been conducted. All independent studies have proven the beneficial effect on animal survival after treatment with SRBAL compared to standard therapy. Moreover, the safety of SRBAL was also confirmed (no zoonotic disease transmission). The studies also concluded that longer treatment (up to 24 hours), initiation of therapy immediately after ALF induction, and the use of large amounts of porcine spheroids positively affect the survival rate (Glorioso *et al.*, 2015; Li *et al.*, 2018; Chen *et al.*, 2019).

The newest report published by Wang et al. described the development of a new BAL device called hiHep-BAL, which utilizes human induced hepatocyte-like cells (iHep). The heart of the system is a multilayer flat-plate bioreactor containing polycarbonate scaffolds. The hiHep-BAL device consists of blood and cell circuits. The mechanism of action is as follows: the patient's blood passes through the dialyzer, where the plasma is separated. Then, plasma flows through the plasma component separator and finally enters the bioreactor. In the end, purified plasma is mixed with blood cells and returned to the bloodstream (Shi *et al.*, 2016; Wang *et al.*, 2023). The scheme of the hiHep-BAL system and its mechanism of action are presented in the figure below (Figure 15).

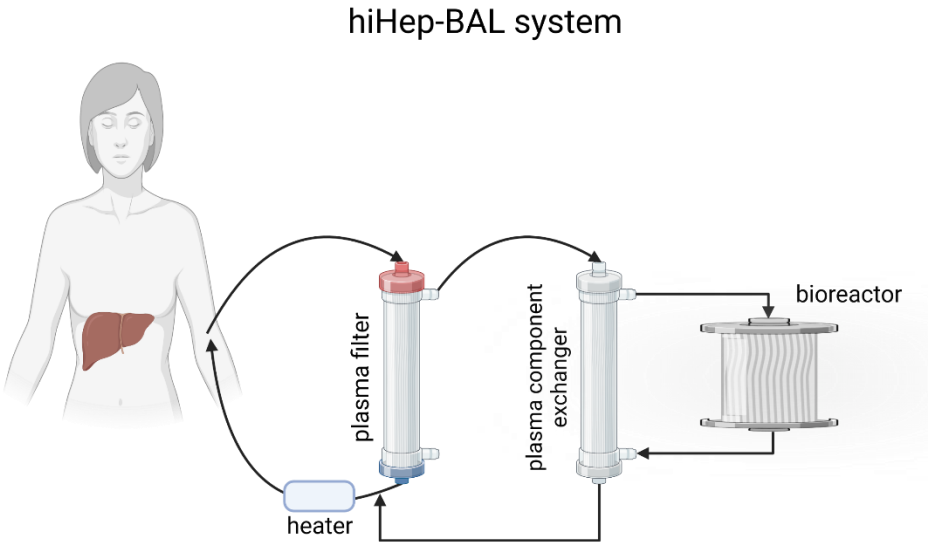

Figure 15. Scheme of the hiHep-BAL support system. Created with BioRender.com.

First, a newly developed BAL system was tested in an animal model. After extended liver resection, pigs were treated with the hiHep-BAL device for 3 hours. The treatment efficacy was very satisfactory, and all the pigs survived after the session with the hiHep-BAL system. Therefore, the Wang group proceeded to carry out clinical trials. This clinical study was a prospective, nonrandomized trial, and its aim was to evaluate the safety and feasibility of the proposed new BAL device. Seven patients, who underwent extended liver resection, participated in this study. Treatment with the hiHep-BAL system lasted 6 hours. The obtained results showed that no serious adverse events occurred (Wang *et al.*, 2023). Although promising outcome, randomized and controlled clinical trials should be performed in the future to draw the correct conclusions.

Future of LSS devices

Over the last thirty years, more than 30 external BAL devices have been developed. Despite the utilization of various cell sources, different bioreactor designs or culture configurations, only half of them have reached clinical trials. There are still several challenges that BAL devices have to address to increase their efficacy, such as bile reduction, insufficient oxygen delivery, limited mass transfer, and aspects concerning vascularization and the time it takes for cells to remain viable and functional. To date, only two BAL devices have entered the third phase of clinical trials. Despite the beneficial effects on patient survival shown in nonrandomized trials, no significant improvements compared to standard treatment have been achieved (Chamuleau, 2009; Zhao, Pan and Li, 2012; Legallais *et al.*, 2018; Starokozhko and Groothuis, 2018).

It is difficult to compare data from clinical trials conducted with the abovementioned LSS due to the various design of the experiments and different analyzed primary or secondary endpoints of the studies (e.g., overall survival rate, transplant-free survival rate, one-year survival rate after liver transplantation). Notwithstanding, on the basis of two clinical trials that compared similar parameters, it can be concluded that LSS are beneficial as a bridging therapy; however their use does not affect patient survival after liver transplantation (Demetriou *et al.*, 2004; Saliba *et al.*, 2013). Nevertheless, scientists and clinicians are still returning to the idea of developing more successful system for bridging therapy. It is worth mentioning that this research area is very challenging yet very relevant because it addresses growing social needs. Therefore, new artificial devices (e.g., DIALIVE) as well as bioartificial devices (e.g., hiHep-BAL, SRBAL) are still being developed (Felgendreff *et al.*, 2022; Agarwal *et al.*, 2023; Wang *et al.*, 2023).

1.4 Human hepatocytes – the most suitable source of cells for use in liver support therapies

The best choice of cells for use in liver failure therapies as well as in *in vitro* studies connected with searching for new drugs and testing their hepatotoxicity are isolated human liver parenchymal cells (Lee and Lee, 2014). The isolation procedure is usually based on the Seglen two-step collagenase perfusion technique (Seglen, 1976). It is regarded as the gold standard, but in our laboratory, we developed a simpler and less stressful (for cells) method, which based on mechanical defragmentation and enzymatic digestion of liver tissue (Zakrzewska *et al.*, 2017). Commonly, human hepatocytes are obtained from the liver, which was rejected for transplantation, or from resected liver tissue. Interestingly, Bhogal et al. showed that there is a possibility of obtaining primary human hepatocytes even from diseased liver (Bhogal *et al.*, 2011). However, the use of isolated human hepatocytes has very strong limitations. First, due to the limited availability of human liver tissue, the amount of good quality material for research is insufficient. Second, human hepatocytes *in vivo* are differentiated cells, which are specialized to perform many vital functions. Therefore, when cultured *in vitro*, these cells are not able to proliferate. Moreover, they dedifferentiate very quickly, which results in a decline in their functionality (Rowe *et al.*, 2013). Thus, a wide variety of methods for the preservation of human hepatocytes culture for a longer time have been developed. The most promising approaches are connected with enhancing cell adhesion (an appropriate growth substratum), enabling cell–cell interactions (cocultures with nonparenchymal liver cells or other cell types), resembling *in vivo* conditions (3D cultures), and media supplementation. Moreover, it is also worth considering the physiological conditions of the liver and ensuring appropriate oxygen tension. It is an

essential parameter due to liver zonation and thus variability in oxygen concentration. In effect, in each liver zone, different processes occur, for which hepatocytes are responsible. Furthermore, for prolonging the *in vitro* culture of human hepatocytes, fluid flow systems have also been studied. Although all of these methods positively affect the *in vitro* culture of human hepatocytes, no gold standard has yet been established (Bachmann *et al.*, 2015; Ruoß *et al.*, 2020; Pluta *et al.*, 2021). The approaches used to preserve the functionality of human hepatocytes are presented graphically in the figure below (Figure 16).

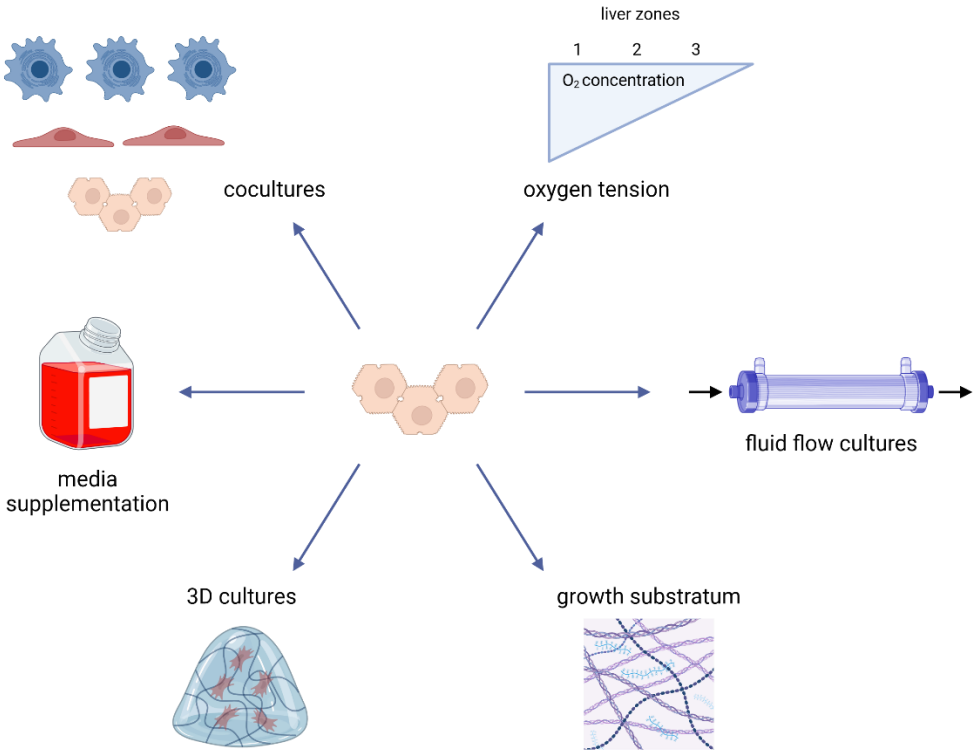

Figure 16. Approaches to preserving the functionality of human hepatocytes *in vitro*. Created with BioRender.com.

1.5 Alternative sources of cells resembling the functionality of human hepatocytes

The challenges connected with the *in vitro* culture of human hepatocytes initiated studies toward developing alternative sources of cells for use in liver support therapies. The best characterized and widely used cells are porcine hepatocytes (Donato, Castell and Gómez-Lechón, 1999) and human tumor-derived cell lines such as HepG2 cells (Nyberg *et al.*, 1994), its subclone C3A cells (Kelly *et al.*, 1992) and HepaRG cells (van Wenum *et al.*, 2016). Other promising alternatives are hepatocyte-like cells obtained from stem cells (for instance, induced pluripotent stem cells) (Song *et al.*, 2009), adult cells (Huang *et al.*, 2011) or hepatic progenitor cells (Malhi *et al.*, 2002). A literature review concerning the advantages and disadvantages of the mentioned sources of cells is provided in the section below. Nevertheless, it is worth

emphasizing that thus far, none of them has been able to fully replace human hepatocytes (Palakkan *et al.*, 2013).

Human tumor-derived cell lines

The great advantages of human tumor-derived cell lines are their high capacity to proliferate *in vitro* and unlimited availability. However, major doubts concerning their usage are connected with their tumorigenicity. To date, in BAL devices that have entered clinical trials, two different cell lines have been utilized: C3A cells in the ELAD system and HepaRG cells in the AMC-BAL system. The C3A cell line is a subclone of HepG2 cells derived from hepatocellular carcinoma (HCC). C3A cells are similar to human hepatocytes – in terms of phenotype, and the ability to metabolize nitrogen and synthetize albumin and alpha fetoprotein. However, they are characterized by some metabolic deficiencies. Due to the nonfunctional urea cycle (lack or low expression of genes encoding two crucial enzymes – arginase 1 and ornithine transcarbamylase), C3A cells are unable to eliminate ammonia properly. Moreover, these cells exhibit decreased activity of several isoforms of cytochrome P450, which results in their lower detoxifying capacity (Mavri-Damelin *et al.*, 2008). Therefore, several attempts have been undertaken to improve the functional capabilities of C3A cells, for example, by increasing the enzymatic activity of CYP3A4 (Han *et al.*, 2018) or restoring the urea cycle (Pluta *et al.*, 2020; Jakubowska *et al.*, 2024). Scientists have also focused on the HepaRG cell line (derived from HCC associated with chronic hepatitis C) due to its greater detoxification capability. Moreover, these cells are more mature than C3A cells because of lower alpha fetoprotein expression. Interestingly, HepaRG cells also have the ability to differentiate into both biliary-like cells and hepatocyte-like cells and thus are recognized as human progenitor bipotent cells. Nonetheless, as in the C3A cell line, the urea cycle does not function properly (Moedas *et al.*, 2017).

Immortalized human hepatocyte cell lines

The immortalization of human hepatocytes has gained much attention because hepatic cell lines obtained during this process are able to proliferate *in vitro* and perform liver-related functions. The most commonly used immortalization strategies include forced expression of human telomerase reverse transcriptase (hTERT) and overexpression of viral oncogenes, such as Simian virus 40 large T antigen (SV40 TAg) or human papillomavirus (HPV) genes. Such gene transfer is conducted with the use of viral (viral transduction) and non-viral (plasmid transfection, human artificial chromosome vectors) methods. Interestingly, for the controlled expansion of human hepatocytes, conditional immortalization has been performed using the

following strategies: temperature-based regulation, recombinase-based regulation, and transcriptional regulation. To date, several hepatic cell lines (derived from adult or fetal hepatocytes) have been established, such as Fa2N-4, HepLL, IHH-A5, THLE or OUMS-29. They are predominantly utilized in pharmacotoxicological studies; however, published results show that immortalized hepatic cell lines possess rather limited liver-specific functionality (Ramboer *et al.*, 2015).

Porcine hepatocytes

Interestingly, the majority of bioartificial liver support systems tested in clinical trials (HepatAssist system, AMC-BAL, etc.) utilized freshly isolated or cryopreserved porcine hepatocytes. The reason for this is the similarity of pig physiology to humans and the easier accessibility of animal liver tissue. However, this source of cells has drawbacks. At first, porcine hepatocytes, similar to human hepatocytes, lose their specific functions during *in vitro* culture (Lee, Kim and Choi, 2015). Moreover, despite the biological barrier (membrane) used in BAL devices, the transmission of zoonotic disease is possible (Yang *et al.*, 2010). Last, as reported in the literature, due to the incompatibility of some human and porcine proteins, the effectiveness of porcine hepatocytes in clinical applications is limited (te Velde *et al.*, 1997; Schrem *et al.*, 2006).

Hepatocyte-like cells from induced pluripotent stem cells (iPSCs)

The development of hepatocyte-like cells from iPSCs consists of two stages. First, adult somatic cells (for example fibroblasts) are converted into iPSCs, and then hepatocyte-like cells are generated from the obtained pluripotent cells. The main advantages of iPSCs are their ability to proliferate *in vitro*, unlimited accessibility, and lack of ethical concerns. Moreover, these cells can be patient specific, which prevents an immunological response. However, the potential risk of tumor formation may limit their clinical application. According to the literature, the method for obtaining hepatocyte-like cells from iPSCs is easy and can be divided into four steps: induction of the iPSCs into the endoderm, induction of the endoderm into hepatic specification, expansion of hepatoblasts, and hepatocytes maturation. Each stage requires the addition of specific growth factors (for example dexamethasone and hepatocyte growth factor (HGF)) (Song *et al.*, 2009). The performance of liver-specific functions by hepatocyte-like cells is confirmed – they synthetize albumin, produce urea, and detoxify xenobiotics, however not at the same level as in the case of human hepatocytes. This may result from the fact that hepatocyte-like cells express alpha fetoprotein and thus are not fully mature (Yu *et al.*, 2012).

However, changes in culture conditions (from static to dynamic) improve liver-related functionality and cell maturity (Ren *et al.*, 2015). Moreover, to achieve more functional hepatocyte-like cells, gene manipulation or supplementation with various substances has been performed (Saito *et al.*, 2021). Hepatocyte-like cells from iPSCs are mainly used for disease modeling or drug screening (Blaszkiewicz and Duncan, 2022). To date, cell-based therapies have been tested in animal models. For example, the Takebe group transplanted liver buds created from human iPSCs into immunodeficient mice. This resulted in the generation of functional and vascularized liver, which stimulated the maturation of buds into tissue resembling adult liver. Moreover, the ability to perform liver-related functions was confirmed (Takebe *et al.*, 2013). Later, the same group successfully transplantated human iPSCs-derived liver organoids into infantile piglets (Tsuchida *et al.*, 2020). Although promising results have shown a potential strategy for the treatment of liver diseases, several studies have reported the tumorigenicity, genetic instability, and immunogenicity of iPSCs (Zhao *et al.*, 2011; Hansel *et al.*, 2016). Therefore, before clinical application, the safety of iPSCs should be thoroughly investigated. Hence, currently, no clinical studies concerning the utilization of iPSC-derived hepatocyte-like cells for the treatment of liver diseases have been conducted (Li *et al.*, 2022).

Hepatocyte-like cells from embryonic stem cells (ESCs)

The other group of cells from which hepatocyte-like cells can be generated are embryonic stem cells. They are a valuable source of cells due to their pluripotency and thus their capacity to differentiate into any type of cell. Moreover, ESCs are characterized by the ability to proliferate *in vitro* and unlimited availability (Oh *et al.*, 2009). Interestingly, Hay et al. showed that hepatocyte-like cells from ESCs were able to synthetize albumin. Moreover, the activity of different P450 cytochrome isoforms was observed (Hay *et al.*, 2008). The method for the generation of hepatocyte-like cells from ESCs is similar to that described for iPSCs. However, due to the lack of protocols for obtaining these differentiated cells on a large scale, they are used for testing the cytotoxicity of drugs (Zhou *et al.*, 2012). The main drawbacks of the utilization of hepatocyte-like cells from ESCs are the possible formation of teratomas from nondifferentiated cells, incompatibility, and ethical concerns (Payne *et al.*, 2011).

Hepatocyte-like cells from adult stem cells

Adult stem cells have advantages over ESCs because of the lack of tumorigenic potential and controversy regarding their usage. Moreover, they are characterized by multipotency and self-renewal capacities. According to the literature, hepatocyte-like cells can be generated from

mesenchymal stem cells (MSCs) due to their ability to transdifferentiate into hepatocytes. MSCs are generally obtained from different adult tissues, including bone morrow or adipose tissue. Many studies have shown that hepatocyte-like cells generated from MSCs exhibit specific features characteristic of adult and fetal hepatocytes (Stock *et al.*, 2008). Interestingly, several clinical trials concerning the transplantation of differentiated hepatocyte-like cells to patients suffering from different liver diseases have been performed; however, the results were not satisfactory. The major obstacles are connected with the fact that initial engraftment was inefficient, and thus, the level of subsequent proliferation of transplanted cells was low (Saito *et al.*, 2021).

Induced hepatocyte-like cells (iHep)

Induced hepatocyte-like cells, called iHep, are directly generated from adult somatic cells such as fibroblasts. Contrary to the protocol for the generation of hepatocyte-like cells from iPSCs, the reprogramming process omits the step in which the cells are in the pluripotency stage. Therefore, the whole procedure is simpler, and the obtained iHep cells have less tumorigenic potential. Moreover, iHep cells can be specific to patients, and thus, therapies using hepatocyte-like cells might not require taking immunosuppressive drugs (Sekiya and Suzuki, 2011). The Huang team was the first to successfully reprogram human fibroblasts into human hepatocyte-like cells. iHep cells were generated using lentiviral vectors carrying genes encoding the following transcription factors: *HNF4A*, *HNF1A*, and *FOXA3*. Overexpression of these genes resulted in the generation of hepatocyte-like cells with a phenotype similar to that of human hepatocytes and the ability to perform liver-specific functions, such as biliary excretion, albumin production and xenobiotics detoxification. Moreover, transplantation of iHep cells into mice with liver injury resulted in prolonged survival (Huang *et al.*, 2014). Although methodology concerning cell reprogramming has been developed, several reports have shown a loss of liver-specific phenotype after cell passaging, suggesting phenotypic instability (Rezvani *et al.*, 2016; Song *et al.*, 2016; Orge *et al.*, 2020).

Human fetal hepatocytes

Human fetal hepatocytes are derived from fetal livers and are characterized by the ability to undergo multiple cell divisions *in vitro*. Therefore, to enable their availability, these cells have been immortalized (Deurholt *et al.*, 2009). However, it is worth mentioning that the fetal liver consists of immature liver cells, which have high levels of alpha fetoprotein and the CYP3A7 isoform. Moreover, human fetal hepatocytes have a much lower capacity to produce

urea and remove ammonia, which limits their application in BAL devices (Poyck *et al.*, 2007). Other concerns are related to ethical issues, possible tumorigenicity, and poor availability (Diekmann, Bader and Schmitmeier, 2006).

Hepatic progenitor cells (HPCs)

Hepatic progenitor cells (HPCs) are located in the normal liver. These cells have a bipotential nature due to their ability to differentiate into hepatocytes or cholangiocytes during liver injury (adult HPCs) or liver organogenesis (fetal HPCs; hepatoblasts). Therefore, they are regarded as a promising alternative to human hepatocytes. The literature shows that adult HPCs have enhanced activity of phase I and II enzymes and metabolize ammonia into urea. However, the tumorigenic potential and poor availability of HPCs limit their use (Khuu *et al.*, 2011; Tanimizu and Mitaka, 2014).

2. Aim and research theses

Aim:

The aim of the presented research was the development of the model system for dynamic cell culture based on hollow fiber bioreactors populated with various hepatocellular carcinoma cells. The primary goal was to establish a new genetically modified hepatocellular carcinoma cell line with a restored urea cycle. The secondary goal was to evaluate the functionality of the obtained cell line under static and dynamic conditions.

Main thesis:

1. The new approach to genetic modification of the hepatocellular carcinoma cell line (C3A) will permanently restore its urea cycle and will provide a potential source of cells for use in bioartificial liver devices.

Supportive theses:

1. The newly established genetically modified hepatocellular carcinoma cell line will have a better overall performance in static culture.

2. The constructed system for dynamic cell culture will provide a better environment for the growth of hepatic cells, manifested in the overproduction of albumin, the main protein liver product.

3. Materials

3.1 Bacterial strains

The table below (Table 1) lists the bacterial strains used during the experiments.

Table 1. List of bacterial strains used in this study.

Bacterial strain	Application	Origin/Company
E.coli STBL2	transformation; preservation of amplified plasmid DNA sequence	Institute of Biochemistry and Biophysics, Polish Academy of Sciences

3.2 Bacterial media

In the course of the experiments, liquid or solid Luria-Bertani (LB) broth was used for bacterial culture. To prepare liquid LB, 1 g of casein tryptone (Diag-Med, Warsaw, Poland), 0.5 g of yeast extract (Diag-Med, Warsaw, Poland) and 1 g of NaCl were weighed, and then the pH was adjusted to 7.5 with NaOH and filled up to 100 mL with distilled water. The medium was sterilized for 20 minutes at 121 °C. The following antibiotic was added to the culture medium: ampicillin (TZF, Warsaw, Poland) at a final concentration of 100 μg/mL. For preparing the solid medium, agar (Becton Dickinson, Warsaw, Poland) was added to the liquid LB. The medium was poured into plates, allowed to set, and then the plates were dried at 37 °C for approximately one hour.

3.3 Plasmid DNA

The table below (Table 2) lists the plasmid DNA used during the experiments.

Table 2. List of plasmid DNA used in this study.

Plasmid DNA	Characteristic	Origin/Company
pLTR-G	Plasmid containing the gene encoding viral envelope protein (Vesicular Stomatitis Virus glycoprotein – VSV-G)	Plasmid DNA constructed and provided by Jakob Reiser, PhD (FDA, Bethesda, USA)
pCD/NL-BH*ΔΔΔ	Second-generation helper/packaging plasmid	
pNL-DsRED2/CMV-WPREΔU3	Transfer plasmid containing gene coding for fluorescent protein DsRed2	
pReceiver_Lv105/ ARG1_P2A_OTC_P2A_DsRed/CMV (in short pl_ARG1_OTC_DsRed)	Transfer plasmid containing genes encoding human arginase 1 (h*ARG1*), human ornithine transcarbamylase (h*OTC*), and the fluorescent protein DsRed.	Genecopoeia, Rockville, Maryland, USA

3.4 Cell lines

The table below (Table 3) lists the cell lines used during the experiments.

Table 3. List of cell lines used in this study.

Cell line	Characteristic	Origin/Company
C3A (CRL-10741)	The cell line derived from human hepatocellular carcinoma (HCC)	American Type Culture Collection, Manassas, Virginia, USA
HEK293T (CRL-3216)	Human embryonic kidney cell line	
HOS (CRL-1543)	Human osteosarcoma cell line	
C3A_ARG1_OTC_III (in short C3A_AO_III)	A cell line derived from HCC (Pluta *et al.*, 2020) after triple transduction with lentiviral vectors carrying human genes coding for urea cycle proteins - arginase 1 (*ARG1*) and ornithine transcarbamylase (*OTC*)	Laboratory of Tissue Engineering, Nalecz Institute of Biocybernetics and Biomedical Engineering, Polish Academy of Sciences
C3A_DsRed2	A cell line derived from HCC (Samluk, Zakrzewska and Pluta, 2013) after transduction with lentiviral vector carrying gene coding for red fluorescent protein DsRed2	
C3A_AO_P2A	A cell line derived from HCC (Jakubowska *et al.*, 2024) after transduction with lentiviral vector carrying human genes coding for urea cycle proteins - arginase 1 (*ARG1*) and ornithine transcarbamylase (*OTC*) and bacterial gene for resistance to puromycin	The new established cell line obtained during this study

3.5 Medium composition for cell culture

The reagents used for cell culture are listed in the table below (Table 4).

Table 4. List of medium components used for cell culture.

Component	Characteristic	Origin/Company
DMEM	Dulbecco's Modified Eagle Medium with 2 mM L-glutamine and high D-glucose content (4.5 g/L)	Sigma Aldrich, Poznan, Poland
FBS	Heat-inactivated fetal bovine serum	Genos, Lodz, Poland
MEM NEAA	Nonessential amino acids solution	Genos, Lodz, Poland
PBS	Balanced salt solution in phosphate buffer without magnesium and calcium ions	Lab Empire, Rzeszow, Poland
Trypsin	0.25% enzyme solution with EDTA	Genos, Lodz, Poland

3.6 Antibodies used for flow cytometry and for protein detection using ELISA and Western blot methods

The antibodies used during the experiments are listed in the table below (Table 5).

Table 5. List of antibodies used in this study.

Antibody	Catalog number	Marker	Dilution	Application	Origin/Company
Goat anti-human albumin	A80-129A	-	1:500	ELISA	Bethyl, Warsaw, Poland
Goat anti-human albumin	A80-129P	HRP	1:5000 1:50 000	Western blot ELISA	Bethyl, Warsaw, Poland
Goat anti-human albumin	A80-129F	FITC	1:150	FACS IF	Bethyl, Warsaw, Poland
Mouse anti-human arginase 1	sc-365547	-	1:50	Western blot	Santa Cruz, Dallas, Texas, USA
Rabbit anti-human OTC	PA5-28197	-	1:500	Western blot	Thermo Fisher Scientific, Waltham, Massachusetts, USA
Rabbit anti-human GAPDH	PA1-988	-	1:5000	Western blot	Thermo Fisher Scientific, Waltham, Massachusetts, USA
Goat anti-human A1AT	A80-122F	FITC	1:750	FACS	Bethyl, Warsaw, Poland
Mouse anti-human CD54	555511	PE	1:1000	FACS	Becton Dickinson, Warsaw, Poland
Goat anti-rabbit IgG	ab97051-1	HRP	1:10 000	Western blot	Symbios, Straszyn, Poland
Goat anti-mouse IgG	31439	HRP	1:2000	Western blot	Thermo Fisher Scientific, Waltham, Massachusetts, USA
goat IgG isotype control	ab37374	FITC	1:100 1:150	FACS IF	Abcam, Cambridge, Great Britain
rabbit IgG isotype control	ab37407	PE	1:100	FACS	Abcam, Cambridge, Great Britain

3.7 Kits used in the experimental procedures

The following table (Table 6) lists the kits used in the course of the experiments.

Table 6. List of kits used in this study.

Name	Application	Origin/Company
Kit for the determination of glucose concentration	Measurement of glucose concentration in culture medium	BioMaxima, Lublin, Poland
Pierce BCA Protein Assay Kit	Determination of protein concentration	Thermo Fisher Scientific, Waltham, Massachusetts, USA
QuantiChrom Urea Assay Kit	Measurement of urea concentration in post-culture medium or cell lysates	BioAssay Systems, Hayward, California, USA
Plasmid Mini Plasmid Midi AX	Plasmid DNA isolation	A&A Biotechnology, Gdansk, Poland

Genomic Mini	Genomic DNA isolation	A&A Biotechnology, Gdansk, Poland
Total RNA Mini Plus	RNA isolation	A&A Biotechnology, Gdansk, Poland
CytoPainter F-Actin Staining Kit	Apical vacuoles visualization	Abcam, Cambridge, Great Britain
Lipofectamine 3000 Transfection Kit	Cell transfection using lipofection method	Thermo Fisher Scientific, Waltham, Massachusetts, USA
Arginase Activity Assay Kit	Measurement of enzymatic activity of arginase	Sigma Aldrich, Poznan, Poland
TURBO DNA-free Kit	DNA removal	Thermo Fisher Scientific, Waltham, Massachusetts, USA
QuantiTect Reverse Transcription Kit	Reverse transcription	QIAGEN, Hilden, Germany

3.8 Primers used for PCR and RT-qPCR

The tables below (Table 7; Table 8) list the primers used in the course of the experiments.

Table 7. List of primers used for PCR.

Primer	Nucleotide sequence of primer	Melting temperature [°C]	Content of GC nucleotides [%]	Origin/Company
ARG1_1 (reverse)	5’ CACCAGGCTGATTCTTCCGT 3’	60	55	Oligo.pl, Warsaw, Poland
OTC_1 (reverse)	5’ TGTAGTGGTTGTCCACACCG 3’	59.9	55	
CMV_2 (forward)	5’ AAGTACGCCCCCTATTGACG 3’	59.5	55	

Table 8. List of primers used for RT-qPCR.

Genes	Nucleotide sequence of primers	Efficiency	Annealing temperature [°C]	Origin/ company
ALB	F: 5' GCTGACTTGCCTTCATTAGC 3' R: 5' AGCAGCACGACAGAGTAATC 3'	0.995	60	Institute of Biochemistry and Biophysics, Polish Academy of Sciences
ARG1	F: 5' TGGCTGGCAAGGTGGCAGAA 3' R: 5' CTGGCATGGCCAGAGATGCT 3'	0.965	60	
OTC	F: 5' ATCCTGGCTGATTACCTCAC 3' R: 5' ACTAGCATCCGGCTCATAAC 3'	1	60	
HNF1A	F: 5' ACAGCCTGCTGAGTACAGAA 3' R: 5' AGGAAGTGAGGCCATGATGA 3'	0.920	54	
HNF4A	F: 5' GGAAGCCGTCCAGAATGAGC 3' R: 5' CCGAATGTCGCCGTTGATCC 3'	0.980	60	
HSPA1A	F: 5' CTGGAGTCCTACGCCTTCAA 3' R: 5' CAGCCACGAGATGACCTCTT 3'	0.990	60	
NFKB1	F: 5' TAATGCCTTCCGGCTGAGTC 3' R: 5' GGCTGCCTGGATCACTTCAA 3'	0.980	60	
GAPDH	F: 5' TGGCACCGTCAAGGCTGAGA 3' R: 5' GGTGGCAGTGATGGCATGGA 3'	0.980	57	
RPL13A	F 5' CGTGCGTCTGAAGCCTACAA 3' R 5' CACGTTCTTCTCGGCCTGTT 3'	0.955	58	

3.9 Nucleic acid and protein size standards

The table below (Table 9) shows the protein and nucleic acid size standards used in the experiments.

Table 9. List of protein and nucleic acid size standards used in this study.

Name	Application	Range	Origin/Company
Perfect Plus 1 kb DNA Ladder	Electrophoretic separation of DNA	250 – 10000 bp	Eurx, Gdansk, Poland
DNA Marker Lambda/Ava II	Electrophoretic separation of DNA	151 – 8126 bp	A&A Biotechnology, Gdansk, Poland
PageRuler or PageRulerPlus Prestained Protein Ladder	Electrophoretic separation of protein	10 – 180 kDa 10 – 250 kDa	Thermo Fisher Scientific, Waltham, Massachusetts, USA

3.10 Enzymes used for PCR, RT-qPCR, and enzymatic digestion

The following enzymes were used during the experiments:

- Taq RUN DNA Polymerase (200 U) with buffer (A&A Biotechnology, Gdansk, Poland),
- Restriction enzymes: BamH1 (20 U/µL) with Anza 10x buffer (Thermo Fisher Scientific, Waltham, Massachusetts, USA),
- LightCycler®480 FastStart SYBR Green I Master Mix, which contains FastStart Taq DNA Polymerase (Roche, Basel, Switzerland).

All used enzymes were stored at -20 °C.

3.11 Buffers and solutions

Reagents for protein detection using ELISA test:

Human albumin standard: a standard for albumin protein with a concentration of 22 mg/mL (Bethyl, Warsaw, Poland) was diluted to a concentration of 400 ng/mL, aliquoted and stored at -20 °C.

Coating Buffer: the ready-to-use powder (Sigma Aldrich, Poznan, Poland) was dissolved in 100 mL of deionized water and stored at 4 °C.

Postcoat Solution (blocking solution): the ready-to-use powder (Sigma Aldrich, Poznan, Poland) was dissolved in 1 L of deionized water and stored at 4 °C.

Conjugent Diluent: 0.5 mL of 10% Tween-20 was added to 100 mL of Postcoat Solution. Prepared reagent was stored at 4 °C.

Wash Solution: 6.06 g of Tris Base and 8.2 g of NaCl were weighed, then 6 mL of 6 M HCl was added, and filled up to 1 L with deionized water. The reagent was stored at 4 °C.

TMB: substrate for horseradish peroxidase (HRP); ready-to-use product (Biomibo, Warsaw, Poland), which was stored at 4 °C.

Buffer for protein isolation:

RIPA buffer (Thermo Fisher Scientific, Waltham, Massachusetts, USA) was stored at 4 °C. Just before cell lysis, the buffer was supplemented with protease inhibitors at a ratio of 1:100 (Halt Protease Inhibitor Cocktail 100x; Thermo Fisher Scientific, Waltham, Massachusetts, USA), phosphatase inhibitors at a ratio of 1:100 (Halt Phosphate Inhibitor Cocktail 100x; Thermo Fisher Scientific, Waltham, Massachusetts, USA) and EDTA at a ratio of 1:100 (EDTA 100x; Thermo Fisher Scientific, Waltham, Massachusetts, USA).

Cell lysis buffer:

Triton X-100 was added to 1 M Tris-HCl buffer, pH 7.4, so that its final concentration was 0.4%. The solution was stored at 4 °C. Before cell lysis, the buffer was supplemented with the following protease inhibitors: pepstatin A (Sigma Aldrich, Poznan, Poland) and leupeptin (Sigma Aldrich, Poznan, Poland). The final concentrations of the compounds in the buffer were 1 μM.

Reagents used for nucleic acid electrophoresis:

TAE electrophoresis buffer 50x: 242 g of Tris Base was weighed, then 57.1 mL of glacial acetic acid and 18.6 mL of 0.5 M EDTA were added, and the volume was adjusted to 1 L with distilled water. The stock solution was stored at 4 °C.

1-1.5% agarose gel: an appropriate amount of agarose (Thermo Fisher Scientific, Waltham, Massachusetts, USA) was dissolved in 50 mL of TAE buffer (1x) using a water bath. To visualize the bands, 2 μL of a solution of 0.5 μg/mL ethidium bromide (Thermo Fisher Scientific, Waltham, Massachusetts, USA) was added to the solution. The gel was poured into a tray and allowed to polymerize.

6x Blue Gel Loading Dye (Blirt, Gdansk, Poland): samples were mixed with loading buffer at a ratio of 1:6 before loading on the gel.

3.12 Reagents used for protein electrophoresis and Western blot analysis

The reagents used for the preparation of polyacrylamide gels for SDS-PAGE are listed in the tables below (Table 10; Table 11).

Table 10. Reagents used for the preparation of 10% and 12% separating gels.

Component	Volume – 10% [mL]	Volume – 12% [mL]
30% solution of acrylamide/bis-acrylamide 37.5:1	3.33	4
1.88 M Tris-HCl pH 8.8	2.4	2.4
10% SDS	0.1	0.1
10% APS	0.1	0.1
TEMED	0.02	0.02
Distilled water	4.05	3.38

Table 11. Reagents used for the preparation of the 4% resolving gel.

Component	Volume [mL]
30% solution of acrylamide/bis-acrylamide 37.5:1	0.6
0.8 M Tris-HCl pH 6.8	0.96
10% SDS	0.04
10% APS	0.04
TEMED	0.006
Distilled water	2.35

Electrophoresis buffer 10x: 30.28 g of Tris Base and 144.14 g of glycine were weighed, and then 100 mL of 10% SDS solution was added. The pH of the buffer was adjusted to 8.3 with 6 M HCl, and the buffer was then refilled with distilled water to 1 L. The stock was diluted 10 times just before use and stored at room temperature (RT).

Transfer buffer 10x: 30.28 g of Tris Base and 144.14 g of glycine were weighed, then the pH of the buffer was adjusted to 8.3 with 6 M HCl, and finally the buffer was filled up to 1 L with distilled water. The stock solution was stored at 4 °C. Just before use, the stock was diluted 10 times, and methanol was added to a final concentration of 20%.

TBST buffer 10x: 24.23 g of Tris Base and 87.66 g of NaCl were weighed, and then 10 mL of Tween-20 was added. The pH of the buffer was adjusted to 7.4 with 6 M HCl, and the buffer was then refilled with distilled water to 1 L. The stock was diluted 10 times just before use and stored at RT.

Stripping buffer: 1.5 g of glycine and 0.1 g of SDS were weighed and 1 mL of Tween-20 was added. The buffer pH was adjusted to 2.2 with 6 M HCl and then filled up to 100 mL with distilled water. Stored at RT.

Sample buffer 5x: 5 g of SDS was weighed, and then 25 mL of glycerol, 6.25 mL of 2 M Tris-HCl pH 6.8 and 1 mL of bromophenol blue (Sigma Aldrich, Poznan, Poland) were added. The obtained solution was refilled with distilled water to 50 mL. The stock solution was stored at -20 °C. Before use, the stock was diluted 3.33 times to obtain 1.5x sample buffer.

Blocking solution: 5 g of nonfat milk (SM, Gostyn, Poland) was dissolved in 100 mL of TBST 1x buffer and stored at 4 °C.

ECL – enhanced chemiluminescence substrate for HRP (Bio-Rad, Hercules, California, USA): the A and B components were mixed at a ratio of 1:1 just before use and applied to the membrane.

3.13 Reagents used for determination of the retention of the polysulfone membrane

The table below (Table 12) lists the reagents used for determining the retention of the polysulfone capillary membranes.

Table 12. List of reagents used for retention measurements.

Name	Size	Origin/Company
Bovine serum albumin (BSA)	67 kDa (7.1 nm)	Fluka, Charlotte, North Carolina, USA
Red fluorescent polystyrene microspheres	100 nm	EPRUI Biotech, Suzhou, China
Red fluorescent polystyrene microspheres	200 nm	EPRUI Biotech, Suzhou, China
Red fluorescent polystyrene microspheres	500 nm	EPRUI Biotech, Suzhou, China
Cytometer Setup and Tracking Beads	2-3 μm	Becton Dickinson, Warsaw, Poland

3.14 Other reagents used in the course of the experiments

The table below (Table 13) lists the other reagents used in the course of the experiments.

Table 13. List of other reagents used during the experiments.

Name	Origin/Company
38% solution of formaldehyde	Sigma Aldrich, Poznan, Poland
Trypan blue	Sigma Aldrich, Poznan, Poland

DAPI	Sigma Aldrich, Poznan, Poland
DMSO	ATCC, Manassas, Virginia, USA
MTT	Sigma Aldrich, Poznan, Poland
SDS	Sigma Aldrich, Poznan, Poland
Glycine	POCH, Gliwice, Poland
APS	Sigma Aldrich, Poznan, Poland
TEMED	PanReacAplliChem ITW Reagents, Darmstadt, Germany
30% solution of acrylamide/bis-acrylamide 37.5:1	Sigma Aldrich, Poznan, Poland
β-mercaptoethanol	Sigma Aldrich, Poznan, Poland
dNTP Mix (10 mM each)	Thermo Fisher Scientific, Waltham, Massachusetts, USA
TCA	Sigma Aldrich, Poznan, Poland
Acetone	WARCHEM, Warsaw, Poland
L-ornithine hydrochloride	Thermo Fisher Scientific, Waltham, Massachusetts, USA
Carbamoyl phosphate dilithium salt	Sigma Aldrich, Poznan, Poland
2,3-butanedione monoxime	Sigma Aldrich, Poznan, Poland
Phosphoric acid (H_3PO_4)	POCH, Gliwice, Poland
OptiMEM	Thermo Fisher Scientific, Waltham, Massachusetts, USA
Glycerol	Sigma Aldrich, Poznan, Poland
Isopropanol	POCH, Gliwice, Poland
Sulfuric acid (H_2SO_4)	POCH, Gliwice, Poland
EDTA	POCH, Gliwice, Poland
Hydrochloric acid (HCl)	POCH, Gliwice, Poland
Ammonium chloride (NH_4Cl)	POCH, Gliwice, Poland
Propidium Iodide	Sigma Aldrich, Poznan, Poland
Tween-20	Sigma Aldrich, Poznan, Poland
Triton X-100	Sigma Aldrich, Poznan, Poland
Tris Base	Lab Empire, Rzeszow, Poland
Sodium chloride (NaCl)	Sigma Aldrich, Poznan, Poland
BSA	Sigma Aldrich, Poznan, Poland
RNA*later* Stabilization Solution	Thermo Fisher Scientific, Waltham, Massachusetts, USA
Puromycin	Thermo Fisher Scientific, Waltham, Massachusetts, USA
Polyurethane resin FC 52/HPE 85; polyol; component A	JASSKOR, Warsaw, Poland
Polyurethane resin FC 52/HPE 40-85A-ISO; isocyanine; component B	JASSKOR, Warsaw, Poland
Silicone grease ROTISILON C	Carl Roth, Karlsruhe, Germany
Sodium hydroxide (NaOH)	POCH, Gliwice, Poland
Glacial acetic acid	POCH, Gliwice, Poland
70% solution of ethanol	Linegal Chemicals, Warsaw, Poland
95% solution of ethanol	POCH, Gliwice, Poland

3.15 Laboratory equipment

The table below (Table 14) summarizes the laboratory equipment used in the course of the research.

Table 14. List of laboratory equipment.

Name	Origin/Company
Flow cytometer BD FACSCanto II	Becton Dickinson, Warsaw, Poland
Spectrophotometer with plate reader Synergy HT Bio-Tek	BIOKOM, Janki, Poland
Incubator CO_2 for cell culture NuAire	NuAire, Plymouth, Massachusetts, USA
Biological safety cabinet class II NuAire LABGARD	NuAire, Plymouth, Massachusetts, USA
Fluorescence inverted microscope IX-71	Olympus, Warsaw, Poland
Inverted phase contrast microscope CKX41	Olympus, Warsaw, Poland
Centrifuge MPW-352R	MPW, Warsaw, Poland
Centrifuge 5415 R	Eppendorf, Warsaw, Poland
Mini centrifuge D1008	DLAB Scientific, Rowland St., California, USA
Autoclave Classic Prestige Medical	Bionovo, Legnica, Poland
Liquid nitrogen dewar Lab Systems LS3000	Worthington Industries, Columbus, Ohio, USA
Spectrophotometer UV-Vis NanoDrop One	Thermo Fisher Scientific, Waltham, Massachusetts, USA
Spectrophotometer UV-Vis Spectronic Genesys 2	Thermo Fisher Scientific, Waltham, Massachusetts, USA
Scanning electron microscope TM-1000	Hitachi High-Technologies, Tokyo, Japan
Sputter coater Emitech K550X	Quorum Technologies, Ashford, Great Britain
Goniometer DSA25	Krüss Optronic, Hamburg, Germany
Spectrophotometer UV-Vis U-3010	Hitachi High-Technologies, Tokyo, Japan
Water Bath SWB	Stuart, Stone, Great Britain
Thermomixer HCM100-Pro	DLAB Scientific, Rowland St., California, USA
Chemiluminescent system for digital documentation of gels Alliance Q4 Advanced	UVITEC, Cambridge, Great Britain
Set for vertical electrophoresis and transfer Mini PROTEAN 3 Cell	Bio-Rad, Hercules, California, USA
Set for horizontal electrophoresis Mini-Sub Cell GT	Bio-Rad, Hercules, California, USA
Shaker IKA Vortex 2	IKA, Warsaw, Poland
Magnetic stirrer with heating IKA RTC basic	IKA, Warsaw, Poland
Incubator Shaker Innova 44	Eppendorf, Warsaw, Poland
Peristaltic pump Reglo-Digital ISM597A	Ismatec, Glattburg, Switzerland
Peristaltic pump L/S easy-load II 77202-60	Masterflex, Plock, Poland

Multifunctional instrument CX-705	Elmetron, Zabrze, Poland
Laboratory cradle KL-945	JW Electronic, Warsaw, Poland
Laboratory scales WTB2000	Radwag, Warsaw, Poland
Thermocycler iCycler T100	Bio-Rad, Hercules, California, USA
LightCycler®96 System	Roche, Basel, Switzerland
Transilluminator 3UV	UVP, Cambridge, Great Britain
Automatic pipettes	Eppendorf, Warsaw, Poland
Automatic pipettor	Eppendorf, Warsaw, Poland
Multichannel pipettes	Medlab, Raszyn, Polska
Incubator KBC-65G	WAMED, Warsaw, Poland
Heater	Termiko, Cieszyn, Poland
Vacuum dryer SPT-200 BCM	Conbest, Krakow, Poland
Centrifuge (for pouring resin on modules)	Laboratory of Semi-Permeable Membranes and Bioreactors, Institute of Biocybernetics and Biomedical Engineering, Polish Academy of Sciences

3.16 Other materials

The table below (Table 15) summarizes the other materials used during the research.

Table 15. List of other materials used in the course of the experiments.

Name	Origin/Company
Polysulfone capillary membranes (pore size 0.2 μm)	Vestergaard Frandsen, Lozanna, Switzerland
PVDF membrane filters (pore size 0.22 μm)	Merck, Darmstadt, Germany
PVDF membrane (pore size 0.2 μm)	Thermo Fisher Scientific, Waltham, Massachusetts, USA
PVDF membrane mini filters (pore size 0.22 μm) Millex-GV	Merck, Darmstadt, Germany
Flasks for cell culture (surface 25 cm^2 and 75 cm^2)	Googlab Scientific, Rokocin, Poland
Serological pipettes (volume 5 mL, 10 mL, 25 mL, and 50 mL)	Googlab Scientific, Rokocin, Poland
Injection syringes (volume 1 mL, 2 mL, and 5 mL)	Becton Dickinson, Warsaw, Poland
6, 12, 24, and 96-well plates	Nest Scientific Biotechnology, Wuxi, Jiangsu, China
96-well maxi binding plates (for ELISA test)	Nest Scientific Biotechnology, Wuxi, Jiangsu, China
Centrifuge tubes (volume 15 mL and 50 mL)	Googlab Scientific, Rokocin, Poland
Microcentrifuge tubes (volume 1.5 mL and 2 mL)	Bionovo, Legnica, Poland
Cryovials (volume 2 mL)	Biologix Plastics, Changzhou, Jiangsu, China
Round-bottom tubes (for cytometric analysis)	Sarstedt, Nümbrecht, Germany
Pipette tips (volume 10 μL, 200 μL, and 1 mL)	Profilab, Warsaw, Poland

Pipette filter tips (volume 10 µL, 200 µL, and 1 mL)	Googlab Scientific, Rokocin, Poland
Glass bottles	Bionovo, Legnica, Poland
Glass beakers	Bionovo, Legnica, Poland
Bürker counting chamber	Equimed, Warsaw, Poland
Mr. Frosty Freezing Container	Bionovo, Legnica, Poland
Cell culture dishes (size 60 mm)	Nest Scientific Biotechnology, Wuxi, Jiangsu, China
Scalpels Cutfix	Linegal Chemicals, Warsaw, Poland
Cell scrapers	Biologix Plastics, Changzhou, Jiangsu, China
Pump tubing (interior diameter 1.85 mm)	Ismatec, Glattburg, Switzerland
Hemodialysis tubing A/V Set for Dialog	B.Braun Aeskulap Chifa, Nowy Tomysl, Poland

3.17 Computer programs

The following computer programs were used for the research:

ImageJ (microscopy image analysis),

Facs Diva (flow cytometry analysis),

CellSens (microscopy image analysis),

Gen5 (software for analysis of data obtained from a microplate reader BioTek),

Primer-BLAST (tool for designing primers for PCR),

COMSOL Multiphysics 5.5 (software for conducting mathematical simulations),

Alliance Q4 Advanced (software for chemiluminescence imaging),

Statistica 10 (software for statistical analysis),

Origin (software for analysis and visualization of obtained data),

REST 2009 (software for analysis of relative gene expression changes),

BioRender (tool for creating scientific images).

4. Methods

4.1 Basic activities related to cell culture

4.1.1 Preparation of the culture medium

Powdered DMEM High Glucose was dissolved in 500 mL of deionized water. Then, 3.7 g of sodium bicarbonate was added, and the mixture was filled up to 1 L with deionized water. The obtained medium was filtered with a 0.22 μm filter and stored at 4 °C. The cell culture medium was supplemented with fetal bovine serum (10% by volume) and nonessential amino acids solution (1% by volume). The obtained medium was filtered with a 0.22 μm filter and stored at 4 °C.

4.1.2 Cell thawing

The cryovial with frozen cells was removed from the liquid nitrogen reservoir and thawed in the warm water. Then, 1 mL of fresh medium was added to the partially thawed cells. The cell suspension was transferred immediately to a sterile centrifuge tube and centrifuged (5 min, 163 RCF, 15 °C). Next, the supernatant was removed, and the obtained pellet was resuspended in 1 mL of fresh medium. Then, whole cell suspension was seeded in culture bottle and transferred to an incubator (37 °C; atmosphere containing 5% CO_2).

4.1.3 Cell passage

The medium was removed from the flask and the cells were washed with PBS. After that, the buffer was removed, and an appropriate volume of 0.25% trypsin solution was added (1 mL for a T25 flask, 3 mL for a T75 flask). Then the mixture was incubated at 37 °C for 5 minutes. Trypsinization was stopped by adding the same amount of culture medium. Then, the cell suspension was transferred to a centrifuge tube and centrifuged (5 min, 163 RCF, 15 °C). The obtained supernatant was removed, and the remaining pellet was thoroughly resuspended in 1 mL of fresh medium. The cells were then seeded onto new culture bottles at the appropriate density and cultured in an incubator (37 °C; atmosphere containing 5% CO_2).

4.1.4 Counting cells using the Bürker chamber

The first steps of this procedure were the same as those in the case of cell passage. Then, after the pellet suspension, the final volume was checked. If the volume was not 1 mL, fresh medium was added, or the excess medium was removed. If necessary, the cell suspension was

diluted in PBS. Then, 10 µL of the cell suspension was mixed with 10 µL of 0.2% trypan blue solution, which penetrates into the nuclei of dead cells and intercalates DNA. Half of the obtained mixture was transferred to a Bürker chamber, and viable cells were then counted from at least five large squares. The final number of cells was calculated using the following formula:

$$n_f = n_a \cdot d \cdot 10^4$$

where:

n_f – final number of cells

n_a – average number of cells obtained from counted squares

d – dilution

4.1.5 Freezing cells

The first steps of this procedure were the same as those in the case of cell passage. Then, after the pellet was resuspended, an appropriate volume of the cell suspension was transferred to a cryovial, and fresh medium (if necessary) and DMSO (10% by volume) were added. The freezing container with the cryovial was left at -80 °C. The next day, the cryovial was transferred to a dewar with liquid nitrogen.

4.1.6 Bacterial cultures in a solid medium

E.coli bacteria were plated as single colonies on solid LB medium (with or without antibiotics) and incubated overnight at 37 °C. Bacterial cultures on solid medium were stored at 4 °C for approximately 2 weeks. After that time, the cultures were passaged.

4.1.7 Bacterial cultures in a liquid medium

E.coli bacteria were inoculated from a single colony. Bacterial cultures in liquid LB medium (with or without antibiotics) were carried out for 18-20 hours in a shaker incubator at 37 °C. For small scale culture, the bacterial cultures were performed in 3-5 mL of LB, and for medium scale culture in 30-100 mL of LB.

4.1.8 Storage of bacterial cells

For long-term storage of bacterial cells, the cultures in liquid medium were mixed with sterile glycerol at a 1:1 ratio and stored at -80 °C.

4.2 Isolation of genomic DNA using SDS cell lysis

The first step of cell lysis was the addition of 2 mL of 5% SDS for 3 minutes at RT. Then, an equivalent amount of cold 95% ethanol was added to the samples, which were gently mixed and centrifuged (15 min, 4081 RCF, 15 °C). After that, the supernatant was removed, and the obtained pellet was rinsed with 1 mL of cold 70% ethanol and again centrifuged (5 min, 163 RCF, 15 °C). The resulting DNA pellet was dried for 10 minutes at RT and then resuspended in 3 mL of water. The concentration of the isolated DNA was determined using a NanoDrop spectrophotometer from Thermo Fisher Scientific by measuring the absorbance of the samples at wavelengths of 230, 260, and 280 nm.

4.3 Determination of glucose concentration in the culture medium

The glucose concentration in the culture medium was measured using a commercial kit from BioMaxima according to the manufacturer's recommendations. Briefly, 2 µl of the analyzed samples and standard were added to 200 µl of the colored reagent and incubated for 10 minutes at RT. A colored reagent was used as a blank, and DMEM with a known glucose concentration (4.5 g/L) was used as a control. The absorbance was read at 505 nm using a Synergy HT spectrophotometer.

4.4 Determination of albumin secretion using the immunoenzymatic method - ELISA

The amount of albumin secreted by the cells was determined using the sandwich variant of ELISA. First, the anti-human albumin antibody was diluted in Coating Buffer at a ratio of 1:500. After that, the special maxi binding 96-well plate was covered with 100 µL of diluted antibody per well. The plate was then incubated for one hour at RT in the dark. At the end of this time, the solution was removed from the wells. Then, the plate was dried and washed twice with 200 µL of Wash Solution per well. To avoid nonspecific binding, the plate was incubated with 200 µL of Postcoat solution (blocking solution) per well for 30 minutes at RT in the dark. Then, the washing procedure was repeated. After that, the medium samples and the human albumin standard appropriately diluted in PBS were applied to the plate. The incubation lasted one hour at RT in the dark. After this time, the procedure for washing the wells was repeated. Then, the anti-human albumin antibody conjugated with HRP was diluted at a ratio of 1:50 000 in Conjugent Diluent, added to the plate (100 µL per well) and incubated again under the same conditions. The next step was to wash the wells and add a colored substrate for HRP (TMB). The plate was incubated at 37 °C with shaking for 15 minutes. The reaction was stopped by

adding 0.2 M sulfuric acid. The absorbance at a wavelength of 450 nm was measured using a Synergy HT spectrophotometer. The albumin concentration in the tested samples was determined on the basis of a standard curve made with the use of serial dilutions of human albumin.

4.5 Preparation and labeling of cells for analysis using fluorescence microscopy

To prepare cells for fluorescence microscopy analysis, the medium was removed from the wells, and the cells were washed with PBS. Then, the cells were fixed by incubation with 4% formaldehyde solution for 15 minutes at RT in the dark. After this time, the formaldehyde was removed, and the wells were washed three times with PBS. The fixed cells were permeabilized by incubation with 0.1% Triton X-100 solution for 10 minutes at RT in the dark. After Triton X-100 was removed, the wells were washed three times with PBS. To block nonspecific binding, the cells were incubated with 1% BSA solution for 30 minutes at RT in the dark. Then, appropriately diluted primary antibodies were added to the wells and incubated. for one hour at RT in the dark. The antibodies were then removed, and the wells were washed three times with PBS. If needed, the secondary antibodies were added to the wells and incubated for 30 minutes at RT in the dark. After the antibodies were removed, the wells were washed three times with PBS. To stain the cell nuclei, the cells were incubated with a DAPI solution at a final concentration of 10 μg/mL. Staining was performed for 5 minutes at RT in the dark. After the DAPI was removed, the wells were washed three times with PBS and observed under an Olympus IX-71 fluorescence microscope. For the analysis, appropriate UV filters were used: UMN-B for green fluorescence, UMN-G for red fluorescence and UMN-B for DAPI.

4.6 Preparation and labeling of cells for flow cytometry analysis

First, the cells were detached using trypsin and counted in a Bürker chamber with a 0.2% trypan blue solution. The cells were then fixed with a 4% formaldehyde solution by adding 100 μL of formaldehyde per $1 \cdot 10^6$ cells. The samples were incubated for 10 minutes at RT in the dark. After this time, the cells were centrifuged (6 min, 700 RCF, 4 °C). Then, the supernatant was removed, and the pellet was gently resuspended in 1 mL of PBS and centrifuged again (6 min, 700 RCF, 4 °C). The next step was permeabilization of the cell membranes. Briefly, the supernatant was removed, and 100 μL of 0.1% Triton X-100 solution was added per $1 \cdot 10^6$ cells. The samples were incubated for 10 minutes at RT in the dark and then centrifuged (6 min, 700 RCF, 4 °C). After that, the supernatant was removed, and 1 mL of PBS was added and again centrifuged (6 min, 700 RCF, 4 °C). Then, the pellet was gently

resuspended in 100 µL of PBS with 2% FBS per $1 \cdot 10^6$ cells, and appropriately diluted primary antibodies were added and incubated for one hour at RT in the dark. The samples were then centrifuged (6 min, 700 RCF, 4 °C). After the supernatant was removed, the cells were again resuspended in 100 µL of PBS supplemented with 2% FBS, and appropriately diluted secondary antibodies were added. The samples were incubated for 30 minutes at RT in the dark. If the primary antibody was conjugated to a fluorophore, this step was omitted. After 30 minutes, the samples were centrifuged (6 min, 700 RCF, 4 °C). Then, the supernatant was removed, and the cells were resuspended in 100 µL of PBS and transferred to round bottom FACS tubes. The prepared samples were analyzed using a BD FACSCanto II flow cytometer.

4.7 Genetic modification of the C3A cell line using lentiviral vectors – establishment of the new genetically modified cell line - C3A_AO_P2A

4.7.1 Transformation of chemocompetent bacteria using the heat shock method

0.5 µL of the pl_ARG1_OTC_DsRed plasmid was added to 50 µL of *E.coli* STBL2 chemically competent bacteria. The mixture was incubated for 20 minutes on ice and then transferred to a water bath (42 °C) for 30 seconds. After this time, the samples were incubated for 2 minutes on ice. Then, 1 mL of liquid LB (prewarmed to 37 °C) was added. Subsequently, the samples were shaken for 40 minutes at 37 °C. Then, the chemocompetent bacteria were seeded on LB plates with ampicillin. Bacteria without plasmid were also seeded as a control. The plates were incubated overnight at 37 °C.

4.7.2 Isolation of plasmid DNA

After transformation, one colony from the obtained bacteria was inoculated into 5 mL of liquid LB containing ampicillin at a concentration of 100 µg/mL. The bacteria were cultured in a shaker incubator (18 h, 37 °C). The next day, the optical density of the culture was measured at a wavelength of 600 nm using a Spectronic Genesys 2 spectrophotometer from Thermo Fisher Scientific. If the analyzed value was between 0.8 and 1.2, plasmid DNA was isolated using a Plasmid Mini kit from A&A Biotechnology in accordance with the manufacturer's recommendations. If needed, medium scale bacterial culture was performed. Briefly, 20 µL of small scale culture was inoculated into 50 mL of liquid LB with ampicillin and transferred to a shaker incubator (18 h, 37 °C). Then, plasmid DNA isolation was conducted using a Plasmid Midi AX kit from A&A Biotechnology according to the manufacturer's protocol. The concentration and purity of the isolated plasmid DNA were determined using a NanoDrop

spectrophotometer from Thermo Fisher Scientific. The absorbance of the samples was measured at wavelengths of 230, 260, and 280 nm. Pure DNA should have an A_{260}/A_{280} ratio in the range of 1.6-1.8 and an A_{260}/A_{230} ratio between 1.8-2.2. The isolated plasmid DNA was further used for the production of lentiviral vectors.

4.7.3 Digestion with restriction enzymes

To confirm the size and purity of the obtained plasmid DNA, digestion with restriction enzymes was conducted. The chosen restriction enzyme was BamH1, which cleaves the analyzed plasmid DNA at two sites. The expected sizes of the plasmid DNA fragments were 8249 and 2578 bp. For the digestion procedure, the following mixtures were prepared (Table 16).

Table 16. List of components for preparing the mixture for digestion with restriction enzymes.

Component	Amount
Plasmid DNA	0.5 µg
Anza Buffer 10x	2 µL
BamH1	1 µL (20 U)
Milli-Q water	Up to 20 µL

The enzymatic digestion was conducted at 37 °C for 15 minutes. To confirm the results of enzymatic digestion, the plasmid DNA was separated on a 1% agarose gel with the addition of ethidium bromide (0.5 µg/mL). Electrophoresis was carried out in TAE buffer at a voltage of 85 V. Before loading on the gel, the samples were mixed with 6x Blue Gel Loading Dye (loading buffer). As a control, nondigested plasmid DNA was loaded on the gel. The molecular weights of the analyzed plasmid DNA fragments were determined on the basis of a Lambda/Ava II DNA marker from A&A Biotechnology (range: 151 – 8126 bp). The result of DNA separation in the agarose gel was visualized under UV light at a wavelength of 254 nm using a UVP transilluminator.

4.7.4 Production of lentiviral vectors - transfection of HEK293T cells using the lipofection method

Before transfection, HEK293T cells were seeded at a density of $2.5 \cdot 10^5$ cells per well in a 12-well plate in 1 mL of DMEM supplemented with 10% FBS and 1% nonessential amino acids solution. The next day, cells were triple transfected with the following plasmids: the transfer plasmid pl_ARG1_OTC_DsRed, the plasmid encoding the viral envelope protein

pLTR-G, and the helper/packaging plasmid pCD/NL-BH*ΔΔΔ. As a control, the cells were also transfected with the transfer plasmid pNL-DsRED2/CMV-WPREΔU3, which encodes the fluorescent protein DsRed2. Two variants of the total amount of DNA per well (3 μg or 5 μg) were checked. The proportion of plasmid DNA (the transfer plasmid to the helper/packaging plasmid to the envelope plasmid) was also evaluated. The following proportions were used to optimize the transfection procedure: 3:2:1, 4:2:1, and 5:2:1. Transfection was performed using a Lipofectamine 3000 Transfection kit in accordance with the manufacturer's protocol. Briefly, before transfection, two mixtures were prepared. The first mixture contained an appropriate amount of three types of plasmid DNA (3 μg or 5 μg) in the proportions mentioned above enriched to 62.5 μL with OptiMEM medium. The second mixture contained 3 μL of Lipofectamine 3000 and was also enriched to 62.5 μL with OptiMEM medium. Subsequently, the two mixtures were incubated for 15 minutes at RT. Then, the mixture with Lipofectamine 3000 was transferred to the mixture with plasmid DNA, mixed and incubated for 15 minutes at RT. Then, the DNA-LP3000 complexes were added gently (by droplets) to the cell cultures and mixed well. The transfected cells were incubated under standard conditions for 16 hours. After this time, the medium was replaced with fresh medium, and the cells were cultured for another two days. The efficiency of transfection was analyzed on the third day under UV light using an Olympus IX-71 fluorescence microscope. For the analysis, UMN-G for red fluorescence (DsRed/DsRed2 protein) was used.

4.7.5 Collection and storage of lentiviral vectors

Three days after the transfection of HEK293T cells, media containing lentiviral vectors (LV_ARG1_OTC_DsRed or LV_DsRed2) were collected and filtered through 0.22 μm PVDF membranes to sterile probes. The lentiviral vectors were stored at -80 °C.

4.7.6 Transduction of human HCC cells using lentiviral vectors

The day before transduction, C3A cells were seeded at a density of $1 \cdot 10^5$ cells per well in a 12-well plate in 1 mL of DMEM supplemented with 10% FBS and 1% nonessential amino acids solution. The following day, the media from the wells were replaced with 500 μL of fresh media. Then, 500 μL of medium containing lentiviral vectors (LV_ARG1_OTC_DsRed or LV_DsRed2) was added to each well. Transduction of C3A cells was conducted using all versions of lentiviral vector preparations obtained during the transfection procedure (in the case of LV_DsRed2 only 5 μg; 5:2:1 variant). The cells were cultured for 20 hours at 37 °C in an

incubator in an atmosphere of 5% CO_2. After that, the media were replaced with fresh media, and the cells were cultured for another five days.

4.7.7 Antibiotic selection

Seven days after transduction, the transduced cells were selected with puromycin (concentrations ranging from 1 to 5 μg/mL). The aim of this process was to obtain a population of 100% genetically modified C3A cells. For selection, C3A cells transduced with the following lentiviral particles were chosen: LV_DsRed2, LV_ARG1_OTC_DsRed (5:2:1; 5 μg), and LV_ARG1_OTC_DsRed (3:2:1; 3 μg). The selection lasted nine days.

4.7.8 Evaluation of transduction efficiency using fluorescence microscopy

The efficiency of transduction of C3A cells was evaluated on the basis of the expression of gene encoding DsRed fluorescent protein. Fluorescence analysis was performed under UV light using an Olympus IX-71 microscope. For the analysis, UMN-G for red fluorescence (DsRed protein) was used.

4.7.9 Determination of the integration of transgenes into the genome using polymerase chain reaction (PCR)

4.7.9.1 Isolation of genomic DNA

The C3A, C3A_AO_III, C3A_AO_P2A, and HOS cell lines were seeded at a density of $1 \cdot 10^6$ cells per well in a 6-well plate and cultured in DMEM supplemented with 10% FBS and 1% nonessential amino acids for two days. At the end of this time, the cells were detached using trypsin and counted in a Bürker chamber with a 0.2% trypan blue solution. Then, an appropriate volume corresponding to $1 \cdot 10^6$ cells was transferred to a microcentrifuge tube and centrifuged (6 min, 700 RCF, 4 °C). After that, the supernatant was removed, and 1 mL of PBS was added and centrifuged again (6 min, 700 RCF, 4 °C). The isolation of genomic DNA from the abovementioned cell lines was performed using the Genomic Mini kit from A&A Biotechnology. The isolation procedure was conducted in accordance with the manufacturer's instructions. The obtained DNA was suspended in sterile Milli-Q water and stored at -20 °C. The concentration and purity of the isolated DNA were determined using a NanoDrop spectrophotometer from Thermo Fisher Scientific. The absorbance of the samples was measured at wavelengths of 230, 260 and 280 nm. The isolated DNA was further used as a DNA template in the PCR experiments.

4.7.9.2 PCR conditions

To confirm the genetic modification of C3A cells, polymerase chain reaction was conducted using genomic DNA templates. Primers for PCR were designed using the Primer-BLAST tool. The ARG1 and OTC primers (reverse primers) were complementary to the fragments of nucleotide sequences of human genes encoding arginase 1 and ornithine transcarbamylase. The CMV primer (forward primer) was complementary to the fragment of the nucleotide sequence of the CMV promoter. The characteristics of the primers used in the PCR experiments are described in section 3.8.

The table below (Table 17) lists the components and their amounts used for PCR.

Table 17. List of compounds used for PCR.

Compound	Volume [µL]		
	Sample	Positive control	Negative control
Taq RUN DNA Polymerase (1 U/µL)	0.5	0.5	0.5
Buffer 10x for DNA Polymerase with Mg^{2+}	2.5	2.5	2.5
dNTPs mix (10 mM each)	1	1	1
Forward starter (10 µM)	1	1	1
Reverse starter (10 µM)	1	1	1
DNA	20	1	-
Milli-Q sterile water	-	19	20

The final volume of one mixture for PCR was 26 µL. The negative control was a mixture without a DNA template. The positive control was a mixture containing 10 ng of the plasmid pl_ARG1_OTC_DsRed.

The table below (Table 18) shows the conditions for the PCR experiments.

Table 18. Conditions of PCR.

Step	Temperature [°C]	Time	Number of cycles
Initial denaturation	94	4 min	-
Denaturation	94	40 s	35
Annealing	58	40 s	
Extension	72	1 min 30 s	
Final extension	72	3 min	-

4.7.9.3 Horizontal electrophoresis

The electrophoretic separation of DNA (after PCR) was performed on a 1.5% agarose gel with the addition of ethidium bromide at a final concentration of 0.5 µg/mL. Electrophoresis was conducted in TAE buffer at a voltage of 80 V. Before loading on the gel, DNA samples were mixed with 6x Blue Gel Loading Dye (loading buffer). The molecular weights of the

analyzed plasmid DNA fragments were determined on the basis of a Perfect Plus DNA Ladder from Eurx (range: 250 – 10 000 bp). The result of DNA separation in the agarose gel was visualized under UV light at a wavelength of 254 nm using a UVP transilluminator.

4.7.10 Determination of gene expression at the mRNA level using RT-qPCR

4.7.10.1 RNA isolation

The C3A, C3A_AO_III, and C3A_AO_P2A cell lines were seeded at a density of $1 \cdot 10^6$ cells per well in a 6-well plate and grown in DMEM supplemented with 10% FBS and 1% nonessential amino acids. After 24 hours, the medium was removed, and fresh medium containing 40 mM ammonium chloride was added and incubated for another 24 hours. In the control wells, the medium was replaced with standard medium. At the end of this time, the cells were detached using trypsin and counted in a Bürker chamber with a 0.2% trypan blue solution. Then, from each culture variant, an appropriate volume corresponding to $1 \cdot 10^6$ cells was transferred to a microcentrifuge tube. Then, the cell suspensions were centrifuged (6 min, 700 RCF, 4 °C). After that, the supernatant was removed, and 1 mL of PBS was added and centrifuged again (6 min, 700 RCF, 4 °C). After removing the supernatant, the pellet was resuspended in 180 µL of RNA*later* Stabilization Solution and stored at 4 °C. RNA isolation was performed the next day with a Total RNA Mini Plus kit from A&A Biotechnology according to the manufacturer's protocol. The obtained RNA was suspended in water for molecular biology and stored at -20 °C. The concentration and purity of the isolated RNA were determined using a NanoDrop spectrophotometer from Thermo Fisher Scientific. The absorbance of the samples was measured at wavelengths of 230, 260, and 280 nm. Pure RNA should have an A_{260}/A_{280} ratio in the range of 1.6-1.8 and an A_{260}/A_{230} ratio between 1.8-2.2. The isolated RNA was further used as a RNA template in the RT-qPCR experiments.

4.7.10.2 RT-qPCR conditions

RT-qPCR experiments were performed in cooperation with the Institute of Biochemistry and Biophysics PAS. Briefly, RNA templates were purified from DNA for 30 minutes at 37 °C using a TURBO DNA-free Kit from Thermo Scientific. Then, 400 ng of total RNA was used for reverse transcription. This procedure was conducted for 30 minutes at 42 °C using a QuantiTect Reverse Transcription Kit. After that, RT-qPCR was performed using a LightCycler®96 System from Roche. To the appropriate amount of cDNA (obtained after reverse transcription) and primers, LightCycler®480 FastStart SYBR Green I Master Mix was

added. It is ready to use mix containing Taq DNA polymerase, buffer for this enzyme, and double-stranded DNA specific dye (SYBR Green I), enabling the real-time detection of PCR products. The primers used for RT-qPCR are described in section 3.8. *GAPDH* and *RPL13A* were used as reference genes. All steps concerning RT-qPCR experiments were performed in accordance with MIQE guidelines (Bustin *et al.*, 2009). For data analysis, the Pfaffl model (Pfaffl, Horgan and Dempfle, 2002) and relative expression software tool (REST 2009) were used.

4.7.11 Semiquantitative protein determination using the Western blot method

4.7.11.1 Protein isolation

The C3A, C3A_AO_III, C3A_AO_P2A, and HOS cell lines were seeded at a density of $3 \cdot 10^6$ cells per 6 cm dish and grown in DMEM supplemented with 10% FBS and 1% nonessential amino acids. After 24 hours, the medium was removed, and fresh medium supplemented with or without 40 mM ammonium chloride was added and incubated for another 24 hours. After this time, the dishes were placed on ice, the culture medium was removed, and the cells were washed twice with 2 mL of PBS. Then, 500 µL of RIPA buffer containing protease and phosphatase inhibitors and EDTA was added to the dishes and incubated on ice for 5 minutes. After this time, the cells were scraped and transferred to microcentrifuge tubes and incubated in a thermomixer (25 min, 300 RPM, 4 °C). Subsequently, the obtained lysates were centrifuged (20 min, 12000 RCF, 4 °C). The collected supernatant was frozen in liquid nitrogen and then stored at -80 °C. In the case of obtaining protein samples from isolated human hepatocytes, frozen isolates from human liver (Zakrzewska *et al.*, 2017) were thawed. Then, fresh medium was added and the cells were centrifuged (5 min, 163 RCF, 15 °C). Subsequently, the supernatant was removed, and 500 µL of RIPA buffer with EDTA and protease and phosphatase inhibitors was added. Then, the sample was incubated in a thermomixer (25 min, 300 RPM, 4 °C) and centrifuged (20 min, 12 000 RCF, 4 °C). The obtained lysate was stored at -80 °C.

4.7.11.2 Measurement of protein concentration

The total protein concentration in the obtained cell lysates was determined colorimetrically with the bicinchoninic acid (BCA) method. The analysis was performed using the commercial Pierce BCA Protein Assay Kit from Thermo Fisher Scientific according to the manufacturer's recommendations. The absorbance at a wavelength of 562 nm was measured

using a Synergy HT spectrophotometer. The protein concentration in the test samples was calculated on the basis of a standard curve made with serial dilutions of BSA.

4.7.11.3 Sample preparation

An equal volume of 10% trichloroacetic acid (TCA) solution was added to the volume of lysate, which corresponded to the appropriate μg of analyzed proteins. Then, the mixture was incubated for 15 minutes on ice. After that, the samples were centrifuged (10 min, 16 100 RCF, 4 °C). The supernatant was removed, and 500 μL of ice-cold acetone was added. The microcentrifuge tubes were flipped several times (gently). Then, the samples were again centrifuged (4 min, 16 100 RCF, 4 °C). Subsequently, the supernatant was removed, and the pellet was dried. After that, the pellet was suspended in the appropriate volume of sample buffer (1.5x). Then, the samples were incubated in a thermomixer (40 min, 1300 RPM, 55 °C). Finally, the obtained samples were stored at -20 °C for further use.

4.7.11.4 Electrophoresis under denaturing conditions (SDS-PAGE)

Immediately before loading on the gel, the samples were denatured at 95 °C for 5 minutes. Then the samples were vortexed and spun. An appropriate amount of total protein (25 to 75 μg for the analyzed cell lines and 10 μg for liver cell isolate) was loaded on the gel. To determine and compare the molecular weights of the analyzed proteins, 5 μL of the marker (PageRuler Prestained Protein Ladder or PageRuler Plus Prestained Protein Ladder) was applied to the gel. Proteins were separated on a 10% or 12% polyacrylamide gel in Electrophoresis Buffer in the presence of SDS (denaturing conditions). Electrophoresis was initially conducted at a voltage of 80 V. After the samples left the resolving gel, the voltage was increased to 120 V.

4.7.11.5 Transfer

After electrophoresis, electrophoretic wet transfer of the separated proteins (from the gel to the membrane) was performed. First, the PVDF membrane was activated by soaking in methanol for 1 minute and then for 5 minutes in Transfer Buffer. Then, the transfer sandwich was set up. The transfer of separated proteins was conducted for 2 hours at a current of 210 mA.

4.7.11.6 Immunoblotting

To block nonspecific binding sites, the membrane was incubated for 30 minutes with 5% nonfat milk. At the end of this time, primary antibodies were added (at an appropriate ratio),

and incubated overnight at 4 °C. The next day, the membrane was washed for 7 minutes in TBST buffer. The procedure was repeated three times. Then, the secondary antibodies conjugated with HRP were added and incubated for one hour. After this time, the membrane was washed three times for 7 minutes in TBST buffer. The specific signal was detected by exposing the membrane to ECL (substrate for HRP) for 3 minutes. The chemiluminescent signal was read using the UVITEC Alliance Q4 Advanced. The value of the obtained signal was calculated with ImageJ software. The reference protein GAPDH was used to determine the relative amount of the analyzed proteins.

4.7.11.7 Stripping

If proteins with similar molecular weights were analyzed on one membrane, the stripping technique was used, i.e., removing primary and secondary antibodies bound to the target protein band. Briefly, the membrane was incubated for 8 minutes in stripping buffer. The procedure was repeated. After that, the membrane was washed three times for 7 minutes in TBST buffer. Then, the membrane was ready for further preparation as described above (section: 4.7.11.6).

4.8 Comparison of the performance of the C3A cell line and its genetically modified counterparts – the C3A_AO_III and C3A_AO_P2A cell lines

4.8.1 Analysis of cell morphology using flow cytometry and microscopy

The differences in morphology between the C3A, C3A_AO_III, and C3A_AO_P2A cell lines were evaluated using an inverted phase contrast microscope Olympus CKX41. Furthermore, the granularity and size of the cells were analyzed with a BD FACSCanto II flow cytometer (side and forward scatter, respectively).

4.8.2 Determination of cell viability using the trypan blue exclusion method

The C3A, C3A_AO_III, C3A_AO_P2A, and HOS cell lines were seeded at a density of $5 \cdot 10^4$ cells per well in a 12-well plate and grown in DMEM supplemented with 10% FBS and 1% nonessential amino acids. After three days, cell viability was determined. Briefly, cells were detached using trypsin solution and centrifuged (6 min, 700 RCF, 4 °C). Then, the cell pellet was thoroughly suspended in 1 mL of fresh medium. After appropriate dilution, 10 µL of cell suspension was mixed with 10 µL of 0.2% trypan blue solution. Half of the volume was then transferred to a Bürker chamber, and both live and dead cells (stained blue) were counted from

at least five squares. Cell viability was calculated as the ratio of the number of viable cells to the total number of cells and expressed as a percentage. The cell culture lasted for twelve days, and the above-described procedure was repeated on the 6, 9, and 12 day of the culture.

4.8.3 Determination of the mitochondrial/metabolic activity of cells using the MTT assay

The C3A, C3A_AO_III, C3A_AO_P2A, and HOS cell lines were seeded at a density of $5 \cdot 10^4$ cells per well in a 12-well plate and grown in DMEM supplemented with 10% FBS and 1% nonessential amino acids. After three days, the culture medium was removed from the wells, and MTT solution at a final concentration of 0.25 mg/mL was added and incubated at 37 °C for 2 hours. Subsequently, isopropanol was added to each well, and the plates were incubated for 15 minutes at 37 °C. After that time, undissolved crystals of MTT salt were carefully suspended by repeated pipetting. The absorbance was measured at a wavelength of 570 nm using a Synergy HT spectrophotometer. The cell culture lasted for twelve days and the above-described procedure was repeated on the 6, 9, and 12 day of the culture.

4.8.4 Determination of metabolic activity - glucose consumption

The C3A, C3A_AO_III, C3A_AO_P2A, and HOS cell lines were seeded at a density of $5 \cdot 10^4$ cells per well in a 12-well plate and grown in DMEM supplemented with 10% FBS and 1% nonessential amino acids. The cell culture lasted for twelve days. On days 3, 6, 9, and 12 of culture, the culture medium was collected and stored at -20 °C for further analysis. Determination of the glucose concentration in the medium samples was performed as described in section 4.3.

4.8.5 Determination of albumin secretion using ELISA

The C3A, C3A_AO_III, C3A_AO_P2A, and HOS cell lines were seeded at a density of $5 \cdot 10^4$ cells per well in a 12-well plate and grown in DMEM supplemented with 10% FBS and 1% nonessential amino acids. The cell culture lasted for twelve days. On days 3, 6, 9, and 12 of culture, the culture medium was collected and stored at -20 °C for further use. Determination of the albumin concentration in the medium samples was performed as described in section 4.4.

4.8.6 Evaluation of albumin production using microscope imaging

The C3A, C3A_AO_III, and C3A_AO_P2A cell lines were seeded at a density of $2 \cdot 10^5$ cells per well in a 12-well plate and grown in DMEM supplemented with 10% FBS and 1% nonessential amino acids. After three days, the cells were fixed and prepared for

microscopic immunofluorescence analysis as described in section 4.5. For albumin detection, the cells were labeled with an antibody against human albumin conjugated with FITC (1:150). The same ratio of antibody was used for labeling with an isotype control.

4.8.7 Comparison of marker protein expression using flow cytometry

The C3A, C3A_AO_III, and C3A_AO_P2A cell lines were seeded at a density of $3 \cdot 10^6$ cells per T25 flask and grown in DMEM supplemented with 10% FBS and 1% nonessential amino acids. After three days, the cells were fixed and prepared for cytometric analysis as described in section 4.6.

4.8.8 Determination of cell membrane polarization

The C3A, C3A_AO_III, and C3A_AO_P2A cell lines were seeded at a density of $5 \cdot 10^4$ cells per well in a 12-well plate and grown in DMEM supplemented with 10% FBS and 1% nonessential amino acids. The cells were cultured for six days. To determine the degree of cell membrane polarization, the medium was removed from the wells, and the cells were washed with PBS. The cells were then incubated with 4% formaldehyde solution for 15 minutes at RT in the dark. After this time, the formaldehyde was removed, and the wells were washed three times with PBS. The fixed cells were then incubated with 0.1% Triton X-100 solution for 10 minutes at RT in the dark. After Triton X-100 was removed, the wells were washed three times with PBS. To visualize the apical vacuoles, which are made of fibrillar actin, the CytoPainter F-Actin Staining Kit was used in accordance with the manufacturer's instructions. Briefly, incubation with phalloidin was carried out for 15 minutes at RT in the dark. After this time, the wells were washed three times with PBS. Then, to stain the nuclei, the cells were incubated with a DAPI solution at a final concentration of 10 µg/mL. Staining was performed for 5 minutes at RT in the dark. After the DAPI was removed, the wells were washed three times with PBS and observed under an Olympus IX-71 fluorescence microscope. For the analysis, appropriate UV filters were used: UMN-G for red fluorescence and UMN-B for DAPI. The number of cell nuclei and apical vacuoles was counted using ImageJ software. The degree of cell membrane polarization was defined as the ratio of apical vacuoles to cell nuclei.

4.8.9 Determination of enzymatic activity of arginase 1 (ARG1)

The C3A, C3A_AO_III, C3A_AO_P2A, and HOS cell lines were seeded at a density of $1 \cdot 10^6$ cells per well in a 6-well plate and grown in DMEM supplemented with 10% FBS and 1% nonessential amino acids. After three days of culture, the cell lysates were prepared. Briefly,

cells were detached from the wells and counted in a Bürker chamber with a 0.2% trypan blue solution. Subsequently, an appropriate volume corresponding to $1 \cdot 10^6$ cells was transferred to a microcentrifuge tube. Then, the cell suspensions were centrifuged (10 min, 1000 RCF, 4 °C). After that time, the supernatant was removed, and 100 μL of lysis buffer per $1 \cdot 10^6$ cells was added and incubated on ice for 10 minutes. Subsequently, the samples were centrifuged (10 min, 13 000 RCF, 4 °C), and the supernatant was collected and stored at -20 °C. In the case of liver cell isolate, samples were prepared as described in section 4.7.11.1. To determine the enzymatic activity of arginase 1, an Arginase Activity Assay Kit was used in accordance with the manufacturer's instructions. The absorbance was measured at 430 nm using a Synergy HT spectrophotometer.

4.8.10 Determination of enzymatic activity of ornithine transcarbamylase (OTC)

Samples for determination of OTC activity were prepared as described in section 4.7.11.1. An appropriate volume of cell lysates (100 μg for liver cell isolate, 200 μg for cell lines) was added to the mixture containing 10 mM Tris-HCl pH 8.5, 5 mM ornithine and 15 mM carbamoyl phosphate. As final volume of the reaction was 700 μL, the mixture was filled with Milli-Q water. The prepared mixtures were incubated at 37 °C for 30 minutes. To stop the enzymatic reaction, 250 μL of a 7.4 M phosphoric acid and 3 M sulfuric acid mixture (3:1) was added. To determine citrulline production, 50 μL of 3% 2,3-butanedione monoxime was added, and the samples were incubated at 95 °C in the dark for 15 minutes. After that time, the absorbance was measured at 490 nm using a Synergy HT spectrophotometer. The concentration of the produced citrulline was determined from the calibration curve.

4.8.11 Determination of urea production

The C3A, C3A_AO_III, and C3A_AO_P2A cell lines were seeded at a density of $2 \cdot 10^6$ cells per well in a 6-well plate and grown in DMEM supplemented with 10% FBS and 1% nonessential amino acids. After 24 hours, the medium was removed, and fresh medium containing 40 mM ammonium chloride was added and incubated for another 24 hours. After this time, the medium was replaced with DMEM supplemented with 1% FBS and 1% nonessential amino acids, and the cells were cultured for another 24 hours. Then, the medium samples were collected and stored at -20 °C. Subsequently, the cell lysates were prepared. Briefly, cells were detached from the wells and counted in a Bürker chamber with a 0.2% trypan blue solution. Then, from each culture variant, an appropriate volume corresponding to $1 \cdot 10^6$ cells was transferred to a microcentrifuge tube. Then, the cell suspensions were centrifuged

(10 min, 1000 RCF, 4 °C). After that time, the supernatant was removed, and 100 µL of lysis buffer per $1 \cdot 10^6$ cells was added and incubated on ice for 10 minutes. Then, the samples were centrifuged (10 min, 13 000 RCF, 4 °C), and the supernatant was collected and stored at -20 °C. To determine urea production, the concentrations of this substance both in the post-culture medium and in the cell lysates were measured using a QuantiChrom Urea Assay Kit in accordance with the manufacturer's recommendations. Briefly, a 200 µL mixture of reagents A and B (at a ratio of 1:1) was added to 50 µL of each sample and incubated for 50 minutes at RT. The absorbance was measured at 430 nm using a Synergy HT spectrophotometer.

4.8.12 Resistance to ammonia toxicity - determination of the effect of oxidative/nitrosative stress induced by ammonium chloride on cell viability and metabolic activity

4.8.12.1 Determination of metabolic activity using the MTT test

The C3A, C3A_AO_III, C3A_AO_P2A, and HOS cell lines were seeded at a density of $3 \cdot 10^4$ cells per well in a 96-well plate and grown in DMEM supplemented with 10% FBS and 1% nonessential amino acids. The next day, the cells were treated for 24 hours with ammonium chloride at three different concentrations – 20 mM, 40 mM, and 60 mM. After this time, the media from the wells were replaced with fresh media and incubated for another 24 hours. Then, the culture medium was removed from the wells, and MTT solution at a final concentration of 0.25 mg/mL was added and incubated at 37 °C for 2 hours. Subsequently, isopropanol was added to each well, and the plate was incubated for 15 minutes at 37 °C. After that time, undissolved crystals of MTT salt were carefully suspended by repeated pipetting. Then, the absorbance was measured at a wavelength of 570 nm using a Synergy HT spectrophotometer.

4.8.12.2 Determination of cell viability using the trypan blue exclusion method

The C3A, C3A_AO_III, C3A_AO_P2A, and HOS cell lines were seeded at a density of $1.5 \cdot 10^5$ cells per well in a 12-well plate and grown in DMEM supplemented with 10% FBS and 1% nonessential amino acids. After three days, the culture medium was replaced with fresh medium containing 20 mM or 40 mM ammonium chloride. Untreated cells were used as the control group. After 24 hours, the cells were detached using trypsin solution and centrifuged (6 min, 700 RCF, 4 °C). Then, the cell pellet was thoroughly suspended in 1 mL of fresh medium. After appropriate dilution, both live and dead cells were counted from at least five squares using a Bürker chamber. Cell viability was calculated as the ratio of the number of viable cells to the total number of cells and expressed as a percentage.

4.8.12.3 Determination of cell viability using flow cytometry analysis

The C3A, C3A_AO_III, C3A_AO_P2A, and HOS cell lines were seeded at a density of $1.5 \cdot 10^5$ cells per well in a 12-well plate and grown in DMEM supplemented with 10% FBS and 1% nonessential amino acids. After three days, the culture medium was replaced with fresh medium containing 20 mM or 40 mM ammonium chloride. Untreated cells were used as a control. After 24 hours, the cells were detached using trypsin solution and centrifuged (6 min, 700 RCF, 4 °C). Then, the supernatant was removed, and the cell pellet was resuspended in 200 µL of PBS. Next, propidium iodide (PI), which penetrates through the membranes of dead cells, was added to the samples. Its final concentration was 5 µg/mL. The percentage of dead cells was determined using a BD FACSCanto II flow cytometer.

4.8.12.4 Determination of albumin secretion using ELISA

The C3A, C3A_AO_III, C3A_AO_P2A, and HOS cell lines were seeded at a density of $3 \cdot 10^6$ cells per T25 flask and grown in DMEM supplemented with 10% FBS and 1% nonessential amino acids. The next day, the cells were treated with 20 mM or 40 mM ammonium chloride. Untreated cells were used as a control. After 24 hours, the culture media were replaced with fresh media. After three days, the medium samples were collected and stored at -20 °C. Determination of the albumin concentration in the medium samples was performed as described in section 4.4.

4.9 The construction of hollow fiber bioreactors

4.9.1 Characterization of the polysulfone capillary membrane

4.9.1.1 Determination of polysulfone membrane structure using scanning electron microscopy (SEM)

To prepare samples for electron microscopy analysis, the membrane was cut into smaller pieces with a scalpel and then immersed in ethanol for 15 minutes. Then, the capillaries were submerged in liquid nitrogen and cut into smaller pieces. Then, the samples were dried for 20 minutes at 80 °C. Finally, the pieces of membrane were placed on the microscope stage by sticking to graphene tape and coated with gold for 90 seconds using a Sputter Coater Emitech K550X. Then, SEM analysis of the membrane structure was conducted, and the following parameters were determined: the pore size, internal and external diameters, and porosity.

4.9.1.2 Measurement of wettability

The wettability of the polysulfone membrane was evaluated by measuring the contact angle formed between the water drops and the analyzed surface using a DSA25 Krüss goniometer. For this purpose, drops of water were mounted on the surface with a microsyringe, and then the contact angle was measured. The results were obtained from ten different areas of the polysulfone membrane.

4.9.2 Biocompatibility of the polysulfone membrane

4.9.2.1 Determination of the cytotoxic effect of capillary membranes – MTT test

The biocompatibility of the polysulfone membrane was evaluated in C3A cells stably expressing the fluorescent protein DsRed2. Briefly, cells were seeded at a density of $2 \cdot 10^5$ per well in a 12-well plate and grown in medium containing 10 capillaries (each with a length of 1 cm) or with medium after daily incubation with capillaries (conditioned medium). As a control, cells were cultured in standard medium (DMEM supplemented with 10% FBS and 1% nonessential amino acids). After three days, the cytotoxic effect of the membrane was evaluated using the MTT test. The detailed procedure is described in section 4.8.3. The absorbance was measured at a wavelength of 570 nm using a Synergy HT spectrophotometer.

4.9.2.2 Determination of the effect of capillary membranes on cell viability

The biocompatibility of the polysulfone membrane was evaluated in C3A cells stably expressing the fluorescent protein DsRed2. Briefly, cells were seeded at a density of $2 \cdot 10^5$ per well in a 12-well plate and grown in medium containing 10 capillaries (each with a length of 1 cm) or with medium after daily incubation with capillaries (conditioned medium). As a control, cells were cultured in standard medium (DMEM supplemented with 10% FBS and 1% nonessential amino acids). After three days, cell viability was analyzed using the trypan blue exclusion method. The live and dead cells were counted from at least five squares using a Bürker chamber. Cell viability was calculated as the ratio of the number of viable cells to the total number of cells and expressed as a percentage. Moreover, microscopic analysis was performed to evaluate the impact of the analyzed material on cell morphology.

4.9.3 Preparation of hollow fiber bioreactors

First, 20 polysulfone capillaries (with a length of 12 cm) were tied with thread at both ends. Then, they were put into a cylinder-shaped housing made of styrene and acrylonitrile. To

avoid getting the resin inside the capillaries, their ends were welded using a heater. Then, the special mold for pouring the modules with resin was coated with silicone. After that, the module was put into the mold and transferred to the centrifuge. The next step was to prepare the polyurethane resin. The two components were mixed at a ratio of 3:1 (polyol: isocyanate) and transferred to a vacuum dryer for 3 minutes. After that, the reservoirs in the mold were filled with polyurethane resin with a syringe. Then, the module was centrifuged (2 h, 600 RPM, 45 °C). After the end of centrifugation, the module was removed from the mold and placed in a dryer (24 h, 40 °C). The next day, the excess resin was removed with a scalpel, and the caps were placed on. The permeability of the capillaries was checked under a microscope. The tightness of the module was checked using air. The growth area was calculated using the following formula:

$$A = \pi \cdot d \cdot L \cdot n$$

where:

A – surface [mm^2]

d – external diameter of the capillary [mm]

L – length of the module (without part containing resin) [mm]

n – number of capillaries (in this research n=20)

The figure below (Figure 17) shows the process of preparing hollow fiber bioreactors, which were used for the construction of the system for dynamic cell culture.

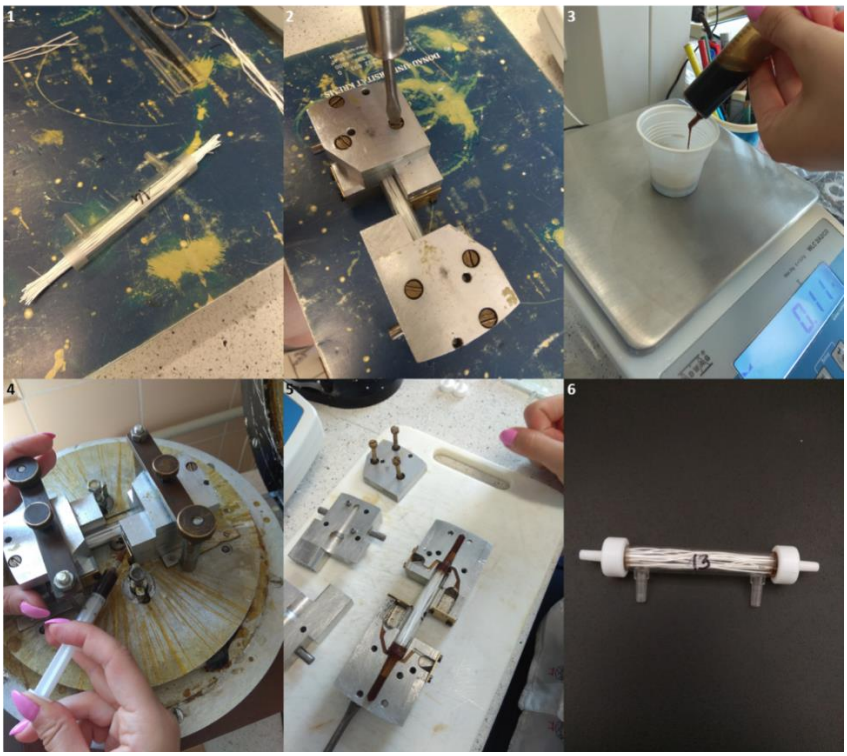

Figure 17. Preparation of hollow fiber bioreactors. The pictures show the following steps of construction of the hollow fiber culture module: 1 – 20 tied polysulfone capillaries after putting into the housing; 2 – preparing for centrifugation – putting the module into the special mold; 3 – resin weighting; 4 – pouring the resin into the special reservoir in the mold; 5 – module after centrifugation; 6 – ready-to-use module.

4.9.4 Ultrafiltration measurement

To measure ultrafiltration of the polysulfone membrane, the volume of water that passed through the capillaries was weighed. The time of the experiment as well as the pressure of the pump were set as follows: 2 minutes and 100 hPa. As the ultrafiltration changes over time, it was again measured after one week. Measurements were made for three different modules. Ultrafiltration was calculated using the following formula:

$$UFC = \frac{V}{A \cdot p \cdot t}$$

where:

UFC – ultrafiltration [$cm^3/(m^2 \cdot hPa \cdot min)$]

V – volume of water that passed through the module [cm^3]

A – surface [m^2]

p – pressure [hPa]

t – time [min]

4.9.5 Retention measurement

4.9.5.1 Retention measurement using bovine serum albumin (BSA)

The retention for BSA was measured spectrophotometrically. First, a solution of BSA at a concentration of 1 g/L was prepared. Then, the obtained solution was filtered. Subsequently, the flow rate at the peristaltic pump was set at 8 mL/min, and then the BSA solution was passed through the analyzed module. After stabilization (10 minutes), the overpressure was adjusted so that the permeate and retentate were collected for measurement at the same rate. The absorbance of BSA in the feed and in both collected fractions was measured at a wavelength of 278 nm using a Hitachi U-3010 spectrophotometer. The concentration of BSA was determined from the calibration curve. The retention was calculated using the following formula:

$$R = \left(1 - \frac{C_p}{C_o}\right) \cdot 100\%$$

where:

R – retention [%]

C_p – concentration of albumin in the permeate [g/L]

C_o – concentration of albumin in the feed [g/L]

4.9.5.2 Retention measurement using polystyrene microspheres of different sizes

The retention for polystyrene microspheres was measured using flow cytometry. The microspheres with particle sizes of 100 nm, 200 nm, and 500 nm (red fluorescence) or 2 μm and 3 μm (red and green fluorescence) were appropriately diluted and passed through the module. After stabilization (5 minutes), the overpressure was adjusted so that the permeate and retentate were collected at the same rate. Then, the number of events in the feed and in both collected fractions was measured using a BD FACSCanto II flow cytometer.

4.10 Construction of the system for dynamic cell culture

4.10.1 Simulations

Mathematical modeling of polysulfone fiber was conducted using COMSOL Multiphysics 5.5. Changes in the concentrations of albumin and glucose in different areas of the membrane were simulated. Moreover, the effect of applying different flow rates (from 1 to 10 mL/min) on the transport of albumin and glucose was investigated. For the modelling of incompressible fluid flow, the continuity equation and the Navier-Stocks momentum balance

equation were used. As a type of fluid flow, the laminar flow was chosen. Our model assumed that the culture medium flows through the intracapillary space of the capillary membrane, whereas the cells grow on the extracapillary surface of the capillary membrane. Moreover, the cells produce albumin, which is transported through the semi-permeable capillary membrane (pore size: 0.2 μm) to the flowing culture medium, and simultaneously consume glucose, which is delivered to them from the flowing culture medium. During mathematical modeling, the increase in the number of cells was not taken into account; however, indirectly, it was reflected in constant increase of albumin concentration and constant decrease of glucose concentration. To simplify the model, the circulation of culture medium in the system was omitted; however, in our experimental system for dynamic culture the circulation of medium occurred. A picture showing the geometry of the hollow fiber and the directions of fluid, glucose, and albumin transport is presented below (Figure 18).

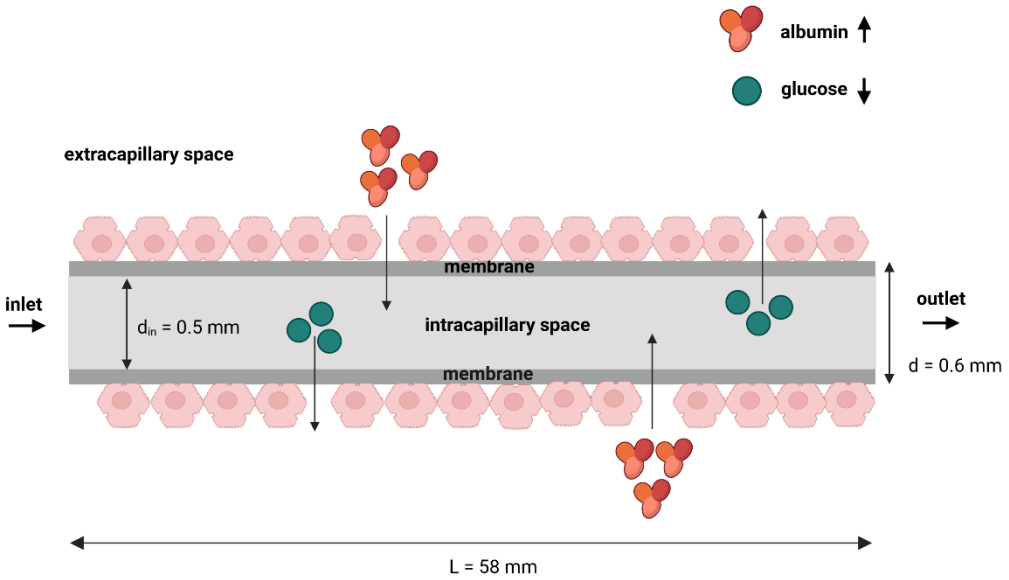

Figure 18. Schematic view of the modeled object – a single hollow fiber. The picture represents the geometry of the modeled capillary with the dimensions concerning the outer diameter, internal diameter and length of the fiber. Moreover, the picture shows the direction of fluid flow and the directions of mass transport of albumin (which is produced by cells during the culture) and glucose (which is consumed by cells during the culture). Abbreviations: L – length of the fiber; d – outer diameter; d_{in} – internal diameter. Created with the Biorender.com.

For the purpose of the mathematical simulations, the initial parameters (in the intracapillary space of the membrane) were set as follows: velocity, pressure, and albumin concentration equal to zero, whereas the glucose concentration in the culture medium equals

22.94 mol/m^3. The below table (Table 19) presents the other parameters used during the simulations.

Table 19. List of the parameters used during mathematical modeling.

Parameter	Value
Coefficient of membrane porosity	0.75
Permeability of membrane	$1.69 \cdot 10^{-13}$ m^2
Albumin diffusion coefficient	$6.1 \cdot 10^{-11}$ m^2/s
Albumin production	$3.28 \cdot 10^{-9}$ $kg/(m^3 \cdot s)$
Albumin molecular weight	67 kg/mol
Albumin molar production	$4.89 \cdot 10^{-11}$ $mol/(m^3 \cdot s)$
Glucose diffusion coefficient	$6 \cdot 10^{-10}$ m^2/s
Glucose consumption	$1.37 \cdot 10^{-6}$ $kg/(m^3 \cdot s)$
Glucose molecular weight	0.18 kg/mol
Glucose concentration in the culture medium	4.13 kg/m^3
Glucose molar concentration in the culture medium	22.94 mol/m^3
Glucose molar consumption	$7.6 \cdot 10^{-6}$ $mol/(m^3 \cdot s)$

4.10.2 Preparation of the system for dynamic cell culture

The heart of the dynamic culture system is a hollow fiber bioreactor (culture module). It was constructed of 20 semipermeable capillary membranes made of polysulfone from Vestergaard Frandsen company. Its culture surface area is ca. 22 cm^2. The capillary membranes have a pore size of 0.2 μm. To construct the system for dynamic culture, a peristaltic pump, a tubbing, a gas trap, a medium reservoir, needles, adapters, and connectors were used. Before assembly, the hollow fiber bioreactor was pasteurized twice (2 hours, 60 °C). The tubbing for the peristaltic pump and medium reservoir were sterilized in an autoclave. The rest of tubbing and gas trap were purchased in sterile packages. The needles, adapters and connectors were sterilized in an autoclave or using 70% ethanol solution. The picture below (Figure 19) shows the assembled system for dynamic cell culture.

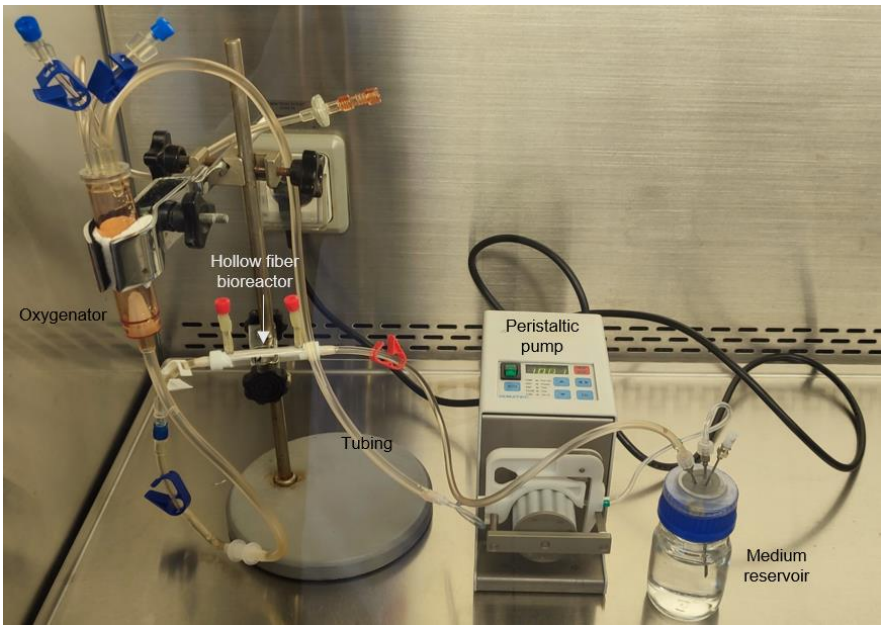

Figure 19. The system for dynamic cell culture. A hollow fiber bioreactor sets the heart of the constructed system.

4.10.3 Cell culture under dynamic conditions

The day before seeding, sterile PBS was passed through the system and circulated for 24 hours in an incubator (37 °C; atmosphere containing 5% CO_2). The next day, the bottle with PBS was replaced with sterile culture medium (DMEM supplemented with 10% FBS and 1% nonessential amino acids). The PBS in the tubbing was removed by passing 50 mL of culture medium through the system. After that, an appropriate number of cells were seeded on the extracapillary space of the polysulfone membrane with a syringe. Then, the whole system was transferred to the incubator. For cell attachment to the membrane surface, the hollow fiber bioreactor was rotated every 5 minutes for 1 hour. After that time, the peristaltic pump was turned on, and the culture was started. As a control for dynamic conditions, the same number of cells was seeded on a T25 flask (static culture) to achieve a similar cell number per growth surface area. The cell culture lasted for twelve days. On days 2, 5, 7, 9, and 12 of culture, the samples from dynamic and static conditions were collected and stored at -20 °C for further analysis.

The optimization of two parameters associated with dynamic culture was conducted using the C3A cell line. Two different flow rates (5 mL/min and 10 mL/min) and two different seeding densities ($0.5 \cdot 10^6$ or $5 \cdot 10^6$ cells per bioreactor) were tested. The final experiments were conducted using the C3A, C3A_AO_III, and C3A_AO_P2A cell lines. The fluid flow was set at 10 mL/min, and the cell density was set at $5 \cdot 10^6$ cells per bioreactor. The figure below (Figure 20) shows the above-described steps of cell culture under dynamic conditions.

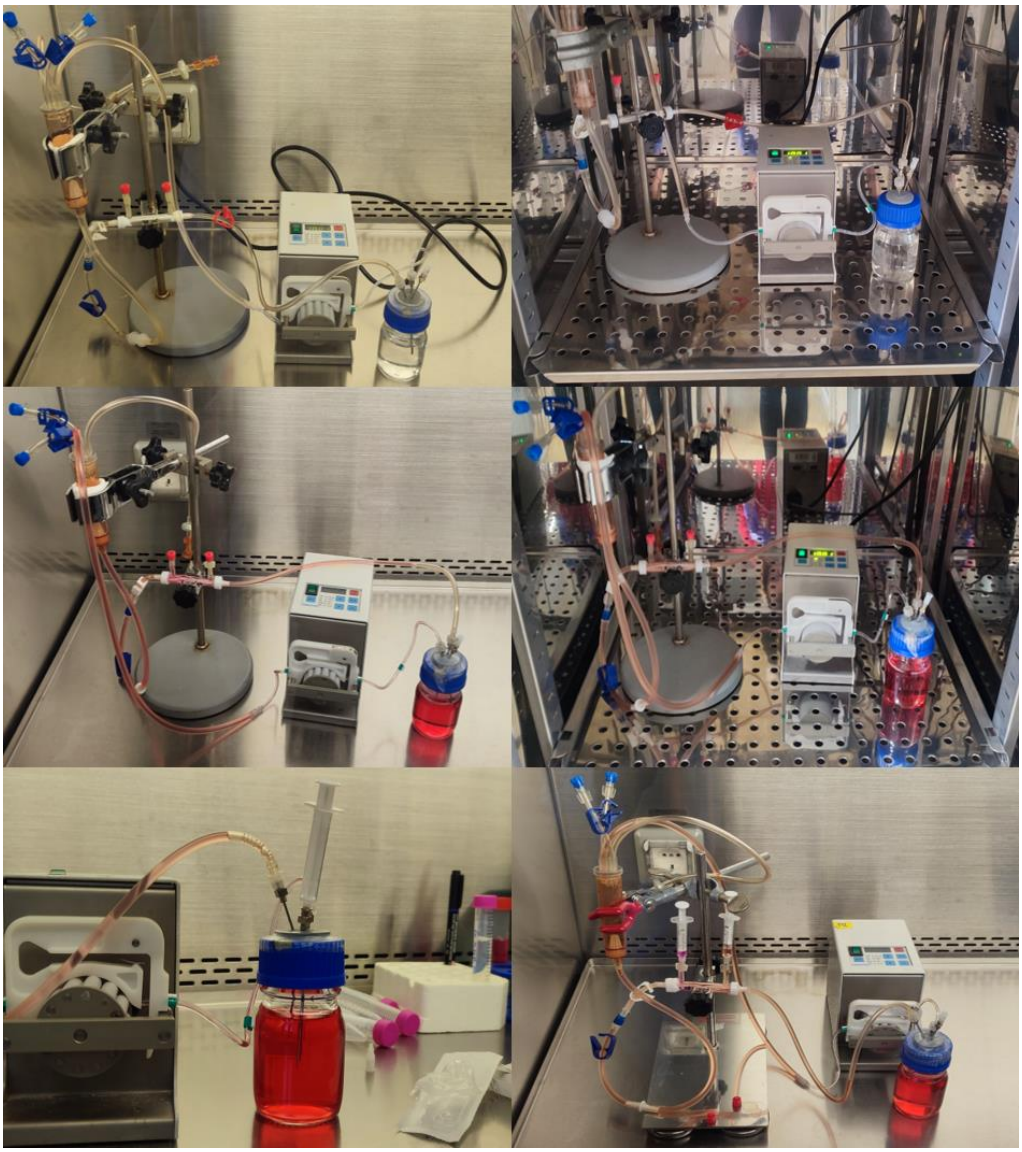

Figure 20. Cell culture under dynamic conditions. The pictures show the following steps of dynamic culture: 1 – assembled system for dynamic culture; 2 – daily incubation with circulating PBS (with the same flow rate as for cell culture); 3 – cells seeding into the bioreactor (extracapillary space of capillary membranes); 4 – dynamic cell culture carried out in the incubator for twelve days; 5 – sample collection from the medium reservoir (on days 2, 5, 7, 9, and 12 of culture); 6 – sample collection from the bioreactor (on days 2, 5, 7, 9, and 12 of culture).

4.10.4 Determination of cell viability, albumin production, and glucose consumption

On the last day of the dynamic culture, after collecting the samples, the medium from the module was removed. Then, the capillaries inside the bioreactor were washed with PBS. Then, the trypsin solution was added, and the module was incubated for 6 minutes at 37 °C. Subsequently, fresh medium was added to the module, and the cells were detached from the capillary membranes using a syringe. The obtained cell suspension was centrifuged (5 min,

163 RCF, 15 °C). After removing the supernatant and suspending the cells in 1 mL of PBS, the live and dead cells were counted using the trypan blue exclusion method. The trypsinization process was repeated (as many times as possible). The viability of cells cultured under static conditions was also determined using the trypan blue exclusion method.

To check whether the cells were still attached to the capillary surface, the capillaries inside the module were fixed for 10 minutes using 4% formaldehyde solution. Then, the formaldehyde was removed, and the fibers were washed with PBS. Then, the capillaries were stained with DAPI solution at a final concentration of 10 μg/mL. Subsequently, the polysulfone membrane was observed under an Olympus IX-71 fluorescence microscope using a UMN-B UV filter for DAPI. The collected media samples from dynamic and static cell culture were used for determination of albumin production and glucose consumption. The measurements were conducted as described in sections 4.3 and 4.4.

4.11 Statistical analysis

Statistical analysis was performed with Statistica 10 software. The statistical significance of the obtained results was checked using one-way or multivariate analysis of variance (ANOVA/MANOVA) with Duncan's *post-hoc* test. *P*-values less than 0.05 were considered as statistically significant.

5. Results

5.1 Genetic modification of C3A cells with lentiviral vectors

The C3A cell line is characterized by a nonfunctional urea cycle, which results from decreased expression of the human arginase 1 (h*ARG1*) and ornithine transcarbamylase (h*OTC*) genes (Mavri-Damelin *et al.*, 2008). Therefore, efforts toward the restoration of the urea cycle using genetic modification tools (lentiviral vectors) have been undertaken. The utilized lentiviral vectors, based on the genome of human immunodeficiency virus-1 (HIV-1), belong to the second-generation system and consist of three plasmids: transfer (containing the gene of interest), helper/packaging, and envelope (Pluta and Kacprzak, 2009). Our previous approach to urea cycle correction was based on the transduction of C3A cells with two different lentiviral vectors: one carrying the h*ARG1* gene and the other carrying the h*OTC* gene. Therefore, the obtained C3A_AO_III cell line constitutes a mixed population of genetically modified cells expressing none, one or, in minority, both transgenes (Pluta *et al.*, 2020). In the present study, C3A cells were transduced with a single lentiviral vector carrying both transgenes in one transcription unit. Moreover, antibiotic selection using puromycin was performed to obtain a pure population of 100% genetically modified cells (the so-called C3A_AO_P2A cell line). More details concerning the production of lentiviral vectors, cell transduction, and selection are provided below.

5.1.1 Determination of the purity and quality of plasmid DNA (digestion with restriction enzymes)

As mentioned above, for genetic modification of C3A cells, a single lentiviral vector with a polycistronic expression cassette was used. Vector plasmid containing genes encoding the human h*ARG1* and h*OTC* genes under the control of CMV promoter was purchased from Genecopoeia (size: 10827 bp). The open reading frames (ORFs) of interest were split by the sequence encoding the P2A peptide, a short viral oligopeptide that mediates the “cleavage” of polypeptides during translation in eukaryotic cells. The sequence encoding the fluorescent protein DsRed was placed downstream and was also preceded by the P2A sequence. The puromycin resistance gene was chosen as a selection antibiotic. A map of the transfer plasmid is presented in the figure below (Figure 21).

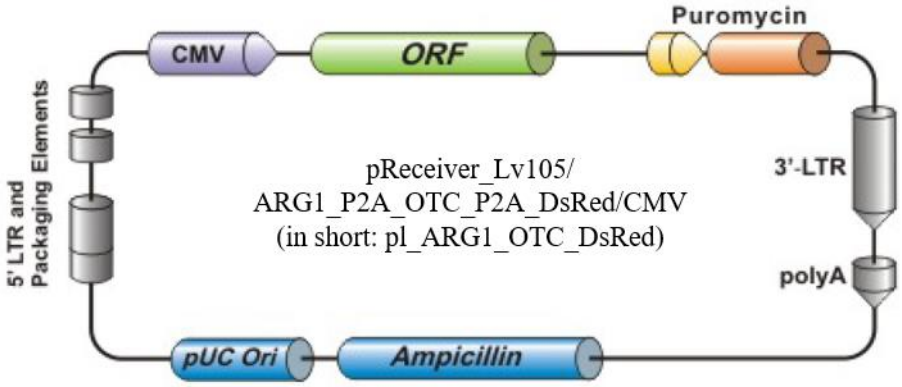

Figure 21. Map of vector plasmid encoding the h*ARG1*, h*OTC* and *DsRed* genes synthetized by Genecopoeia. The scheme of plasmid DNA was obtained from Genecopoeia. The *ORF* represents the polycistronic expression cassette.

Before the evaluation of the quality and purity of plasmid preparation, plasmid DNA was introduced into chemocompetent *E.coli* STBL2 bacteria using the heat shock method. Transformed bacteria were cultured on solid LB media supplemented with ampicillin. From the obtained bacterial colonies, four clones were selected, transferred to liquid LB medium supplemented with ampicillin and cultured overnight. The isolation of plasmid DNA from cultivated bacteria was performed using a Plasmid Mini kit. The purity of the obtained plasmid DNA was then checked using a NanoDrop spectrophotometer. In turn, identity was evaluated by digestion with the BamH1 restriction enzyme. Details concerning enzymatic digestion are presented in section 4.7.3. The results of electrophoretic separation of the digested plasmid DNA are presented below (Figure 22).

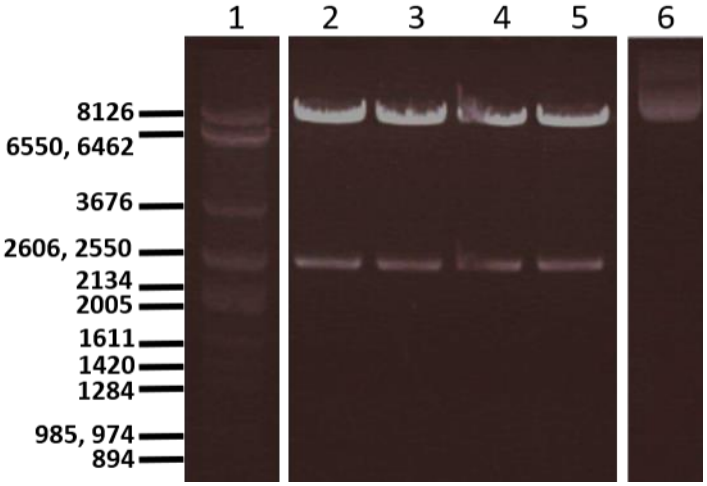

Figure 22. Determination of the quality and identity of the amplified plasmid DNA using enzymatic digestion. The results of electrophoresis of digested plasmid DNA. 1 – nucleic acid size standard - DNA Marker Lambda/Ava II; 151 – 8126 bp; 2 – digested pl_ARG1_OTC_DsRed clone 1; 3 – digested pl_ARG1_OTC_DsRed clone 2; 4 – digested pl_ARG1_OTC_DsRed clone 3; 5 – digested pl_ARG1_OTC_DsRed clone 4; 6 – nondigested control, pl_ARG1_OTC_DsRed (size: 10827 bp).

Electrophoretic separation revealed that for the digested plasmid DNA, two fragments with sizes of approximately 8200 bp and 2500 bp were obtained. The results were consistent with the expected sizes based on DNA sequence analysis. For further experiments, the pl_ARG1_OTC_DsRed clone 1 was chosen. The selected plasmid DNA was multiplied for larger scale and isolated using the Plasmid Midi kit. Its purity was evaluated using a NanoDrop spectrophotometer. The obtained plasmid DNA was utilized as a template (transfer vector) for the production of lentiviral particles.

5.1.2 Production of lentiviral vectors - transfection of HEK293T cells using the lipofection method

The production of lentiviral vectors carrying additional copies of the human h*ARG1* and h*OTC* genes was performed using the HEK293T cell line, which is characterized by high transfectability. For the purpose of this research, HEK293T cells were transfected with three types of plasmids (transfer, helper/packaging, and envelope) in three different proportions (3:2:1, 4:2:1, and 5:2:1) using a Lipofectamine 3000 kit. The effect of the utilization of two different amounts of total DNA per well (3 µg or 5 µg) was also evaluated. HEK293T cells were also transfected with the pNL-DsRED2/CMV-WPREΔU3 plasmid (encoding the fluorescent protein DsRed2) as a positive control for the reaction. The detailed procedure for the production of lentiviral vectors is described in section 4.7.4. Microphotographs of transfected cells are presented below (Figure 23A, Figure 23B).

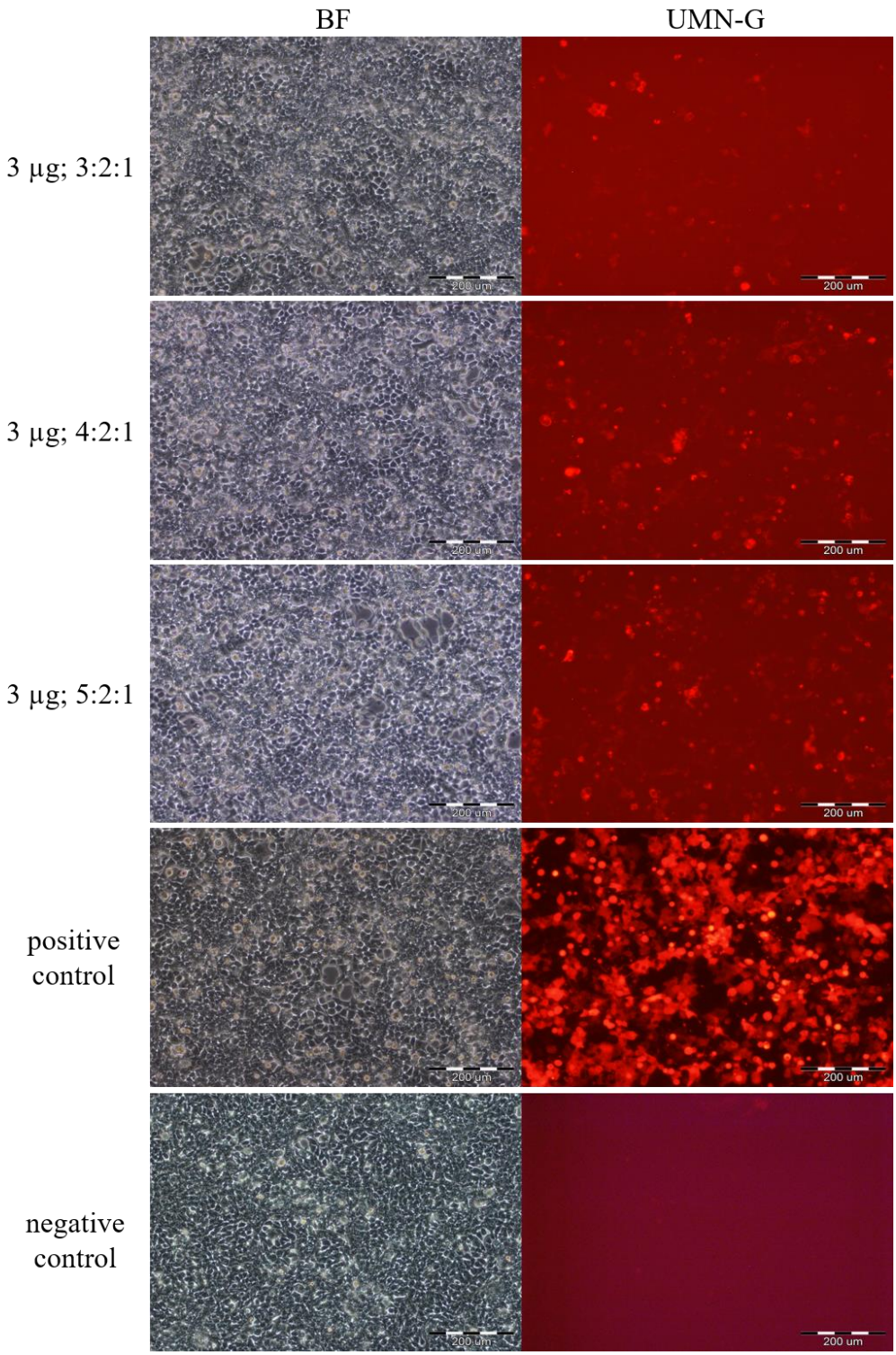

Figure 23A. Evaluation of transfection of HEK293T cells. HEK293T cells were transfected with three types of plasmids (transfer, helper/packaging, and envelope) in three different proportions (3:2:1, 4:2:1, and 5:2:1) using a lipofection method. The total amount of DNA per well was 3 µg. As a positive control, HEK293T cells were transfected with a transfer plasmid carrying a gene encoding the fluorescent protein DsRed2. As a negative control, nontransfected HEK293T cells were utilized. Three days after transfection, microphotographs of HEK293T cells were taken with a bright-field (BF) illumination and UMN-G filter (for red fluorescence) using an Olympus IX-71 fluorescence microscope. Scale bar: 200 µm.

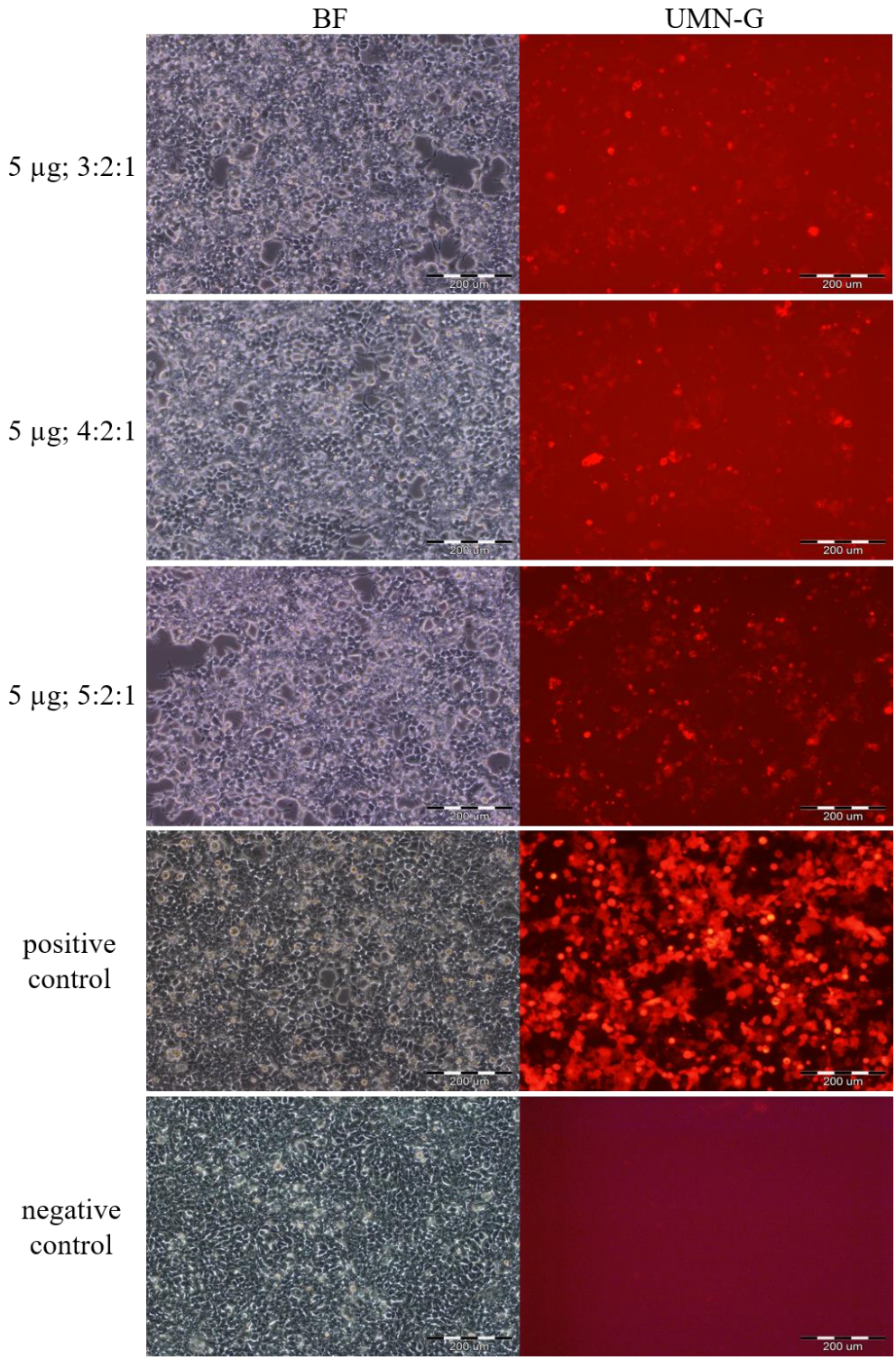

Figure 23B. Evaluation of transfection of HEK293T cells. HEK293T cells were transfected with three types of plasmids (transfer, helper/packaging, and envelope) in three different proportions (3:2:1, 4:2:1, and 5:2:1) using a lipofection method. The total amount of DNA per well was 5 µg. As a positive control, HEK293T cells were transfected with a transfer plasmid carrying a gene encoding the fluorescent protein DsRed2. As a negative control, nontransfected HEK293T cells were utilized. Three days after transfection, microphotographs of HEK293T cells were taken with a bright-field (BF) illumination and UMN-G filter (for red fluorescence) using an Olympus IX-71 fluorescence microscope. Scale bar: 200 µm.

Microscopic analysis revealed successful transfection of HEK293T cells. Media potentially containing the obtained lentiviral vectors (LV_ARG1_OTC_DsRed and LV_DsRed2) were collected on the third day after transfection and used in further experiments (i.e., transduction of human hepatic cells).

5.1.3 Transduction of a human hepatic cell line using self-prepared lentiviral vectors and evaluation of their efficiency using fluorescence microscopy

Before the transduction of target cells, the titer, expressed as the number of transducing units per milliliter (TU/mL), of lentiviral preparations should be determined using, for example, the HOS cell line. Despite many attempts, cytometric analysis revealed that the percentage of transduced HOS cells expressing a red fluorescent protein marker (DsRed) was below the detection level. Therefore, due to low titers or low expression of marker protein, the titer of self-prepared lentiviral vectors (LV_ARG1_OTC_DsRed) was not determined. Then, the target cells (C3A cells) were transduced with 500 µl of conditioned medium containing self-prepared lentiviruses. Transduction of C3A cells was performed using each transfection variant of LV_ARG1_OTC_DsRed vectors. Nontransduced cells were used as a negative control, whereas the positive control constituted C3A cells treated with the selected variant of the LV_DsRed2 vector (5 µg of total plasmid DNA; proportion of plasmids: 5:2:1). More details are provided in section 4.7.6. Microphotographs presenting the effect of lentiviral transduction are shown in the figures below (Figure 24A, Figure 24B).

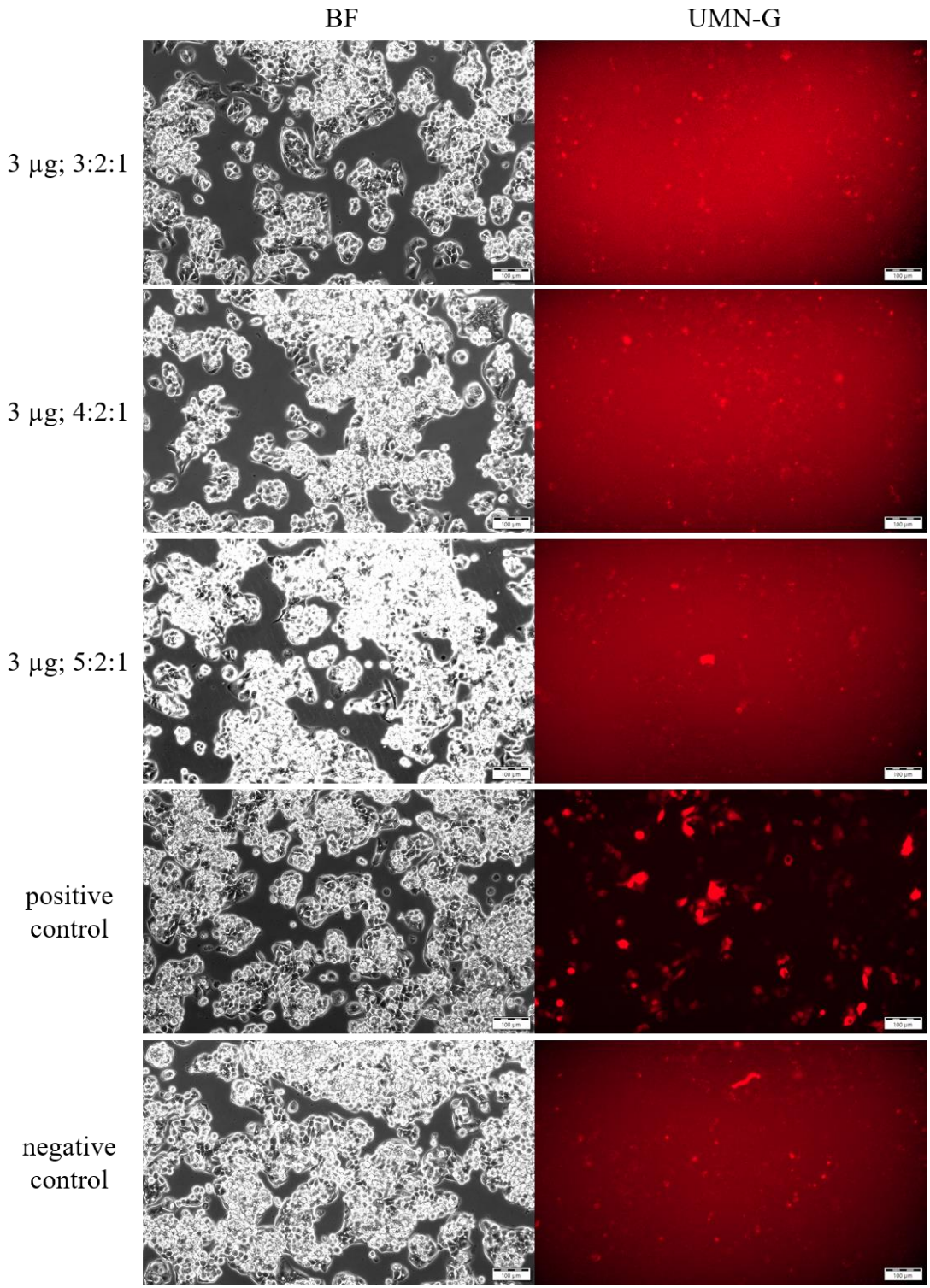

Figure 24A. Evaluation of the efficiency of transduction of human hepatic cells. C3A cells were transduced using the following transfection variants of LV_ARG1_OTC_DsRed vectors - total amount of DNA: 3 µg; proportion of plasmids: 3:2:1, 4:2:1, and 5:2:1. As a positive control, C3A cells were transduced with lentiviral vectors carrying a gene encoding the fluorescent protein DsRed2. As a negative control, nontransduced C3A cells were used. Three days after transduction, microphotographs of C3A cells were taken with a bright-field (BF) illumination and UMN-G filter (for red fluorescence) using an Olympus IX-71 fluorescence microscope. Scale bar: 100 µm.

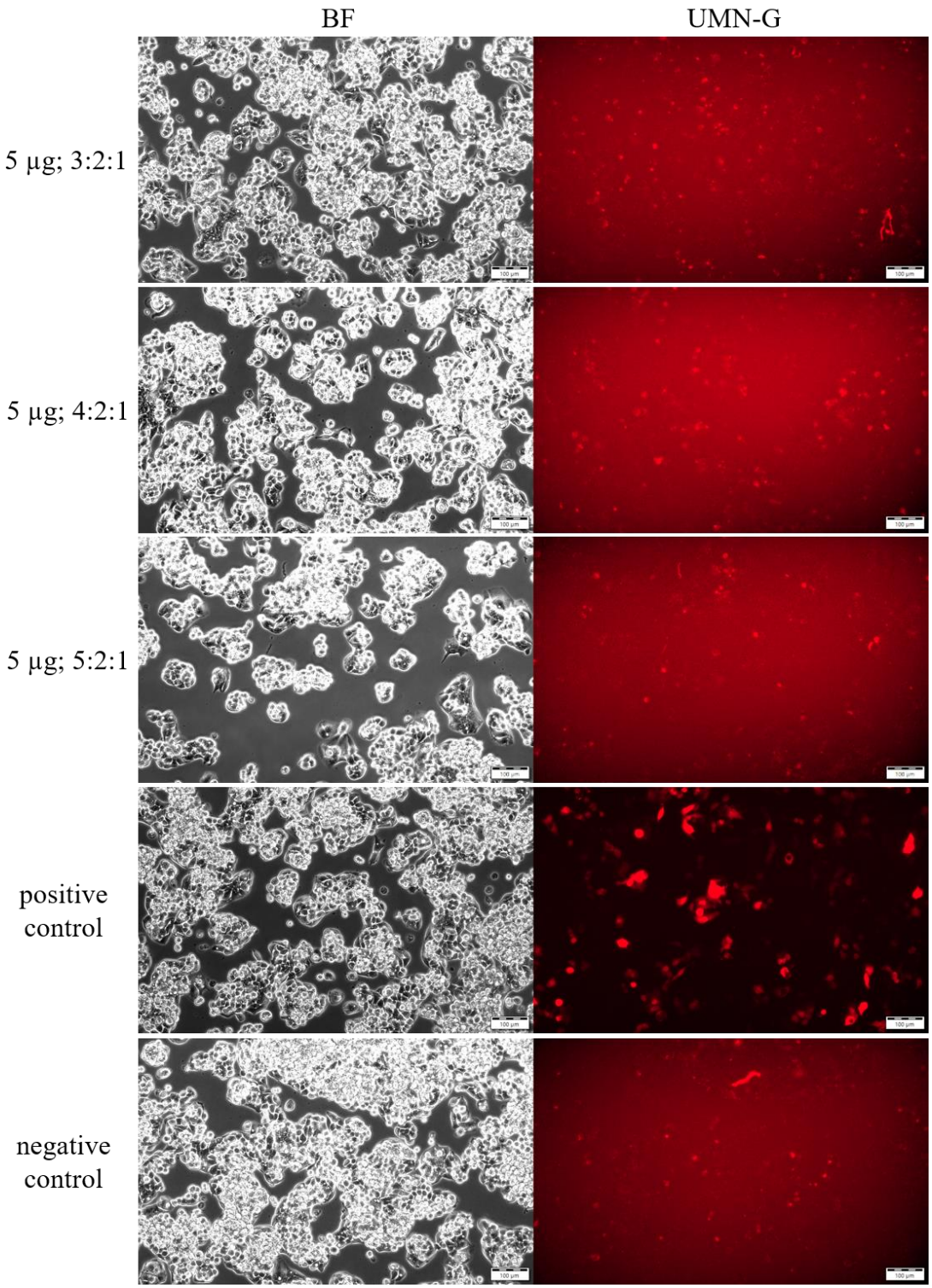

Figure 24B. Evaluation of the efficiency of transduction of human hepatic cells. C3A cells were transduced using the following transfection variants of LV_ARG1_OTC_DsRed vectors - total amount of DNA: 5 µg; proportion of plasmids: 3:2:1, 4:2:1, and 5:2:1. As a positive control, C3A cells were transduced with lentiviral vectors carrying a gene encoding the fluorescent protein DsRed2. As a negative control, nontransduced C3A cells were used. Three days after transduction, microphotographs of C3A cells were taken with a bright-field (BF) illumination and UMN-G filter (for red fluorescence) using an Olympus IX-71 fluorescence microscope. Scale bar: 100 µm.

Comparison of C3A cells transduced with the LV_ARG1_OTC_DsRed vectors with their nontransduced counterparts revealed that the specific signal from the fluorescent protein DsRed was not detected. In contrast, microscopic analysis of cells transduced with LV_DsRed2 vectors revealed successful genetic modification. The reason for this could be the low titer of the obtained lentiviral vectors. However, the fact that the gene encoding the fluorescent protein DsRed is located far from the CMV promoter, at the very end of the 3-cistronic expression cassette (Figure 21), may result in lower expression of this ORF and decreased efficiency of protein synthesis. Therefore, to enrich the population of transduced cells, antibiotic selection was conducted.

5.1.4 Antibiotic selection

As mentioned above (section: 5.1.1), the transfer plasmid contains a puromycin resistance gene; thus, cells which were successfully genetically modified are resistant to this antibiotic. In turn, unmodified cells die during exposure to puromycin. Thus, to obtain a population of nearly 100% genetically modified cells, antibiotic selection was performed. For this procedure, C3A cells transduced with 5 μg of total plasmid DNA at a ratio of 5:2:1 and 3 μg of total plasmid DNA at a ratio of 3:2:1 were chosen. Nontransduced human hepatic cells were selected as the negative control. The detailed protocol used for antibiotic selection is described in section 4.7.7. The obtained results are presented below (Figure 25).

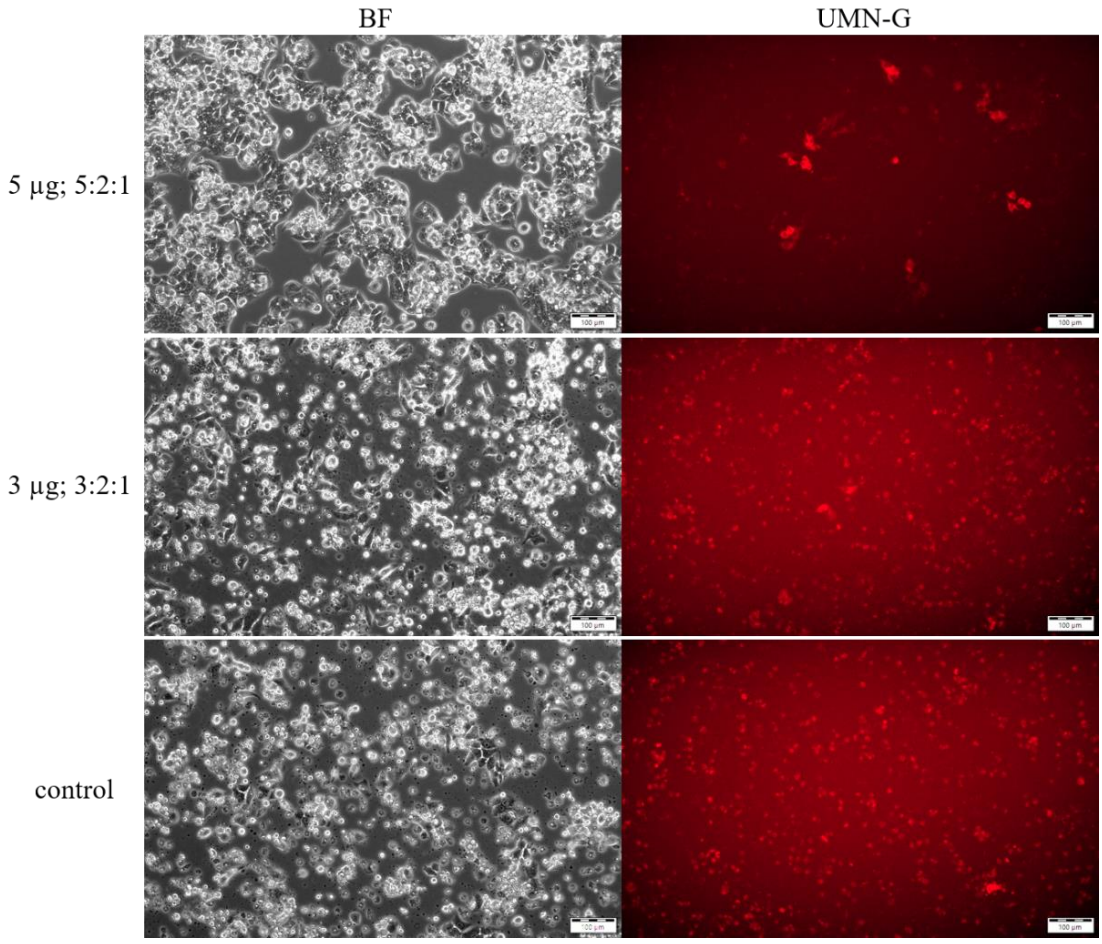

Figure 25. Determination of the effect of antibiotic selection. Selection with puromycin was conducted using C3A cells transduced with 5 µg of total plasmid DNA at a ratio of 5:2:1 and 3 µg of total plasmid DNA at a ratio of 3:2:1. Nontransduced human hepatic cells were used as the negative control. After 48 hours of puromycin selection, microphotographs of the transduced C3A cells were taken with a bright-field (BF) illumination and UMN-G filter (for red fluorescence) using an Olympus IX-71 fluorescence microscope. As a negative control, nontransduced C3A cells were used. Scale bar: 100 µm.

Microscopic analysis revealed that after 48 hours of puromycin selection, nontransduced C3A cells and C3A cells transduced with 3 µg of total plasmid DNA at a ratio of 3:2:1 started to die. In contrast, in the case of C3A cells transduced with 5 µg of total plasmid DNA at a ratio of 5:2:1, cell division and fluorescent cells were observed. After 72 hours of puromycin selection, control cells and cells transduced with lower amount and proportion of plasmid DNA were completely dead. In turn, C3A cells transduced with 5 µg of total plasmid DNA at a ratio of 5:2:1 grew very quickly, and the number of fluorescent cells increased. Nevertheless, this finding supported our hypothesis that not every cell that was successfully transduced (puromycin resistant) expresses fluorescent marker. Antibiotic selection lasted nine days. Exemplary microphotographs after eight days of this procedure are presented below (Figure 26).

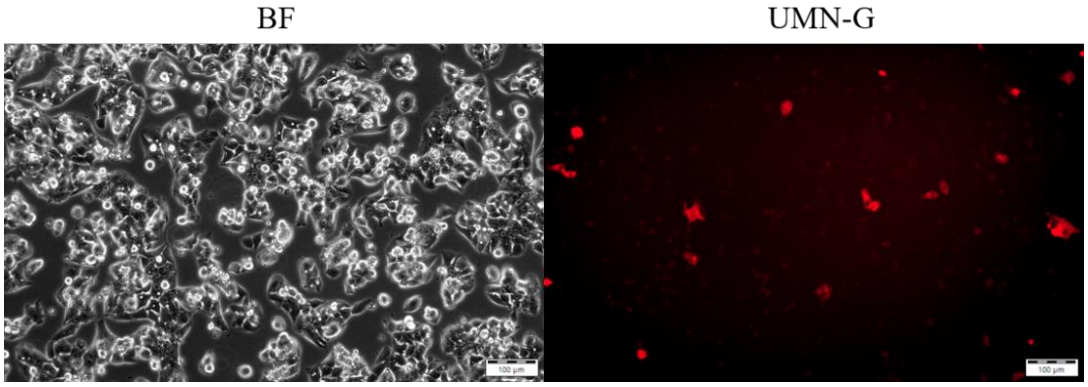

Figure 26. Determination of the effect of antibiotic selection. Microphotographs of transduced C3A cells (5 µg; 5:2:1) after 192 hours of puromycin selection were taken with a bright-field (BF) illumination and UMN-G filter (for red fluorescence) using an Olympus IX-71 fluorescence microscope. Scale bar: 100 µm.

After nine days of puromycin selection, this antibiotic was removed from the culture medium, and the newly obtained cell line C3A_AO_P2A was cultivated. Each passage was cryopreserved for further experiments.

5.1.5 Confirmation of DNA integration into the cell genome by PCR

To confirm the integration of the h*ARG1* and h*OTC* genes into the C3A genome, polymerase chain reaction (PCR) was performed. The genomic DNA isolated from C3A, C3A_AO_III, C3A_AO_P2A, and HOS was used as a template for PCR. The plasmid pl_ARG1_OTC_DsRed (size: 10827 bp) was used as a positive control for the reaction. The negative control (e.g., control of the purity of reagents) was a reaction mixture without a DNA template. The nucleotide sequences of the forward and reverse primers are presented in section 3.8. The composition of the reaction mixtures and PCR conditions are described in section 4.7.9. The results of electrophoresis for the amplified DNA fragments are shown below (Figure 27).

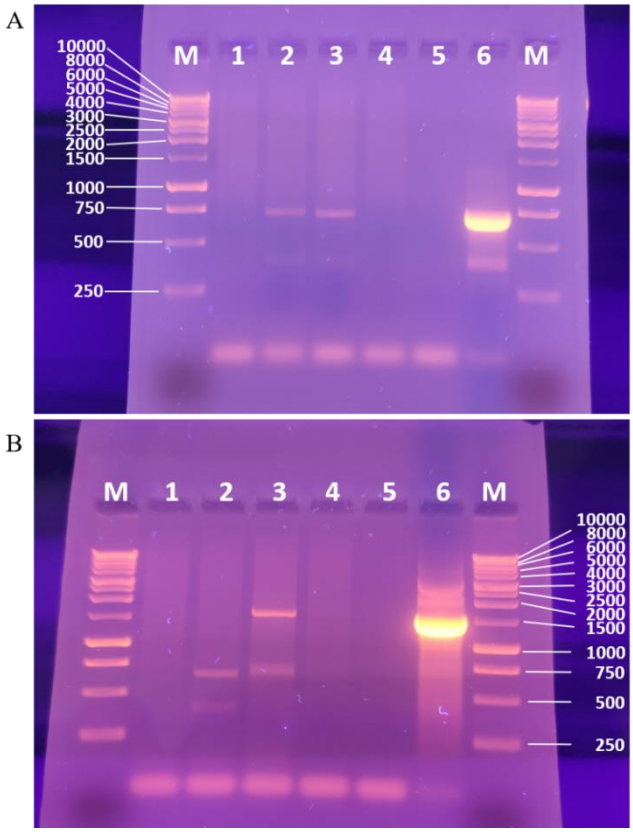

Figure 27. Determination of the integration of the h*ARG1* and h*OTC* genes into the C3A genome. A Results of horizontal electrophoresis of PCR products obtained from genomic DNA templates using the CMV promoter and ARG1 primers. Lanes: M – DNA size standard Perfect Plus 1 kb DNA Ladder; 250 – 10000 bp; 1 – C3A; 2 – C3A_AO_III; 3 – C3A_AO_P2A; 4 – HOS; 5 – negative control (PCR conducted without a DNA template); 6 – positive control – plasmid DNA (pl_ARG1_OTC_DsRed). **B** Results of horizontal electrophoresis of PCR products obtained from genomic DNA templates using the CMV promoter and OTC primers. Lanes: M – DNA size standard Perfect Plus 1 kb DNA Ladder; 250 – 10000 bp; 1 – C3A; 2 – C3A_AO_III; 3 – C3A_AO_P2A; 4 – HOS; 5 – negative control (PCR conducted without a DNA template); 6 – positive control – plasmid DNA (pl_ARG1_OTC_DsRed).

The expected sizes of products, based on DNA sequence analysis, were as follows: for ARG1, 697 bp (for the C3A_AO_P2A cell line) and 712 bp (for the C3A_AO_III cell line); for OTC, 1527 bp (for the C3A_AO_P2A cell line) and 672 bp (for the C3A_AO_III cell line). It is worth emphasizing that the lack of PCR products for C3A cells is connected to the absence of the CMV promoter sequence in front of the h*ARG1* and h*OTC* genes in the nontransduced cell genomes. Moreover, the differences in the sizes of the products for OTC between C3A_AO_III and C3A_AO_P2A were the result of the use of different LVs for the genetic modification of C3A cells (C3A_AO_III – two different plasmids, each containing other missing genes; C3A_AO_P2A – one transfer plasmid consisting of a sequence of both transgenes – longer product). To sum up, the obtained results confirmed the integration of the h*ARG1* and h*OTC* genes into the C3A genome in the newly constructed cell line.

5.1.6 Determination of transgene expression at the mRNA level using RT-qPCR

The comparison of gene expression between C3A cells and their genetically modified counterparts (C3A_AO_III and C3A_AO_P2A) was conducted using RT-qPCR. The experiments were carried out for cells treated with 40 mM NH_4Cl and their untreated counterparts. Data normalization was performed against the *RPL13A* and *GAPDH* reference genes (housekeeping genes whose expression is stable in all types of cells and in all experimental conditions). Since for the purpose of the study the treatment with ammonium chloride was performed, the expression stability of the reference genes under these conditions was verified and confirmed (data not shown). The results of RT-qPCR analysis obtained for h*ARG1* and h*OTC* genes are presented in the figure below (Figure 28).

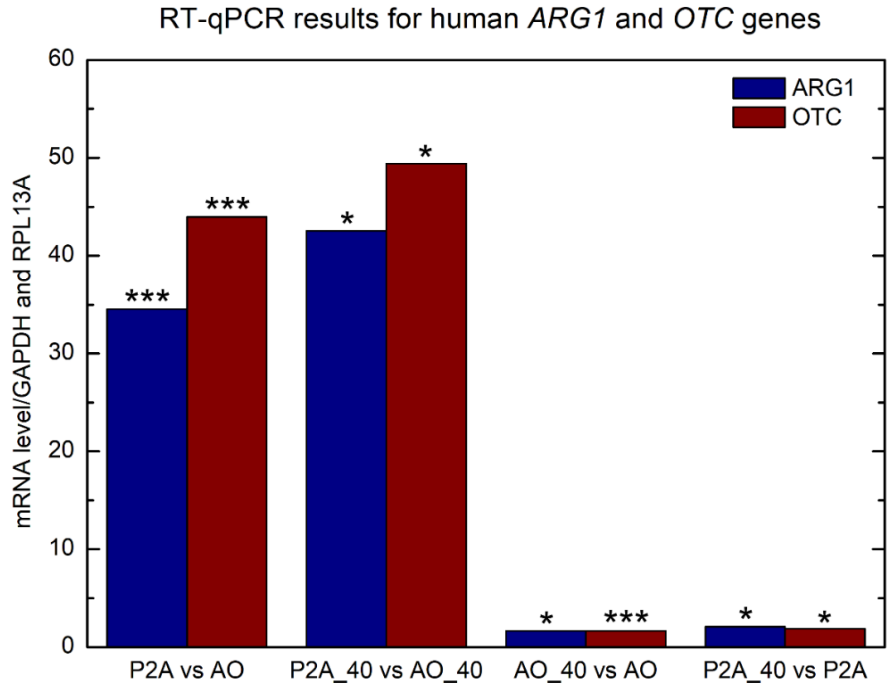

Figure 28. Analysis of the expression of the h*ARG1* and h*OTC* genes in genetically modified hepatic cells. The results of RT-qPCR experiments conducted for C3A_AO_P2A and C3A_AO_III cells cultured with or without 40 mM NH_4Cl. To determine the changes in mRNA levels, REST 2009 software and the Pfaffl model were used. Data normalization was performed using the *RPL13A* and *GAPDH* genes. Number of biological replicates: 4. The levels of significance were marked as follows: *p*-value < 0.05 (*); *p*-value < 0.01 (**); *p*-value < 0.001 (***). Abbreviations: P2A – C3A_AO_P2A cell line; AO – C3A_AO_III cell line.

The expression of the h*ARG1* gene was 34.5-fold (*p*-value < 0.001) greater when comparing C3A_AO_P2A and C3A_AO_III cells, and 42.5-fold (*p*-value = 0.022) greater when comparing these cell lines after incubation with 40 mM NH_4Cl. A similar effect was observed for the h*OTC* gene. The expression of this gene was 43.9-fold (*p*-value < 0.001)

greater when comparing C3A_AO_P2A and C3A_AO_III cells and 49.4-fold (*p*-value = 0.025) greater when comparing these cell lines after incubation with 40 mM NH_4Cl. Interestingly, ammonium chloride treatment increased the mRNA levels of the h*ARG1* and h*OTC* genes in the genetically modified cells. For the C3A_AO_P2A cell line, the expression of the h*ARG1* and h*OTC* genes was 2.1-fold (*p*-value = 0.024) and 1.9-fold (*p*-value = 0.015) greater, respectively. Similarly, for C3A_AO_III cells, the mRNA levels of the h*ARG1* and h*OTC* genes were 1.69-fold (*p*-value = 0.036) and 1.68-fold (*p*-value < 0.001) greater, respectively. As expected, the levels of h*ARG1* and h*OTC* transcripts in unmodified C3A cells were under the detection limit.

Differences in the expression of genes encoding albumin (*ALB*), hepatocyte nuclear factor 4 alpha (*HNF4A*), hepatocyte nuclear factor 1 homeobox A (*HNF1A*), heat shock protein family A (Hsp70) member 1A (*HSPA1A*), and nuclear factor kappa B (*NF-κB*) between C3A cells and their genetically modified counterparts were also evaluated. Data normalization was performed against the *GAPDH* reference gene. The obtained results are shown below (Figure 29).

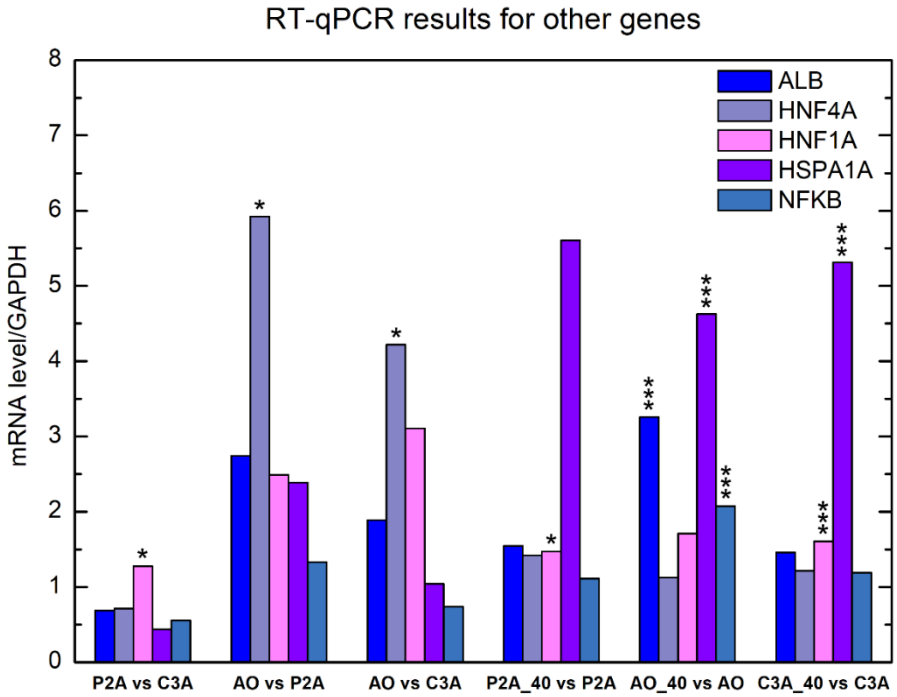

Figure 29. Analysis of the expression of the *ALB*, *HNF4A*, *HNF1A*, *HSPA1A*, and *NF-κB* genes in human HCC cells. The results of RT-qPCR experiments conducted for C3A, C3A_AO_P2A, and C3A_AO_III cells cultured with or without 40 mM NH_4Cl. To determine the changes in mRNA levels, REST 2009 software and the Pfaffl model were used. Data normalization was performed using the *GAPDH* gene. Number of biological replicates: 3. The levels of significance were marked as follows: *p*-value < 0.05 (*); *p*-value < 0.01 (**); *p*-value < 0.001 (***). Abbreviations: P2A – C3A_AO_P2A cell line; AO – C3A_AO_III cell line.

The expression of the *ALB* gene was 2.7-fold and 1.9-fold greater in C3A_AO_III cells than in C3A_AO_P2A and C3A cells, respectively. In turn, the mRNA level of the analyzed gene in C3A_AO_P2A cells was decreased (0.7-fold) in comparison with that in the C3A cell line. Interestingly, the obtained results revealed that the presence of 40 mM NH_4Cl induced an increase in the mRNA level of albumin in both the genetically modified cells and their unmodified counterparts. The level of *ALB* gene expression after ammonium chloride treatment was 1.6-fold greater for C3A_AO_P2A cells, 3.3-fold (p-value < 0.001) greater for the C3A_AO_III cell line, and 1.5-fold greater for C3A cells.

Analysis of the expression of the *HNF4A*, *HNF1A*, *HSPA1A*, and *NF-κB* genes showed that C3A_AO_III cells were characterized by 5.9-fold (p-value = 0.032) and 4.2-fold (p-value = 0.016) greater expression of the *HNF4A* gene than the C3A_AO_P2A and C3A cell lines, respectively. Moreover, the expression of the *HNF1A* gene in C3A_AO_III cells was also upregulated. Its value was 2.5-fold and 3.1-fold greater than that of C3A_AO_P2A and C3A cells, respectively. In turn, in the case of C3A_AO_P2A cells, downregulation of the expression of the *HNF4A*, *HSPA1A*, and *NF-κB* genes and upregulation of the *HNF1A* gene were observed when compared to the C3A cell line. Interestingly, RT-qPCR analysis revealed the upregulation of the expression of the *HSPA1A* gene (encoding a heat-shock protein) in all analyzed cell lines after ammonium chloride treatment, which confirmed that NH_4Cl induced oxidative/nitrosative stress.

5.1.7 Semiquantitative determination of protein levels using Western blot analysis

As the genetic modification of C3A_AO_P2A cells was confirmed at both the DNA and mRNA levels, the expression of arginase 1, ornithine transcarbamylase, and albumin proteins was evaluated. The protein extracts from C3A cells and their genetically modified counterparts were prepared as described in section 4.7.11.1. As a negative control, the HOS cell line was used, and as a positive control, the human liver cell isolate was used. The results of the Western blot analysis performed for albumin protein are presented below (Figure 30).

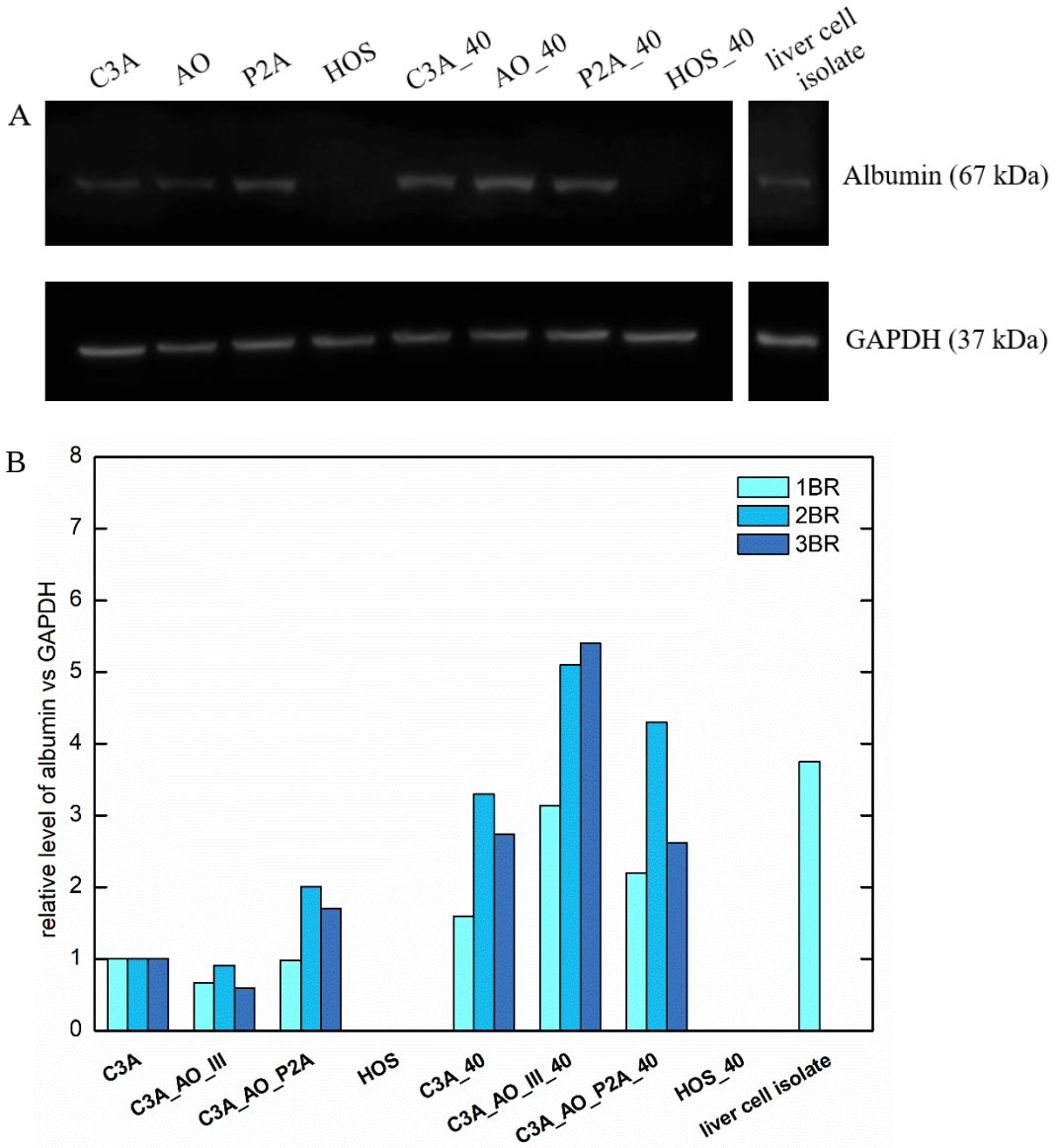

Figure 30. Determination of albumin levels in human HCC cell lysates. Western blot analysis showing the immunoreactivity levels of albumin and GAPDH in protein samples isolated from C3A, C3A_AO_III, C3A_AO_P2A, and HOS cells cultured with or without 40 mM NH_4Cl. Liver cell isolate was used as a positive control. The total amount of protein per well for each cell line was 25 µg, whereas for liver cell isolate, it was 10 µg. **A** Representative image of albumin expression in human HCC cells. Abbreviations: AO - C3A_AO_III cell line; P2A – C3A_AO_P2A cell line. **B** Graph showing the relative albumin levels normalized to the level of GAPDH. The plot presents the results for three independent biological repetitions. Abbreviations: 1BR – first biological repetition; 2BR – second biological repetition; 3BR – third biological repetition.

Figure 30A shows an exemplary image comparing albumin expression by C3A cells and their genetically modified counterparts. The obtained results indicated that the highest albumin levels in standard culture conditions were observed for C3A_AO_P2A cells. Interestingly, the performed analysis confirmed the induction of albumin expression after treatment with 40 mM ammonium chloride. In the presence of this substance, the highest amount of albumin was

observed for C3A_AO_III cells. Figure 30B shows the relative ratio between the levels of albumin and GAPDH proteins for three independent biological replicates obtained using the ImageJ tool. The results obtained for the first biological repetition revealed that in standard culture, C3A_AO_P2A cells expressed a similar amount of albumin as C3A cells, while for C3A_AO_III cells, the level of this protein was decreased. In turn, after incubation with 40 mM NH_4Cl, C3A cells were characterized by approximately 1.6-fold greater expression of the analyzed protein. Compared with untreated C3A cells, genetically modified C3A_AO_III and C3A_AO_P2A cells after exposure to NH_4Cl expressed approximately 3.1-fold and 2.2-fold more albumin, respectively. As expected, albumin expression in the HOS cell line was not detected. In the case of liver cell isolate, the level of the analyzed protein was 3.75-fold greater than that in C3A cells. As the multiple conditions for biological replicates can differ from each other, instead of averaging the results, each repetition was presented separately on the same graph (Figure 30B). Despite minor differences, all three biological repetitions showed similar tendencies in terms of albumin expression.

The results of the Western blot analysis performed for ARG1 protein are presented in the figure below (Figure 31).

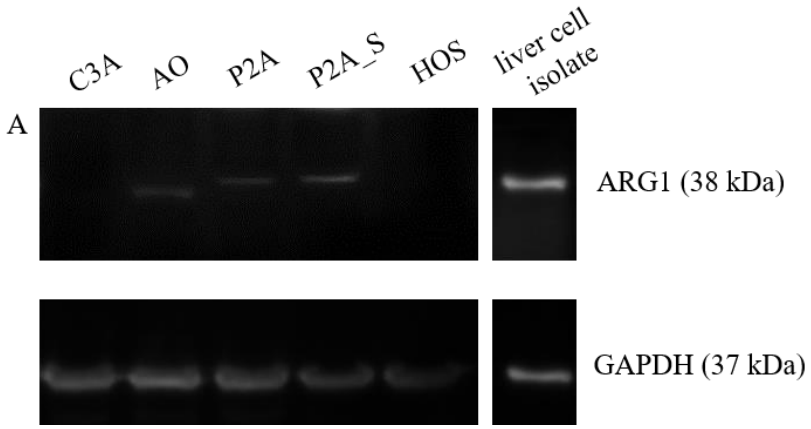

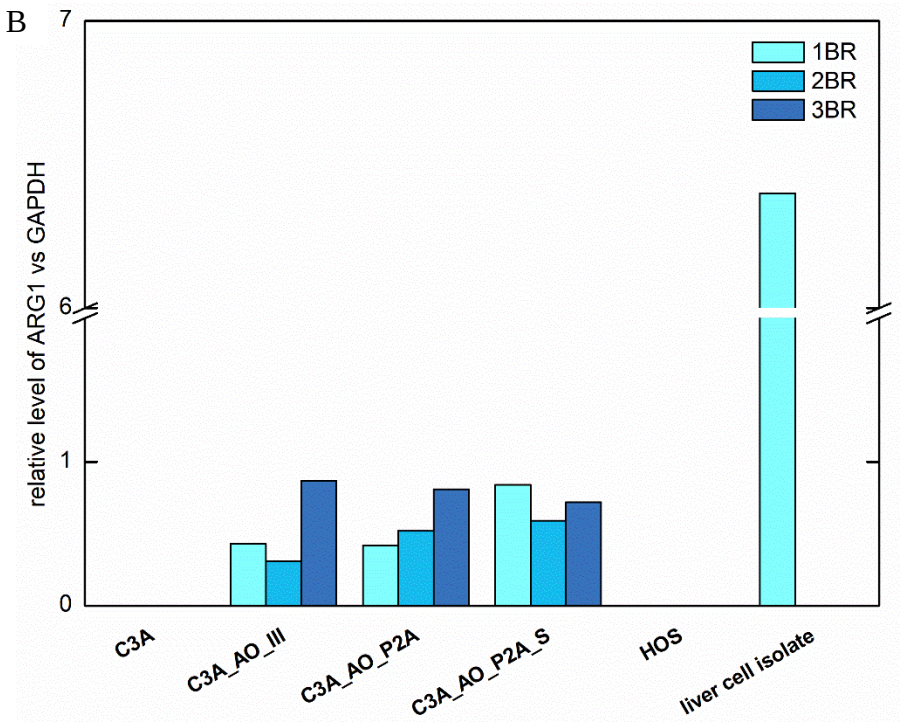

Figure 31. Determination of ARG1 levels in human HCC cell lysates. Western blot analysis showing the immunoreactivity levels of ARG1 and GAPDH in protein samples isolated from C3A, C3A_AO_III, C3A_AO_P2A, and HOS cells. Liver cell isolate was used as a positive control. The total amount of protein per well for each cell line was 75 µg, whereas for liver cell isolate, it was 10 µg. **A** Representative image of ARG1 expression in human HCC cells. Abbreviations: AO - C3A_AO_III cell line; P2A – C3A_AO_P2A cell line; P2A_S – C3A_AO_P2A cell line after additional antibiotic selection. **B** Graph showing the relative ARG1 levels normalized to the level of GAPDH. The plot presents the results for three independent biological repetitions. Abbreviations: 1BR – first biological repetition; 2BR – second biological repetition; 3BR – third biological repetition.

Figure 31A presents an exemplary image showing ARG1 expression in human HCC cells. The results revealed that the analyzed protein was not detected in extracts from the C3A and HOS cell lines. In turn, the expression of ARG1 in both genetically modified cell lines was observed. Figure 31B shows the relative ratio between ARG1 and GAPDH proteins obtained using the ImageJ tool. The results obtained for the first biological repetition indicated that the level of ARG1 protein in C3A_AO_P2A cells was similar to that in C3A_AO_III cells. Moreover, the expression of the analyzed protein in C3A_AO_P2A cells (after additional selection with puromycin) increased approximately 2-fold compared with that in C3A_AO_P2A (without additional selection) and C3A_AO_III cells. In the case of liver cell isolate, the expression of ARG1 was approximately 7-fold greater than that in C3A_AO_P2A cells (after additional antibiotic selection). The results of Western blot analysis obtained for the second and third biological repetitions are also presented in Figure 31B. Compared to the first

biological repetition, the second repetition revealed a similar trend in ARG1 expression, while the third repetition showed the opposite trend.

The results of Western blot analysis for the OTC protein are presented below (Figure 32).

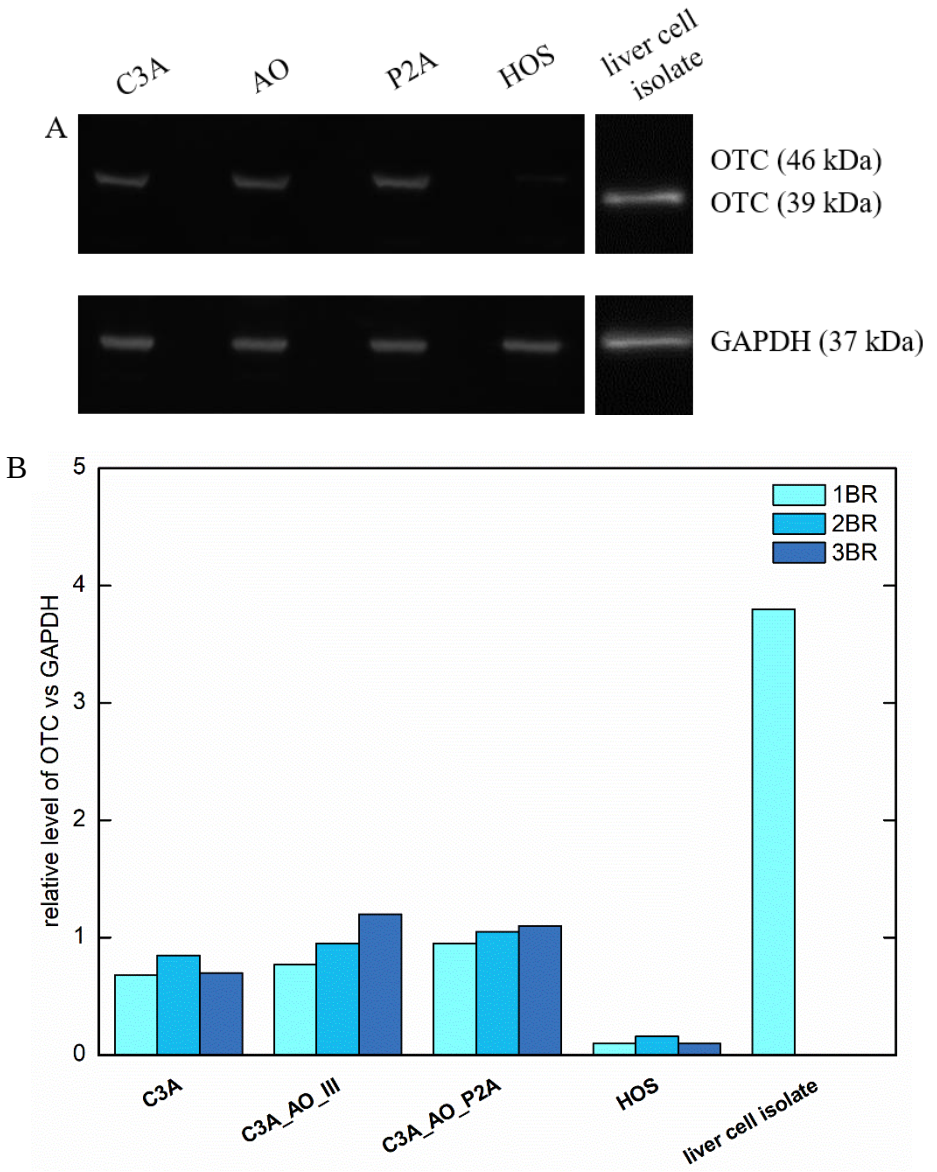

Figure 32. Determination of OTC levels in human HCC cell lysates. Western blot analysis showing the immunoreactivity levels of OTC and GAPDH in protein samples isolated from C3A, C3A_AO_III, C3A_AO_P2A, and HOS cells. Liver cell isolate was used as a positive control. The total amount of protein per well for each cell line was 40 µg, whereas for liver cell isolate, it was 10 µg. **A** Representative image of OTC expression in human HCC cells. Abbreviations: AO - C3A_AO_III cell line; P2A – C3A_AO_P2A cell line. **B** Graph showing the relative OTC levels normalized to the level of GAPDH. The plot presents the results for three independent biological repetitions. Abbreviations: 1BR – first biological repetition; 2BR – second biological repetition; 3BR – third biological repetition.

A representative image from the Western blot analysis (Figure 32A) shows the expression of the OTC protein in human HCC cell lines. The results obtained for the first

biological repetition indicated that the new generation of genetically modified cells (C3A_AO_P2A) was characterized by the highest level of the analyzed protein (Figure 32B). Compared to those in C3A_AO_III and C3A cells, the amount of OTC protein (counted using the ImageJ tool) was 1.2-fold and 1.4-fold greater, respectively. Interestingly, despite not identifying the OTC transcript in the C3A cell line, the analyzed protein was detected. In turn, in contrast to ARG1, the OTC protein is present in HOS cells, but not at the same level as it is in human hepatic cells (approximately 8-fold lower). Moreover, the results obtained for the liver cell isolate revealed approximately 4-fold greater expression of OTC than in C3A_AO_P2A cells. The results of Western blot analysis obtained for the second and third biological repetitions are also presented in Figure 32B. Compared to the first biological repetition, both repeats revealed similar trends at the OTC level.

5.2 Comparison of the performance of C3A cells and their genetically modified counterparts

5.2.1 Analysis of cell morphology using flow cytometry and microscopy

The differences in morphology between the C3A cell line and its genetically modified counterparts was evaluated using a BD FACSCanto II cytometer and an inverted phase contrast microscope Olympus CKX41. The results of the performed analysis are shown in the figure below (Figure 33).

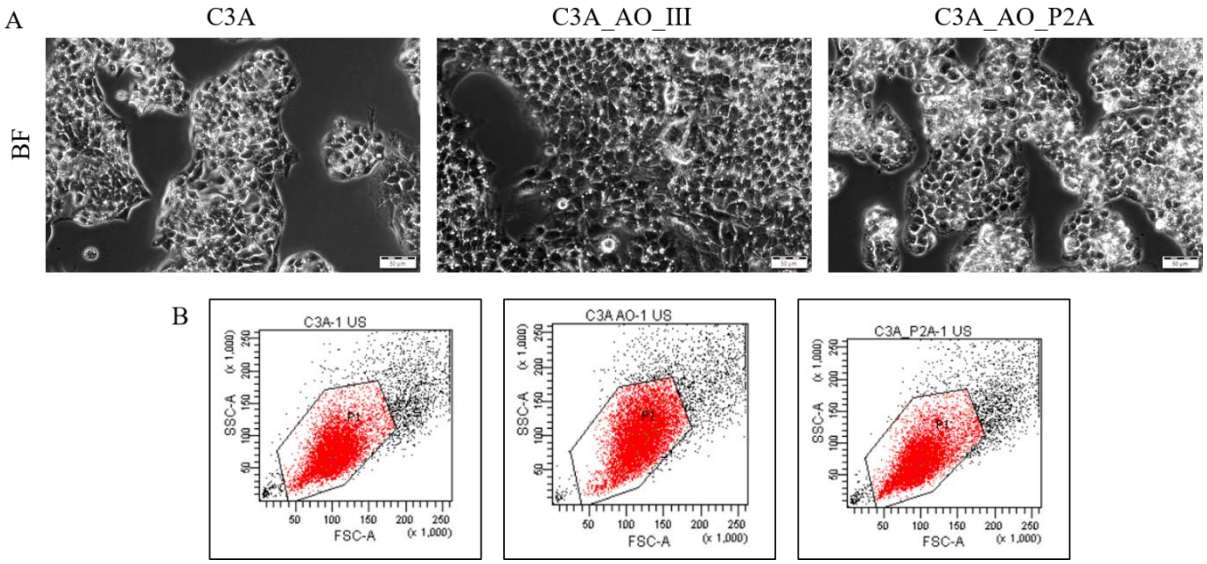

Figure 33. Determination of differences in cell morphology. A Bright field (BF) microphotographs of C3A, C3A_AO_III, and C3A_AO_P2A cells were taken using an inverted phase contrast microscope Olympus CKX41. Scale bar: 50 µm. **B** Results of cytometric analysis conducted using a BD FACSCanto II flow cytometer (side and forward scatters).

The results obtained from cytometric analysis confirmed that cells of the newly established cell line C3A_AO_P2A have similar size and granularity to those of C3A (Figure 33B). In contrast, the forward scatter (FSC) and side scatter (SSC) values for C3A_AO_III cells were greater, which indicated that the analyzed cells were larger and more grainy. These conclusions were also confirmed by microscopic observation (Figure 33A). Interestingly, the greater granularity of C3A_AO_III cells could correspond to their increased albumin production. Moreover, microphotographs of C3A and C3A_AO_P2A cells showed their tendency to aggregate and grow on each other. In contrast, the C3A_AO_III cell line formed a monolayer (Figure 33A), suggesting a stronger tendency toward adherence.

5.2.2 Determination of cell viability using the trypan blue exclusion method

The differences in cell viability in long-term culture (lasted for twelve days) between human hepatic cell lines were evaluated. Briefly, C3A cells and their genetically modified counterparts (C3A_AO_P2A and C3A_AO_III) were seeded on plates in standard culture medium. The HOS cell line (cells that are not derived from the liver) was used as a control. Every third day, the cells were detached and counted using the trypan blue exclusion method. Cell viability was expressed as the ratio between the number of live cells and their total number. More details are presented in section 4.8.2. The obtained results are shown in the figure below (Figure 34).

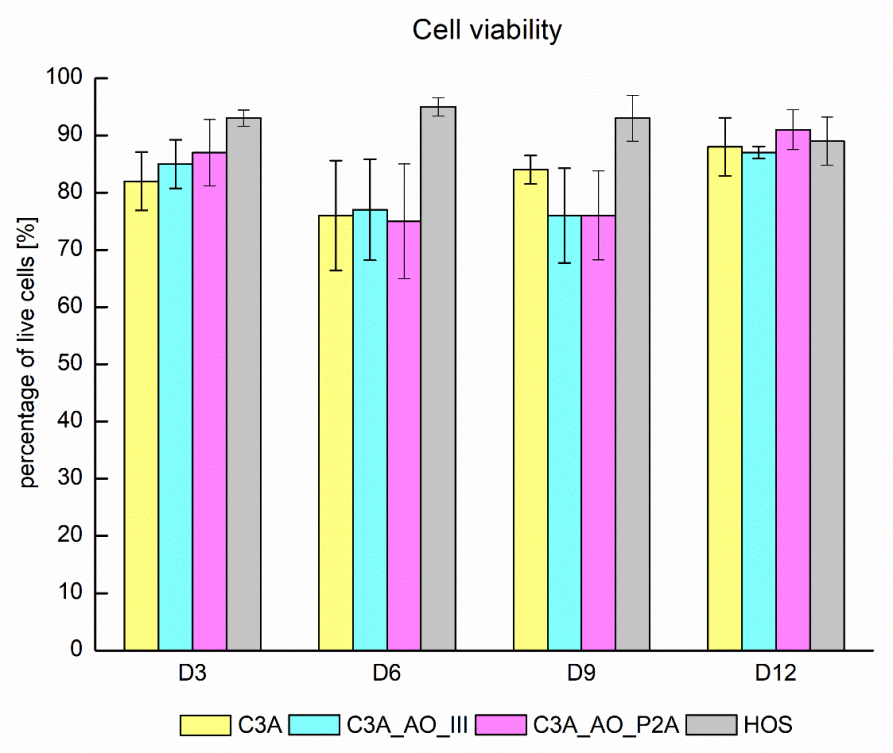

Figure 34. Determination of the viability of human HCC and HOS cells in long-term culture using the trypan blue exclusion method. C3A cells and their genetically modified counterparts, C3A_AO_III and C3A_AO_P2A, were cultured on 12-well plates for twelve days. The HOS cell line was used as a control. Every third day, the cells were detached and counted. Cell viability was expressed as the percentage of live cells. Number of biological replicates: 3. The results are presented as an average of analyzed biological replicates (with standard deviation values). Statistical analysis was conducted using MANOVA with Duncan's *post hoc* test. All obtained *p*-values (statistically significant in red) are presented in the table below. Levels of significance: *p*-value < 0.05 (*); *p*-value < 0.01 (**); *p*-value < 0.001 (***).

Duncan's *post hoc* test		D3				D6				D9				D12			
		C3A	AO	P2A	HOS	C3A	AO	P2A	HOS	C3A	AO	P2A	HOS	C3A	AO	P2A	HOS
D3	C3A		0.664097	0.411267	0.063599	0.215959	0.244413	0.196670	0.033615	0.751186	0.250595	0.241384	0.076422	0.330360	0.402718	0.135927	0.272169
D3	AO	0.664097		0.661432	0.134321	0.110678	0.140266	0.098704	0.076232	0.884048	0.132796	0.130786	0.157616	0.552421	0.643807	0.260319	0.470806
D3	P2A	0.411267	0.661432		0.259057	0.050955	0.069093	0.044632	0.158243	0.579390	0.062935	0.062613	0.296104	0.849373	0.996836	0.453276	0.743454
D3	HOS	0.063599	0.134321	0.259057		0.003539	0.005433	0.002977	0.727656	0.108108	0.004675	0.004697	0.907658	0.327108	0.262973	0.659085	0.390148
D6	C3A	0.215959	0.110678	0.050955	0.003539		0.837309	0.932182	0.001539	0.136248	0.896323	0.889049	0.004516	0.036376	0.049537	0.009976	0.027226
D6	AO	0.244413	0.140266	0.069093	0.005433	0.837309		0.782443	0.002414	0.164308	0.927460	0.937105	0.006824	0.050621	0.065276	0.014669	0.038743
D6	P2A	0.196670	0.098704	0.044632	0.002977	0.932182	0.782443		0.001283	0.122575	0.839942	0.832852	0.003815	0.031632	0.043588	0.008509	0.023524
D6	HOS	0.033615	0.076232	0.158243	0.727656	0.001539	0.002414	0.001283		0.060074	0.002060	0.002071	0.663146	0.205909	0.160964	0.459127	0.251798
D9	C3A	0.751186	0.884048	0.579390	0.108108	0.136248	0.164308	0.122575	0.060074		0.161374	0.156969	0.127982	0.477993	0.568240	0.216186	0.402784
D9	AO	0.250595	0.132796	0.062935	0.004675	0.896323	0.927460	0.839942	0.002060	0.161374		0.985083	0.005932	0.045446	0.060896	0.012882	0.034357
D9	P2A	0.241384	0.130786	0.062613	0.004697	0.889049	0.937105	0.832852	0.002071	0.156969	0.985083		0.005940	0.045397	0.059929	0.012888	0.034435
D9	HOS	0.076422	0.157616	0.296104	0.907658	0.004516	0.006824	0.003815	0.663146	0.127982	0.005932	0.005940		0.369157	0.302001	0.723179	0.434238
D12	C3A	0.330360	0.552421	0.849373	0.327108	0.036376	0.050621	0.031632	0.205909	0.477993	0.045446	0.045397	0.369157		0.855744	0.548814	0.873633
D12	AO	0.402718	0.643807	0.996836	0.262973	0.049537	0.065276	0.043588	0.160964	0.568240	0.060896	0.059929	0.302001	0.855744		0.461252	0.749640
D12	P2A	0.135927	0.260319	0.453276	0.659085	0.009976	0.014669	0.008509	0.459127	0.216186	0.012882	0.012888	0.723179	0.548814	0.461252		0.631227
D12	HOS	0.272169	0.470806	0.743454	0.390148	0.027226	0.038743	0.023524	0.251798	0.402784	0.034357	0.034435	0.434238	0.873633	0.749640	0.631227	

The obtained results indicated that C3A cells and their genetically modified counterparts were characterized by similar cell viability in long-term culture. On the third day, the percentage of live cells among human hepatic cell lines ranged from 80-85%. In turn, on the 6th and 9th days of culture, the C3A, C3A_AO_P2A, and C3A_AO_III cell lines were characterized by the same percentage of dead cells, which equaled approximately 25%. The results obtained on the last day of long-term culture indicated that the viability of human hepatic cells slightly

increased. The percentage of live cells for C3A cells and their genetically modified counterparts was similar and equaled approximately 90%. The highest cell viability was observed for the HOS cell line. They were characterized by an invariable percentage of live cells during the course of long-term culture, which equaled approximately 93%. It might be concluded that the genetic modification of C3A cells had no negative impact on their viability.

5.2.3 Determination of the metabolic activity of cells using the MTT test

Analysis of mitochondrial activity in long-term culture was performed for both genetically modified cells (C3A_AO_P2A and C3A_AO_III) and their unmodified counterparts. The HOS cell line was used as a control. The cell lines were seeded on plates in standard medium and cultured for twelve days. Every third day, their metabolic activity was determined using the MTT test. The detailed procedure is described in section 4.8.3. The results of the mitochondrial activity assay are presented in the figure below (Figure 35).

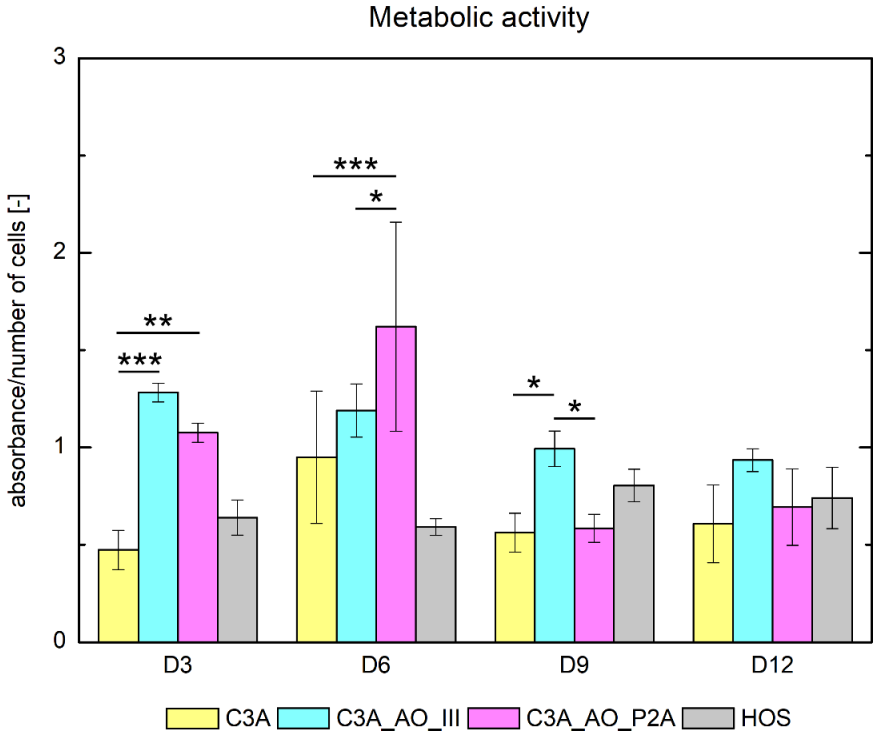

Figure 35. Determination of mitochondrial activity of HCC and HOS cells in long-term culture using the MTT assay. C3A cells and their genetically modified counterparts, C3A_AO_III and C3A_AO_P2A, were cultured on 12-well plates for twelve days. The HOS cell line was used as a control. Every third day, the metabolic activity of the cells was evaluated. The obtained results are expressed as the ratio of the absorbance to the number of living cells. Number of biological replicates: 3. The results are presented as an average of analyzed biological replicates (with standard deviation values). Statistical analysis was conducted using MANOVA with Duncan's *post hoc* test. Selected statistically significant differences were marked in the graph as follows: p-value < 0.05 (*); p-value < 0.01 (**); p-value < 0.001 (***). All obtained p-values (statistically significant in red) are presented in the table below.

Duncan's *post hoc* test		D3				D6				D9				D12			
		C3A	AO	P2A	HOS	C3A	AO	P2A	HOS	C3A	AO	P2A	HOS	C3A	AO	P2A	HOS
D3	C3A		0.000074	0.002143	0.358574	0.013210	0.000328	0.000010	0.501818	0.577092	0.007232	0.511588	0.077868	0.452181	0.015595	0.230237	0.149626
D3	AO	0.000074		0.220082	0.000932	0.064007	0.562825	0.037921	0.000460	0.000310	0.100034	0.000431	0.010431	0.000578	0.057178	0.002131	0.004239
D3	P2A	0.002143	0.220082		0.020325	0.454900	0.464371	0.002502	0.011191	0.007979	0.606150	0.010616	0.131138	0.013607	0.420697	0.039485	0.067222
D3	HOS	0.358574	0.000932	0.020325		0.089346	0.003881	0.000020	0.769019	0.660184	0.055585	0.747964	0.344101	0.837387	0.099846	0.731857	0.546537
D6	C3A	0.013210	0.064007	0.454900	0.089346		0.167626	0.000404	0.054596	0.040976	0.778415	0.052177	0.389970	0.064233	0.925851	0.153107	0.232936
D6	AO	0.000328	0.562825	0.464371	0.003881	0.167626		0.012901	0.001985	0.001369	0.242904	0.001877	0.034928	0.002466	0.152578	0.008353	0.015612
D6	P2A	0.000010	0.037921	0.002502	0.000020	0.000404	0.012901		0.000012	0.000011	0.000752	0.000012	0.000053	0.000013	0.000353	0.000022	0.000028
D6	HOS	0.501818	0.000460	0.011191	0.769019	0.054596	0.001985	0.000012		0.863111	0.032618	0.966319	0.237670	0.914080	0.062469	0.552965	0.398133
D9	C3A	0.577092	0.000310	0.007979	0.660184	0.040976	0.001369	0.000011	0.863111		0.023974	0.887273	0.189565	0.792019	0.047545	0.464650	0.326925
D9	AO	0.007232	0.100034	0.606150	0.055585	0.778415	0.242904	0.000752	0.032618	0.023974		0.031037	0.278855	0.038911	0.725367	0.099661	0.157933
D9	P2A	0.511588	0.000431	0.010616	0.747964	0.052177	0.001877	0.000012	0.966319	0.887273	0.031037		0.228842	0.888230	0.060093	0.536935	0.385017
D9	HOS	0.077868	0.010431	0.131138	0.344101	0.389970	0.034928	0.000053	0.237670	0.189565	0.278855	0.228842		0.269112	0.411414	0.509049	0.686305
D12	C3A	0.452181	0.000578	0.013607	0.837387	0.064233	0.002466	0.000013	0.914080	0.792019	0.038911	0.888230	0.269112		0.072772	0.607323	0.443031
D12	AO	0.015595	0.057178	0.420697	0.099846	0.925851	0.152578	0.000353	0.062469	0.047545	0.725367	0.060093	0.411414	0.072772		0.168208	0.250879
D12	P2A	0.230237	0.002131	0.039485	0.731857	0.153107	0.008353	0.000022	0.552965	0.464650	0.099661	0.536935	0.509049	0.607323	0.168208		0.763872
D12	HOS	0.149626	0.004239	0.067222	0.546537	0.232936	0.015612	0.000028	0.398133	0.326925	0.157933	0.385017	0.686305	0.443031	0.250879	0.763872	

The results of the performed analysis indicated that C3A_AO_III cells were characterized by the highest metabolic activity among all analyzed cell lines. On the third day of culture, C3A_AO_III cells had 1.2-fold and 2.7-fold (p-value < 0.001) greater mitochondrial activity than C3A_AO_P2A and C3A cells, respectively. The results obtained on the next day of measurements were reversed. On the 6th day of long-term culture, the most metabolically active cells were genetically modified C3A_AO_P2A. The values of the analyzed parameter were 1.4-fold (p-value = 0.013) and 1.7-fold (p-value < 0.001) greater than those of the C3A_AO_III and C3A cell lines, respectively. This could be attributed to differences in the number of living cells among three independent biological replicates. Averaged results for C3A_AO_P2A cells are characterized by large standard deviations, and therefore, it is difficult to draw the correct conclusions. In turn, on the 9th and 12th days of culture, the mitochondrial activity of the C3A and C3A_AO_P2A cell lines was similar. Again, the highest metabolic activity was observed for C3A_AO_III cells. Compared with those of C3A and C3A_AO_P2A cells, their mitochondrial activity was 1.8-fold (p-value = 0.024) and 1.7-fold (p-value = 0.031) greater (on the 9th day) and 1.5-fold and 1.3-fold greater (on the 12th day), respectively. Interestingly, the obtained results indicated that the HOS cell line was characterized by rather similar metabolic activity during the course of long-term culture.

5.2.4 Determination of metabolic activity - glucose consumption

Metabolic activity in long-term culture was also evaluated by measuring glucose consumption in the conditioned culture medium. The C3A, C3A_AO_P2A, C3A_AO_III, and HOS cell lines were cultured for twelve days. Every third day, the media samples were collected, and the glucose concentration was determined using a commercial kit. The detailed protocol is presented in section 4.8.4. The obtained results are shown in the figure below (Figure 36).

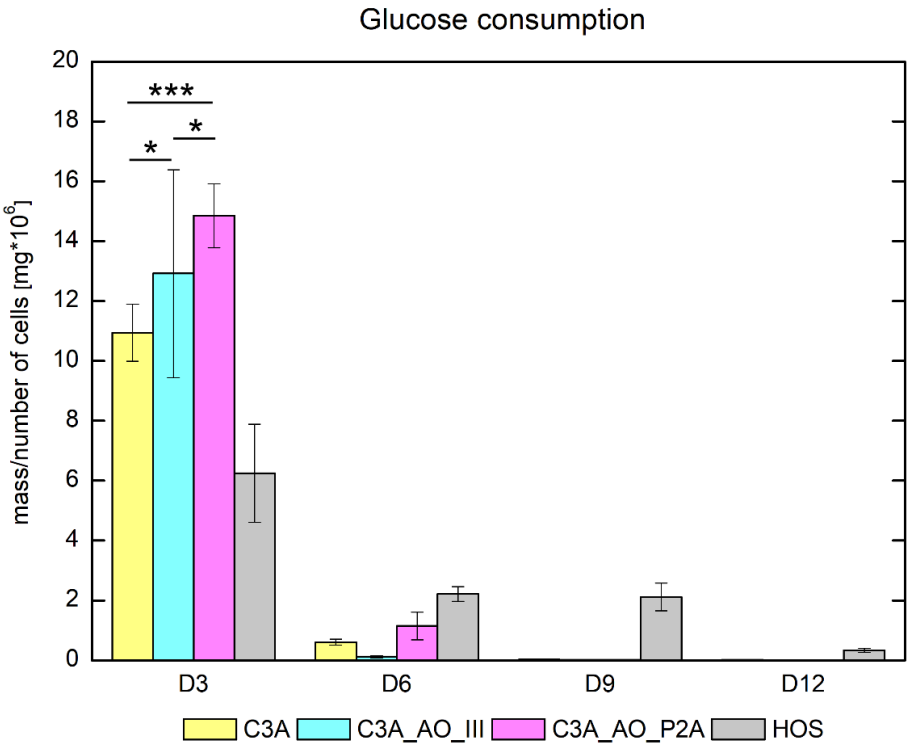

Figure 36. Evaluation of glucose consumption by HCC and HOS cells in long-term culture. C3A cells and their genetically modified counterparts, C3A_AO_III and C3A_AO_P2A, were cultured on 12-well plates for twelve days. The HOS cell line was used as a control. Every third day, the medium samples were collected, and the glucose content was measured using a commercial kit. The obtained results are expressed as the ratio of glucose mass per number of living cells. Number of biological replicates: 3. The results are presented as an average of analyzed biological replicates (with standard deviation values). Statistical analysis was conducted using MANOVA with Duncan's *post hoc* test. Selected statistically significant differences were marked in the graph as follows: *p*-value < 0.05 (*); *p*-value < 0.01 (**); *p*-value < 0.001 (***). All obtained *p*-values (statistically significant in red) are presented in the table below.

Duncan's *post hoc* test		D3				D6				D9				D12			
		C3A	AO	P2A	HOS	C3A	AO	P2A	HOS	C3A	AO	P2A	HOS	C3A	AO	P2A	HOS
D3	C3A		0.025789	0.000141	0.000137	0.000026	0.000020	0.000033	0.000062	0.000018	0.000018	0.000012	0.000055	0.000018	0.000011	0.000012	0.000023
D3	AO	0.025789		0.029832	0.000062	0.000023	0.000018	0.000026	0.000055	0.000018	0.000018	0.000012	0.000033	0.000012	0.000010	0.000011	0.000020
D3	P2A	0.000141	0.029832		0.000055	0.000020	0.000018	0.000023	0.000033	0.000018	0.000012	0.000011	0.000026	0.000012	0.000010	0.000010	0.000018
D3	HOS	0.000137	0.000062	0.000055		0.000033	0.000023	0.000056	0.000169	0.000020	0.000018	0.000019	0.000097	0.000018	0.000012	0.000012	0.000026
D6	C3A	0.000026	0.000023	0.000020	0.000033		0.596525	0.525892	0.090454	0.540939	0.547063	0.555083	0.099963	0.552443	0.551647	0.552133	0.756819
D6	AO	0.000020	0.000018	0.000018	0.000023	0.596525		0.278571	0.034975	0.911341	0.913481	0.916959	0.040856	0.918385	0.907048	0.910153	0.798850
D6	P2A	0.000033	0.000026	0.000023	0.000056	0.525892	0.278571		0.243417	0.247296	0.252966	0.260852	0.260364	0.257904	0.260340	0.259988	0.376127
D6	HOS	0.000062	0.000055	0.000033	0.000169	0.090454	0.034975	0.243417		0.029578	0.030878	0.033157	0.909909	0.032163	0.033950	0.033442	0.054415
D9	C3A	0.000018	0.000018	0.000018	0.000020	0.540939	0.911341	0.247296	0.029578		0.996124	0.993667	0.035107	0.995657	0.982799	0.986298	0.731242
D9	AO	0.000018	0.000018	0.000012	0.000018	0.547063	0.913481	0.252966	0.030878	0.996124		0.997114	0.036995	0.999091	0.986118	0.989656	0.737126
D9	P2A	0.000012	0.000012	0.000011	0.000019	0.555083	0.916959	0.260852	0.033157	0.993667	0.997114		0.040130	0.997811	0.988879	0.991533	0.745628
D9	HOS	0.000055	0.000033	0.000026	0.000097	0.099963	0.040856	0.260364	0.909909	0.035107	0.036995	0.040130		0.038783	0.041311	0.040604	0.062073
D12	C3A	0.000018	0.000012	0.000012	0.000018	0.552443	0.918385	0.257904	0.032163	0.995657	0.999091	0.997811	0.038783		0.986904	0.990517	0.742547
D12	AO	0.000011	0.000010	0.000010	0.000012	0.551647	0.907048	0.260340	0.033950	0.982799	0.986118	0.988879	0.041311	0.986904		0.995920	0.738905
D12	P2A	0.000012	0.000011	0.000010	0.000012	0.552133	0.910153	0.259988	0.033442	0.986298	0.989656	0.991533	0.040604	0.990517	0.995920		0.741385
D12	HOS	0.000023	0.000020	0.000018	0.000026	0.756819	0.798850	0.376127	0.054415	0.731242	0.737126	0.745628	0.062073	0.742547	0.738905	0.741385	

Glucose consumption reflects the metabolic activity and proliferation rate of cells. The lower the glucose content in the medium was, the greater the cell proliferation rate. The results of the analysis revealed that C3A_AO_III cells were characterized by the fastest glucose consumption during long-term culture among the tested human hepatic cell lines as clearly shown on day 6. On the 3rd day, C3A cells were characterized by the lowest amount of glucose in the medium. The obtained values were 1.4-fold (*p*-value = 0.03) and 1.2-fold

(*p*-value < 0.001) lower than those for the C3A_AO_III and C3A_AO_P2A cell lines, respectively. Nevertheless, the large standard deviation between three independent biological repetitions obtained for C3A_AO_III cells indicated that it is difficult to compare the analyzed cell lines. On the 6th day of culture, C3A_AO_III cells consumed 1.8-fold and 11-fold more glucose than C3A and C3A_AO_P2A cells, respectively. On the other days of measurements, a lack of glucose in the culture medium was observed for all human hepatic cell lines. Interestingly, HOS cells were characterized by the fastest glucose consumption on the 3rd day. However, on the 6th day, the proliferation rate decreased and remained invariable on the 9th day of culture. Only on the last day of the long-term culture, the amount of glucose consumed by HOS cells was close to the value obtained for human hepatic cells. In summary, the results of the performed analysis are consistent with the results obtained using the MTT test and confirmed that the most metabolically active cell line is the genetically modified C3A_AO_III.

5.2.5 Determination of albumin production using ELISA

Comparison of albumin secretion by C3A cells and their genetically modified counterparts in long-term culture was performed using a quantitative immunoenzymatic technique. The HOS cell line was used as a negative control. The cell lines were seeded on plates in standard medium and cultured for twelve days. Every third day, the media samples were collected, and the albumin content was measured. More details are described in section 4.8.5. The results of the analysis are presented in the figure below (Figure 37).

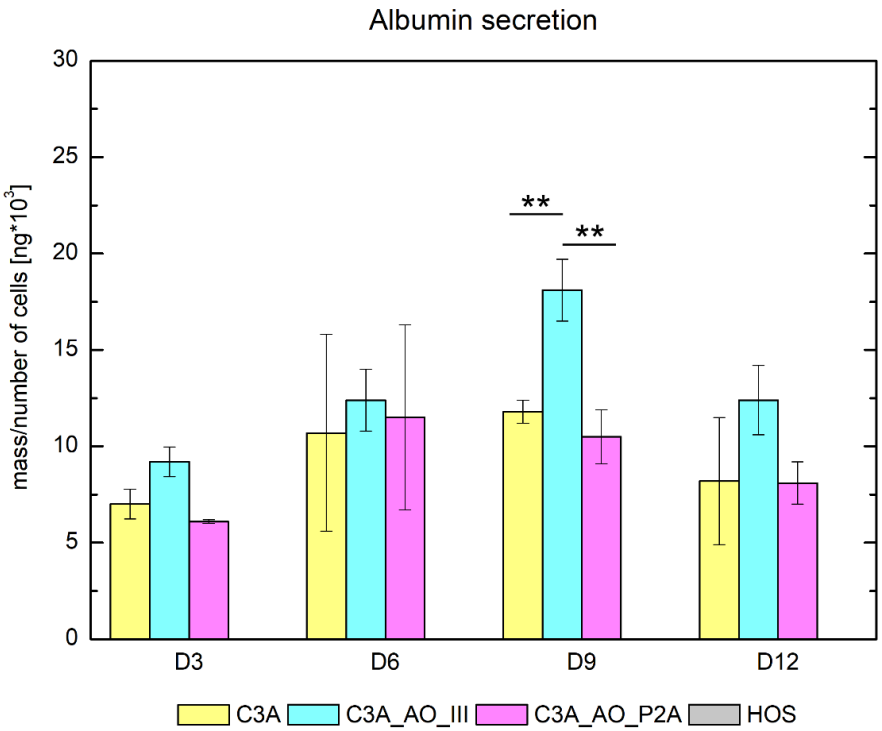

Figure 37. Determination of albumin secretion by human HCC and HOS cells in long-term culture using ELISA. C3A cells and their genetically modified counterparts, C3A_AO_III and C3A_AO_P2A, were cultured on 12-well plates for twelve days. The HOS cell line was used as a control. Every third day, the medium samples were collected, and albumin production was measured. The obtained results are expressed as the ratio of the albumin mass to the number of living cells. Number of biological replicates: 3. The results are presented as an average of analyzed biological replicates (with standard deviation values). Statistical analysis was conducted using MANOVA with Duncan's *post hoc* test. Selected statistically significant differences were marked in graph as follows: *p*-value < 0.05 (*); *p*-value < 0.01 (**); *p*-value < 0.001 (***). All obtained *p*-values (statistically significant in red) are presented in the table below.

Duncan's *post hoc* test		D3			D6			D9			D12		
		C3A	AO	P2A	C3A	AO	P2A	C3A	AO	P2A	C3A	AO	P2A
D3	C3A		0.324377	0.654185	0.123119	0.030906	0.064684	0.051608	0.000068	0.138304	0.597406	0.030814	0.614595
D3	AO	0.324377		0.175610	0.514717	0.187020	0.325196	0.276099	0.000634	0.551169	0.598638	0.186407	0.582570
D3	P2A	0.654185	0.175610		0.058502	0.012912	0.028748	0.022485	0.000029	0.066680	0.360207	0.012899	0.372355
D6	C3A	0.123119	0.514717	0.058502		0.454181	0.694184	0.613761	0.002774	0.923123	0.269947	0.453715	0.258119
D6	AO	0.030906	0.187020	0.012912	0.454181		0.684797	0.773285	0.012210	0.413166	0.081598	0.985648	0.076171
D6	P2A	0.064684	0.325196	0.028748	0.694184	0.684797		0.885772	0.006220	0.645115	0.155470	0.682591	0.147393
D9	C3A	0.051608	0.276099	0.022485	0.613761	0.773285	0.885772		0.007550	0.564949	0.128291	0.773432	0.120521
D9	AO	0.000068	0.000634	0.000029	0.002774	0.012210	0.006220	0.007550		0.002429	0.000199	0.009784	0.000185
D9	P2A	0.138304	0.551169	0.066680	0.923123	0.413166	0.645115	0.564949	0.002429		0.293319	0.410424	0.285219
D12	C3A	0.597406	0.598638	0.360207	0.269947	0.081598	0.155470	0.128291	0.000199	0.293319		0.081599	0.953998
D12	AO	0.030814	0.186407	0.012899	0.453715	0.985648	0.682591	0.773432	0.009784	0.410424	0.081599		0.075702
D12	P2A	0.614595	0.582570	0.372355	0.258119	0.076171	0.147393	0.120521	0.000185	0.285219	0.953998	0.075702	

Measurements of albumin secretion in long-term culture indicated that, unlike in cell lysates (Figure 30), genetically modified C3A_AO_III cells produced the greatest amount of the analyzed protein. In turn, genetically modified C3A_AO_P2A cells and their parental C3A cells were characterized by similar levels of synthetized albumin. On the third day of culture, C3A_AO_III cells produced 1.3-fold and 1.5-fold more albumin than C3A and C3A_AO_P2A cells, respectively. In turn, on the 6th day, genetically modified and unmodified cell lines were

characterized by similar secretion of the analyzed protein. This could be attributed to the differences in the number of living cells among three independent biological replicates. Averaged results for C3A and C3A_AO_P2A cells are characterized by high standard deviation, and therefore, it is difficult to make any comparison. The results obtained on the next days revealed that C3A_AO_III outperformed the other two human hepatic cell lines in terms of albumin secretion. The production of the analyzed protein by C3A_AO_III cells on the 9th day was 1.5-fold (*p*-value = 0.008) and 1.7-fold (*p*-value = 0.002) greater than that by C3A and C3A_AO_P2A cells, respectively. Similar results were obtained on the 12th day of long-term culture. As expected, albumin production by the HOS cell line was not observed.

5.2.6 Evaluation of albumin production using immunofluorescence technique

The evaluation of albumin synthesis by C3A cell lines and their genetically modified counterparts was also conducted using immunofluorescence. For this experiment, cells were prepared as described in section 4.5. The microscopic analysis was performed using an inverted fluorescence microscope Olympus IX-71. The obtained results are shown in the figure below (Figure 38).

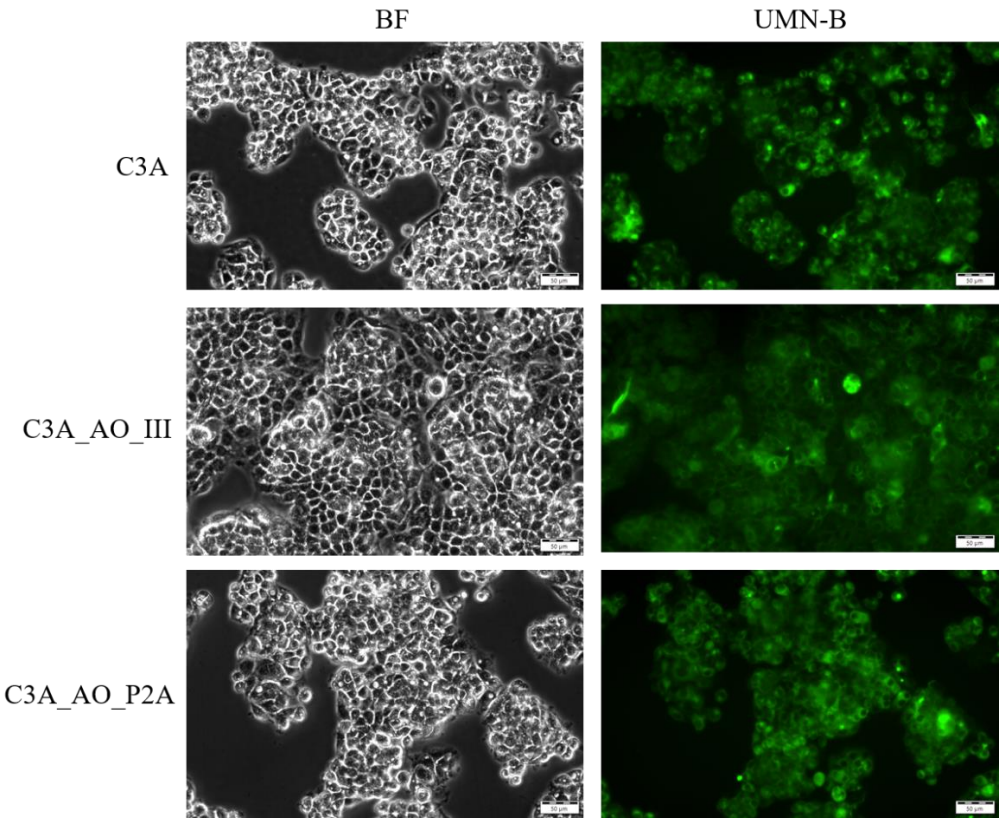

Figure 38. Comparison of albumin secretion by human HCC cell lines. Microphotographs of C3A, C3A_AO_III, and C3A_AO_P2A cells were taken with a bright-field (BF) illumination and UMN-B filter (for FITC fluorophore visualization) using an Olympus IX-71 fluorescence microscope. Scale bar: 50 μm.

Cell staining with an anti-human albumin antibody conjugated with FITC indicated that each of the analyzed cell lines produced this protein. However, the possible differences in albumin secretion between human HCC cells are difficult to distinguish.

5.2.7 Evaluation of marker protein expression using flow cytometry

Comparison of the expression of liver-specific marker proteins, such as albumin, A1AT, and CD54, in human hepatic cell lines was conducted using a BD FACSCanto II flow cytometer. The cells were prepared for cytometric analysis as described in section 4.6. The obtained results are presented in the figure below (Figure 39).

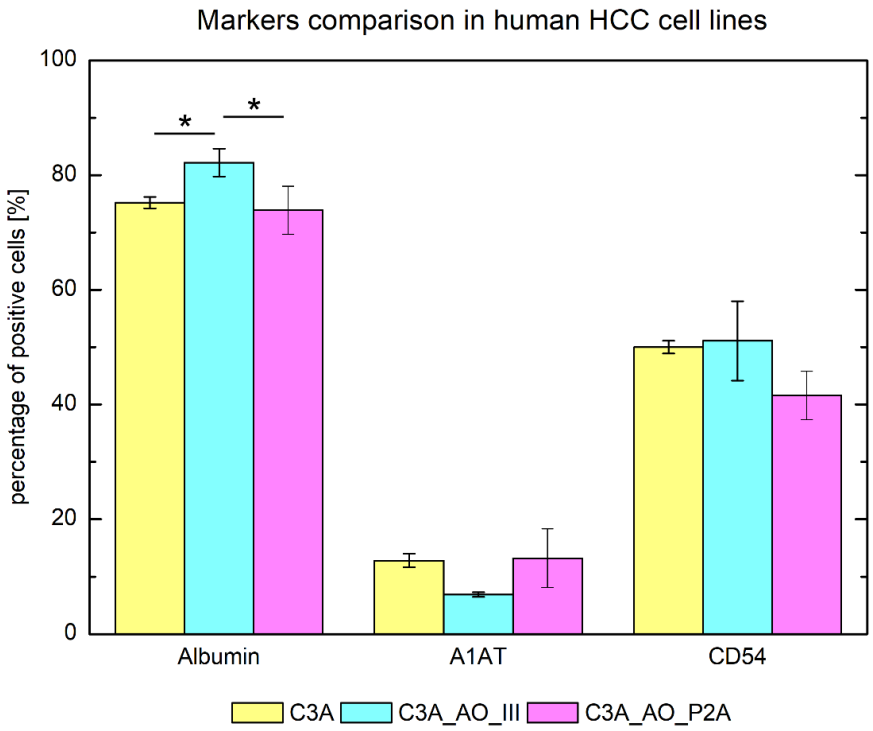

Figure 39. Analysis of liver-specific marker protein expression in C3A cells and their genetically modified counterparts. Comparison of the percentage of albumin-, A1AT-, and CD54-positive cells was conducted using cytometric analysis. Number of biological replicates: 3. The results are presented as an average of analyzed biological replicates (with standard deviation values). Statistical analysis was conducted using one-way ANOVA with Duncan's *post hoc* test. Statistically significant differences were marked as follows: p-value < 0.05 (*); p-value < 0.01 (**); p-value < 0.001 (***). Abbreviations: A1AT - alpha-1- antitrypsin; CD54 – cluster of differentiation 54 responsible for intercellular adhesion.

Cytometric analysis revealed that the percentage of albumin-positive cells was similar in the C3A and C3A_AO_P2A cell lines and equal to 75.2% (± 1.0) and 73.9% (± 4.2), respectively. In the case of the C3A_AO_III cell line, this value was greater – 82.2% (± 2.4) and was statistically significant in comparison to C3A (p-value = 0.045) and C3A_AO_P2A cells (p-value = 0.028). The obtained results indicated that the lowest percentage of

A1AT-posivite cells was received for C3A_AO_III cells and equaled 6.9% (± 0.4). In turn, for C3A and C3A_AO_P2A cells, these values were similar and equaled 12.8% (± 1.2) and 13.2% (± 5.1), respectively. The percentage of CD54-positive cells in the genetically modified cell line - C3A_AO_P2A was the lowest and equaled 41.6% (± 4.2). This parameter was similar for C3A and C3A_AO_III cells and equaled 50% (± 1.1) and 51.1% (± 6.9), respectively. The differences in A1AT and CD54 production between the analyzed cell lines were not statistically significant.

5.2.8 Determination of cell membrane polarization

To determine the level of cellular membrane polarization, the number of apical vacuoles, which are precursors of *bile canaliculi*, was evaluated. The comparison between C3A cells and their genetically modified counterparts was conducted using a CytoPainter F-Actin Staining kit and an inverted fluorescence microscope Olympus IX-71. The cells were prepared as described in section 4.5 and stained with phalloidin conjugated with TRITC (for fibrillar actin visualization) and DAPI. The obtained results are shown in the figure below (Figure 40).

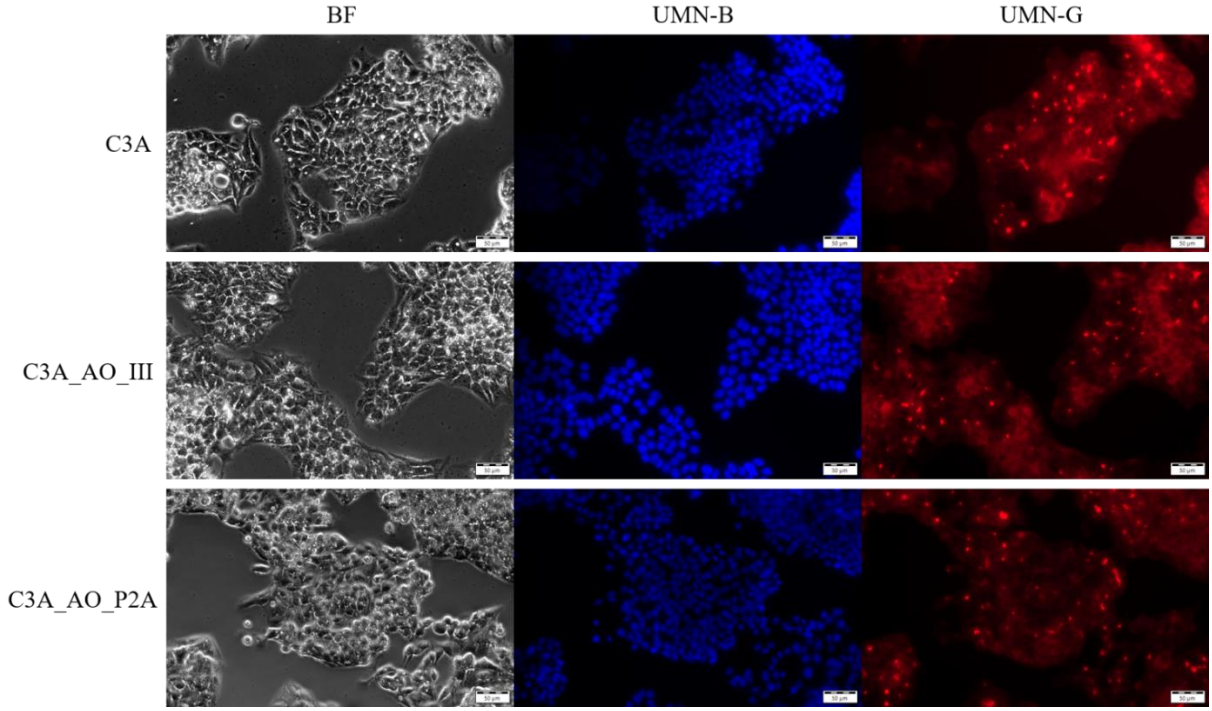

Figure 40. Formation of apical vacuoles by human hepatic cell lines. Microphotographs of C3A, C3A_AO_III, and C3A_AO_P2A cells were taken with a bright-field (BF) illumination, UMN-B filter for DAPI, and UMN-G filter for phalloidin conjugated with TRITC using an Olympus IX-71 fluorescence microscope. Apical vacuoles are present at the junctions of two or more cells (red dots). Scale bar: 50 µm.

To compare the level of membrane polarization between genetically modified and unmodified C3A cells, apical vacuoles and nuclei from microphotographs were counted. Cell membrane polarization was expressed as the ratio between the number of *bile canaliculi* precursors and the number of nuclei. The obtained results are presented below (Figure 41).

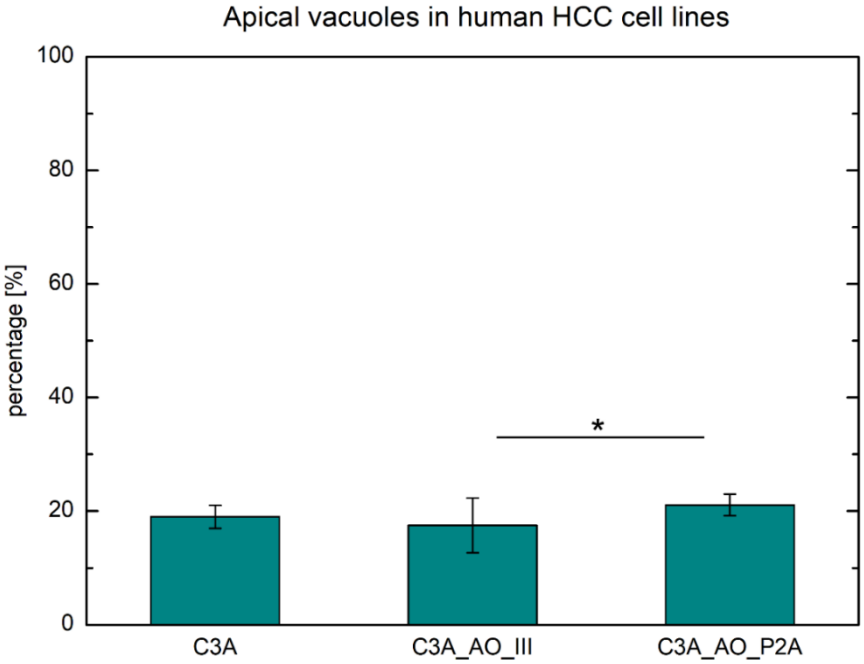

Figure 41. Determination of cell membrane polarization in human hepatic cell lines. Number of biological replicates: 9. The results are presented as an average of analyzed biological replicates (with standard deviation values). Statistical analysis was conducted using one-way ANOVA with Duncan's *post hoc* test. Statistically significant differences were marked as follows: *p*-value < 0.05 (*); *p*-value < 0.01 (**); *p*-value < 0.001 (***).

The percentage of apical vacuoles for nontransduced C3A cells was 19% (± 2). The highest value was obtained for C3A_AO_P2A and equaled 21.1% (± 1.9). This value was significantly greater than that received for C3A_AO_III cells - 17.5% (± 4.8) (*p*-value = 0.036).

5.2.9 Determination of the enzymatic activity of arginase 1 (ARG1)

Although the production of arginase 1 (ARG1) by genetically modified cells (C3A_AO_III and C3A_AO_P2A) was confirmed using Western blot analysis, this protein can be unfunctional. Therefore, as ARG1 participates in the urea cycle and catalyzes the conversion of arginine into ornithine, the enzymatic activity of this enzyme was measured using an Arginase Activity Assay kit. The obtained results are shown in the figure below (Figure 42).

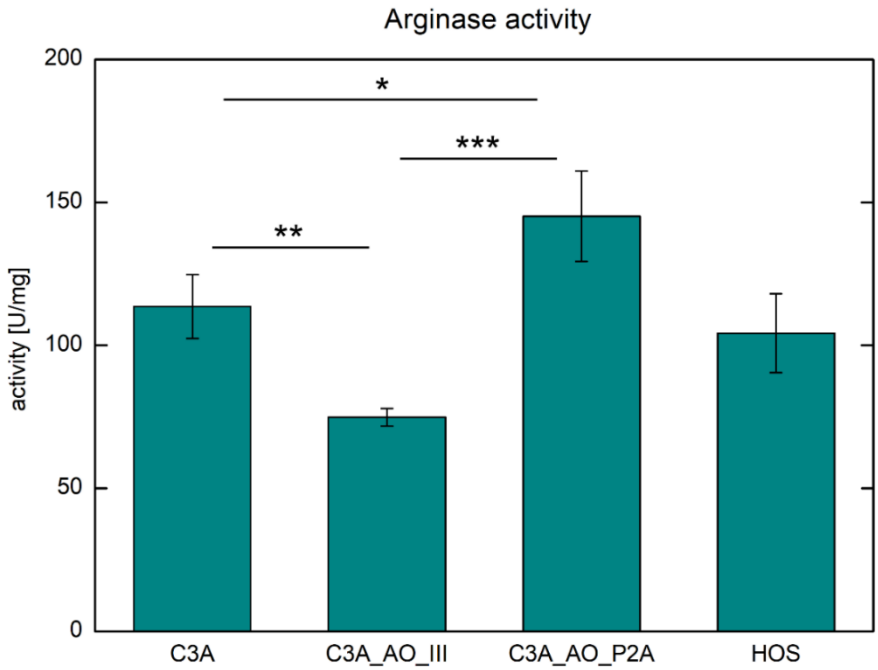

Figure 42. Determination of arginase activity. Measurements of enzymatic activity in cell lysates were conducted for the C3A cell line and its genetically modified counterparts (C3A_AO_III and C3A_AO_P2A). The HOS cell line was used as the negative control. Number of biological replicates: 3. The results are presented as an average of analyzed biological replicates (with standard deviation values). Statistical analysis was conducted using one-way ANOVA with Duncan's *post hoc* test. Statistically significant differences were marked as follows: *p*-value < 0.05 (*); *p*-value < 0.01 (**); *p*-value < 0.001 (***).

First, it is worth mentioning that this assay measured the enzymatic activity of both arginases – 1 and 2 (both isoforms take part in the conversion of arginine into urea and ornithine). The presented results indicated that the highest enzymatic activity of arginases among human hepatic cells was obtained for C3A_AO_P2A cells, and the lowest was received for the C3A_AO_III cell line. The value of enzymatic activity in C3A_AO_P2A cells was 1.2-fold (*p*-value = 0.012) and 2-fold (*p*-value = 0.005) greater than that in C3A and C3A_AO_III cells, respectively., The HOS cell line was selected as a negative control for the experiment. The results obtained for these cells showed that the enzymatic activity of both arginases was similar to the activity received for C3A cells. Importantly, considering that ARG1 was not detected in C3A and HOS cells by Western blot analysis, the results obtained for these cell lines reflect the activity of arginase 2. As a positive control for the experiment, liver cell isolate was used (data not shown in the graph). The enzymatic activity of arginases for the liver cell isolate was approximately 60-fold greater than the values obtained for all analyzed cell lines. In summary, although C3A_AO_P2A cells were characterized by the highest activity of arginases, no significant increase in enzymatic activity was observed in comparison to their parental cells. It was expected that after genetic modification this value would be much greater.

5.2.10 Determination of enzymatic activity of ornithine transcarbamylase (OTC)

As mentioned above, although the production of ornithine transcarbamylase (OTC) by genetically modified cells (C3A_AO_III and C3A_AO_P2A) was confirmed using Western blot analysis, the functionality of the analyzed protein should be evaluated. As the OTC enzyme catalyzes the conversion of ornithine into citrulline in the presence of carbamoyl phosphate, its enzymatic activity during this reaction was measured using a biochemical assay. More details are presented in section 4.8.10. The obtained calibration curve for citrulline is shown in the figure below (Figure 43).

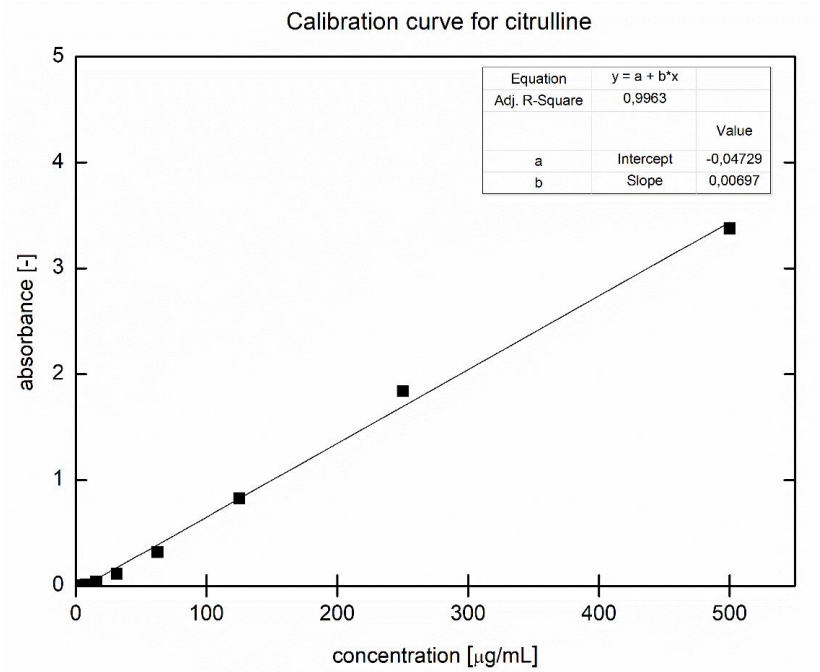

Figure 43. Calibration curve for citrulline, a product of the enzymatic reaction catalyzed by ornithine transcarbamylase (OTC).

The concentration of citrulline was calculated based on the equation from the calibration curve. For liver cell isolate, the activity of the OTC enzyme was detected and equaled 31.9 μg/mL. However, the enzymatic activity of OTC for all analyzed human hepatic cell lines was not calculated because the absorbance values obtained for citrulline were below the limit of quantification and, in some cases, were below the limit of detection. Thus, it might be concluded that the enzymatic activity of OTC in cell lysates from all analyzed human hepatic cell lines was too low to be detected using this method.

5.2.11 Determination of urea production

The evaluation whether restoration of the urea cycle in the newly obtained cell line - C3A_AO_P2A was successful was performed using a QuantiChrom Urea Assay Kit. To determine the production of total urea, measurements were conducted both in culture media and in cell lysates. More details are presented in section 4.8.11. The results of total urea production are shown below (Figure 44).

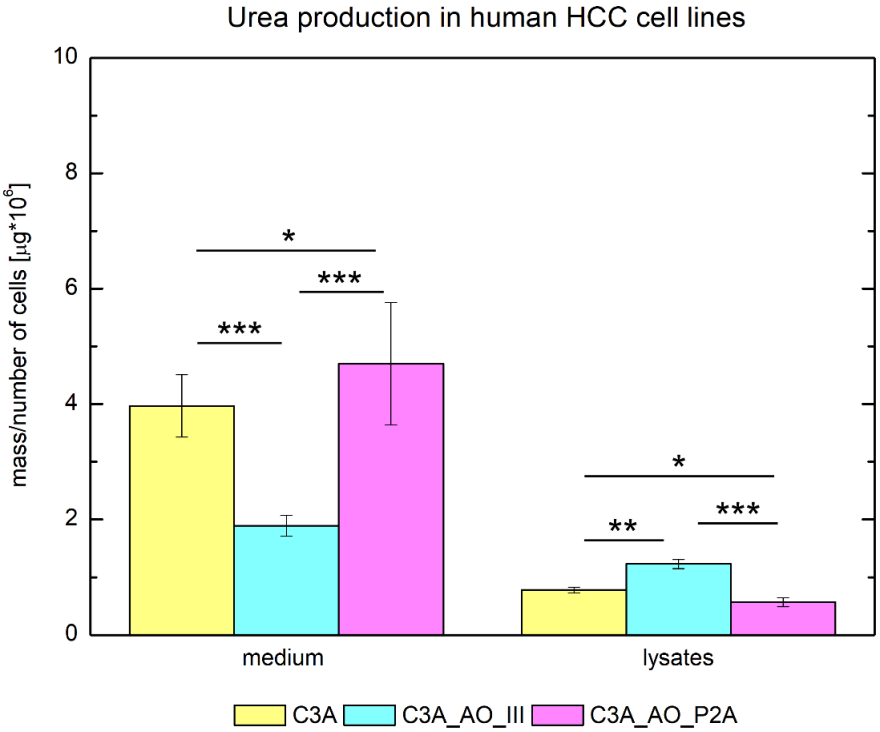

Figure 44. Evaluation of urea production by human HCC cells. C3A cells and their genetically modified counterparts were cultured for one day and then treated with 40 mM ammonium chloride for 24 hours. Next, the medium was replaced with fresh medium supplemented with a reduced amount of FBS, after which the cells were cultured for another 24 hours. The next day, samples were collected. Urea production was determined both in culture media and in cell lysates using a QuantiChrom Urea Assay Kit. Number of biological replicates: 3. The results are presented as an average of analyzed biological replicates (with standard deviation values). Statistical analysis was conducted using one-way ANOVA with Duncan's *post hoc* test. Selected statistically significant differences were marked in the graph as follows: p-value < 0.05 (*); p-value < 0.01 (**); p-value < 0.001 (***).

The measurements of urea production in media samples revealed that the newly established C3A_AO_P2A cell line was characterized by the highest production of the analyzed metabolite. The results obtained for nontransduced C3A cells and for genetically modified C3A_AO_III were 1.2-fold (p-value = 0.047) and 2.5-fold (p-value < 0.001) lower, respectively, than those obtained for C3A_AO_P2A cells. Interestingly, the urea measurements in cell lysates revealed quite different results. The greatest amount of urea was produced by

C3A_AO_III cells. Compared to C3A_AO_III cells, the results obtained for C3A and C3A_AO_P2A cells were 1.5-fold (p-value < 0.001) and 2.1-fold (p-value < 0.001) lower, respectively. A similar situation was shown previously (Pluta *et al.*, 2020). Nevertheless, after summing the mass of urea measured both in medium and in cell lysates, C3A_AO_P2A cells were characterized by the highest production of total urea, while C3A_AO_III was characterized by the lowest. Comparison of these results to measurements conducted for liver cell isolate (data not shown) revealed that, in the case of cell lysates, HCC cells were characterized by approximately 20-fold lower urea production.

5.2.12 Resistance to ammonia toxicity - determination of the effect of oxidative/nitrosative stress induced by ammonium chloride on human hepatic cells

The evaluation whether the introduction of additional copies of the h*ARG1* and h*OTC* genes into the C3A genome affects the cell resistance to nitrosative/oxidative stress was performed. The impact of oxidative/nitrosative stress on cell viability, metabolic activity, and albumin synthesis was determined. The results of the mentioned experiments are presented in the section below.

5.2.12.1 Determination of metabolic activity using the MTT test

To evaluate the cytotoxic effect of ammonium chloride on human hepatic cells, metabolic activity was measured using the MTT test. Treatment with different concentrations of this substance (20 mM, 40 mM, and 60 mM) was conducted for 24 hours. More details are presented in section 4.8.12.1. The results of the mitochondrial activity assay are shown in the figure below (Figure 45).

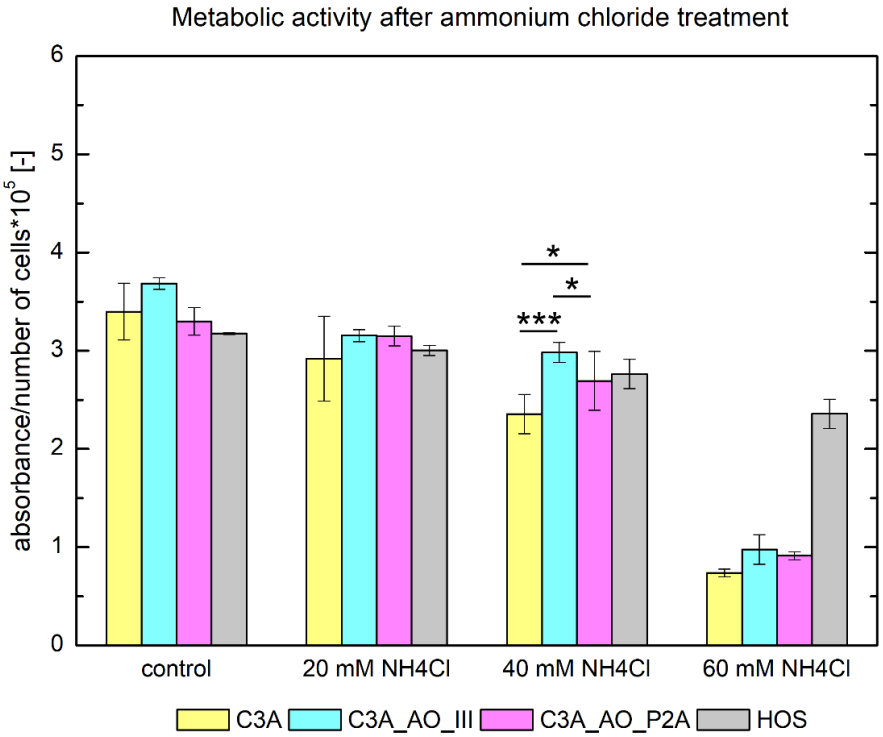

Figure 45. Evaluation of mitochondrial activity in human hepatic cells after treatment with different concentrations of ammonium chloride using MTT test. C3A cells and their genetically modified counterparts were treated with 20 mM, 40 mM, and 60 mM ammonium chloride for 24 hours. The HOS cell line was used as a control. After this time, the metabolic activity was measured. Number of biological replicates: 4. The results are presented as an average of analyzed biological replicates (with standard deviation values). Statistical analysis was conducted using MANOVA with Duncan's *post hoc* test. Selected statistically significant differences were marked in the graph as follows: *p*-value < 0.05 (*); *p*-value < 0.01 (**); *p*-value < 0.001 (***). All obtained *p*-values (statistically significant in red) are presented in the table below.

Duncan's		C				20 mM				40 mM				60 mM			
post hoc test		C3A	AO	P2A	HOS	C3A	AO	P2A	HOS	C3A	AO	P2A	HOS	C3A	AO	P2A	HOS
C	C3A		0.027402	0.428644	0.111100	0.001398	0.082630	0.084565	0.006676	0.000011	0.004947	0.000021	0.000046	0.000011	0.000011	0.000011	0.000018
C	AO	0.027402		0.004832	0.000454	0.000018	0.000283	0.000289	0.000029	0.000011	0.000022	0.000018	0.000017	0.000010	0.000011	0.000011	0.000011
C	P2A	0.428644	0.004832		0.363699	0.010960	0.291178	0.295061	0.040217	0.000018	0.031569	0.000083	0.000380	0.000011	0.000011	0.000011	0.000017
C	HOS	0.111100	0.000454	0.363699		0.075813	0.828644	0.815689	0.203194	0.000017	0.168983	0.001112	0.004775	0.000011	0.000018	0.000011	0.000018
20 mM	C3A	0.001398	0.000018	0.010960	0.075813		0.106527	0.104622	0.551526	0.000141	0.627644	0.095659	0.220844	0.000019	0.000029	0.000023	0.000143
20 mM	AO	0.082630	0.000283	0.291178	0.828644	0.106527		0.973914	0.264074	0.000018	0.225062	0.001892	0.007653	0.000011	0.000017	0.000018	0.000019
20 mM	P2A	0.084565	0.000289	0.295061	0.815689	0.104622	0.973914		0.248624	0.000019	0.219832	0.001864	0.007411	0.000018	0.000017	0.000017	0.000023
20 mM	HOS	0.006676	0.000029	0.040217	0.203194	0.551526	0.264074	0.248624		0.000041	0.880084	0.032439	0.091385	0.000017	0.000019	0.000017	0.000043
40 mM	C3A	0.000011	0.000011	0.000018	0.000017	0.000141	0.000018	0.000019	0.000041		0.000052	0.013748	0.003948	0.000056	0.000117	0.000063	0.989632
40 mM	AO	0.004947	0.000022	0.031569	0.168983	0.627644	0.225062	0.219832	0.880084	0.000052		0.040383	0.108394	0.000017	0.000023	0.000019	0.000057
40 mM	P2A	0.000021	0.000018	0.000083	0.001112	0.095659	0.001892	0.001864	0.032439	0.013748	0.040383		0.582032	0.000029	0.000056	0.000033	0.010725
40 mM	HOS	0.000046	0.000017	0.000380	0.004775	0.220844	0.007653	0.007411	0.091385	0.003948	0.108394	0.582032		0.000023	0.000033	0.000029	0.003311
60 mM	C3A	0.000011	0.000010	0.000011	0.000011	0.000019	0.000011	0.000018	0.000017	0.000056	0.000017	0.000029	0.000023		0.119538	0.178389	0.000033
60 mM	AO	0.000011	0.000011	0.000011	0.000018	0.000029	0.000017	0.000017	0.000019	0.000117	0.000023	0.000056	0.000033	0.119538		0.757906	0.000063
60 mM	P2A	0.000011	0.000011	0.000011	0.000011	0.000023	0.000018	0.000017	0.000017	0.000063	0.000019	0.000033	0.000029	0.178389	0.757906		0.000056
60 mM	HOS	0.000018	0.000011	0.000017	0.000018	0.000143	0.000019	0.000023	0.000043	0.989632	0.000057	0.010725	0.003311	0.000033	0.000063	0.000056	

The results revealed that the presence of ammonium chloride exerted a negative effect on mitochondrial activity, which decreased with increasing concentrations of this toxic substance. The strongest impact was observed for nontransduced C3A cells. In turn, the genetically modified cell lines were characterized by greater metabolic activity after exposure to NH_4Cl and their values were similar when comparing different concentrations of the analyzed substances. The results of this analysis indicated that mitochondrial activity in the

HOS cell line was not strongly affected by ammonium chloride, and the effect was not as visible as it was for human hepatic cells, especially after treatment with 60 mM NH_4Cl.

5.2.12.2 Determination of cell viability using the trypan blue exclusion method

The cytotoxic effect of ammonium chloride on cell viability was evaluated for C3A cells and their genetically modified counterparts. These cell lines (and the HOS cell line as a control) were cultured for three days and then treated for 24 hours with two different concentrations of ammonium chloride (20 mM and 40 mM). After that, the cells were detached and counted. The detailed procedure is presented in section 4.8.12.2. The obtained results are shown in the figure below (Figure 46).

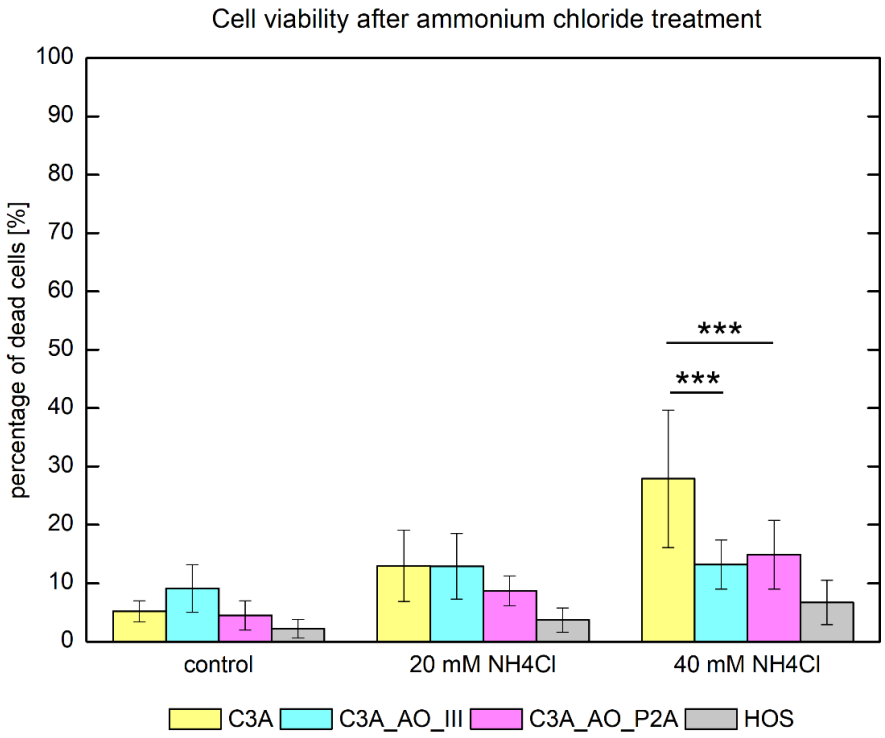

Figure 46. Determination of cell viability after treatment with different concentrations of ammonium chloride using the trypan blue exclusion method. The human HCC cell line - C3A and its genetically modified counterparts (C3A_AO_III and C3A_AO_P2A) were treated with 20 mM and 40 mM ammonium chloride for 24 hours. The HOS cells were used as a control. After this time, analysis of cell viability was performed. Live and dead cells were counted, and the cell viability was expressed as the percentage of dead cells. Number of biological replicates: 6. The results are presented as an average of analyzed biological replicates (with standard deviation values). Statistical analysis was conducted using MANOVA with Duncan's *post hoc* test. Selected statistically significant differences were marked in the graph as follows: p-value < 0.05 (*); p-value < 0.01 (**); p-value < 0.001 (***). All obtained p-values (statistically significant in red) are presented in the table below.

Duncan's *post hoc* test		C				20 mM				40 mM			
		C3A	AO	P2A	HOS	C3A	AO	P2A	HOS	C3A	AO	P2A	HOS
C	C3A		0.239730	0.803710	0.362897	0.021928	0.021836	0.274416	0.634500	0.000018	0.020929	0.005322	0.628210
C	AO	0.239730		0.171499	0.046749	0.217392	0.204258	0.892240	0.116198	0.000027	0.215750	0.086410	0.443718
C	P2A	0.803710	0.171499		0.476266	0.013050	0.013202	0.201094	0.795040	0.000017	0.012290	0.002866	0.492855
C	HOS	0.362897	0.046749	0.476266		0.001910	0.001981	0.058041	0.616119	0.000011	0.001751	0.000326	0.188048
20 mM	C3A	0.021928	0.217392	0.013050	0.001910		0.967926	0.189504	0.007225	0.000060	0.957007	0.560767	0.058523
20 mM	AO	0.021836	0.204258	0.013202	0.001981	0.967926		0.185938	0.007401	0.000042	0.930314	0.551346	0.057533
20 mM	P2A	0.274416	0.892240	0.201094	0.058041	0.189504	0.185938		0.139317	0.000022	0.184287	0.071198	0.495120
20 mM	HOS	0.634500	0.116198	0.795040	0.616119	0.007225	0.007401	0.139317		0.000017	0.006723	0.001436	0.371127
40 mM	C3A	0.000018	0.000027	0.000017	0.000011	0.000060	0.000042	0.000022	0.000017		0.000066	0.000152	0.000019
40 mM	AO	0.020929	0.215750	0.012290	0.001751	0.957007	0.930314	0.184287	0.006723	0.000066		0.570396	0.056562
40 mM	P2A	0.005322	0.086410	0.002866	0.000326	0.560767	0.551346	0.071198	0.001436	0.000152	0.570396		0.017149
40 mM	HOS	0.628210	0.443718	0.492855	0.188048	0.058523	0.057533	0.495120	0.371127	0.000019	0.056562	0.017149	

The results of the performed analysis revealed that ammonium chloride treatment affects cell viability. In the case of genetically modified cells, the percentage of dead cells increased approximately 2-3-fold in the presence of different concentrations of NH_4Cl. In turn, the viability of C3A cells was more strongly affected by the analyzed substance. The results obtained for nontransduced cells showed approximately 3-fold and 6-fold increases in the percentage of dead cells during treatment with 20 mM and 40 mM ammonium chloride, respectively. A moderate effect on cell viability was observed for the HOS cell line. This observation is consistent with the results of the MTT test. In summary, genetically modified C3A_AO_III and C3A_AO_P2A cells seemed to be more resistant to nitrosative/oxidative stress. This effect is especially visible for a 40 mM solution of ammonium chloride.

5.2.12.3 Determination of cell viability using cytometric analysis

The cytotoxic effect of ammonium chloride on cell viability was additionally evaluated using flow cytometry. The experiment was performed in the same way as described above. After 24 hours of treatment, the percentage of dead cells after the addition of propidium iodide (PI) was determined using a BD FACSCanto II flow cytometer. More details are given in section 4.8.12.3. The results of the conducted cytometric analysis are shown in the figure below (Figure 47).

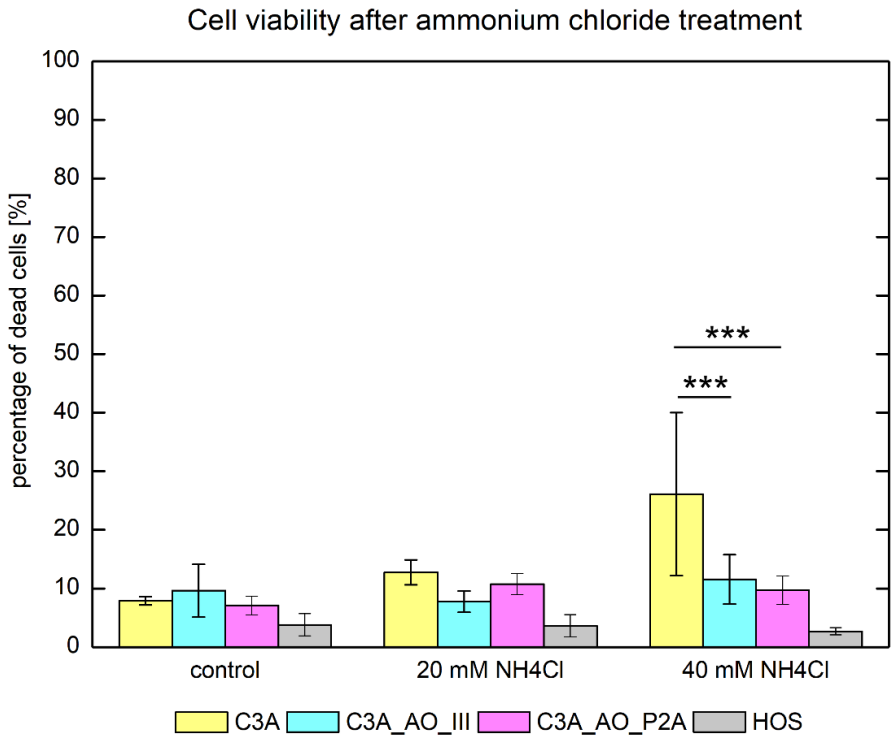

Figure 47. Determination of cell viability after treatment with different concentrations of ammonium chloride using flow cytometry. The human HCC cell line - C3A and its genetically modified counterparts (C3A_AO_III and C3A_AO_P2A) were treated with 20 mM and 40 mM ammonium chloride for 24 hours. The HOS cells were used as a control. Cell viability was determined using PI staining and a BD FACSCanto II flow cytometer and expressed as the percentage of dead cells. Number of biological replicates: 4. The results are presented as an average of analyzed biological replicates (with standard deviation values). Statistical analysis was conducted using MANOVA with Duncan's *post hoc* test. Selected statistically significant differences were marked in the graph as follows: *p*-value < 0.05 (*); *p*-value < 0.01 (**); *p*-value < 0.001 (***). All obtained *p*-values (statistically significant in red) are presented in the table below.

Duncan's *post hoc* test		C				20 mM				40 mM			
		C3A	AO	P2A	HOS	C3A	AO	P2A	HOS	C3A	AO	P2A	HOS
C	C3A		0.596689	0.826035	0.265600	0.200825	0.969899	0.431779	0.256681	0.000029	0.323203	0.599654	0.174623
C	AO	0.596689		0.489871	0,120579	0.403891	0.594736	0.749568	0.115817	0.000059	0.593799	0.975934	0.073356
C	P2A	0.826035	0.489871		0.320715	0.147247	0.843986	0.337584	0.325016	0.000021	0.245743	0.483116	0.229486
C	HOS	0.265600	0,120579	0.320715		0.023442	0.263638	0.072332	0.957809	0.000017	0.046788	0.120413	0.754979
20 mM	C3A	0.200825	0.403891	0.147247	0.023442		0.194980	0.570449	0.021816	0.000347	0.722123	0.408191	0.012180
20 mM	AO	0.969899	0.594736	0.843986	0.263638	0.194980		0.422918	0.259803	0.000026	0.315009	0.589080	0.178026
20 mM	P2A	0.431779	0.749568	0.337584	0.072332	0.570449	0.422918		0.068215	0.000119	0.802764	0.756353	0.041273
20 mM	HOS	0.256681	0.115817	0.325016	0.957809	0.021816	0.259803	0.068215		0.000018	0.043828	0.114384	0.779460
40 mM	C3A	0.000029	0.000059	0.000021	0.000017	0.000347	0.000026	0.000119	0.000018		0.000173	0.000065	0.000012
40 mM	AO	0.323203	0.593799	0.245743	0.046788	0.722123	0.315009	0.802764	0.043828	0.000173		0.599654	0.025642
40 mM	P2A	0.599654	0.975934	0.483116	0.120413	0.408191	0.589080	0.756353	0.114384	0.000065	0.599654		0.072159
40 mM	HOS	0.174623	0.073356	0.229486	0.754979	0.012180	0.178026	0.041273	0.779460	0.000012	0.025642	0.072159	

Cytometric analysis revealed a similar tendency in cell viability to the results obtained using the trypan blue exclusion method. The greatest effect on the percentage of dead cells after exposure to different concentrations of ammonium chloride was observed for C3A cells. The analyzed parameter increased more than 3-fold after treatment with 20 mM and 40 mM NH_4Cl. In turn, the viability of the genetically modified cells was not strongly affected. The percentage

of dead cells increased less than 2-fold after exposure to two different concentrations of ammonium chloride. The obtained results confirmed that the C3A_AO_III and C3A_AO_P2A cell lines are more resistant to nitrosative/oxidative stress. Similarly, in the case of HOS cells, a moderate effect on cell viability was observed.

5.2.12.4 Determination of albumin production using ELISA

The influence of ammonium chloride treatment on albumin secretion was evaluated in C3A cells and their genetically modified counterparts. Human hepatic cells (and the HOS cell line as a negative control) were cultured under standard conditions and then treated for 24 hours with 20 mM or 40 mM NH_4Cl. Albumin production in collected media samples was measured quantitatively using ELISA. More details are presented in section 4.8.12.4. The obtained results are shown in the figure below (Figure 48).

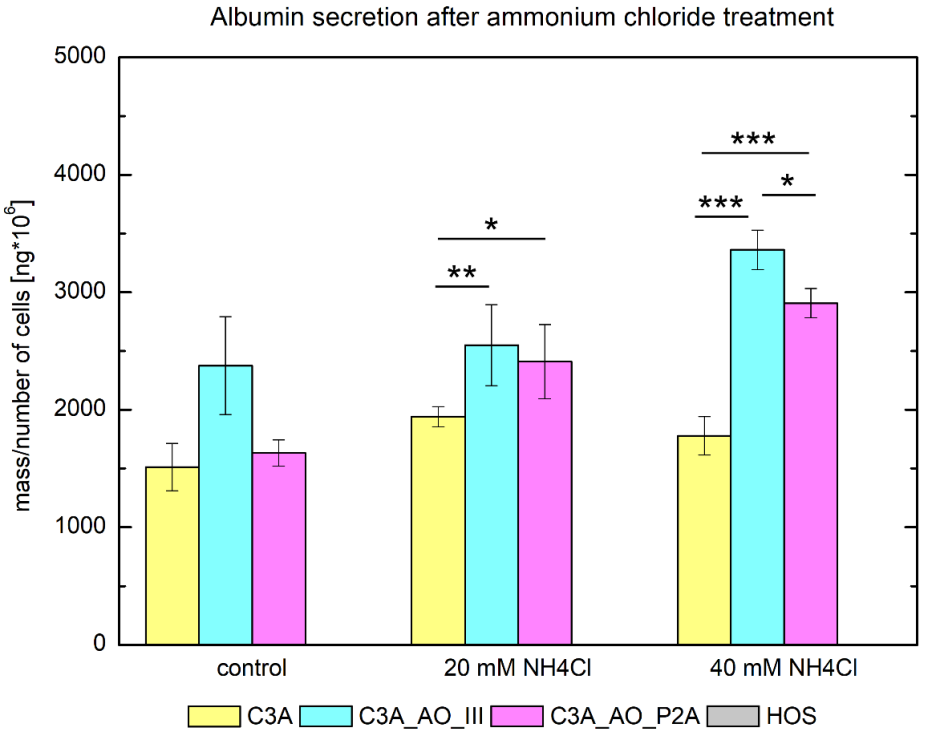

Figure 48. Evaluation of albumin secretion by human HCC cells after treatment with different concentrations of ammonium chloride using ELISA. C3A cells and their genetically modified counterparts were treated with 20 mM and 40 mM ammonium chloride for 24 hours. The HOS cell line was used as a negative control. At the end of the experiment, the medium samples were collected, and the amount of produced albumin was measured. Number of biological replicates: 3. The results are presented as an average of analyzed biological replicates (with standard deviation values). Statistical analysis was conducted using MANOVA with Duncan's *post hoc* test. Selected statistically significant differences were marked in the graph as follows: p-value < 0.05 (*); p-value < 0.01 (**); p-value < 0.001 (***). All obtained p-values (statistically significant in red) are presented in the table below.

Duncan's *post hoc* test		C			20 mM			40 mM		
		C3A	AO	P2A	C3A	AO	P2A	C3A	AO	P2A
C	C3A		0.000746	0.553660	0.059322	0.000163	0.000582	0.217083	0.000022	0.000027
C	AO	0.000746		0.002305	0.040396	0.417532	0.863943	0.009344	0.000221	0.022101
C	P2A	0.553660	0.002305		0.152942	0.000476	0.001834	0.465189	0.000023	0.000036
20 mM	C3A	0.059322	0.040396	0.152942		0.009940	0.035388	0.419486	0.000033	0.000265
20 mM	AO	0.000163	0.417532	0.000476	0.009940		0.490633	0.002006	0.000927	0.086065
20 mM	P2A	0.000582	0.863943	0.001834	0.035388	0.490633		0.007704	0.000283	0.027021
40 mM	C3A	0.217083	0.009344	0.465189	0.419486	0.002006	0.007704		0.000028	0.000074
40 mM	AO	0.000022	0.000221	0.000023	0.000033	0.000927	0.000283	0.000028		0.033067
40 mM	P2A	0.000027	0.022101	0.000036	0.000265	0.086065	0.027021	0.000074	0.033067	

Measurements of albumin secretion indicated that ammonium chloride induced synthesis of the analyzed protein by human hepatic cells. Both genetically modified cell lines produced more albumin than their parental C3A cells. The highest secretion of this protein was observed for C3A_AO_III cells. Under standard conditions, albumin production by C3A_AO_III cells was 1.6-fold (p-value < 0.001) and 1.5-fold (p-value = 0.002) greater than that by C3A and C3A_AO_P2A cells, respectively. After treatment with 20 mM ammonium chloride, the synthesis of analyzed protein by both genetically modified cell lines was similar and the differences were not statistically significant. In turn, albumin production by C3A cells was 1.3-fold (p-value = 0.009) and 1.2-fold (p-value = 0.035) lower than that by C3A_AO_III and C3A_AO_P2A cells, respectively. Finally, after treatment with 40 mM ammonium chloride, C3A_AO_III cells were characterized by 1.9-fold (p-value < 0.001) and 1.2-fold (p-value = 0.033) greater secretion of the analyzed protein than C3A and C3A_AO_P2A cells, respectively. This tendency is similar to the Western blot results in cell lysates (Figure 30). As expected, albumin production by the HOS cell line was not observed.

5.3 Construction of hollow fiber bioreactors – the heart of the system for dynamic cell culture

5.3.1 Characterization of the polysulfone capillary membrane

For the construction of hollow fiber bioreactors, semipermeable polysulfone capillary membranes were selected and purchased from Vestergaard Frandsen. Their characteristics are presented in the section below.

5.3.2 Determination of polysulfone membrane structure using scanning electron microscopy (SEM)

Evaluation of the structure (porosity, pore size etc.) of the chosen polysulfone membrane was conducted using scanning electron microscopy (SEM). Details concerning

probe preparation are described in section 4.9.1.1. The obtained results are presented in the figure below (Figure 49).

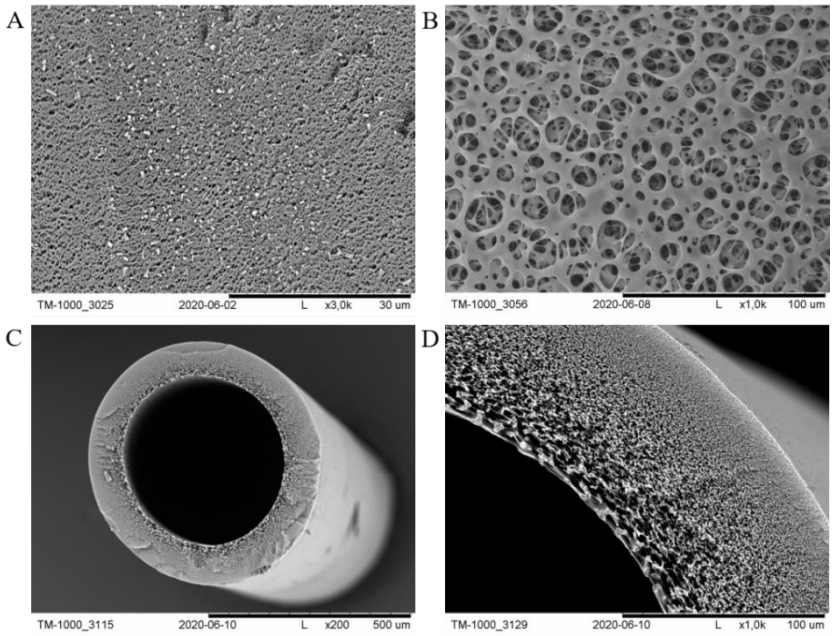

Figure 49. Determination of polysulfone capillary membrane structure. **A** SEM image of the external structure of the membrane. **B** SEM image of the internal structure of the membrane. **C** SEM image of the cross-section of the membrane – showing the internal and external diameter. **D** SEM image of the cross-section of the membrane showing the porosity of membrane. Scale bars: 30 μm (A), 100 μm (B; D), and 500 μm (C).

The results of SEM analysis revealed that the structure of the membrane varied. The pores are larger closer to the intracapillary space of the membrane. The size of the pores of the external structure was evaluated for comparison with the value of this parameter reported by the producer (0.2 μm). One hundred measurements were made and presented as the average. The obtained results indicated that the pore size of the polysulfone membrane was 0.26 μm (± 0.08). Moreover, the diameter and internal diameter were dimensioned. The results of the conducted measurements were as follows: 588 μm (± 24) and 400 μm (± 38.5).

5.3.3 Evaluation of the wettability of the polysulfone membrane

Determination of the wettability of the polysulfone membrane was essential because the hydrophilic surfaces promote cell attachment. Therefore, measurements of the contact angle between the water droplet and the analyzed surface were performed using a DSA25 Krüss goniometer. More details are described in section 4.9.1.2. A picture of the shape of the water droplet after deposition on the polysulfone membrane is presented below (Figure 50).

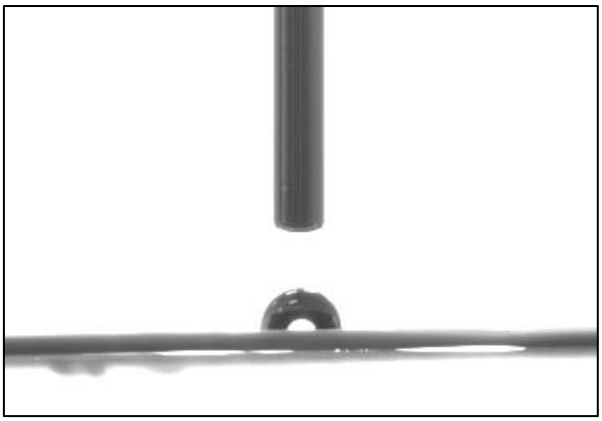

Figure 50. Evaluation of the wettability of the polysulfone membrane. Exemplary photograph from contact angle measurements obtained after settling the water droplet on the analyzed surface. The photograph was taken by a camera in a DSA25 Krüss goniometer.

The contact angle was measured for different areas of the membrane and expressed as an average. The value of the analyzed parameter was 60.2° (± 4.7). For hydrophilic materials, the contact angle should be less than 90°, and for hydrophobic materials, the contact angle should be greater than 90°. Therefore, the obtained results indicated the hydrophilicity of the tested surface.

5.3.4 Evaluation of the biocompatibility of the polysulfone membrane

Because polysulfone capillary membranes were chosen as a surface for hepatic cell growth in hollow fiber bioreactors, their biocompatibility was determined. Evaluation of their potential cytotoxic effects on cell viability and metabolic activity was performed. Moreover, the impact of the presence of this material on the secretion of albumin (a crucial hepatic marker) was evaluated. For cytotoxicity analysis, the C3A_DsRed2 cell line (stably overexpressing the fluorescent protein DsRed2) was chosen. The results of the experiments are presented in the section below.

5.3.4.1 Determination of the cytotoxic effect of capillary membranes on cells – MTT test

The cytotoxic influence of the polysulfone membrane on the metabolism of human hepatic cells was evaluated using the MTT test. Details concerning the entire procedure are described in section 4.9.2.1. The results of MTT assay conducted for each culture variant are presented in the figure below (Figure 51).

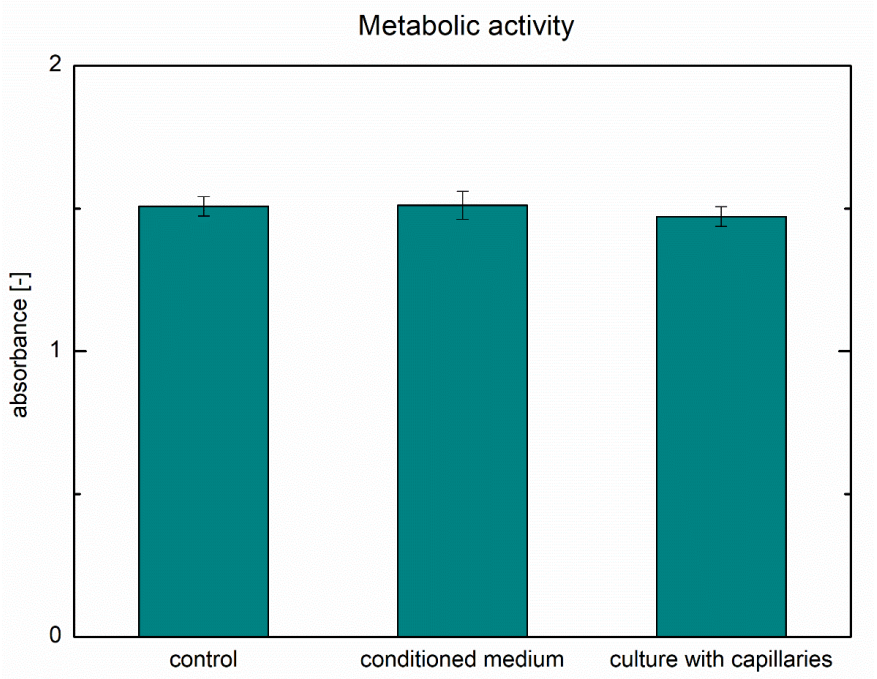

Figure 51. Evaluation of the cytotoxic effect of the polysulfone membrane on a human hepatic cell line using the MTT assay. To determine metabolic activity, C3A_DsRed2 cells were cultured with 10 capillaries (each with a length of 1 cm) or with conditioned medium (medium after daily incubation with capillaries). The control cells were cultured in standard medium. After three days, the mitochondrial activity was measured. Number of biological replicates: 6. The results are presented as an average of analyzed biological replicates (with standard deviation values). Statistical analysis was conducted using one-way ANOVA with Duncan's *post hoc* test. Levels of significance: p-value < 0.05 (*); p-value < 0.01 (**); p-value < 0.001 (***).

The obtained results indicated that there were no differences in mitochondrial activity between C3A_DsRed2 cells cultured in standard conditions and in the presence of capillary membranes. Therefore, polysulfone material did not exert an impact on the metabolic activity of hepatic cells.

5.3.4.2 Determination of the effect of capillary membranes on cell viability and morphology

The differences in cell morphology after culturing in the presence of the polysulfone capillary membrane were evaluated using an Olympus IX-71 fluorescence microscope. The C3A_DsRed2 cell line was cultured with capillaries or in conditioned medium (obtained after daily incubation with membranes). During this time, microscopic observation was performed. Representative microphotographs of C3A_DsRed2 cells cultured under different conditions are presented below (Figure 52).

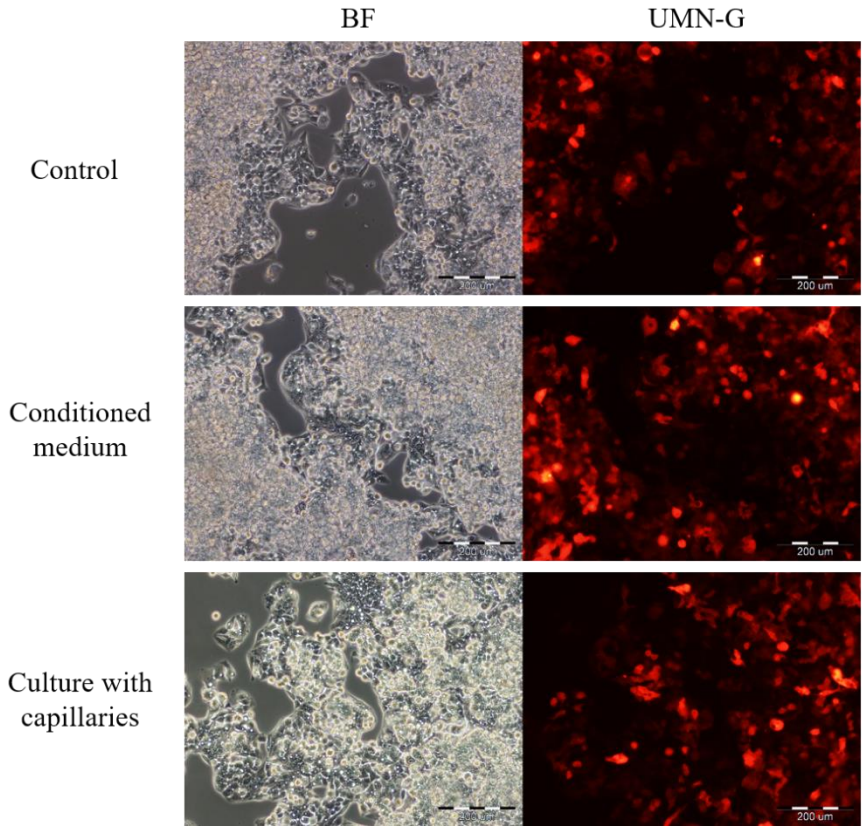

Figure 52. Determination of the effect of the polysulfone membrane on cell morphology. Microphotographs of C3A_DsRed2 cells were taken with a bright-field (BF) illumination and UMN-G filter (for red fluorescence) using an inverted fluorescence microscope Olympus IX-71. Scale bar: 200 µm.

Microscopic analysis did not reveal a cytotoxic effect of the polysulfone membrane on cell morphology. Moreover, an impact on cell fluorescence intensity was not observed. The effect of the presence of a capillary membrane on cell viability was also evaluated. C3A_DsRed2 cells were cultured for three days under the conditions described above. Then, the live and dead cells were counted using the trypan blue exclusion method. More details are presented in section 4.9.2.2. The obtained results are shown in the figure below (Figure 53).

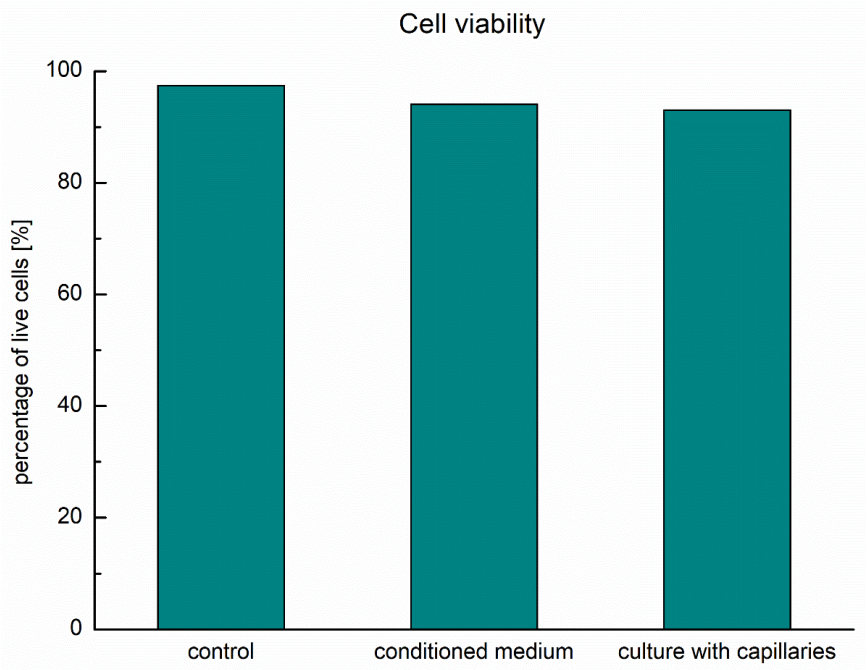

Figure 53. Evaluation of the cytotoxic effect of polysulfone membranes on the viability of hepatic cells. C3A_DsRed2 cells were cultured for three days with 10 capillaries (each with a length of 1 cm) or with conditioned medium (medium after daily incubation with capillaries). The control cells were cultured in standard medium. The cell viability was determined using the trypan blue exclusion method and expressed as the percentage of live cells.

The viability of cells after exposure to the polysulfone membrane was slightly lower than that of control cells and equaled 94.1% (for conditioned medium) and 93% (for cell culture with capillaries). In turn, the viability of C3A_DsRed2 cells cultured under standard conditions was 97.4%. Nevertheless, the differences were not significant enough to classify this material as cytotoxic for hepatic cells. Because only one biological repetition was conducted, statistical analysis of the obtained results was not performed.

5.3.4.3 Determination of the effect of capillary membranes on albumin production

Comparison of albumin secretion between human HCC cells (C3A_DsRed2) cultured under standard conditions and cultured in the presence of a polysulfone membrane was conducted using ELISA. After three days of culture, the medium was collected, and albumin synthesis was measured. The detailed procedure is described in section 4.4. The results of the conducted measurements are presented below (Figure 54).

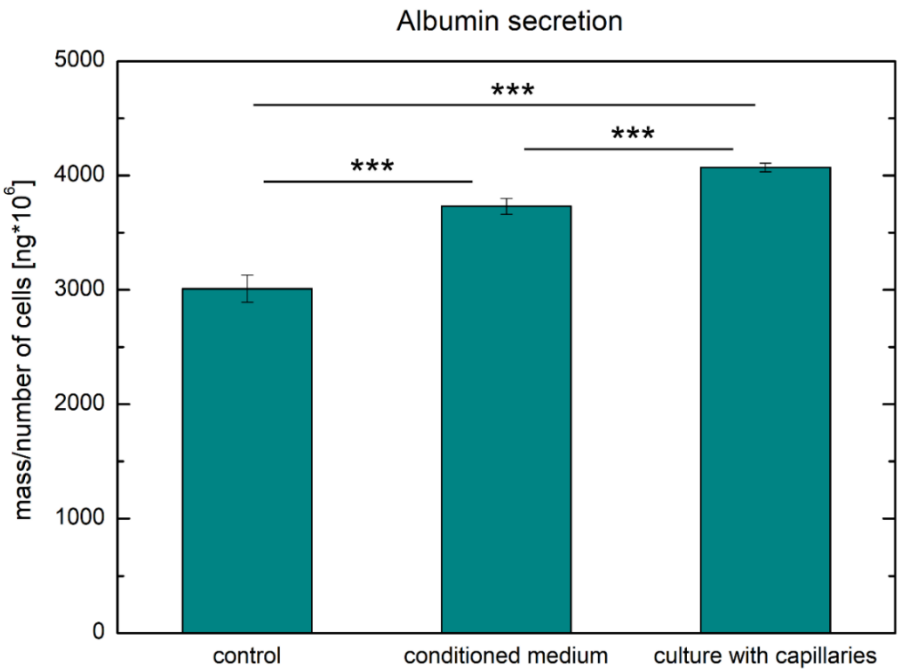

Figure 54. Evaluation of the effect of the polysulfone membrane on albumin secretion by human HCC cells using ELISA. C3A_DsRed2 cells were cultured with 10 capillaries (each with a length of 1 cm) or with conditioned medium (medium after daily incubation with capillaries). The control cells were cultured in standard medium. After three days, albumin production was measured. Number of biological replicates: 3. The results are presented as an average of analyzed biological replicates (with standard deviation values). Statistical analysis was conducted using one-way ANOVA with Duncan's *post hoc* test. Selected statistically significant differences were marked in the graph as follows: p-value < 0.05 (*); p-value < 0.01 (**); p-value < 0.001 (***).

The obtained results revealed that the presence of a polysulfone membrane had no negative effect on albumin production. Compared with the control (cell culture under standard conditions), synthesis of the analyzed protein increased 1.2-fold during culture in conditioned medium (p-value < 0.001) and 1.4-fold during culture with capillaries (p-value < 0.001). Therefore, the analyzed material can be classified as nontoxic to hepatic cells.

5.3.5 Determination of ultrafiltration and retention for constructed hollow fiber bioreactors

After polysulfone membrane characterization and determination of its possible cytotoxic effect, hollow fiber bioreactors (each consisting of twenty capillaries) were prepared. A detailed description is provided in section 4.9.3. The properties of the constructed culture modules were evaluated by ultrafiltration and retention measurements. The obtained results are presented in the section below.

5.3.6 Determination of ultrafiltration for hollow fiber bioreactors

Ultrafiltration measurements were conducted for three independent hollow fiber bioreactors. Because ultrafiltration changes over time, the entire procedure was repeated after one week. More details are described in section 4.9.4. The obtained results are presented in the table below (Table 20).

Table 20. The results of ultrafiltration measurements.

Module	Ultrafiltration 1 [$cm^3/(m^2 \cdot hPa \cdot min)$]	Ultrafiltration 2 [$cm^3/(m^2 \cdot hPa \cdot min)$]
1	185	117
2	186	127
3	192	137

The conducted measurements revealed that the ultrafiltration value was between 185 and 192 $cm^3/(m^2 \cdot hPa \cdot min)$ (U1). The obtained results also showed that this parameter decreased after one week and equaled between 117 and 137 $cm^3/(m^2 \cdot hPa \cdot min)$ (U2). Nevertheless, the similarity of ultrafiltration values between the three hollow fiber bioreactors indicated the repeatability of their preparations.

5.3.7 Determination of the cutoff point for polysulfone capillary membrane - retention measurement

To define the cutoff point for the polysulfone capillary membrane, retention measurements were conducted. This parameter was evaluated using bovine serum albumin (BSA) and fluorescent polystyrene microspheres of different sizes. The retention for BSA was measured using a spectrophotometer. In turn, to determine the retention for fluorescent polystyrene microspheres, cytometric analysis was performed. More details are described in section 4.9.5. The obtained values of retention are presented in the table below (Table 21).

Table 21. The results of retention measurements.

Compound	Retention [%]
BSA (67 kDa; 7.1 nm)	2
Red fluorescent polystyrene microspheres (100 nm)	69
Red fluorescent polystyrene microspheres (200 nm)	99
Red fluorescent polystyrene microspheres (500 nm)	100
Cytometer Setup and Tracking Beads (2 µm and 3 µm)	100

The studies confirmed that substances smaller than 0.2 µm pass completely (BSA) or partially (polystyrene microspheres with a particle size of 100 nm) through the capillary

membrane. The results obtained for the larger objects (polystyrene microspheres with particle sizes ≥ 200 nm) revealed that the analyzed substances were completely retained.

Because the value of retention obtained for green fluorescent microspheres with a particle size of 100 nm (data not shown) was completely different (microspheres passed easily through the membrane) than that for red microspheres, microscopic observation of their shape was conducted using an Olympus IX-71 fluorescence microscope. The obtained results are presented below (Figure 55).

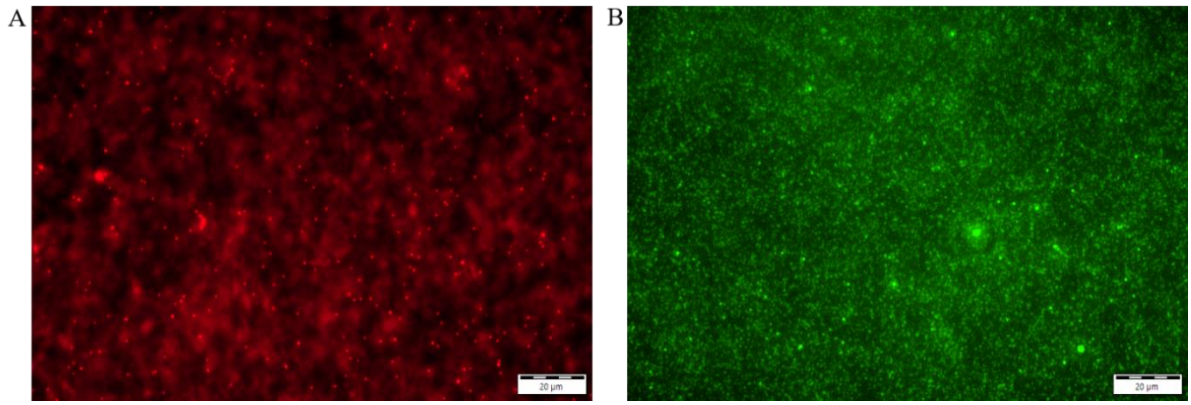

Figure 55. Evaluation of the morphology of the fluorescent polystyrene microspheres. A Representative microphotograph of red fluorescent polystyrene microspheres with a particle size of 100 nm. **B** Representative microphotograph of green fluorescent polystyrene microspheres with a particle size of 100 nm. Microphotographs were taken using UMN-B (for green fluorescence) and UMN-G (for red fluorescence) filters. Scale bar: 20 μm.

Notably, according to the microscopic analysis, the red polystyrene microspheres showed a tendency to form clusters (aggregates). This effect was not observed for green polystyrene microspheres and could be the reason for the observed discrepancies in their retention.

5.4 Comparison of the performance of C3A cells and their genetically modified cell lines under dynamic conditions

5.4.1 Mathematical modeling of hepatic cell culture under dynamic conditions

To conduct the mathematical modeling of the polysulfone fiber, the COMSOL Multiphysics 5.5 tool was used. During the analysis, changes in the albumin and glucose concentrations in dynamic culture were evaluated. Moreover, simulations concerning the determination of the effect of applying different flow rates (from 1 to 10 mL/min) on albumin and glucose diffusion were performed. More details are presented in section 4.10.1. The obtained results are shown in the figures below (Figure 56A, Figure 56B).

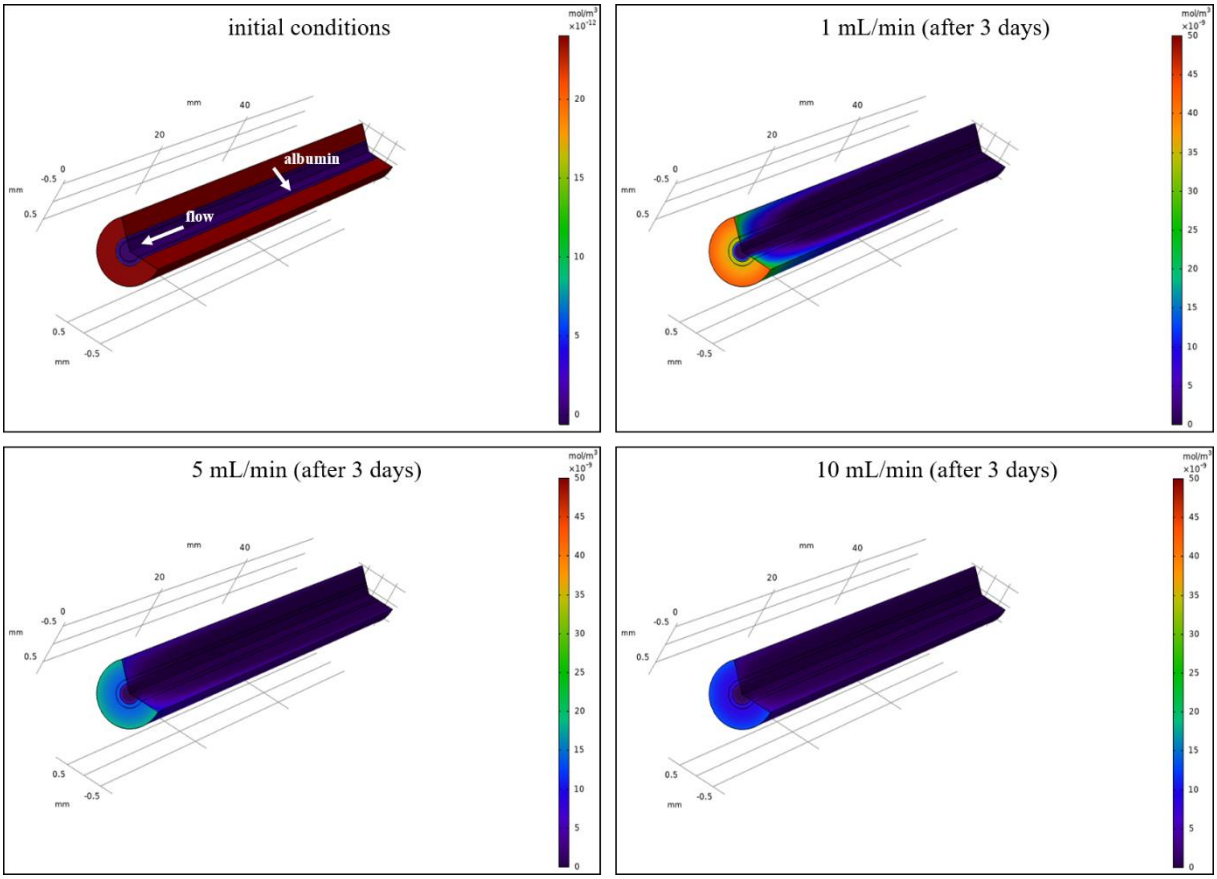

Figure 56A. Mathematical modeling of changes in albumin concentrations under dynamic conditions ensured by hollow fiber bioreactors. The simulation of polysulfone fiber was conducted using COMSOL Multiphysics 5.5. The first picture on the left shows the albumin concentration at the beginning of the simulation. The other pictures show the albumin concentration after three days calculated for three different flow rates (1 mL/min, 5 mL/min, and 10 mL/min).

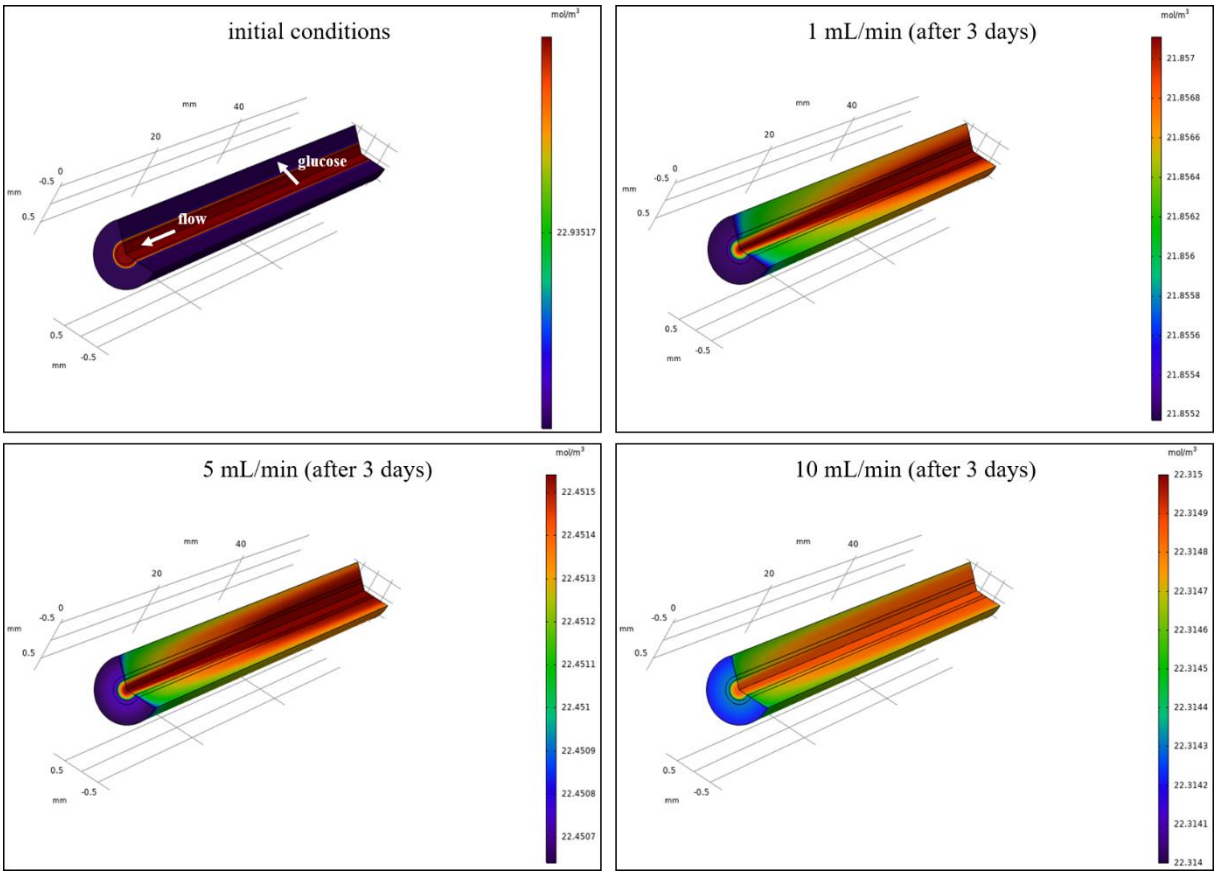

Figure 56B. Mathematical modeling of changes in glucose concentrations under dynamic conditions ensured by hollow fiber bioreactors. The simulation of polysulfone fiber was conducted using COMSOL Multiphysics 5.5. The first picture on the left shows the glucose concentration at the beginning of the simulation. The other pictures show the glucose concentration after three days calculated for three different flow rates (1 mL/min, 5 mL/min, and 10 mL/min).

The conducted simulations revealed that the diffusion of the analyzed substances was affected by the flow rate. The higher the flow rate used, the quicker the mass transfer of albumin and glucose occurred. Nevertheless, all the obtained results were evaluated experimentally.

5.4.2 Hepatic cell culture under dynamic conditions

The constructed system for dynamic culture (section: 4.10.2) was used to compare the culture of C3A cells and their genetically modified counterparts. Initially, optimization of crucial parameters (flow rate, number of seeded cells) was conducted. For the optimization process, C3A cells were chosen. The results of the performed experiments are presented in the section below.

5.4.2.1 Optimization of parameters concerning dynamic culture

Optimization of two parameters connected with dynamic cell culture in medium flow was conducted using the C3A cell line. The cells were cultured for twelve days under dynamic conditions. The impact of different flow rates (5 mL/min and 10 mL/min) and seeding densities ($0.5 \cdot 10^6$ and $5 \cdot 10^6$) on glucose consumption and albumin production was evaluated. Appropriate static culture controls were performed at the same time. More details are described in section 4.10.3. The results of glucose usage during both types of culture are presented below (Figure 57).

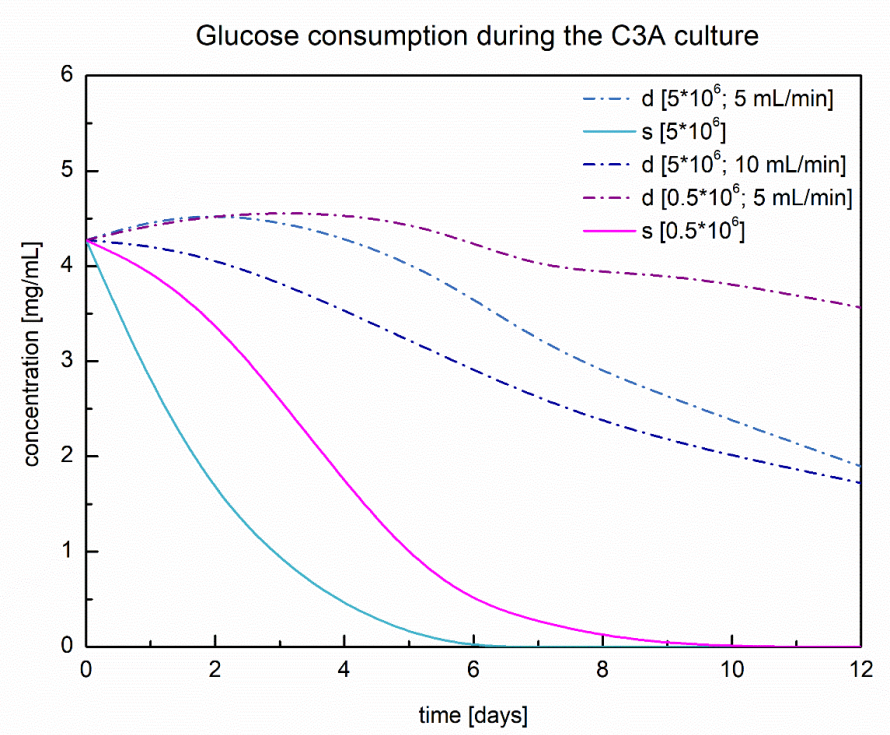

Figure 57. Evaluation of glucose consumption by human hepatic cells in long-term culture. C3A cells were cultured under dynamic conditions for twelve days. The influence of different flow rates and seeding densities on glucose usage was determined. The glucose concentration in medium samples collected on days 3, 5, 7, 9, and 12 of culture was measured using a commercial kit. Abbreviations: s – static culture; d – dynamic culture.

The obtained results indicated faster glucose consumption under static conditions. Depletion of glucose in static culture was observed on the 6th day of culture (starting seeding density: $5 \cdot 10^6$ cells) and on the 10th day of culture (starting seeding density: $0.5 \cdot 10^6$ cells). In turn, during culture under dynamic conditions, only half of the glucose was utilized due to the larger volume of medium (ca. 17 times). In the case of the culture variant in which ten times fewer cells were seeded, practically no consumption of glucose from the medium was observed. The use of different flow rates (5 mL/min and 10 mL/min) did not significantly affect the rate of glucose usage. In summary, the optimization process revealed that the initial number of

seeded cells had a more significant influence on glucose consumption than the medium flow rate.

Interestingly, the results obtained for static conditions indicated intensive glucose consumption, especially in the first days of culture. The reason for this could be the lack of fresh medium. In turn, the dynamic conditions ensured constant access to fresh medium. During the flow culture, 100 mL of medium circulated through the system, while C3A cells under static conditions were cultured in only 6 mL of medium.

A comparison of albumin synthesis during dynamic and static culture of C3A cells is presented in the figure below (Figure 58).

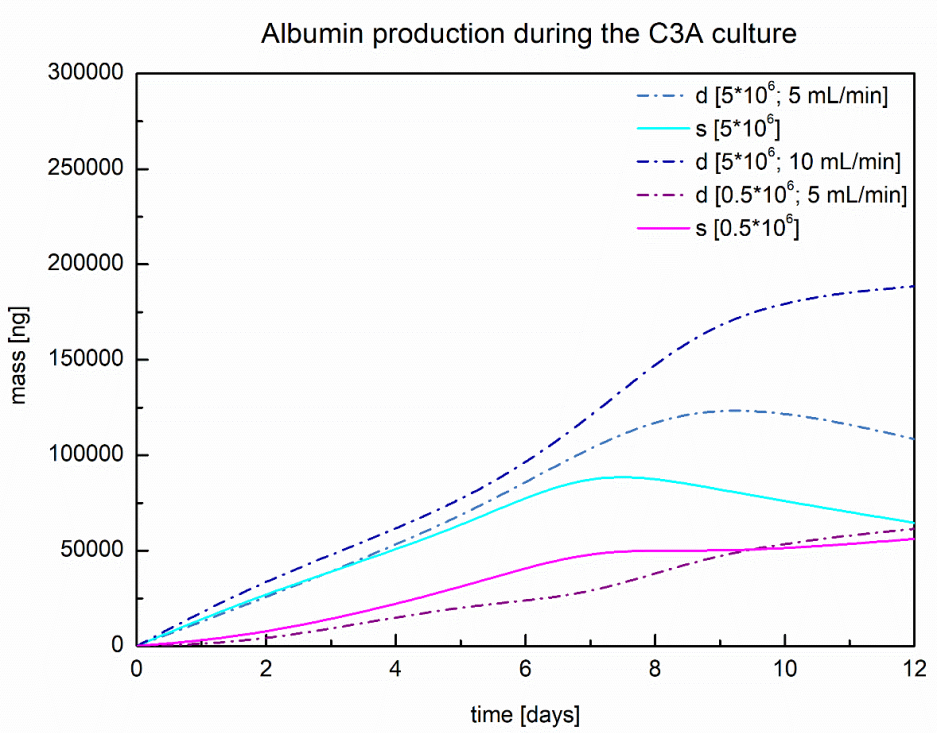

Figure 58. Evaluation of albumin secretion by human hepatic cells in long-term culture. C3A cells were cultured under dynamic conditions for twelve days. The influence of different flow rates and seeding densities on albumin production was determined. The albumin concentration in medium samples collected on days 3, 5, 7, 9, and 12 of culture was measured using ELISA. Abbreviations: s – static culture; d – dynamic culture.

In the case of albumin production, the optimization process revealed that this parameter was strongly affected by both the flow rate and the initial number of seeded cells. The highest albumin secretion was observed for the C3A cell line cultured at a 10 mL/min flow rate and with a starting seeding density of $5 \cdot 10^6$ cells per bioreactor. Interestingly, decreasing the flow rate to 5 mL/min resulted in a decrease in the amount of synthesized protein (without changing the initial number of seeded cells). Analysis of the variant with a starting seeding density of $5 \cdot 10^6$ cells confirmed that dynamic culture ensured greater albumin secretion than static culture.

In turn, a 10-fold decrease in the initial number of seeded cells showed that the production of the analyzed protein under flow and static conditions was comparable.

In summary, after analysis of the obtained results, for further experiments, a flow rate of 10 mL/min and $5 \cdot 10^6$ cells as the initial number of seeded cells were chosen. Interestingly, optimization experiments revealed significant differences between dynamic and static conditions. Flow culture was more efficient, and thanks to medium circulation, could be conducted for a longer time.

5.4.2.2 Comparison of hepatic cell culture under dynamic conditions

First biological repetition

Comparison of genetically modified C3A cells and their unmodified counterparts under static conditions was previously described (section: 4.8). A similar analysis was performed for culture under dynamic conditions. C3A, C3A_AO_III, and C3A_AO_P2A cells were seeded ($5 \cdot 10^6$ cells per bioreactor) on the extracapillary space of polysulfone membranes and cultured for twelve days at a flow rate of 10 mL/min. Afterwards, a comparison of cell viability, metabolic activity and albumin production was conducted. Details concerning culture under dynamic conditions are presented in section 4.10.3.

Cell viability was determined using the trypan blue exclusion method. For the static controls, the obtained values of the analyzed parameters were as follows: 91.5% for C3A cells, 88% for C3A_AO_III, and 91% for C3A_AO_P2A. In turn, the evaluation of cell viability under dynamic conditions was not entirely successful. Trypsinization of C3A cells enabled the detachment of approximately $20 \cdot 10^6$ living cells, while for their genetically modified counterparts, the number of living cells was approximately $10 \cdot 10^6$. Because the cells were still visible on the membranes (and further trypsinization processes were not effective), polysulfone capillaries were fixed with a 4% solution of formaldehyde, stained with DAPI and observed under an Olympus IX-71 fluorescence microscope. The details are described in section 4.10.4. The results obtained from microscopic analysis are presented below (Figure 59).

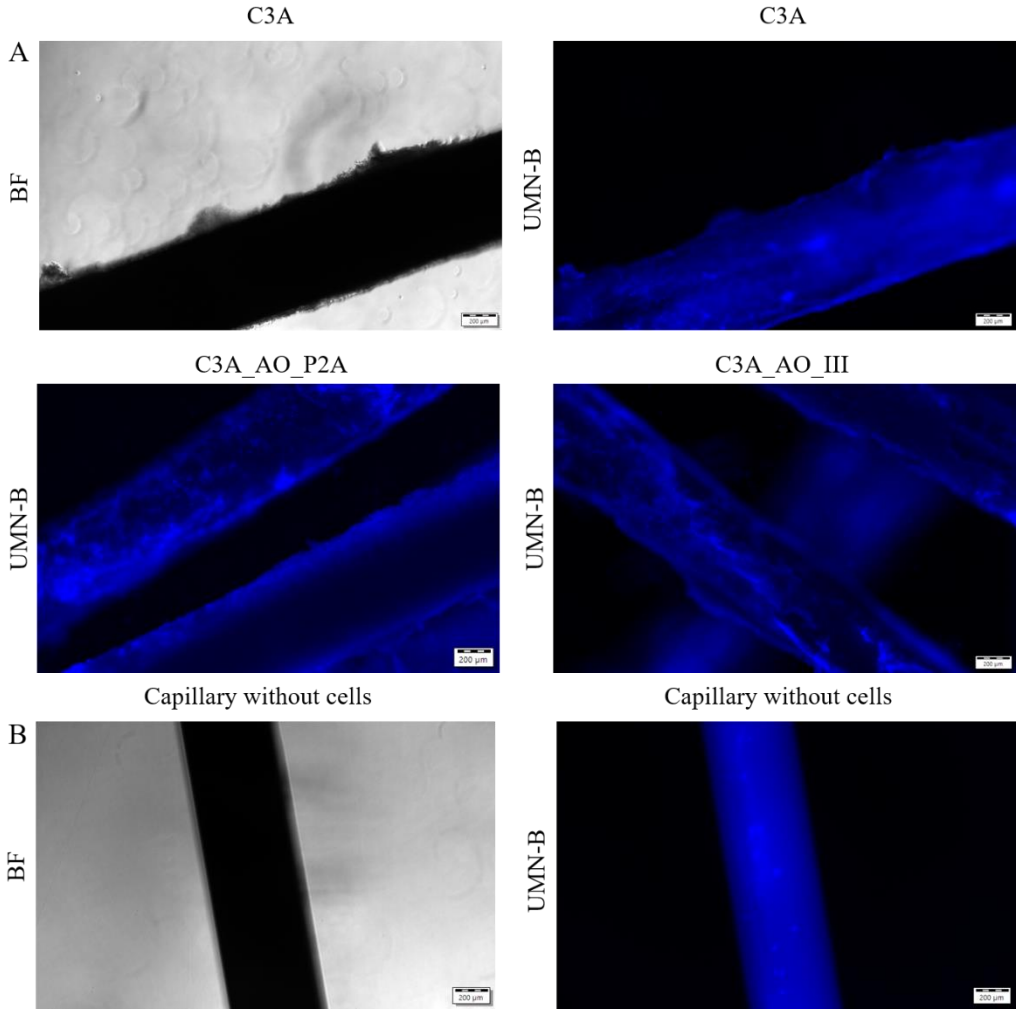

Figure 59. Evaluation of cell adhesion to the capillary membrane. A Microphotographs of polysulfone capillary membranes after the end of dynamic culture of C3A, C3A_AO_III, and C3A_AO_P2A cells were taken with bright-field (BF) illumination and the UMN-B filter (for DAPI visualization) using an inverted fluorescence microscope Olympus IX-71. **B** Microphotographs of polysulfone capillary membranes were taken in the BF and in the UMN-B filter (for DAPI visualization) using an inverted fluorescence microscope Olympus IX-71. Scale bar: 200 µm.

Microscopic analysis revealed that human hepatic cells strongly attach to the polysulfone capillary membrane. Moreover, C3A cells and their genetically modified counterparts formed aggregates and presumably produced a large amount of extracellular matrix (ECM). The obtained results indicated that even estimation of the number of nuclei would not be reliable because there is no possibility to count cells that form aggregates and grow one on another. Moreover, each capillary membrane from the same bioreactor looked different (data not shown), so even efforts toward counting cells from one membrane and averaging the obtained result would not be reliable. Therefore, there is no possibility to estimate the cell viability in flow cultures and make any comparisons.

Glucose consumption under dynamic and static conditions was measured in medium samples collected during culture. A comparison of glucose usage between C3A, C3A_AO_III, and C3A_AO_P2A cells cultured under different conditions is presented below (Figure 60).

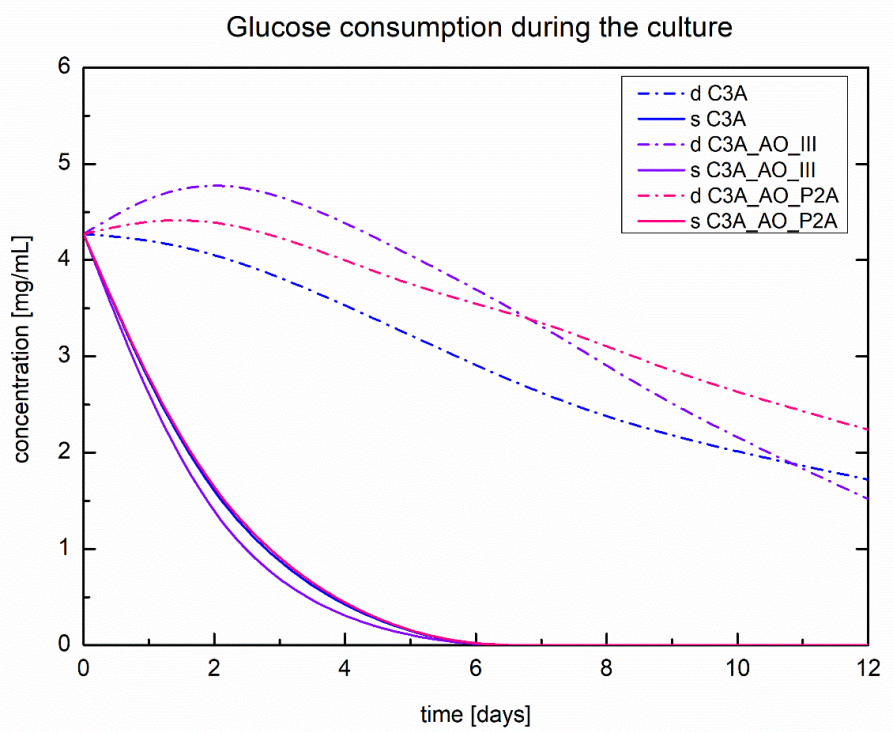

Figure 60. Comparison of glucose consumption between C3A cells and their genetically modified counterparts in dynamic and static cultures. Human HCC cells were cultured under flow conditions for twelve days. Appropriate static controls were performed at the same time. The glucose concentration in medium samples collected on days 3, 5, 7, 9 and 12 of culture was measured using a commercial kit. Abbreviations: s – static culture; d – dynamic culture.

The obtained results indicated that human hepatic cells completely consumed glucose from the culture medium on the 6th day of static culture. In contrast, during culture under dynamic conditions only half of the glucose was used. Interestingly, the rates of glucose consumption by C3A cells and their genetically modified counterparts were very similar in both culture conditions. Nevertheless, C3A_AO_III cells were the most metabolically active under static conditions, while the C3A cell line under dynamic conditions. The differences in the rate of glucose consumption between both culture variants were similar to the results obtained during the optimization process. Therefore, it might be concluded that flow culture constituted a more efficient type of culture and ensured better conditions for the growth of human hepatic cells.

Albumin secretion under dynamic and static conditions was measured in medium samples collected during culture. A comparison of albumin production among C3A,

C3A_AO_III, and C3A_AO_P2A cells cultured under different conditions is presented below (Figure 61).

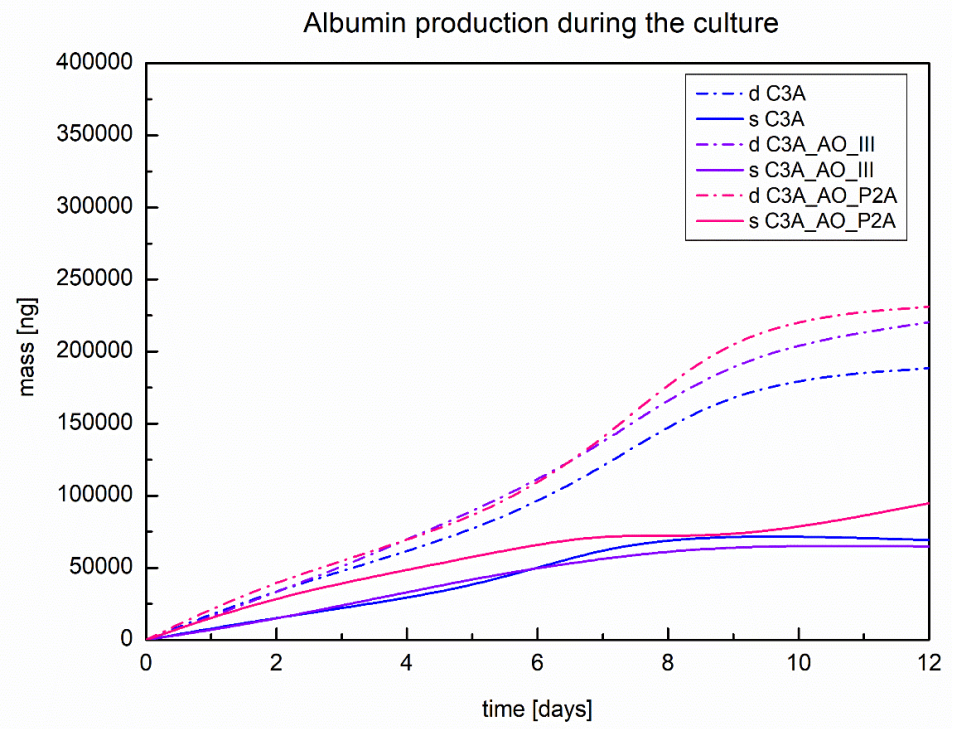

Figure 61. Comparison of albumin synthesis between C3A cells and their genetically modified counterparts in dynamic and static cultures. Human HCC cells were cultured under flow conditions for twelve days. Appropriate static controls were performed at the same time. The albumin content in medium samples collected on days 3, 5, 7, 9 and 12 of culture was measured using ELISA. Abbreviations: s – static culture; d – dynamic culture.

Analysis of albumin secretion indicated that under dynamic conditions all types of human hepatic cells produced greater amounts of the analyzed protein, especially those genetically modified, and that the newest genetically modified cell line (C3A_AO_P2A) outperformed the older one (C3A_AO_III).

Second biological repetition

At the end of the dynamic cultures described above, cell viability was determined using the trypan blue exclusion method. However, human hepatic cells were strongly attached to the capillary membrane, and as a result, it was impossible to detach all cells (despite multiple attempts to trypsinize them) and thus to estimate the final number of cells. With subsequent dynamic cultures (second biological replication), the viability determination method was modified. In the case of the static controls, the method for cell viability evaluation was not changed. The obtained values of the analyzed parameter were as follows: 89% for C3A cells and 92% for C3A_AO_III and C3A_AO_P2A cells. Moreover, no changes were made in the

dynamic culture of C3A cells, and multiple rounds of trypsinization enabled the detachment of approximately $19 \cdot 10^6$ living cells. In the case of the C3A_AO_P2A cell line, some cells were detached and counted ($19 \cdot 10^6$ living cells), while the remaining cells in the culture module were lysed with 5% SDS. After that, the DNA was precipitated using 95% ethanol. The obtained pellet was dried and then suspended in water. The DNA concentration was measured using a NanoDrop spectrophotometer. The obtained concentration was 8 ng/µl (total). As reported in the literature, $1 \cdot 10^6$ cells corresponds to 6 µg of DNA (Gillooly, Hein and Damiani, 2015), so in the culture module remained $4 \cdot 10^6$ cells. In the case of the C3A_AO_III cell line, the trypsinization process was omitted, and immediately after removing the medium from the bioreactor, 5% SDS was added. The concentration of the obtained DNA was 40.5 ng/µl, which corresponds to approximately $7 \cdot 10^6$ cells. Importantly, it was observed that not all cells from the bioreactor were lysed. It seems that for future experiments, both methods should be combined – first, the trypsinization process, and then cell lysis.

Glucose consumption under dynamic and static conditions was measured in medium samples collected during culture. A comparison of glucose usage between C3A, C3A_AO_III, and C3A_AO_P2A cells cultured under different conditions is presented below (Figure 62).

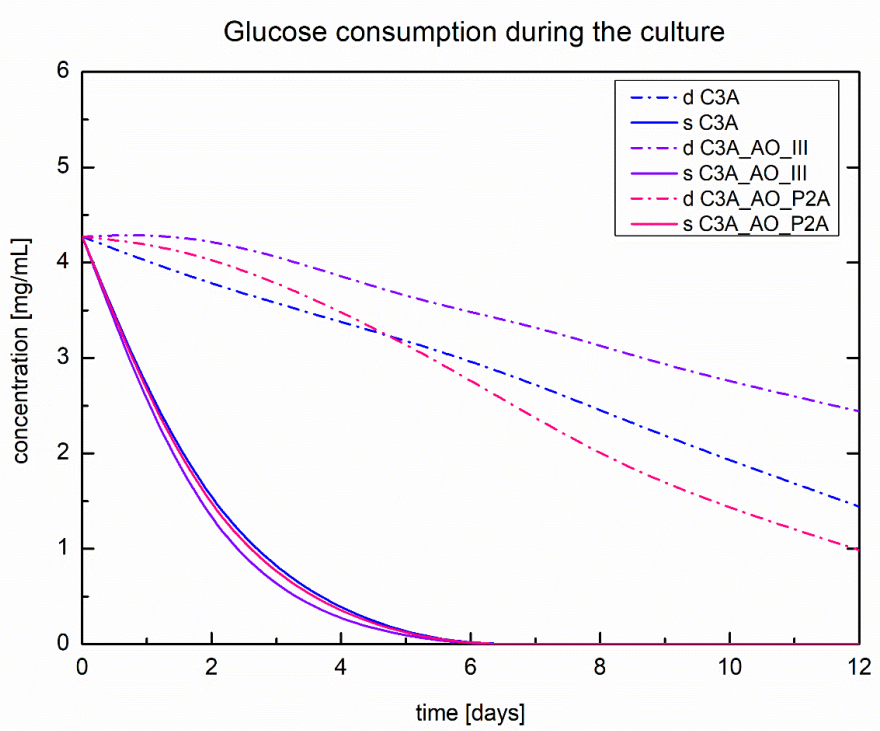

Figure 62. Comparison of glucose consumption between C3A cells and their genetically modified counterparts in dynamic and static cultures. Human HCC cells were cultured under flow conditions for twelve days. Appropriate static controls were performed at the same time. The glucose concentration in medium samples collected on days 3, 5, 7, 9, and 12 of culture was measured using a commercial kit. Abbreviations: s – static culture; d – dynamic culture.

The second biological repetition revealed a similar tendency in the rate of glucose consumption under both culture conditions to that of the first one. The obtained results indicated that C3A_AO_III cells were again the most metabolically active under static conditions, but under dynamic conditions. C3A_AO_P2A cells consumed glucose faster.

Albumin secretion under dynamic and static conditions was measured in medium samples collected during culture. A comparison of albumin production among C3A, C3A_AO_III, and C3A_AO_P2A cells cultured under different conditions is presented below (Figure 63).

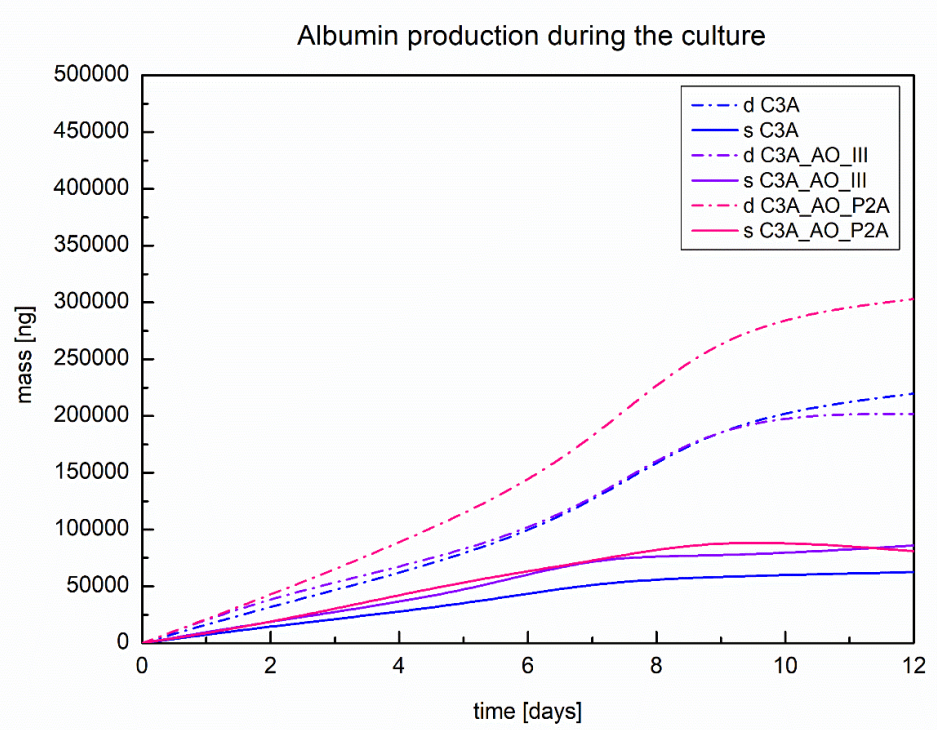

Figure 63. Comparison of albumin synthesis between C3A cells and their genetically modified counterparts in dynamic and static cultures. Human HCC cells were cultured under flow conditions for twelve days. Appropriate static controls were performed at the same time. The albumin content in medium samples collected on days 3, 5, 7, 9, and 12 of culture was measured using ELISA. Abbreviations: s – static culture; d – dynamic culture.

Analysis of albumin secretion indicated a similar tendency in the production of the analyzed protein in the flow culture. Second biological repetition revealed, that again, C3A_AO_P2A cells produced the highest amounts of albumin under dynamic conditions.

6. Discussion

Currently, cardiovascular diseases and cancers are the two main causes of death worldwide. However, liver diseases, with the still increasing prevalence rate, are not far from the aforementioned leading factors. Indeed, liver diseases, with a mortality rate of 2 million deaths per year, are regarded as global public health problems (Cheemerla and Balakrishnan, 2021). Despite the fact that the liver has a tremendous ability to regenerate, usually when organ failure occurs, the only effective medical solution is liver transplantation. Unfortunately, a great limitation to this type of treatment is the chronic shortage of appropriate organ donors. Therefore, other experimental therapies have still been developed, among which bioartificial liver support systems seem to be the most promising. These systems are hybrid extracorporeal devices aimed at bridging patients until organ transplantation or recovery (Pless, 2007). Talking about bioartificial liver support systems, the issue concerning the utilization and choice of biological component cannot be omitted. The main task of the biological component, which in ideal situations should constitute human hepatocytes, is the performance of synthetic, regulatory, and other metabolic liver-related functions, which cannot be replaced by artificial liver support systems (Chamuleau, Poyck and Van De Kerkhove, 2006). Many alternative sources of cells have been tested in experimentally designed bioreactors, although only porcine hepatocytes and tumor-derived C3A cell line have been utilized in advanced devices studied in clinical trials. However, the utilization of porcine hepatocytes has raised concerns due to the potential transmission of zoonotic diseases or protein incompatibility. Moreover, porcine hepatocytes, similar to human hepatocytes, quickly dedifferentiate *in vitro*, which results in rapid deterioration of the performance of liver-specific functions (Schrem *et al.*, 2006). Hence, the C3A cell line derived from human HCC seems to be a more valuable source of cells for use in such devices. This cancer cell line has a very similar phenotype to human hepatocytes, is easy to manipulate, and its availability is unlimited. Additionally, C3A cells proliferate very quickly, which is an especially beneficial feature, as to obtain the therapeutic effect of BAL devices, a minimum of 10^{10} viable cells are needed. Moreover, the C3A cells are able to synthetize albumin, a very essential liver protein product. However, these cells are characterized by some metabolic deficiencies. As reported in the literature, the C3A cell line has decreased activity of several isoforms of cytochrome P450, which results in their lower detoxifying capacity. Moreover, these cells lack (or have low) expression of arginase 1 (*ARG1*) and ornithine transcarbamylase (*OTC*) genes, which implicates a nonfunctional urea cycle and hence an inability to eliminate ammonia properly (Filippi *et al.*, 2004; Mavri-Damelin *et al.*,

2008; Kundu and Brahma, 2016). In fact, the nonfunctional urea cycle could be a reason for the failure of clinical trials conducted with the ELAD system, as the detoxification of ammonia is an essential liver function. Therefore, the aim of my doctoral study was to establish a new genetically modified hepatocellular carcinoma cell line with a restored urea cycle and to evaluate its functionality under static and dynamic conditions. The results obtained for those aforementioned goals will be discussed below.

Establishment of a new genetically modified HCC cell line with a restored urea cycle – C3A_AO_P2A

According to the literature, only a few research groups have attempted to genetically modify human HCC cells in order to improve their metabolic activity related to ammonia detoxification. The genetic modifications, described by others, were based on transient transfection or transduction with retroviruses and were performed on the HepG2 cell line. Two different approaches were proposed to increase the ammonia elimination capacity in HepG2 cells. Some research groups have introduced into the cell genome gene encoding glutamine synthetase, which is involved in alternative ammonia detoxification pathway (Enosawa *et al.*, 2000; Tang *et al.*, 2008). In turn, other teams introduced additional copies of the *ARG1* and *OTC* genes to restore the functionality of the urea cycle (Mavri-Damelin *et al.*, 2007; Tang *et al.*, 2012). These approaches resulted in stable (Tang *et al.*, 2012) or transient (Mavri-Damelin *et al.*, 2007) overexpression of the aforementioned genes and thus improved capacity to detoxify ammonia. However, compared to human hepatocytes, the efficiency of this process was significantly lower. In the case of C3A cells, which are a subclone of the HepG2 cell line, several research papers reporting improvements in the activity of different cytochrome P450 enzymes have been published (Chen *et al.*, 2014; Han *et al.*, 2018). To the best of my knowledge, in terms of genetic modifications aimed at enhancing ammonia elimination capacity, the scientific report released by our group is the one. It presents, as a result of many years of research and development conducted in our laboratory, the C3A_AO_III cell line with a restored urea cycle, which indeed produces more urea than its unmodified counterparts (Pluta *et al.*, 2020). Nonetheless, the chosen method for carrying out the genetic modification allowed us to obtain a mixed cell population, with only half being genetically modified. In addition, our laboratory research has shown that the percentage of genetically modified cells decreases with each cell passage.

Therefore, it was decided to introduce some changes in the previously used methodology and to develop a new genetically modified cell line with a restored urea cycle, which was the first goal of my doctoral thesis. Similar to our previous approach, this aforementioned aim was achieved using a lentiviral vector. This tool for gene transfer was not changed because our group has great experience in conducting successful genetic modifications with lentiviral vectors. Moreover, our previous studies indicated that C3A cells are susceptible to lentiviral transfection and that this process is highly effective (Samluk, Zakrzewska and Pluta, 2013; Pluta *et al.*, 2020). Additionally, lentiviral vectors, which are based on the HIV-1 genome, enable stable integration of transgenes into the genome of the target cell. Moreover, they are able to transduce nondividing cells, which is a very important feature. According to the literature, the high efficiency of gene delivery makes lentiviral vectors very promising tools in different applications, especially in gene therapy (Kamata *et al.*, 2010; Merten, Hebben and Bovolenta, 2016; Picanço-Castro *et al.*, 2020; Ku *et al.*, 2021). It is also worth emphasizing the safety of lentiviral vectors. First, to minimize the risk, all accessory genes associated with virulence are deleted from the vector sequence. Additionally, the lentiviral genome is split into several separate plasmids, which reduces the possibility of virus recombination. Moreover, lentiviral vectors are equipped with a self-inactivating system (Pluta and Kacprzak, 2009). Taken together, it should not be surprising that lentiviral vectors are widely studied in many clinical trials evaluating their use in gene therapy for different human diseases (Naldini, Trono and Verma, 2016; Milone and O'Doherty, 2018; Labbé, Vessillier and Rafiq, 2021). Additionally, in 2017, the FDA approved the first commercial gene therapy (KYMRIAH, Novartis) on the market. KYMRIAH is an immunotherapy utilizing CD19-targeted genetically modified (with the use of lentiviral vectors) autologous T cells (CAR-T cells), which destroy B cells. It is widely used for the treatment of pediatric and young adult patients (up to 25 years old) with acute lymphoblastic leukemia (O'Leary *et al.*, 2019). All of the abovementioned arguments confirmed the validity of utilizing lentiviral vectors.

In our laboratory, both previous and current approaches aimed at developing genetically modified cell lines that have introduced additional copies of the human genes h*ARG1* and h*OTC*. These transgenes, which are stably integrated into the C3A genome, encode arginase 1 (ARG1) and ornithine transcarbamylase (OTC) enzymes, which participate in the urea cycle. Although having the same aim, the used approach was quite different. Previously, C3A cells were transduced with two different lentiviral vectors, each bearing one of the transgenes. As a result, the obtained genetically modified C3A_AO_III cell line is a mixed cell population that consists of unmodified cells, cells expressing a single transgene or, in minority, cells transduced

with both missing genes. As the transfer plasmids contain the gene encoding the fluorescent protein mCherry, the transduction efficiency was evaluated using cytometric analysis. The obtained results showed that the percentage of genetically modified cells represents 53% of total population. However, exact information on how many cells were transduced with vectors carrying both missing genes is lacking. The only provided information is that this value does not exceed 25% (Pluta *et al.*, 2020). Thus, the novelty of the current approach is the use for a transduction a single lentiviral vector carrying one multicistronic transcriptional cassette, which simultaneously expresses the h*ARG1* and h*OTC* transgenes. Therefore, the possibility that cells might overexpress only one of the missing genes was eliminated. Additionally, the DsRed protein was chosen as a fluorescent marker. Thus, the efficiency of transduction with self-prepared lentiviral vectors (LV_ARG1_OTC_DsRed) could be evaluated using fluorescence microscopy (Figure 24A, Figure 24B) and flow cytometry (data not shown). Both techniques revealed that, compared to nontransduced C3A cells, the fluorescent signal from the DsRed protein was not detected. This might have resulted from the fact that a low titer of the prepared lentiviral vectors was achieved. Indeed, microphotographs taken after HEK293T transfection (Figure 23A, Figure 23B) showed transient expression from the transfer plasmid. However, despite many attempts, the measurement of the titer of the obtained lentiviral vectors was not possible, as the signal from DsRed was below the detection level of the flow cytometer (data not shown). Moreover, the lower efficiency of viral particles assembly may result from the insert size. Notably, our construct contains 10827 bp, and according to the literature, lentiviral vectors are able to incorporate inserts with sizes up to 10000 bp (Tolmachov, Tolmachova and Al-Allaf, 2011). Therefore, the conducted research was very close to the limit of technological possibilities. Nonetheless, knowing that the transfer plasmid contains a puromycin resistance gene, it was decided to carry out antibiotic selection to evaluate whether any of the cells were successfully transduced, which was the second novelty of the current approach. Indeed, as shown by microscopy analysis (Figure 25, Figure 26), cells that were not resistant to puromycin died, which resulted in antibiotic resistant cell colonies, enabling cloning of the population consisting of nearly 100% *ARG1*- and *OTC*-expressing cells named the C3A_AO_P2A cell line. However, not all cells that survive antibiotic selection (have resistance to puromycin) express the fluorescent marker DsRed (Figure 26). This might be explained by the fact that the gene encoding this fluorescent protein is located far from the CMV promoter, preceded by the sequences encoding h*ARG1* and h*OTC* separated by P2A. Thus, this may result in its lower expression and hence in decreased efficiency of protein synthesis. Nevertheless, PCR and RT-qPCR analysis confirmed the successful integration of the h*ARG1* and h*OTC*

transgenes into the C3A genome (Figure 27) and the overexpression of both genes (Figure 28), respectively. Moreover, Western blot analysis affirmed that translation of both ARG1 and OTC proteins occurred (Figure 31, Figure 32).

Taking this into account, it might be concluded that genetic modification of C3A cells with the use of lentiviral vectors was successful. Particularly noteworthy is the fact that applied innovations in the previously used methodology, despite the encountered difficulties, have led to the establishment of the C3A_AO_P2A cell line, which consists of nearly 100% of the population of *ARG1*- and *OTC*-expressing cells.

Evaluation of the functionality of the new genetically modified C3A_AO_P2A cell line under static conditions

The second goal of my doctoral thesis was to evaluate the functionality of the newly established C3A_AO_P2A cell line under static and dynamic conditions. In this section, the results obtained for static culture will be discussed. For comparison, all experiments performed for C3A_AO_P2A cells were also conducted for C3A_AO_III and C3A cells.

Microscopic and cytometric analyses concerning the evaluation of the differences in cell morphology revealed that C3A_AO_P2A cells were similar in size and granularity to their parental C3A cell line. Moreover, both cell lines had a tendency to aggregate (Figure 33). In turn, C3A_AO_III cells were larger, more grainy, and had a stronger ability to adhere to the growth surface (Figure 33), which confirmed our previously obtained results (Pluta *et al.*, 2020). Additionally, the impact of the conducted genetic modification on cell viability and metabolic activity was assessed. No significant differences in the percentage of live cells between modified and unmodified cells were observed (Figure 34). Moreover, both genetically modified cell lines were characterized by higher metabolic activity than their parental C3A cells, however, the C3A_AO_III cell line slightly outperformed the results obtained for C3A_AO_P2A cells (Figure 35). Nonetheless, no negative effect of genetic modification on vital cell parameters was observed.

Albumin, an essential protein synthetized by hepatocytes, whose daily production in adults is 10-15 g, performs many vital functions. For example, it is responsible for modulating the osmotic pressure of the blood. Additionally, albumin has a strong binding capacity and thus participates in the transport of many endogenous and exogenous substances. Importantly, this ability is widely utilized in the majority of artificial liver support systems (Moman, Gupta and Varacallo, 2023). Therefore, the synthesis of albumin by the newly developed C3A_AO_P2A

cell line was evaluated. Research at the mRNA level revealed that the expression of albumin was the highest in C3A_AO_III cells. In turn, C3A_AO_P2A cells were characterized by lower expression of the analyzed gene even compared to their parental cell line (Figure 29). This finding might be explained by downregulation of the *HNF4A* gene in C3A_AO_P2A cells, whereas in contrast, in C3A_AO_III cells, this gene was upregulated. Indeed, HNF4A is a liver-related transcription factor that is heavily involved in the regulation of albumin expression (Guzman-Lepe *et al.*, 2018). As reported the literature, HNF4A, FOXA2, and C/EBPA (CCAAT/enhancer-binding protein alpha) bind to the albumin transcription enhancer. When either of these transcription factors was knocked down, a reduction in the expression of albumin was observed (Feng *et al.*, 2022). However, Costa et al. reported that the *HNF1A* gene is also engaged in the regulation of albumin expression (Costa *et al.*, 2003), and in our study, upregulation of the *HNF1A* gene in both genetically modified cell lines was observed (Figure 29). However, C3A_AO_III cells outperformed C3A_AO_P2A cells at the level of upregulation of the analyzed gene. This could be explained by the fact that the *HNF4A* gene plays an important role as a positive regulator of *HNF1A* gene expression. As shown in the literature, overexpression of the *HNF4* gene in human HCC cells resulted in upregulation of the *HNF1A* gene and other genes encoding vital liver-specific proteins, such as albumin (Nagaki and Moriwaki, 2008). Analysis of albumin expression at the protein level revealed contradictory results. Western blot analysis showed that compared with the control C3A cell line, C3A_AO_P2A cells were characterized by the highest albumin level, whereas C3A_AO_III cells – by the lowest (Figure 30). In turn, ELISA revealed that the highest albumin synthesis was observed for C3A_AO_III cells, however, this difference was statistically significant only on the 9th day of culture. The secretion of the analyzed protein by the C3A_AO_P2A cells was similar to that of their parental cell line, without any statistically significant differences (Figure 37). Nonetheless, it is worth emphasizing that Western blot is a semiquantitative technique, and thus, no exact comparison could be made based on these results. Moreover, referring to the ELISA results, due to the large discrepancies in the number of cells from the three independent biological repetitions, large standard deviations were obtained (especially for the 6th day of culture). Therefore, no differences between C3A and C3A_AO_P2A cells could be accurately demonstrated. Additionally, albumin synthesis was evaluated using flow cytometry and immunofluorescence methods. The latter technique showed that the possible differences between human HCC cells were not visible (Figure 38). However, cytometric analysis confirmed the results obtained by ELISA, showing that the percentage of ALB-positive cells was similar for C3A_AO_P2A and C3A cells, whereas for C3A_AO_III cells, this value was

the highest (Figure 39). This may explain the more granular structure of C3A_AO_III cells (Figure 33), which implicates increased protein production and accumulation (Pluta *et al.*, 2020).

Therefore, it might be concluded that genetic modification did not negatively affect albumin synthesis in the newly developed C3A_AO_P2A cell line; however, an increase in the secretion of this protein to the same extent as in the case of C3A_AO_III cells has not been confirmed. Moreover, it might be speculated that the previously conducted genetic modification occurred via a quite different mechanism, which affects cell phenotype and albumin synthesis, whereas such implications were not observed for the newly developed C3A_AO_P2A cell line. Additionally, it might be speculated that these discrepancies may result from different passages of C3A cells used for genetic modification.

Many scientific reports have revealed the antioxidative properties of albumin under conditions of oxidative/nitrosative stress generated by reactive oxygen species (ROS) and reactive nitrogen species (RNS) (Roche *et al.*, 2008; Taverna *et al.*, 2013; Belinskaia *et al.*, 2021). However, the exact effect of ammonia-induced oxidative/nitrosative stress on albumin synthesis by human hepatic cells remains elusive. In our previous study, a very interesting phenomenon was observed. After ammonium chloride treatment, genetically modified C3A_AO_III cells and their unmodified counterparts were characterized by increased expression of albumin at both the mRNA and protein levels (Pluta *et al.*, 2020). Thus, the investigation whether a similar effect would be observed in the newly developed C3A_AO_P2A cell line was conducted. Additionally, to confirm whether ammonium chloride indeed induces oxidative/nitrosative stress in human HCC cell lines, analysis of the expression of the *HSPA1A* gene was performed, as this family of proteins is produced in response to such conditions (Szyller and Bil-Lula, 2021). Notably, the obtained results showed upregulation of the analyzed gene in all three human HCC cell lines. Moreover, the analysis confirmed that oxidative/nitrosative stress affected the expression of albumin. Increased mRNA levels of albumin were observed in both genetically modified cell lines and their unmodified counterparts; however, this phenomenon was most prominent in C3A_AO_III cells. Previously, it was reported that this was connected with the upregulation of the *HNF4A* gene in all analyzed cell lines, and it was speculated that this could be part of the mechanism concerning the response of human HCC cells to ammonia-induced oxidative/nitrosative stress (Pluta *et al.*, 2020). A similar correlation was observed in the current study, which additionally supported our hypothesis. Increased albumin synthesis was also confirmed at the protein level. Western blot analysis and ELISA showed that under oxidative/nitrosative stress, both genetically modified

cell lines produced more albumin; however, the degree of this induction in C3A_AO_III cells was much greater than that in the newly developed C3A_AO_P2A cell line. However, despite the presence of scientific papers showing the synthesis of albumin after treatment with ammonium chloride, the phenomenon observed in our laboratory has not been confirmed by others. The Baudoin group showed no effect of ammonium chloride on the secretion of this protein by C3A cells, however, they mentioned that due to the large standard deviations, their results were not conclusive. Moreover, they used a 10 mM concentration as the maximal dose for treatment, whereas in our studies, 20 mM and 40 mM ammonium chloride were utilized (Baudoin *et al.*, 2011; Pluta *et al.*, 2020). Therefore, this difference in dose may result in the lack of the phenomenon observed in our laboratory. In turn, the Laemmle group reported that ammonium chloride reduces the secretion of albumin (Laemmle *et al.*, 2016). However, they also utilized a 10 mM concentration of ammonium chloride for the treatment. Additionally, the Laemmle group showed only the concentration of secreted albumin, and they did not count the amount of synthetized protein per number of living cells as was done in our research. Moreover, as they performed their studies on human hepatocytes, the decrease in albumin synthesis may have resulted from their phenotypic instability during *in vitro* culture. Therefore, based on the abovementioned scientific reports, it is difficult to draw the correct conclusions. Nonetheless, it might be speculated that the observed phenomenon is connected with cellular defense mechanisms, and albumin, as it has unusual antioxidant properties and the ability to bind various toxic substances, is involved in these processes.

Additionally, two other markers related to human hepatic cells (A1AT and CD54) were investigated using flow cytometry. Alpha-1-antitrypsin (A1AT) is a serum protein synthetized by hepatocytes and other cell types (Janciauskiene and Welte, 2016). Nonetheless, it is used in our laboratory as a characteristic marker for liver parenchymal cells. In turn, the CD54 receptor, also known as intercellular adhesion molecule-1 (ICAM-1), participates in cell-cell interactions. This protein is widely distributed in normal tissue and neoplastic tissue, also called tumor (Maio and Del Vecchio, 1992; Gorgoulis *et al.*, 2003). Cytometric analysis revealed no statistically significant differences in the percentages of A1AT- and CD54-positive cells among the three human HCC cell lines (Figure 39). Thus, it might be concluded that genetic modification did not have any effect on the analyzed markers.

The polarity of the hepatocyte membrane is a unique feature. Hepatocytes possess two domains of the membrane – apical (canalicular) and basolateral (sinusoidal). In this way, they can contact sinusoids or neighboring hepatocytes, which facilitates the performance of vital liver-specific functions. In the apical domain, liver parenchymal cells form vacuoles, which are

precursors of *bile canaliculi* (Treyer and Müsch, 2013). As the formation of apical vacuoles is a characteristic parameter for hepatocytes and this parameter was not previously compared, the possible differences between both the genetically modified cells and their unmodified counterparts were analyzed. The obtained results revealed that the greatest number of apical vacuoles was achieved for C3A_AO_P2A cells. The value of the analyzed parameter for C3A cells was slightly lower, however the differences between these cell lines were not statistically significant. Interestingly, it was observed that C3A_AO_P2A cells significantly outperformed C3A_AO_III cells in the formation of apical vacuoles, which implies that these cells have more polarized membranes (Figure 40, Figure 41).

Ammonia elimination is regarded as a key function of BAL devices, hence, this parameter is continuously monitored in patients suffering from liver failure, as ammonia at high concentrations is toxic (Van Wenum *et al.*, 2014). Normally, the ammonia concentration in the blood of healthy adults ranges from 11-32 μmol/L (Braissant, McLin and Cudalbu, 2013). However, pathological stages associated with liver diseases often correlate with a decrease in metabolic activity related to ammonia detoxification. Thus, it implicates the accumulation of this compound in the body, which is called hyperammonemia. This phenomenon is an essential contributing factor to hepatic encephalopathy, which in turn causes damage to the central nervous system. Persistently high levels of ammonia in the blood (over 150 μmol/L), if no effective therapy is used, in many cases can lead to cerebral edema or even death (Bernal *et al.*, 2007; Kumar *et al.*, 2012; Walker, 2014; Romero-Gómez, Montagnese and Jalan, 2015). Therefore, the issue concerning effective ammonia elimination in therapies for patients suffering from different liver diseases cannot be overlooked. It is worth mentioning that ammonia detoxification occurs through two different metabolic pathways. The first route is connected with the reversible formation of glutamine from ammonia and glutamate. This process is catalyzed by the glutamine synthetase (GS) enzyme and occurs nearly in the whole body. The second pathway is the irreversible urea cycle, which is performed only by liver parenchymal cells. The end product of this cycle, consisting of five enzymatic reactions, is urea, which is then eliminated from the body with the urine (Adeva *et al.*, 2012). Notably, for BAL application, ammonia elimination through the urea cycle is preferable. This is the only way to definitely dispose of this toxic compound, as the conversion of ammonia into glutamine is a reversible process. Thus, the risk of consecutive ammonia formation in the opposite reaction is highly likely (Adam *et al.*, 2019).

The low ammonia detoxification capacity of human hepatocellular C3A cells strongly limits their utilization in the treatment of liver diseases, especially in BAL devices. As

mentioned above, the reason for this metabolic dysfunction of C3A cells (and their parental HepG2 cell line) is the absence of a functional urea cycle. According to the literature, this phenomenon results from a lack or low expression of the *ARG1* and *OTC* genes, which encode enzymes involved in the urea cycle; however, scientific reports have revealed some contradictory conclusions. The Mavri-Damelin group showed that no mRNA levels of *ARG1* and *OTC* genes were observed in HepG2 cells (Mavri-Damelin *et al.*, 2007). In contrast, the Tang group revealed that the *ARG1* and *OTC* genes were expressed in the HepG2 cell line. Moreover, they also showed the presence of ARG1 and OTC proteins (Tang *et al.*, 2012). In turn, the Bobak group confirmed the expression of the *ARG1* and *OTC* genes in HepG2 cells; however, they claimed that the translation of these proteins did not occur (Bobak *et al.*, 2010). Finally, the van Wenum group reported that low mRNA levels of the *ARG1* and *OTC* genes in C3A cells were observed (van Wenum *et al.*, 2016). Notably, our own research showed that the C3A cell line lacks the expression of *ARG1* and *OTC* genes (Pluta *et al.*, 2020; Jakubowska *et al.*, 2024). Nonetheless, it is worth emphasizing that a nonfunctional urea cycle was also observed in HepaRG cells, another cell line derived from human HCC (Moedas *et al.*, 2017). Thus, this phenomenon might be explained by the fact that cancer cells alter the expression of urea cycle genes to maximize nitrogen incorporation into biomass (Keshet *et al.*, 2018).

As mentioned above, our research revealed a lack of *ARG1* and *OTC* transcripts in C3A cells, and thus, in this doctoral study, the mRNA levels of these genes were only compared between both genetically modified cell lines. Interestingly, RT-qPCR analysis revealed that the newly developed C3A_AO_P2A cell line was characterized by approximately 35-fold (p-value < 0.001) and 44-fold (p-value < 0.001) greater expression of the h*ARG1* and h*OTC* genes, respectively, than C3A_AO_III cells (Figure 28). Additionally, the observed effect was enhanced after ammonia-induced oxidative/nitrosative stress, resulting in approximately 43-fold (p-value = 0.022) and 50-fold (p-value = 0.025) overexpression of the analyzed genes compared to that in C3A_AO_III cells (Figure 28). This phenomenon may be explained by the fact that the CMV promoter, which was utilized for the expression of the analyzed genes, is activated in oxidative/nitrosative stress by the NF-κB transcription factor (Speir, 2000). Indeed, the overexpression of the *NF-κB* gene was elevated in both genetically modified cell lines; however, the observed correlation was more prominent for C3A_AO_III cells (Figure 29). Our aim was to compare and discuss our results with scientific reports released by the Mavri-Damelin and Tang groups, who conducted similar research using HepG2 cells. Unfortunately, this was not possible because both scientific groups did not study the expression of *ARG1* and *OTC* genes after performing genetic modification (Mavri-Damelin *et al.*, 2007; Tang *et al.*,

2012). Nonetheless, it is worth emphasizing that changes introduced in the methodology previously used for conducting genetic modification of C3A cells resulted in obtaining significantly greater mRNA levels of the *ARG1* and *OTC* genes, which can be regarded as a success.

Subsequently, the translation of the ARG1 and OTC proteins was evaluated. Western blot analysis revealed that the ARG1 protein was not detected in C3A cells. Thus, comparison with the newly developed C3A_AO_P2A cell line is not possible. Previously, the level of ARG1 protein was 12.5-fold greater in C3A_AO_III cells than in their unmodified counterparts (Pluta *et al.*, 2020). Nonetheless, the current study showed that the expression of the analyzed protein in C3A_AO_P2A cells was approximately 2-fold greater than that in C3A_AO_III cells, suggesting that the newly developed cell line outperformed the other studied cell lines in ARG1 production (Figure 31). In contrast, the OTC protein was detected in the parental C3A cells. Thus, compared to those in C3A_AO_III and C3A cells, the levels of OTC in C3A_AO_P2A cells were 1.2-fold and 1.4-fold greater, respectively (Figure 32). In turn, our former study showed that the level of OTC protein was 2.5-fold greater in C3A_AO_III cells than in their unmodified counterparts (Pluta *et al.*, 2020). This discrepancy may ensue from the use of different antibodies and reagents necessary for performing Western blot analysis. Nonetheless, it might be concluded that the newly developed cell line outperformed the other studied cell lines also in terms of OTC production. Comparison with results obtained by other scientific groups is partially possible. The Mavri-Damelin team did not study protein expression by Western blot, whereas Tang et al. reported that their genetically modified cell line HepG2/(hArgI+hOTC)4 was characterized by 2-fold and 5-fold greater expression of ARG1 and OTC protein, respectively, than unmodified HepG2 (Mavri-Damelin *et al.*, 2007; Tang *et al.*, 2012). As mentioned above, in the present study, ARG1 protein was not detected in C3A cells; thus, only the difference in OTC levels between HepG2/(hArgI+hOTC)4 and C3A_AO_P2A cells could be examined. The lower expression of the OTC protein in the newly developed cell line may be explained by the lower efficiency of genetic modification, which in turn depends on various factors, such as cell condition, but above all, on the size of the introduced DNA construct. Nonetheless, it is worth emphasizing that our assumption was confirmed. The changes introduced in the previously used methodology resulted in the fact that the newly developed C3A_AO_P2A cell line outperformed C3A_AO_III and C3A cells in the expression of ARG1 and OTC proteins. However, it must be admitted that after obtaining very high mRNA levels of the h*ARG1* and h*OTC* transgenes, it was expected that this phenomenon would be reflected by highly elevated protein synthesis. Nevertheless, this assumption was not

confirmed. It might be elucidated by several literature reports suggesting that the correlation between mRNA and protein levels in healthy tissue is relatively poor, whereas in cancerous tissue, it is even worse. The proposed explanation for this phenomenon is inter alia posttranscriptional regulation of gene expression (Vogel and Marcotte, 2012; Kosti *et al.*, 2016; Perl *et al.*, 2017).

Finally, to verify the functionality of the analyzed proteins, their enzymatic activity was evaluated using biochemical assays. The obtained results indicated that enzymatic activity of arginase in C3A_AO_P2A cells was 1.2-fold (p-value = 0.012) and 2-fold (p-value = 0.005) greater than that in C3A and C3A_AO_III cells, respectively (Figure 42). It is worth mentioning that the chosen assay measured the enzymatic activity of both ARG1 and arginase 2 (ARG2). Although both isoforms participate in the conversion of arginine into ornithine, ARG1 is a cytosolic protein, that is mostly expressed in the liver and plays an essential role in the urea cycle aimed at ammonia elimination. In turn, ARG2 is a mitochondrial protein that is present in all tissues (especially in the kidney and endocrine tissues) and is involved in the regulation of ornithine biosynthesis (Clemente *et al.*, 2020). However, the presence of ARG2 protein in C3A and HepG2 cells was confirmed (Mavri-Damelin *et al.*, 2008; Tang *et al.*, 2012; van Wenum *et al.*, 2016). Although the expression of ARG2 in all analyzed cell lines was not investigated in the current study, the following conclusions could be drawn. First, considering that ARG1 was not detected in C3A cells, the results obtained for this cell line reflect the activity of ARG2. Second, the activity between ARG1 and ARG2 could not be distinguished; thus confirming whether the activity of ARG1 is in fact greater in newly developed C3A_AO_P2A cells than in C3A_AO_III cells was not possible. Third, among all analyzed cell lines, C3A_AO_P2A cells were characterized by the highest enzymatic activity of both arginases. However, considering that the enzymatic activity of arginases measured for liver cell isolate was approximately 60-fold greater, it was expected that the functionality of the ARG1 protein in genetically modified C3A_AO_P2A cells will be much greater. In the case of determining the enzymatic activity of the OTC protein, the chosen method did not yield conclusive results. Unfortunately, the results of measurements conducted for all analyzed cell lines were below the detection limit (Figure 43). Therefore, comparison with results obtained by other scientific groups can be difficult. Using biochemical assays, the Tang group confirmed the functionality of ARG1 and OTC proteins in HepG2/(hArgI+hOTC)4 cells. However, differences in the activity of the analyzed enzymes between modified and unmodified cells were visible only at higher concentrations of cell protein lysates (Tang *et al.*, 2012). In turn, the Mavri-Damelin group presented enhanced activity of ARG1 and OTC enzymes using a

radioactive method (Mavri-Damelin *et al.*, 2007). Based on their research, it is planned to use this method for future experiments because, in our opinion, only by using an isotope labeling technique (radiolabeling) can the effectiveness of the urea cycle in the newly developed C3A_AO_P2A cell line be correctly verified.

Despite obtaining not fully conclusive results concerning the activity of ARG1 and OTC proteins, it was considered that the comparison of urea production between all analyzed cell lines would allow for the assessment of the success of the performed genetic modification. Previously, the urea concentration was measured only in cell lysates (Pluta *et al.*, 2020). However, knowing that urea is formed inside the cell and is efficiently transported into the bloodstream, measurements of urea content both in cell lysates and in post-culture medium were performed. The experiments revealed very intriguing results. The highest urea content in cell lysates was observed in C3A_AO_III, whereas regarding urea secretion into the medium, the newly developed C3A_AO_P2A cell line was the most efficient (Figure 44). Nonetheless, analyzing the total amounts of urea (from cell lysates and post-culture medium), it might be concluded that C3A_AO_P2A cells were characterized by the greatest production of the analyzed metabolite among all three HCC cell lines (1.3-fold and 1.7-fold greater than that of C3A and C3A_AO_III cells, respectively). Notably, by measuring urea in cell lysates and in post-culture medium, discrepancies in its content in both fractions were detected. Moreover, the obtained results showed that C3A_AO_III cells accumulate this metabolite inside the cell. Thus, it might be speculated that the active urea transport through the membranes might be disturbed. According to the literature, urea transport is facilitated by UT-A and UT-B transporters (Klein *et al.*, 1999; Lucien *et al.*, 2005). Moreover, aquaporin-9 (AQP9), which is a urea-permeable protein localized at the basolateral membrane of hepatocytes, is also thought to be involved in urea efflux; however, the exact mechanism is not yet fully understood (Jelen *et al.*, 2012; Geyer *et al.*, 2013). The comparison of our results with those obtained by the Mavri-Damelin group was not possible because they used radioisotopic techniques for measurements (Mavri-Damelin *et al.*, 2007). In turn, the Tang group investigated the urea content in conditioned medium using 60 mM ammonium chloride as a substrate for the reaction, which was the lowest studied concentration. Under these conditions, HepG2/(hArgI+hOTC)4 cells produced approximately 1.7-fold more urea than their unmodified counterparts (Tang *et al.*, 2012). Our experiments were performed in the presence of 40 mM ammonium chloride, as 60 mM concentration of this substance was found to be toxic to cells (Figure 45). Moreover, Tang et al. presented in their paper the concentration of produced urea (Tang *et al.*, 2012), whereas our results were expressed as the urea mass counted per cell (Figure 44). Thus, a direct

comparison of the obtained data was not possible. Taking these considerations into account, it might be concluded that the newly developed C3A_AO_P2A cell line produces urea more effectively than C3A and C3A_AO_III cells, suggesting that this success could be attributed inter alia to changes in method used for urea cycle restoration.

Nonetheless, it is worth noting that considering ammonia elimination, newly developed C3A_AO_P2A cells did not achieve the efficacy of primary human hepatocytes. This finding was confirmed by measurements conducted in cell lysates for liver cell isolate, which revealed approximately 20-fold higher urea content than that in the C3A_AO_P2A cell lysates. It is supposed that the reason for this is the low or lack of expression of the *CPS1* gene in the parental C3A cells. The CPS1 enzyme catalyzes the first step of the urea cycle and is regarded as its key limiting factor (Nitzahn and Lipshutz, 2020). According to the literature, DNA methylation suppresses the expression of the *CPS1* gene in human HCC cells, resulting in the abolishment of the urea cycle (Liu *et al.*, 2011). However, looking through scientific reports, contradictory information about the mRNA level of the *CPS1* gene in different HCC cell lines was found. For example, Hoekstra et al. showed that the *CPS1* gene is expressed at a low level in HepaRG cells (Hoekstra *et al.*, 2011). In turn, Tang et al. revealed that HepG2 cells also expressed the analyzed gene, whereas Missiaen et al. reported a lack of mRNA for the *CPS1* gene (Tang *et al.*, 2012; Missiaen *et al.*, 2022). In the case of C3A cells, Mavri-Damelin et al. reported that these cells expressed this gene but at a relatively low level (Mavri-Damelin *et al.*, 2008). These findings were similar to our preliminary research. Our study confirmed that the C3A cell line expressed the *CPS1* gene at a low level, whereas the expression of this gene was slightly upregulated in both genetically modified cell lines (data not shown). Despite these discrepancies, it is supposed that after introducing additional copies of the *CPS1* gene into the C3A_AO_P2A cell genome, the functionality of the urea cycle will be closer to the efficacy of primary human hepatocytes. For example, studies conducted by Adam et al. showed that the overexpression of the *CPS1* gene in the HepaRG cell line significantly improved the process of ureagenesis (Adam *et al.*, 2019). Therefore, it is believed that this is a necessary step toward improving the efficiency of C3A_AO_P2A cells in ammonia elimination. Nonetheless, it is worth mentioning that other factors also have an impact on the urea cycle. First, the urea cycle is predominantly regulated by several transcription factors, such as HNF1A, HNF4A, C/EBPA or the glucocorticoid receptor. They work in response to the amino acid balance or the presence of glucocorticoids, insulin or glucagon (Morris, 2002). Second, mitochondrial transporters, such as ornithine carrier 1 (ORC1), are also involved in maintaining the proper functionality of the urea cycle because they are responsible for protein transport between the cytosol and

mitochondria (Monné *et al.*, 2015). Finally, to activate the CPS1 enzyme, the allosteric cofactor *N*-acetylglutamate (NAG) is needed. The production of NAG is in turn catalyzed by *N*-acetylglutamate synthase (NAGS) (Caldovic *et al.*, 2010). Interestingly, Hoekstra et al. reported that the activity of NAGS in HepaRG cells is not sufficient. Thus, to activate the CPS1 enzyme, they added synthetic NAG to the culture medium (Hoekstra *et al.*, 2011). Therefore, it might be valuable to verify the activity of NAGS in parental C3A cells and in their genetically modified counterparts in future experiments.

Finally, the influence of ammonia on the metabolic activity and viability of the newly developed C3A_AO_P2A cell line was analyzed. Resistance to ammonia toxicity is a very essential issue, especially in BAL devices, where nonphysiological concentrations of this substance are present. Although the neurotoxic effect of ammonia on astrocyte dysfunction is well documented (Ohara *et al.*, 2009; Drews *et al.*, 2020), few studies have evaluated the cytotoxic impact of this substance on liver parenchymal cells. Several reports have shown that hyperammonemia can lead to the disruption of hepatocyte metabolism, cause apoptosis and affect gene expression (Jia *et al.*, 2014; Wang *et al.*, 2022). Moreover, some scientific papers suggest that ammonia may be associated with the development of liver diseases (Jalan *et al.*, 2016; De Chiara *et al.*, 2020). Our own research showed that 20 mM ammonium chloride did not significantly affect the metabolic activity of human HCC cells. In turn, in 40 mM ammonia, both genetically modified cell lines demonstrated greater metabolic activity than their parental C3A cells. This difference in ammonia tolerance was 1.3-fold (p-value < 0.001) and 1.2-fold (p-value = 0.014) greater when comparing C3A_AO_III and C3A_AO_P2A cells with unmodified C3A, respectively. Although, at a 60 mM concentration of ammonia a dramatic reduction in metabolic activity was observed, both genetically modified cell lines were more resistant (approximately 1.3-fold) to ammonia-induced stress than their parental cells (Figure 45). Tang et al. also evaluated the difference in cell tolerance to ammonia between genetically modified HepG2/(hArgI+hOTC)4 cells and unmodified HepG2 cells. However, they started to study this impact only from a 60 mM concentration of ammonia, whereas as mentioned above, this amount was toxic for human HCC cells (Figure 45). Despite this, they reported that at a 60 mM concentration of ammonia, HepG2/(hArgI + hOTC)4 cells were characterized by 1.8-fold greater metabolic activity than unmodified HepG2 cells. The fact that they obtained better results might be explained by the very dense starting cell culture (100 000 cells, whereas in the current study 30 000 cells) and shorter exposure to the toxic substance (12 hours, whereas in our experiments 24 hours) (Tang *et al.*, 2012). In our opinion, the choice of these two parameters by Tang et al. strongly affected the outcome results. In the case of cell viability, our

own research revealed that ammonia affects this parameter, which was confirmed using flow cytometry (Figure 47) and the trypan blue exclusion method (Figure 46). However, after exposure to ammonium chloride, both genetically modified cell lines were characterized by a lower percentage of dead cells than their parental cell line. This effect was especially visible for 40 mM ammonium chloride (Figure 46, Figure 47). Under these conditions, the percentage of dead cells increased approximately 2-fold (p-value < 0.001) and 3-fold (p-value < 0.001) for C3A cells compared to that of C3A_AO_III and C3A_AO_P2A cell lines, respectively (Figure 46, Figure 47). In summary, it might be concluded that both genetically modified cell lines are less prone to ammonia-induced oxidative/nitrosative stress. Moreover, in our previous research, it was speculated that the integration of additional copies of the h*ARG1* and h*OTC* genes may be associated with increased resistance to ammonia (Pluta *et al.*, 2020). Indeed, this phenomenon was confirmed in the present study.

Evaluation of the functionality of the new genetically modified C3A_AO_P2A cell line under dynamic conditions

As mentioned above, the second goal of my doctoral thesis was to evaluate the functionality of the newly established C3A_AO_P2A cell line under static and dynamic conditions. In this section, the results obtained for dynamic culture will be discussed. Similarly, to make a comparison, all experiments performed with C3A_AO_P2A cells were also conducted with C3A_AO_III and C3A cells.

The prevalence of 3D hepatic cell culture systems over standard monolayers (2D) is because such models better resemble the *in vivo* tissue environment. Moreover, such systems have the ability to mimic the complex architecture of the liver, which facilitates the performance of liver-specific functions. Additionally, under 3D conditions, cell polarization is preserved and cell-cell or cell-matrix interactions are ensured, enabling the response to different stimuli (Anton *et al.*, 2015; Polidoro *et al.*, 2021). According to the literature, 3D culture is beneficial for human hepatic cells. For example, Mori and Kida reported that HepG2 cells cultured in a 3D microfluidic perfusion system were characterized by increased expression of genes involved in drug metabolism (Mori and Kida, 2020). Another study showed that C3A cells cultured on alginate scaffolds exhibited enhanced liver-specific performance and phenotype (Elkayam *et al.*, 2006). Research conducted by Stampar et al. concerning the culture of HepG2 cells as spheroids demonstrated similar results. Moreover, compared to standard monolayers, such spheroids were characterized by increased expression of liver-specific genes, suggesting more

mature phenotype (Štampar *et al.*, 2020). In turn, another group showed enhanced functionality of HepaRG cells cultured under dynamic conditions ensured by hollow fiber bioreactors. The obtained results confirmed that this cell line displayed increased albumin synthesis and urea production under these conditions (van Wenum *et al.*, 2016).

There are many different types of 3D hepatic culture systems, including spheroid/organoid culture, scaffolds, hydrogels, flow bioreactors (e.g., hollow fiber bioreactors), and microfluidic platforms (e.g., liver-on-the-chip). The choice of culture system usually depends on the application (Duval *et al.*, 2017). In the case of BAL devices, the majority of them, especially those that are the most advanced, which came to the third phase of clinical trials (HepatAssist and ELAD), utilized hollow fiber bioreactors. Hollow fiber bioreactors consist of a bundle of semipermeable capillary membranes and due to the constant flow through their lumen, conditions existing in the liver (e.g., vascularization, sinusoids – fenestrated capillaries) can be recreated. Moreover, they are characterized by relatively good mass transfer properties. This resulted from the large surface area, which enables effective bidirectional transport of nutrients and waste products. This configuration facilitates the performance of liver-specific functions (Diban and Stamatialis, 2014; Eghbali *et al.*, 2016).

Considering all of the abovementioned advantages and the great application potential, especially in BAL devices, it was decided to construct a system for dynamic culture with self-made hollow fiber bioreactors. First, attention was given to the choice of membrane, and finally, commercially available capillaries made of polysulfone were selected. Polysulfone, due to its good psychological, chemical, and biological properties, is widely used in tissue-engineered BAL. Moreover, polysulfone is characterized by mechanical stability, and thus, various sterilization techniques can be applied (Carpentier, Gautier and Legallais, 2009). Several experimental studies confirmed the validity of using polysulfone capillary membranes (Liu *et al.*, 2001; Dufresne *et al.*, 2013; Ren *et al.*, 2015). However, polysulfone is hydrophobic, which might affect cell adhesion because for adherent cell cultures, hydrophilic surfaces are preferable (Kim *et al.*, 2002; Arima and Iwata, 2007). Thus, there were doubts regarding whether this membrane would be suitable for our experiments. Nonetheless, our own study showed that commercial polysulfone capillary membranes were characterized by contact angle lower than 90°, suggesting their hydrophilicity (Figure 50). Additionally, as polysulfone capillary membranes were intended for dynamic cell culture, the biocompatibility of the chosen material was determined. The conducted research showed that the polysulfone membrane had no negative effect on cell viability, metabolic activity or protein secretion (Figure 51, Figure 53, Figure 54). The other vital issue concerns the choice of the appropriate size of the pores

because hollow fiber membranes must simultaneously serve as isolation barriers and enable proper mass transfer. Thus, this parameter should be small enough to isolate cells and large enough to allow for the exchange of nutrients and waste. As the manufacturer declares, our polysulfone capillary membranes have a pore size of 0.2 μm, which was confirmed using SEM (Figure 49). As reported in the literature, larger pores (i.e., 0.1 μm or 0.2 μm) positively affect the transfer of albumin and urea (Meng, Zhang and Wu, 2004; Iwamuro *et al.*, 2012). Therefore, it might be concluded that the chosen polysulfone capillary membranes should be suitable for dynamic cell culture.

Before developing the system for dynamic cell culture, hollow fiber bioreactors, which serve as the heart of the system, were self-constructed (Figure 17). Each culture module contains 20 capillary membranes and enables cell growth at the surface, which equals approximately 22 cm^2. The physical properties of the membranes (i.e., retention, ultrafiltration) in the constructed hollow fiber bioreactors were evaluated. Retention measurements revealed that our capillaries are permeable to substances smaller than 0.2 μm, which is consistent with the manufacturer's declaration (Table 21). However, red fluorescent microspheres with a size of 0.1 μm were partially retained in the membrane. In our opinion, this might have resulted from their tendency to form clusters (Figure 55). Ultrafiltration measurements of aqueous solution flow through the capillaries were also convenient for cell culture (Table 20). Finally, the system for dynamic cell culture was self-constructed, which basically consisted of a hollow fiber bioreactor (culture module), peristaltic pump, oxygenator/bubble trap, and medium reservoir (Figure 19). The aim of our study was to investigate the performance of human HCC cells in flow culture, not to make innovative improvements; thus, the development of our system was based on experimental studies conducted by other scientific groups. Elder publications (Nyberg *et al.*, 1993; Rozga *et al.*, 1993; Takeshita *et al.*, 1995; Flendrig *et al.*, 1997), which often presented preliminary studies with bioreactors further used as BAL devices, and current reports (Gautier *et al.*, 2009; Sullivan, Harris and Palmer, 2008; Palakkan *et al.*, 2013) utilized those four abovementioned items for the construction of such systems. Sometimes scientists use different bioreactor designs (Jasmund *et al.*, 2002; De Bartolo *et al.*, 2009), but in general, such a configuration is sufficient to conduct dynamic cell culture. For example, Storm et al. presented a step-by-step protocol for how to manufacture a system for flow culture for the purpose of experimental study with different types of mammalian cells (Storm *et al.*, 2016).

In this study, experiments started from an optimization procedure to establish an appropriate flow rate and seeding density, both of which are crucial parameters for dynamic cell culture. Looking through the literature, it was found that for the experimental study, the

following flow rates were used: 1 mL/min (Takeshita *et al.*, 1995), 1.5 mL/min (De Bartolo *et al.*, 2009; Palakkan *et al.*, 2013), 2 mL/min (Ren *et al.*, 2015), 5 mL/min (van Wenum *et al.*, 2016), 5-23 mL/min (Sullivan, Harris and Palmer, 2008) or 10 mL/min (Rozga *et al.*, 1993). Taking this into account, three different flow rates (1 mL/min, 5 mL/min, and 10 mL/min) were chosen, and to investigate their effect on mass transfer, mathematical simulations were conducted. The obtained results revealed that the higher the flow rate was used, the quicker mass exchange occurred (Figure 56A, Figure 56B). Similar research was performed by the Gautier group, who simulated the effect of two different flow rates (3 mL/min and 10 mL/min) on the transport of nutrients. Their observations were consistent with our findings. They also concluded that choosing 10 mL/min as the flow rate should be more beneficial for cell performance in dynamic culture (Gautier *et al.*, 2009). Therefore, it was decided to experimentally study only two flow rates: 5 mL/min and 10 mL/min. In the case of seeding density, the following values were found in the literature: $0.5 \cdot 10^6$ (Gautier *et al.*, 2009), $2 \cdot 10^6$ (Storm *et al.*, 2016), $5 \cdot 10^6$ (Palakkan *et al.*, 2013) or $9\text{-}10 \cdot 10^6$ (Ren *et al.*, 2015). According to Gerlach et al. cell behavior depends on seeding density (Gerlach *et al.*, 1994). Thus, it was decided to experimentally evaluate two different seeding densities: $0.5 \cdot 10^6$ cells per bioreactor and $5 \cdot 10^6$ cells per bioreactor. The optimization process was performed using C3A cells. As described earlier (section 4.10.3), cells were seeded on the extracapillary space of the capillary membrane. According to the literature, such a configuration positively affects the oxygen supply to cells (Eghbali *et al.*, 2016). Moreover, the medium flow through the capillaries provides moderate shear stress, which is typical for the *in vivo* hepatocyte environment (Li *et al.*, 2021). The whole experiment was run for 12 days, and media samples were collected every 2-3 days. For the control, cells were also cultured under static conditions using T25 flasks, as their growth surface area was similar to that in bioreactors.

During the optimization process, the influence of different flow rates and seeding densities on glucose consumption and albumin secretion was analyzed. The obtained results showed that the medium flow rate did not significantly affect glucose usage, whereas the initial number of seeded cells had a more significant impact. As expected, a 10-fold lower seeding density ($0.5 \cdot 10^6$ cells per bioreactor) resulted in a significant decrease in glucose consumption (Figure 57). In the case of albumin, the synthesis of this protein was strongly affected by both analyzed parameters. The best results were obtained when a flow rate of 10 mL/min and seeding density of $5 \cdot 10^6$ cells/module were applied. Interestingly, the use of the lower flow rate (5 mL/min) resulted in a decrease in albumin synthesis. In turn, the lowest albumin secretion, which was comparable to the results obtained for the static controls, was observed for the

culture variant, in which 10-fold lower seeding density was applied ($0.5 \cdot 10^6$ cells per bioreactor). Nonetheless, taking these considerations into account, it was decided to choose the following parameters for further experiments: medium flow rate - 10 mL/min, and initial seeding density - $5 \cdot 10^6$ cells/module.

The final experiments were conducted for both the genetically modified cell lines and their parental C3A cells. The performance of all three cell lines under dynamic conditions was compared, and thus, albumin secretion, glucose consumption, urea production, and cell viability were analyzed. For each cell line, two independent biological repetitions (bioreactors) were carried out. As underlined several times, the ability to synthetize albumin is one of the major indicators of hepatic functions (de Hoyos-Vega *et al.*, 2021). Our own results showed that in dynamic culture, genetically modified cells outperformed their unmodified counterparts in the secretion of this protein. Importantly, both biological repetitions revealed that the newly developed C3A_AO_P2A cell line was characterized by the highest albumin production (calculated as the total mass content) under flow conditions. Additionally, compared to that of the static controls, a significant increase in the secretion of this protein under dynamic conditions was observed for all analyzed cell lines (Figure 61, Figure 63). In our opinion, this might be explained by the fact that flow culture in our bioreactors allows for the establishment of a 3D environment, which provides very essential homotypic cell-cell interactions (Li *et al.*, 2014). This was also confirmed by microscopic analysis, which suggested that some of the cells formed aggregates that resembled spheroids (Figure 59). Moreover, many scientific reports were consistent with our observations and showed an increase in albumin secretion during culture in hollow fiber bioreactors (Palakkan *et al.*, 2013; Ren *et al.*, 2015; van Wenum *et al.*, 2016). In the case of glucose consumption, interesting observations were made. The results of both biological repetitions obtained for static conditions indicated intensive glucose consumption, especially in the first days of culture (Figure 60, Figure 62). This can be explained by the lack of fresh medium, whereas dynamic conditions ensured constant access to nonlimited glucose in a much larger (ca. 20 times) volume of medium. Therefore, it might be concluded that flow culture constituted a more efficient type of culture, which ensures better availability of nutrients and faster gas exchange. Thus, it implicated better conditions for cell growth and enhanced liver-specific functions. As the main function of BAL devices is ammonia elimination, the effect of flow cell culture on urea production was analyzed. However, our method for urea determination (section 4.8.11) is quite complicated to use under dynamic conditions. Briefly, it relies on two medium changes: first, the culture medium is replaced with the fresh medium containing 40 mM ammonium chloride, which, after 24 hours, is replaced

with the fresh medium containing a decreased amount of FBS (at a concentration of 1%). However, our aim was to conduct long-term dynamic culture without any disturbance concerning medium removal. Therefore, it was decided to measure urea in the samples collected every 2-3 days. Unfortunately, the determination of urea content in dynamic culture was not manageable. Two possible explanations are as follows: lack of an appropriate amount of substratum for the urea cycle (ammonia) and too much dilution to detect urea in the used large volume of medium containing 10% FBS. Therefore, in future experiments, the adjustment of our method to dynamic conditions and subsequent proper measurements are planned. The last analyzed parameter was cell viability. As described earlier (section 5.4.2.2), the detachment of all cells from capillaries in hollow fiber bioreactors was not possible due to their strong attachment to the surface of the membrane (Figure 59). Similar problems were reported by the Ren group, who revealed that cell harvesting was inefficient because cells were stuck between fibers. Therefore, they determined cell viability only for detached cells and focused on analyzing more parameters related to cell functionality (Ren *et al.*, 2015). In our opinion, their conclusions are reasonable and could be a good clue for our future experiments. Nevertheless, several attempts have been made, however unsuccessful, to estimate the final number of cells at the end of dynamic culture because our aim was to verify cell proliferation. Moreover, this value was necessary for calculating the albumin secretion per number of cells, as was done in the analysis of static culture. However, in such applications as BAL devices, the capacity to produce albumin by the whole bioreactor is more important than individual cell effectiveness. Thus, there is no need to perform such calculations. Our conclusion is consistent with several scientific reports, which did not present the amount of secreted albumin counted per number of living cells (Palakkan *et al.*, 2013; Ren *et al.*, 2015; van Wenum *et al.*, 2016).

In summary, the self-constructed system enabled successful long-term dynamic cell culture. During culture, significant differences, especially in albumin secretion, between flow and static conditions were observed, indicating that flow culture was more efficient. Importantly, the best results under dynamic conditions were obtained for the newly developed C3A_AO_P2A cell line. Therefore, it might be concluded that C3A_AO_P2A cells could be a new alternative source of cells for improved BAL devices. Obviously, our conclusions are based mostly on albumin secretion; therefore, investigations of additional liver-specific parameters (e.g., metabolism of xenobiotics, expression of liver-related genes) are planned in the future. Moreover, an effective method for determining urea production and ammonia detoxification in dynamic culture will be developed. Additionally, the changes in oxygen concentration during culture will be monitored. As hepatocytes exhibit highly oxygen-

dependent metabolism, this nutrient is regarded as the key limiting factor in hollow fiber bioreactor cultures (Hay, Veitch and Gaylor, 2001; Sullivan, Gordon and Palmer, 2006). Finally, the introduction of changes into the system for dynamic cell culture (e.g., an increase in the number of fibers) will be performed. It is believed that after these modifications are made, more information about cell performance under flow conditions will be received. Nonetheless, on the basis of the obtained results, the conclusion that C3A_AO_P2A cells could serve as a new source of cells in improved BAL devices seems to be reasonable.

7. Conclusions

Currently, the only effective treatment for patients suffering from liver failure is orthotropic transplantation. Unfortunately, donor shortage is a great limitation to this therapy. Therefore, scientists have made many different attempts to support patients suffering from liver failure. It is worth emphasizing the complexity of the problem and the fact that interdisciplinary solutions are needed. Thus, the cooperation of scientists from different fields is very important. Each scientific study has the purpose of being beneficial for patients waiting for liver transplantation. I believe that I also contributed to the field of LSS thanks to my doctoral dissertation. The motivation for my research was the poor outcome of clinical trials with the use of an ELAD device, which is the most advanced bioartificial liver support system. ELAD utilizes as the biological component the C3A cell line, which is characterized by dysfunction of the urea cycle. This resulted from the lack or low expression of the arginase 1 (*ARG1*) and ornithine transcarbamylase (*OTC*) genes, which encode proteins involved in the enzymatic reactions of this cycle. Thus, this metabolic dysfunction limits the use of C3A cells in the treatment of liver diseases, as the detoxification of ammonia is an essential liver function, especially in BAL devices. In patients suffering from liver diseases, reduced activity of metabolic pathways related to ammonia metabolism is often observed. In turn, the persistent high concentration of this compound in the blood can lead to hepatic encephalopathy. Therefore, effective ammonia elimination is one of the bases for the successful treatment of liver failure. Thus, the research presented in this doctoral dissertation aimed to compensate for metabolic dysfunctions related to ammonia detoxification, which exist in the C3A cell line. Although such experiments have been previously performed in our laboratory, several changes in the methodology were made to improve the effectiveness of genetic modification. Thus, in this doctoral study, the newly genetically modified HCC cell line - C3A_AO_P2A was established using self-prepared lentiviral vectors. Moreover, as part of this research, the functionality of the newly developed C3A_AO_P2A cell line was evaluated under static and dynamic conditions. Research conducted in static culture confirmed that the C3A_AO_P2A cell line (1) is characterized by similar secretion of albumin, the main liver marker, to their parental C3A cells; (2) produces a significantly greater amount of urea, indicating an increased capacity to detoxify ammonia; and (3) is more resistant to ammonia-induced oxidative/nitrosative stress. In the case of dynamic culture in the self-constructed system, the newly established C3A_AO_P2A cell line exhibited the highest albumin secretion among all analyzed human HCC cell lines. It is worth emphasizing the importance of the conducted

research because, due to the improved overall cell performance after genetic modification, the use of the newly developed C3A_AO_P2A cell line as a potential source of cells for improved bioartificial liver support systems might be considered.

The studies conducted during this dissertation confirmed the doctoral theses and allowed to make the following conclusions:

1. Conducted genetic modification of the human HCC C3A cell line with the use of lentiviral vectors was successful and allowed to establish the C3A_AO_P2A cell line. Particularly noteworthy is the fact that, thanks to antibiotic selection, the C3A_AO_P2A cell line is a population consisting of nearly 100% genetically modified cells.
2. No negative effect of the performed genetic modification on the morphology, viability, and mitochondrial activity of the C3A_AO_P2A cell line was observed.
3. Conducted genetic modification did not negatively affect albumin synthesis by the newly developed C3A_AO_P2A cell line; however, the increase in the secretion of this protein to the same extent as that in C3A_AO_III cells has not been confirmed.
4. Conducted genetic modification resulted in significantly greater expression of the *ARG1* and *OTC* genes in the newly developed C3A_AO_P2A cells. Although such an extensive effect was not visible at the protein level, the overproduction of ARG1 and OTC proteins was confirmed.
5. Newly developed C3A_AO_P2A cells were characterized by the highest activity of both arginases among all three analyzed HCC cell lines. Unfortunately, the activity of the OTC enzyme was not detectable in any of the HCC cell lines. Therefore, it might be concluded that the obtained results were inconclusive and need further verification.
6. The newly developed C3A_AO_P2A cell line produced urea more effectively than the C3A and C3A_AO_III cell lines.
7. Measurements of urea content in cell lysates and in post-culture medium showed that C3A_AO_III cells accumulate this metabolite inside the cell. Thus, it might be speculated that active urea transport through membranes might be disturbed in these cells.
8. Both genetically modified cell lines are less prone to ammonia-induced oxidative/nitrosative stress. This phenomenon might be associated with the integration of additional copies of the h*ARG1* and h*OTC* genes into the cell genome.
9. The choice of method for conducting genetic modification matters.

10. The dynamic cell culture in the self-constructed system was successful.
11. Among all analyzed HCC cell lines, the newly developed C3A_AO_P2A cell line exhibited the best cell performance under flow conditions, especially in terms of albumin secretion.
12. The newly developed C3A_AO_P2A cell line could constitute a more attractive source of cells for use in BAL devices.

Our future plans concern:

1. Development of methods for evaluating the enzymatic activity of ARG1 and OTC proteins.
2. As the urea cycle performance in C3A_AO_P2A cells requires further improvement, we are planning to introduce the *CPS1* gene into their genome and test the effect of this third gene addition on its functionality.
3. Evaluation of NAGS activity in the C3A cell line and its genetically modified derivatives.
4. Evaluation of the gene and protein expression of the remaining enzymes (ASS, ASL) involved in the urea cycle in the C3A cell line and their genetically modified derivatives.
5. Introduction of some changes to the system for dynamic cell culture. For example, we would like to evaluate how an increase in the number of polysulfone capillary membranes influences cell performance under flow conditions.
6. Development of the method for determining urea production and ammonia detoxification in dynamic culture conditions.
7. We are planning to increase the number of analyzed liver-specific parameters during dynamic cell culture, especially paying attention to the oxygen concentration in the culture medium.
8. We are planning to conduct a dynamic coculture of new C3A_AO_P2A cells with feeder layer cells, e.g., genetically modified fibroblasts overexpressing liver-relevant growth factors.

8. Bibliography

1. Abdel-Misih, S.R.Z. and Bloomston, M. (2010) 'Liver anatomy', *The Surgical clinics of North America*, 90(4), pp. 643–653. Available at: https://doi.org/10.1016/J.SUC.2010.04.017.
2. Acharya, M., Berger, R. and Popov, A.F. (2022) 'The role of the ADVanced Organ Support (ADVOS) system in critically ill patients with multiple organ failure', *Artificial Organs*, 46(5), pp. 735–746. Available at: https://doi.org/10.1111/AOR.14188.
3. Adam, A.A.A. *et al.* (2019) 'Overexpression of carbamoyl-phosphate synthase 1 significantly improves ureagenesis of human liver HepaRG cells only when cultured under shaking conditions', *Mitochondrion*, 47, pp. 298–308. Available at: https://doi.org/10.1016/J.MITO.2019.02.005.
4. Adeva, M.M. *et al.* (2012) 'Ammonium metabolism in humans', *Metabolism*, 61(11), pp. 1495–1511. Available at: https://doi.org/10.1016/J.METABOL.2012.07.007.
5. Agarwal, B. *et al.* (2023) 'Randomized, controlled clinical trial of the DIALIVE liver dialysis device versus standard of care in patients with acute-on- chronic liver failure', *Journal of Hepatology*, 79(1), pp. 79–92. Available at: https://doi.org/10.1016/J.JHEP.2023.03.013.
6. Al-Chalabi, A. *et al.* (2013) 'Evaluation of the Hepa Wash® treatment in pigs with acute liver failure', *BMC Gastroenterology*, 13(1). Available at: https://doi.org/10.1186/1471-230X-13-83.
7. Allen, J.W., Hassanein, T. and Bhatia, S.N. (2001) 'Advances in bioartificial liver devices', *Hepatology*, 34(3), pp. 447–455. Available at: https://doi.org/10.1053/jhep.2001.26753.
8. Anton, D. *et al.* (2015) 'Three-dimensional cell culture: A breakthrough in vivo', *International Journal of Molecular Sciences*, 16(3), pp. 5517–5527. Available at: https://doi.org/10.3390/ijms16035517.
9. Arima, Y. and Iwata, H. (2007) 'Effect of wettability and surface functional groups on protein adsorption and cell adhesion using well-defined mixed self-assembled monolayers', *Biomaterials*, 28(20), pp. 3074–3082. Available at: https://doi.org/10.1016/J.BIOMATERIALS.2007.03.013.
10. Asrani, S.K. *et al.* (2019) 'Burden of liver diseases in the world', *Journal of hepatology*, 70(1), pp. 151–171. Available at: https://doi.org/10.1016/J.JHEP.2018.09.014.
11. Bachmann, A. *et al.* (2015) '3D Cultivation Techniques for Primary Human Hepatocytes', *Microarrays*, 4(1), pp. 64–83. Available at: https://doi.org/10.3390/microarrays4010064.
12. Bañares, R. *et al.* (2013) 'Extracorporeal albumin dialysis with the molecular adsorbent recirculating system in acute-on-chronic liver failure: The RELIEF trial', *Hepatology*, 57(3), pp. 1153–1162. Available at: https://doi.org/10.1002/hep.26185.
13. Baptista, P.M. *et al.* (2011) 'The use of whole organ decellularization for the generation of a vascularized liver organoid', *Hepatology*, 53(2), pp. 604–617. Available at: https://doi.org/10.1002/HEP.24067.
14. De Bartolo, L. *et al.* (2000) 'A novel full-scale flat membrane bioreactor utilizing porcine hepatocytes: Cell viability and tissue-specific functions', *Biotechnology Progress*, 16(1), pp. 102–108. Available at: https://doi.org/10.1021/bp990128o.
15. De Bartolo, L. *et al.* (2009) 'Human hepatocyte functions in a crossed hollow fiber membrane bioreactor', *Biomaterials*, 30(13), pp. 2531–2543. Available at: https://doi.org/10.1016/J.BIOMATERIALS.2009.01.011.
16. Baudoin, R. *et al.* (2011) 'Behavior of HepG2/C3A cell cultures in a microfluidic bioreactor', *Biochemical Engineering Journal*, 53(2), pp. 172–181. Available at: https://doi.org/10.1016/J.BEJ.2010.10.007.
17. Belinskaia, D.A. *et al.* (2021) 'Serum Albumin in Health and Disease: Esterase, Antioxidant, Transporting and Signaling Properties', *International Journal of Molecular*

Sciences, 22(19), p. 10318. Available at: https://doi.org/10.3390/IJMS221910318.
18. Bernal, W. *et al.* (2007) 'Arterial ammonia and clinical risk factors for encephalopathy and intracranial hypertension in acute liver failure', *Hepatology*, 46(6), pp. 1844–1852. Available at: https://doi.org/10.1002/HEP.21838.
19. Bernal, W. and Wendon, J. (2013) 'Acute Liver Failure', *The new England journal of medicine*, 369(26), pp. 2525–2534. Available at: https://doi.org/10.1056/NEJMRA1208937.
20. Bhogal, R.H. *et al.* (2011) 'Isolation of Primary Human Hepatocytes from Normal and Diseased Liver Tissue: A One Hundred Liver Experience', *PLoS ONE*, 6(3), p. e18222. Available at: https://doi.org/10.1371/journal.pone.0018222.
21. Blachier, M. *et al.* (2013) 'The burden of liver disease in Europe: a review of available epidemiological data', *Journal of hepatology*, 58(3), pp. 593–608. Available at: https://doi.org/10.1016/J.JHEP.2012.12.005.
22. Blaszkiewicz, J. and Duncan, S.A. (2022) 'Advancements in Disease Modeling and Drug Discovery Using iPSC-Derived Hepatocyte-like Cells', *Genes*, 13(4), p. 573. Available at: https://doi.org/10.3390/GENES13040573.
23. Bobak, Y.P. *et al.* (2010) 'Cancer cell sensitivity to arginine deprivation in vitro is not determined by endogenous levels of arginine metabolic enzymes', *Cell Biology International*, 34(11), pp. 1085–1089. Available at: https://doi.org/10.1042/CBI20100451.
24. Braissant, O., McLin, V.A. and Cudalbu, C. (2013) 'Ammonia toxicity to the brain', *Journal of inherited metabolic disease*, 36(4), pp. 595–612. Available at: https://doi.org/10.1007/S10545-012-9546-2.
25. Bustin, S.A. *et al.* (2009) 'The MIQE guidelines: minimum information for publication of quantitative real-time PCR experiments.', *Clinical chemistry*, 55(4), pp. 611–22. Available at: https://doi.org/10.1373/clinchem.2008.112797.
26. Caldovic, L. *et al.* (2010) 'N-acetylglutamate synthase: structure, function and defects', *Molecular genetics and metabolism*, 100(Suppl 1), p. S13-S19. Available at: https://doi.org/10.1016/J.YMGME.2010.02.018.
27. Carpentier, B., Gautier, A. and Legallais, C. (2009) 'Artificial and bioartificial liver devices: present and future', *Gut*, 58(12), pp. 1690–1702. Available at: https://doi.org/10.1136/GUT.2008.175380.
28. Chamuleau, R.A. (2009) 'Future of bioartificial liver support', *World Journal of Gastrointestinal Surgery*, 1(1), p. 21-25. Available at: https://doi.org/10.4240/wjgs.v1.i1.21.
29. Chamuleau, R.A.F.M., Poyck, P.P.C. and Van De Kerkhove, M.P. (2006) 'Bioartificial liver: Its pros and cons', *Therapeutic Apheresis and Dialysis*, 10(2), pp. 168–174. Available at: https://doi.org/10.1111/j.1744-9987.2006.00359.x.
30. Cheemerla, S. and Balakrishnan, M. (2021) 'Global Epidemiology of Chronic Liver Disease', *Clinical Liver Disease*, 17(5), p. 365-370. Available at: https://doi.org/10.1002/CLD.1061.
31. Chen, F. *et al.* (2014) 'Up-Regulating CYP3A4 Expression in C3A Cells by Transfection with a Novel Chimeric Regulator of hPXR-p53-AD', *PLOS ONE*, 9(5), p. e95752. Available at: https://doi.org/10.1371/JOURNAL.PONE.0095752.
32. Chen, H.S. *et al.* (2019) 'Randomized Trial of Spheroid Reservoir Bioartificial Liver in Porcine Model of Posthepatectomy Liver Failure', *Hepatology*, 69(1), pp. 329–342. Available at: https://doi.org/10.1002/HEP.30184.
33. De Chiara, F. *et al.* (2020) 'Ammonia Scavenging Prevents Progression of Fibrosis in Experimental Nonalcoholic Fatty Liver Disease', *Hepatology*, 71(3), pp. 874–892. Available at: https://doi.org/10.1002/HEP.30890.
34. Clemente, G.S. *et al.* (2020) 'Arginase as a Potential Biomarker of Disease Progression: A

Molecular Imaging Perspective', *International Journal of Molecular Sciences*, 21(15), p. 5291. Available at: https://doi.org/10.3390/IJMS21155291.
35. Costa, R.H. *et al.* (2003) 'Transcription factors in liver development, differentiation, and regeneration.', *Hepatology*, 38(6), pp. 1331–47. Available at: https://doi.org/10.1016/j.hep.2003.09.034.
36. Crapo, P.M., Gilbert, T.W. and Badylak, S.F. (2011) 'An overview of tissue and whole organ decellularization processes', *Biomaterials*, 32(12), pp. 3233–3243. Available at: https://doi.org/10.1016/J.BIOMATERIALS.2011.01.057.
37. Cunningham, R.P. and Porat-Shliom, N. (2021) 'Liver Zonation – Revisiting Old Questions With New Technologies', *Frontiers in Physiology*, 12, pp. 1–17. Available at: https://doi.org/10.3389/fphys.2021.732929.
38. Damm, G. *et al.* (2013) 'Human parenchymal and non-parenchymal liver cell isolation, culture and characterization', *Hepatology International*, 7(4), pp. 951–958. Available at: https://doi.org/10.1007/s12072-013-9475-7.
39. Davies, N.A. and Bañares, R. (2015) 'A new horizon for liver support in acute liver failure', *Journal of Hepatology*, 63(2), pp. 303–305. Available at: https://doi.org/10.1016/j.jhep.2015.05.020.
40. Demetriou, A.A. *et al.* (1995) 'Early clinical experience with a hybrid bioartificial liver', *Scandinavian journal of gastroenterology. Supplement*, 208, pp. 111–117. Available at: https://doi.org/10.3109/00365529509107771.
41. Demetriou, A.A. *et al.* (2004) 'Prospective, Randomized, Multicenter, Controlled Trial of a Bioartificial Liver in Treating Acute Liver Failure', *Annals of Surgery*, 239(5), p. 660-670. Available at: https://doi.org/10.1097/01.SLA.0000124298.74199.E5.
42. Deurholt, T. *et al.* (2009) 'Novel immortalized human fetal liver cell line, cBAL111, has the potential to differentiate into functional hepatocytes', *BMC Biotechnology*, 9(1), p. 89. Available at: https://doi.org/10.1186/1472-6750-9-89/FIGURES/4.
43. Dhawan, A. *et al.* (2010) 'Human hepatocyte transplantation: current experience and future challenges', *Nature reviews. Gastroenterology & hepatology*, 7(5), pp. 288–298. Available at: https://doi.org/10.1038/NRGASTRO.2010.44.
44. Diban, N. and Stamatialis, D. (2014) 'Polymeric hollow fiber membranes for bioartificial organs and tissue engineering applications', *Journal of Chemical Technology & Biotechnology*, 89(5), pp. 633–643. Available at: https://doi.org/10.1002/JCTB.4300.
45. Diekmann, S., Bader, A. and Schmitmeier, S. (2006) 'Present and Future Developments in Hepatic Tissue Engineering for Liver Support Systems: State of the art and future developments of hepatic cell culture techniques for the use in liver support systems', *Cytotechnology*, 50(1–3), pp. 163–179. Available at: https://doi.org/10.1007/S10616-006-6336-4.
46. Ding, Y.T. *et al.* (2003) 'The development of a new bioartificial liver and its application in 12 acute liver failure patients', *World journal of gastroenterology*, 9(4), pp. 829–832. Available at: https://doi.org/10.3748/WJG.V9.I4.829.
47. Donato, M.T., Castell, J. V. and Gómez-Lechón, M.J. (1999) 'Characterization of drug metabolizing activities in pig hepatocytes for use in bioartificial liver devices: Comparison with other hepatic cellular models', *Journal of Hepatology*, 31(3), pp. 542–549. Available at: https://doi.org/10.1016/S0168-8278(99)80049-X.
48. Drews, L. *et al.* (2020) 'Ammonia inhibits energy metabolism in astrocytes in a rapid and glutamate dehydrogenase 2-dependent manner', *Disease models & mechanisms*, 13(10). Available at: https://doi.org/10.1242/DMM.047134.
49. Duan, Z. *et al.* (2018) 'Comparison of extracorporeal cellular therapy (ELAD®) vs standard of care in a randomized controlled clinical trial in treating Chinese subjects with acute-on-chronic liver failure', *Hepatic Medicine: Evidence and Research*, 10, p. 139-152.

Available at: https://doi.org/10.2147/HMER.S180246.
50. Dufresne, M. *et al.* (2013) 'Human hepatic cell behavior on polysulfone membrane with double porosity level', *Journal of Membrane Science*, 428, pp. 454–461. Available at: https://doi.org/10.1016/j.memsci.2012.10.041ï.
51. Dutkowski, P. *et al.* (2015) 'Challenges to liver transplantation and strategies to improve outcomes', *Gastroenterology*, 148(2), pp. 307–323. Available at: https://doi.org/10.1053/J.GASTRO.2014.08.045.
52. Duval, K. *et al.* (2017) 'Modeling physiological events in 2D vs. 3D cell culture', *Physiology*, 32(4), pp. 266–277. Available at: https://doi.org/10.1152/PHYSIOL.00036.2016.
53. Eghbali, H. *et al.* (2016) 'Hollow fiber bioreactor technology for tissue engineering applications', *International Journal of Artificial Organs*, 39(1), pp. 1–15. Available at: https://doi.org/10.5301/IJAO.5000466.
54. Elkayam, T. *et al.* (2006) 'Enhancing the Drug Metabolism Activities of C3A— A Human Hepatocyte Cell Line—By Tissue Engineering Within Alginate Scaffolds', *Tissue Engineering*, 12(5), pp. 1357–1368. Available at: https://doi.org/10.1089/TEN.2006.12.1357.
55. Ellis, A.J. *et al.* (1996) 'Pilot-controlled trial of the extracorporeal liver assist device in acute liver failure', *Hepatology*, 24(6), pp. 1446–1451. Available at: https://doi.org/10.1002/HEP.510240625.
56. Enosawa, S. *et al.* (2000) 'Long-term culture of glutamine synthetase-transfected HepG2 cells in circulatory flow bioreactor for development of a bioartificial liver', *Cell transplantation*, 9(5), pp. 711–715. Available at: https://doi.org/10.1177/096368970000900520.
57. Falkenhagen, D. *et al.* (1999) 'Fractionated plasma separation and adsorption system: a novel system for blood purification to remove albumin bound substances', *Artificial organs*, 23(1), pp. 81–86. Available at: https://doi.org/10.1046/J.1525-1594.1999.06292.X.
58. Felgendreff, P. *et al.* (2022) 'Preclinical Experience of the Mayo Spheroid Reservoir Bioartificial Liver (SRBAL) in Management of Acute Liver Failure', *Livers*, 2(4), pp. 387–399. Available at: https://doi.org/10.3390/livers2040029.
59. Feng, R. *et al.* (2022) 'A hierarchical regulatory network ensures stable albumin transcription under various pathophysiological conditions', *Hepatology*, 76(6), pp. 1673–1689. Available at: https://doi.org/10.1002/HEP.32414.
60. Ferrell, L. (2000) 'Liver Pathology: Cirrhosis, Hepatitis, and Primary Liver Tumors. Update and Diagnostic Problems', *Modern Pathology*, 13(6), pp. 679–704. Available at: https://doi.org/10.1038/modpathol.3880119.
61. Filippi, C. *et al.* (2004) 'Improvement of C3A cell metabolism for usage in bioartificial liver support systems', *Journal of Hepatology*, 41(4), pp. 599–605. Available at: https://doi.org/10.1016/J.JHEP.2004.06.012.
62. Flendrig, L.M. *et al.* (1997) 'In vitro evaluation of a novel bioreactor based on an integral oxygenator and a spirally wound nonwoven polyester matrix for hepatocyte culture as small aggregates.', *Journal of hepatology*, 26(6), pp. 1379–1392. Available at: http://www.ncbi.nlm.nih.gov/pubmed/9210627.
63. Flendrig, L.M. *et al.* (1999) 'Significantly Improved Survival Time in Pigs with Complete Liver Ischemia Treated with a Novel Bioartificial Liver', *International Journal of Artificial Organs*, 22(10), pp. 701–709. Available at: https://doi.org/10.1177/039139889902201008.
64. Forbes, S.J., Gupta, S. and Dhawan, A. (2015) 'Cell therapy for liver disease: From liver transplantation to cell factory', *Journal of hepatology*, 62(1 Suppl), pp. S157–S169. Available at: https://doi.org/10.1016/J.JHEP.2015.02.040.

65. Fox, I.J. (2014) ‘Hepatocyte Transplantation’, *Gastroenterology & Hepatology*, 10(9), p. 594-596. Available at: /pmc/articles/PMC4991536/ (Accessed: 2 June 2023).
66. Fuhrmann, V. *et al.* (2020) ‘Advanced organ support (ADVOS) in the critically ill: first clinical experience in patients with multiple organ failure’, *Annals of intensive care*, 10(1), p.96. Available at: https://doi.org/10.1186/S13613-020-00714-3.
67. García Martínez, J.J. and Bendjelid, K. (2018) ‘Artificial liver support systems: what is new over the last decade?’, *Annals of Intensive Care*, 8(1), p.109. Available at: https://doi.org/10.1186/s13613-018-0453-z.
68. Gautier, A. *et al.* (2009) ‘Hollow fiber bioartificial liver: Physical and biological characterization with C3A cells’, *Journal of Membrane Science*, 341(1–2), pp. 203–213. Available at: https://doi.org/10.1016/J.MEMSCI.2009.06.007.
69. Gerlach, J. *et al.* (1994) ‘Hepatocyte Culture between Woven Capillary Networks: A Microscopy Study’, *Artificial Organs*, 18(3), pp. 226–230. Available at: https://doi.org/10.1111/j.1525-1594.1994.tb02181.x.
70. Geyer, R.R. *et al.* (2013) ‘Relative CO(2)/NH(3) selectivities of mammalian aquaporins 0-9’, *American journal of physiology. Cell physiology*, 304(10), p. C985-C994. Available at: https://doi.org/10.1152/AJPCELL.00033.2013.
71. Gilbert, T.W., Sellaro, T.L. and Badylak, S.F. (2006) ‘Decellularization of tissues and organs’, *Biomaterials*, 27(19), pp. 3675–3683. Available at: https://doi.org/10.1016/J.BIOMATERIALS.2006.02.014.
72. Gillooly, J.F., Hein, A. and Damiani, R. (2015) ‘Nuclear DNA content varies with cell size across human cell types’, *Cold Spring Harbor Perspectives in Biology*, 7(7), pp. 1–27. Available at: https://doi.org/10.1101/cshperspect.a019091.
73. Gislason, G.T. *et al.* (1994) ‘A treatment system for implementing an extracorporeal liver assist device’, *Artificial organs*, 18(5), pp. 385–389. Available at: https://doi.org/10.1111/J.1525-1594.1994.TB02220.X.
74. Gleißner, M. *et al.* (1997) ‘Immunoisolation of Hybrid Liver Support Systems by Semipermeable Membranes’, *International Journal of Artificial Organs*, 20(11), pp. 644–649. Available at: https://doi.org/10.1177/039139889702001108.
75. Glorioso, J.M. *et al.* (2015) ‘Pivotal preclinical trial of the spheroid reservoir bioartificial liver’, *Journal of hepatology*, 63(2), pp. 388–398. Available at: https://doi.org/10.1016/J.JHEP.2015.03.021.
76. Godoy, P. *et al.* (2013) 'Recent advances in 2D and 3D in vitro systems using primary hepatocytes, alternative hepatocyte sources and non-parenchymal liver cells and their use in investigating mechanisms of hepatotoxicity, cell signaling and ADME', *Archives of Toxicology*, 87(8), p.1315-1530. Available at: https://doi.org/10.1007/s00204-013-1078-5.
77. Gorgoulis, V.G. *et al.* (2003) ‘p53 activates ICAM-1 (CD54) expression in an NF-κB-independent manner’, *The EMBO Journal*, 22(7), p. 1567-1578. Available at: https://doi.org/10.1093/EMBOJ/CDG157.
78. Grodzicki, M. *et al.* (2009) ‘Results of treatment of acute liver failure patients with use of the prometheus FPSA system’, *Transplantation proceedings*, 41(8), pp. 3079–3081. Available at: https://doi.org/10.1016/J.TRANSPROCEED.2009.08.024.
79. Gupta, S. and Bit, A. (2022) ‘3D bioprinting in tissue engineering and regenerative medicine’, *Cell and Tissue Banking*, 23(2), pp. 199–212. Available at: https://doi.org/10.1007/S10561-021-09936-6/FIGURES/11.
80. Guzman-Lepe, J. *et al.* (2018) ‘Liver-enriched transcription factor expression relates to chronic hepatic failure in humans’, *Hepatology Communications*, 2(5), pp. 582–594. Available at: https://doi.org/10.1002/hep4.1172.
81. Han, S. *et al.* (2018) ‘Enhanced intrinsic CYP3A4 activity in human hepatic C3A cells with optically controlled CRISPR/dCas9 activator complex’, *Integrative Biology*, 10(12),

pp. 780–790. Available at: https://doi.org/10.1039/C8IB00109J.
82. Hansel, M.C. *et al.* (2016) 'The Use of Induced Pluripotent Stem Cells for the Study and Treatment of Liver Diseases', *Current Protocols in Toxicology*, 67(1), pp. 14.13.1-14.13.27. Available at: https://doi.org/10.1002/0471140856.TX1413S67.
83. Harm, S. *et al.* (2009) 'Alginate-encapsulated human hepatoma C3A cells for use in a bioartificial liver device - The hybrid-MDS', *International Journal of Artificial Organs*, 32(11), pp. 769–778. Available at: https://doi.org/10.1177/039139880903201102.
84. Hay, D.C. *et al.* (2008) 'Efficient differentiation of hepatocytes from human embryonic stem cells exhibiting markers recapitulating liver development in vivo', *Stem cells*, 26(4), pp. 894–902. Available at: https://doi.org/10.1634/STEMCELLS.2007-0718.
85. Hay, P.D., Veitch, A.R. and Gaylor, J.D.S. (2001) 'Oxygen Transfer in a Convection-Enhanced Hollow Fiber Bioartificial Liver', *Artificial Organs*, 25(2), pp. 119–130. Available at: https://doi.org/10.1046/J.1525-1594.2001.025002119.X.
86. Heidelbaugh, J.J. and Bruderly, M. (2006) 'Cirrhosis and chronic liver failure: Part I. Diagnosis and evaluation', *American family physician*, 74(5), pp. 756–762.
87. Hessel, F.P. *et al.* (2010) 'Cost-effectiveness of the artificial liver support system MARS in patients with acute-on-chronic liver failure', *European journal of gastroenterology & hepatology*, 22(2), pp. 213–220. Available at: https://doi.org/10.1097/MEG.0B013E3283314E48.
88. Heydari, Z. *et al.* (2022) 'Mimicking the liver function in micro-patterned units: Challenges and perspectives in 3D bioprinting', *Bioprinting*, 27, p. e00208. Available at: https://doi.org/10.1016/J.BPRINT.2022.E00208.
89. Hillebrandt, K.H. *et al.* (2019) 'Strategies based on organ decellularization and recellularization', *Transplant International*, 32(6), pp. 571–585. Available at: https://doi.org/10.1111/TRI.13462.
90. Hoekstra, R. *et al.* (2011) 'The HepaRG cell line is suitable for bioartificial liver application', *The International Journal of Biochemistry & Cell Biology*, 43(10), pp. 1483–1489. Available at: https://doi.org/10.1016/J.BIOCEL.2011.06.011.
91. de Hoyos-Vega, J.M. *et al.* (2021) 'Hepatocyte cultures: From collagen gel sandwiches to microfluidic devices with integrated biosensors', *APL Bioengineering*, 5(4). Available at: https://doi.org/10.1063/5.0058798.
92. Huang, P. *et al.* (2011) 'Induction of functional hepatocyte-like cells from mouse fibroblasts by defined factors', *Nature*, 475(7356), pp. 386–391. Available at: https://doi.org/10.1038/nature10116.
93. Huang, P. *et al.* (2014) 'Direct reprogramming of human fibroblasts to functional and expandable hepatocytes', *Cell stem cell*, 14(3), pp. 370–384. Available at: https://doi.org/10.1016/J.STEM.2014.01.003.
94. Huber, W. *et al.* (2017) 'First clinical experience in 14 patients treated with ADVOS: A study on feasibility, safety and efficacy of a new type of albumin dialysis', *BMC Gastroenterology*, 17(1), pp. 1–11. Available at: https://doi.org/10.1186/S12876-017-0569-X/TABLES/4.
95. Hui, T., Rozga, J. and Demetriou, A.A. (2001) 'Bioartificial liver support', *Journal of Hepato-Biliary-Pancreatic Surgery*, 8(1), pp. 1–15. Available at: https://doi.org/10.1007/s005340170045.
96. Iansante, V. *et al.* (2018) 'Human hepatocyte transplantation for liver disease: current status and future perspectives', *Pediatric research*, 83(1–2), pp. 232–240. Available at: https://doi.org/10.1038/PR.2017.284.
97. Ibars, E.P. *et al.* (2016) 'Hepatocyte transplantation program: Lessons learned and future strategies', *World Journal of Gastroenterology*, 22(2), p. 874-886. Available at: https://doi.org/10.3748/WJG.V22.I2.874.

98. Iwamuro, M. *et al.* (2012) ‘A preliminary study for constructing a bioartificial liver device with induced pluripotent stem cell-derived hepatocytes’, *BioMedical Engineering Online*, 11(93), pp. 1–12. Available at: https://doi.org/10.1186/1475-925X-11-93/FIGURES/4.
99. Jakubowska, M. *et al.* (2024) ‘Hollow fiber bioreactor with genetically modified hepatic cells as a model of biologically active function block of the bioartificial liver’, *Biocybernetics and Biomedical Engineering*, 44(1), pp. 9–19. Available at: https://doi.org/10.1016/J.BBE.2023.11.003.
100. Jalan, R. *et al.* (2016) ‘Ammonia produces pathological changes in human hepatic stellate cells and is a target for therapy of portal hypertension’, *Journal of Hepatology*, 64(4), pp. 823–833. Available at: https://doi.org/10.1016/J.JHEP.2015.11.019.
101. Janciauskiene, S. and Welte, T. (2016) ‘Well-Known and Less Well-Known Functions of Alpha-1 Antitrypsin. Its Role in Chronic Obstructive Pulmonary Disease and Other Disease Developments’, *Annals of the American Thoracic Society*, 13 Suppl 4, pp. S280–S288. Available at: https://doi.org/10.1513/ANNALSATS.201507-468KV.
102. Jasmund, I. *et al.* (2002) ‘Cultivation of primary porcine hepatocytes in an OXY-HFB for use as a bioartificial liver device’, *Biotechnology progress*, 18(4), pp. 839–846. Available at: https://doi.org/10.1021/BP025501Y.
103. Jelen, S. *et al.* (2012) ‘Aquaporin-9 and urea transporter-A gene deletions affect urea transmembrane passage in murine hepatocytes’, *American Journal of Physiology - Gastrointestinal and Liver Physiology*, 303(11), pp. G1279–G1287. Available at: https://doi.org/10.1152/ajpgi.00153.2012.
104. Jia, B. *et al.* (2014) ‘Hyperammonaemia induces hepatic injury with alteration of gene expression profiles’, *Liver international*, 34(5), pp. 748–758. Available at: https://doi.org/10.1111/LIV.12365.
105. Kamata, M. *et al.* (2010) ‘Generation of Human Induced Pluripotent Stem Cells Bearing an Anti-HIV Transgene by a Lentiviral Vector Carrying an Internal Murine Leukemia Virus Promoter’, *Human Gene Therapy*, 21(11), p. 1555-1567. Available at: https://doi.org/10.1089/HUM.2010.050.
106. Kaps, L. *et al.* (2021) ‘Applicability and safety of discontinuous ADVanced Organ Support (ADVOS) in the treatment of patients with acute-on-chronic liver failure (ACLF) outside of intensive care’, *PLOS ONE*, 16(4), p. e0249342. Available at: https://doi.org/10.1371/JOURNAL.PONE.0249342.
107. Kelly, J.H. *et al.* (1992) ‘Assessment of an Extracorporeal Liver Assist Device in Anhepatic Dogs’, *Artificial Organs*, 16(4), pp. 418–422. Available at: https://doi.org/10.1111/J.1525-1594.1992.TB00543.X.
108. Van De Kerkhove, M.P. *et al.* (2002) ‘Phase I Clinical Trial with the AMC-Bioartificial Liver’, *International Journal of Artificial Organs*, 25(10), pp. 950–959. Available at: https://doi.org/10.1177/039139880202501009.
109. Van De Kerkhove, M.P. *et al.* (2004) ‘Clinical application of bioartificial liver support systems’, *Annals of Surgery*, 240(2), pp. 216–230. Available at: https://doi.org/10.1097/01.sla.0000132986.75257.19.
110. Keshet, R. *et al.* (2018) ‘Rewiring urea cycle metabolism in cancer to support anabolism’, *Nature reviews. Cancer*, 18(10), pp. 634–645. Available at: https://doi.org/10.1038/S41568-018-0054-Z.
111. Khuu, D.N. *et al.* (2011) ‘In Vitro Differentiated Adult Human Liver Progenitor Cells Display Mature Hepatic Metabolic Functions: A Potential Tool for in Vitro Pharmacotoxicological Testing’, *Cell Transplantation*, 20(2), pp. 287–302. Available at: https://doi.org/10.3727/096368910X516655.
112. Kim, K.S. *et al.* (2002) ‘Surface modification of polysulfone ultrafiltration membrane by oxygen plasma treatment’, *Journal of Membrane Science*, 199(1–2), pp. 135–145.

Available at: https://doi.org/10.1016/S0376-7388(01)00686-X.
113. Klein, J.D. *et al.* (1999) 'UT-A urea transporter protein expressed in liver: upregulation by uremia', *Journal of the American Society of Nephrology: JASN*, 10(10), pp. 2076–2083. Available at: https://doi.org/10.1681/ASN.V10102076.
114. Kmieć, Z. (2001) 'Cooperation of liver cells in health and disease', *Advances in anatomy, embryology, and cell biology*, 161(III-XIII), p. 1-151. Available at: https://doi.org/10.1007/978-3-642-56553-3.
115. Kojima, H. *et al.* (2018) 'Establishment of practical recellularized liver graft for blood perfusion using primary rat hepatocytes and liver sinusoidal endothelial cells', *American Journal of Transplantation*, 18(6), pp. 1351–1359. Available at: https://doi.org/10.1111/AJT.14666.
116. Kortgen, A. *et al.* (2009) 'Albumin dialysis in liver failure: comparison of molecular adsorbent recirculating system and single pass albumin dialysis--a retrospective analysis', *Therapeutic apheresis and dialysis*, 13(5), pp. 419–425. Available at: https://doi.org/10.1111/J.1744-9987.2009.00760.X.
117. Kosti, I. *et al.* (2016) 'Cross-tissue Analysis of Gene and Protein Expression in Normal and Cancer Tissues', *Scientific reports*, 6, p. 24799. Available at: https://doi.org/10.1038/SREP24799.
118. Kribben, A. *et al.* (2012) 'Effects of fractionated plasma separation and adsorption on survival in patients with acute-on-chronic liver failure', *Gastroenterology*, 142(4), pp. 782-789.e3. Available at: https://doi.org/10.1053/j.gastro.2011.12.056.
119. Kryou, C. *et al.* (2019) 'Bioprinting for Liver Transplantation', *Bioengineering*, 6(4), p. 95. Available at: https://doi.org/10.3390/BIOENGINEERING6040095.
120. Ku, M.W. *et al.* (2021) 'Intranasal vaccination with a lentiviral vector protects against SARS-CoV-2 in preclinical animal models', *Cell Host and Microbe*, 29(2), pp. 236-249.e6. Available at: https://doi.org/10.1016/j.chom.2020.12.010.
121. Kumar, R. *et al.* (2012) 'Persistent hyperammonemia is associated with complications and poor outcomes in patients with acute liver failure', *Clinical gastroenterology and hepatology*, 10(8), pp. 925–931. Available at: https://doi.org/10.1016/J.CGH.2012.04.011.
122. Kumar, R., Mehta, G. and Jalan, R. (2020) 'Acute-on-chronic liver failure', *Clinical Medicine*, 20(5), p. 501-504. Available at: https://doi.org/10.7861/CLINMED.2020-0631.
123. Kundu, S. and Brahma, S. (2016) 'Bio-artificial liver: An advanced therapy for liver failure', *International Journal of Applied Research*, 2(5), pp. 920–923. Available at: https://www.allresearchjournal.com/archives/?year=2016&vol=2&issue=5&part=N&ArticleId=2020.
124. Kwong, A.J. *et al.* (2022) 'OPTN/SRTR 2020 Annual Data Report: Liver', *American journal of transplantation*, 22(Suppl 2), pp. 204–309. Available at: https://doi.org/10.1111/AJT.16978.
125. Labbé, R.P., Vessillier, S. and Rafiq, Q.A. (2021) 'Lentiviral Vectors for T Cell Engineering: Clinical Applications, Bioprocessing and Future Perspectives', *Viruses*, 13(8), p. 1528. Available at: https://doi.org/10.3390/V13081528.
126. Laemmle, A. *et al.* (2016) 'Frequency and Pathophysiology of Acute Liver Failure in Ornithine Transcarbamylase Deficiency (OTCD)', *PLOS ONE*, 11(4), p. e0153358. Available at: https://doi.org/10.1371/JOURNAL.PONE.0153358.
127. Laleman, W. *et al.* (2006) 'Review article: Non-biological liver support in liver failure', *Alimentary Pharmacology and Therapeutics*, 23(3), pp. 351–363. Available at: https://doi.org/10.1111/j.1365-2036.2006.02765.x.
128. Lee, D.-H. and Lee, K.-W. (2014) 'Hepatocyte Isolation, Culture, and Its Clinical Applications', *Hanyang Medical Reviews*, 34(4), p. 165-172. Available at: https://doi.org/10.7599/hmr.2014.34.4.165.

129. Lee, H. *et al.* (2017) 'Development of Liver Decellularized Extracellular Matrix Bioink for Three-Dimensional Cell Printing-Based Liver Tissue Engineering', *Biomacromolecules*, 18(4), pp. 1229–1237. Available at: https://doi.org/10.1021/ACS.BIOMAC.6B01908.
130. Lee, S.Y., Kim, H.J. and Choi, D. (2015) 'Cell sources, liver support systems and liver tissue engineering: Alternatives to liver transplantation', *International Journal of Stem Cells*, 8(1), pp. 36–47. Available at: https://doi.org/10.15283/ijsc.2015.8.1.36.
131. Legallais, C. *et al.* (2018) 'Bioengineering Organs for Blood Detoxification', *Advanced Healthcare Materials*, 7(21), pp. e1800430. Available at: https://doi.org/10.1002/adhm.201800430.
132. Legallais, C., David, B. and Doré, E. (2001) 'Bioartificial livers (BAL): Current technological aspects and future developments', *Journal of Membrane Science*, 181(1), pp. 81–95. Available at: https://doi.org/10.1016/S0376-7388(00)00539-1.
133. Lewis, P.L. and Shah, R.N. (2016) '3D Printing for Liver Tissue Engineering: Current Approaches and Future Challenges', *Current Transplantation Reports*, 3(1), pp. 100–108. Available at: https://doi.org/10.1007/S40472-016-0084-Y/FIGURES/1.
134. Li, C.Y. *et al.* (2014) 'Micropatterned cell-cell interactions enable functional encapsulation of primary hepatocytes in hydrogel microtissues', *Tissue Engineering - Part A*, 20(15–16), pp. 2200–2212. Available at: https://doi.org/10.1089/ten.tea.2013.0667.
135. Li, T.T. *et al.* (2022) 'Stem Cell Therapies for Chronic Liver Diseases: Progress and Challenges', *Stem Cells Translational Medicine*, 11(9), pp. 900–911. Available at: https://doi.org/10.1093/STCLTM/SZAC053.
136. Li, W. *et al.* (2021) 'Matrix stiffness and shear stresses modulate hepatocyte functions in a fibrotic liver sinusoidal model', *American journal of physiology. Gastrointestinal and liver physiology*, 320(3), pp. G272–G282. Available at: https://doi.org/10.1152/AJPGI.00379.2019.
137. Li, Y. *et al.* (2018) 'Novel spheroid reservoir bioartificial liver improves survival of nonhuman primates in a toxin-induced model of acute liver failure', *Theranostics*, 8(20), p. 5562-5574. Available at: https://doi.org/10.7150/THNO.26540.
138. Liu, F. *et al.* (2018) 'Progress in organ 3D bioprinting', *International Journal of Bioprinting*, 4(1), p.128. Available at: https://doi.org/10.18063/IJB.V4I1.128.
139. Liu, H. *et al.* (2011) 'DNA Methylation Suppresses Expression of the Urea Cycle Enzyme Carbamoyl Phosphate Synthetase 1 (CPS1) in Human Hepatocellular Carcinoma', *The American Journal of Pathology*, 178(2), pp. 652–661. Available at: https://doi.org/10.1016/J.AJPATH.2010.10.023.
140. Liu, J. *et al.* (2001) 'Growth and Metabolic Activity of Immortalized Porcine Hepatocytes in Extracorporeal Hollow-Fiber Liver Assist Devices', *Artificial Organs*, 25(7), pp. 539–545. Available at: https://doi.org/10.1046/J.1525-1594.2001.025007539.X.
141. Lucien, N. *et al.* (2005) 'UT-B1 urea transporter is expressed along the urinary and gastrointestinal tracts of the mouse', *American Journal of Physiology - Regulatory Integrative and Comparative Physiology*, 288(4 57-4), pp. 1046–1056. Available at: https://doi.org/10.1152/AJPREGU.00286.2004.
142. Ma, L. *et al.* (2020) 'Current Advances on 3D-Bioprinted Liver Tissue Models', *Advanced Healthcare Materials*, 9(24), p. e2001517. Available at: https://doi.org/10.1002/ADHM.202001517.
143. Mahadevan, V. (2020) 'Anatomy of the liver', *Surgery (Oxford)*, 38(8), pp. 427–431. Available at: https://doi.org/10.1016/J.MPSUR.2014.10.004.
144. Maio, M. and Del Vecchio, L. (1992) 'Expression and functional role of CD54/Intercellular Adhesion Molecule-1 (ICAM-1) on human blood cells', *Leukemia & lymphoma*, 8(1–2), pp. 23–33. Available at: https://doi.org/10.3109/10428199209049814.
145. Malhi, H. *et al.* (2002) 'Isolation of human progenitor liver epithelial cells with extensive

replication capacity and differentiation into mature hepatocytes', *Journal of Cell Science*, 115(13), pp. 2679–2688. Available at: https://doi.org/10.1242/jcs.115.13.2679.
146. Manco, R. and Itzkovitz, S. (2021) 'Liver zonation', *Journal of Hepatology*, 74(2), pp. 466–468. Available at: https://doi.org/10.1016/j.jhep.2020.09.003.
147. Marcellin, P. and Kutala, B.K. (2018) 'Liver diseases: A major, neglected global public health problem requiring urgent actions and large-scale screening', *Liver International*, 38(Suppl 1), pp. 2–6. Available at: https://doi.org/10.1111/liv.13682.
148. Matsumura, K.N. *et al.* (1987) 'Hybrid bioartificial liver in hepatic failure: preliminary clinical report', *Surgery*, 101(1), pp. 99–103.
149. Mavri-Damelin, D. *et al.* (2007) 'Ornithine transcarbamylase and arginase I deficiency are responsible for diminished urea cycle function in the human hepatoblastoma cell line HepG2', *The International Journal of Biochemistry & Cell Biology*, 39(3), pp. 555–564. Available at: https://doi.org/10.1016/J.BIOCEL.2006.10.007.
150. Mavri-Damelin, D. *et al.* (2008) 'Cells for bioartificial liver devices: The human hepatoma-derived cell line C3A produces urea but does not detoxify ammonia', *Biotechnology and Bioengineering*, 99(3), pp. 644–651. Available at: https://doi.org/10.1002/bit.21599.
151. Mazza, G. *et al.* (2015) 'Decellularized human liver as a natural 3D-scaffold for liver bioengineering and transplantation', *Scientific reports*, 5, p. 13079. Available at: https://doi.org/10.1038/SREP13079.
152. Mazzocchi, A. *et al.* (2018) 'Optimization of collagen type I-hyaluronan hybrid bioink for 3D bioprinted liver microenvironments', *Biofabrication*, 11(1), p. 015003. Available at: https://doi.org/10.1088/1758-5090/AAE543.
153. Meirelles Júnior, R.F. *et al.* (2015) 'Liver transplantation: history, outcomes and perspectives', *Einstein*, 13(1), pp. 149–152. Available at: https://doi.org/10.1590/S1679-45082015RW3164.
154. Melaram, R. (2021) 'Environmental Risk Factors Implicated in Liver Disease: A Mini-Review', *Frontiers in Public Health*, 9, p. 683719. Available at: https://doi.org/10.3389/FPUBH.2021.683719.
155. Meng, Q., Zhang, G. and Wu, D. (2004) 'Hepatocyte culture in bioartificial livers with different membrane characteristics', *Biotechnology Letters*, 26(18), pp. 1407–1412. Available at: https://doi.org/10.1023/B:BILE.0000045641.81661.DF/METRICS.
156. Merten, O.W., Hebben, M. and Bovolenta, C. (2016) 'Production of lentiviral vectors', *Molecular Therapy - Methods & Clinical Development*, 3, p. 16017. Available at: https://doi.org/10.1038/MTM.2016.17.
157. Miki, T. (2019) 'Clinical hepatocyte transplantation', *Gastroenterologia y hepatologia*, 42(3), pp. 202–208. Available at: https://doi.org/10.1016/J.GASTROHEP.2018.10.007.
158. Millis, J.M. *et al.* (2002) 'Initial experience with the modified extracorporeal liver-assist device for patients with fulminant hepatic failure: system modifications and clinical impact.', *Transplantation*, 74(12), pp. 1735–46. Available at: https://doi.org/10.1097/01.TP.0000038483.93833.21.
159. Milone, M.C. and O'Doherty, U. (2018) 'Clinical use of lentiviral vectors', *Leukemia*, 32(7), pp. 1529–1541. Available at: https://doi.org/10.1038/s41375-018-0106-0.
160. Missiaen, R. *et al.* (2022) 'GCN2 inhibition sensitizes arginine-deprived hepatocellular carcinoma cells to senolytic treatment', *Cell Metabolism*, 34(8), pp. 1151-1167.e7. Available at: https://doi.org/10.1016/j.cmet.2022.06.010.
161. Mito, M., Kusano, M. and Kawaura, Y. (1992) 'Hepatocyte transplantation in man', *Transplantation Proceedings*, 24(6), pp. 3052–3053.
162. Mitzner, S.R. *et al.* (2001) 'Improvement of multiple organ functions in hepatorenal syndrome during albumin dialysis with the molecular adsorbent recirculating system', *Therapeutic apheresis*, 5(5), pp. 417–422. Available at: https://doi.org/10.1046/J.1526-

0968.2001.00388.X.
163. Mitzner, S.R. (2011) 'Extracorporeal liver support-albumin dialysis with the molecular adsorbent recirculating system (MARS)', *Annals of Hepatology*, 10(Suppl 1), pp. S21–S28. Available at: https://doi.org/10.1016/s1665-2681(19)31602-3.
164. Moedas, M.F. *et al.* (2017) 'Advances in methods for characterization of hepatic urea cycle enzymatic activity in HepaRG cells using UPLC-MS/MS', *Analytical Biochemistry*, 535, pp. 47–55. Available at: https://doi.org/10.1016/j.ab.2017.07.025.
165. Moman, R.N., Gupta, N. and Varacallo, M. (2023) 'Physiology, Albumin', *StatPearls* [Internet]. Available at: http://www.ncbi.nlm.nih.gov/pubmed/29083605 (Accessed: 13 July 2023).
166. Monné, M. *et al.* (2015) 'Mitochondrial transporters for ornithine and related amino acids: a review', *Amino acids*, 47(9), pp. 1763–1777. Available at: https://doi.org/10.1007/S00726-015-1990-5.
167. Moon, A.M., Singal, A.G. and Tapper, E.B. (2020) 'Contemporary Epidemiology of Chronic Liver Disease and Cirrhosis', *Clinical gastroenterology and hepatology*, 18(12), pp. 2650–2666. Available at: https://doi.org/10.1016/J.CGH.2019.07.060.
168. Morelli, S. *et al.* (2022) 'Hollow fiber and nanofiber membranes in bioartificial liver and neuronal tissue engineering', *Cells Tissues Organs*, 211(4), p. 447-476. Available at: https://doi.org/10.1159/000511680.
169. Mori, N. and Kida, Y.S. (2020) 'Expression of genes involved in drug metabolism differs between perfusable 3D liver tissue and conventional 2D-cultured hepatocellular carcinoma cells', *FEBS Open Bio*, 10(10), pp. 1985–2002. Available at: https://doi.org/10.1002/2211-5463.12948.
170. Morris, S.M. (2002) 'Regulation of enzymes of the urea cycle and arginine metabolism', *Annual review of nutrition*, 22, pp. 87–105. Available at: https://doi.org/10.1146/ANNUREV.NUTR.22.110801.140547.
171. Morsiani, E. *et al.* (2001) 'Long-term expression of highly differentiated functions by isolated porcine hepatocytes perfused in a radial-flow bioreactor', *Artificial organs*, 25(9), pp. 740–748. Available at: https://doi.org/10.1046/J.1525-1594.2001.06669.X.
172. Morsiani, E. *et al.* (2002) 'Early Experiences with a Porcine Hepatocyte-based Bioartificial Liver in Acute Hepatic Failure Patients', *The International Journal of Artificial Organs*, 25(3), pp. 192–202. Available at: https://doi.org/10.1177/039139880202500305.
173. Mulaikal, T.A. and Emond, J.C. (2012) *Physiology and anatomy of the liver*, *Liver Anesthesiology and Critical Care Medicine*. Springer New York. Available at: https://doi.org/10.1007/9781461451679.
174. Mullon, C. and Pitkin, Z. (1999) 'The HepatAssist bioartificial liver support system: clinical study and pig hepatocyte process', *Expert opinion on investigational drugs*, 8(3), pp. 229–235. Available at: https://doi.org/10.1517/13543784.8.3.229.
175. Nagaki, M. and Moriwaki, H. (2008) 'Transcription factor HNF and hepatocyte differentiation', *Hepatology Research*, 38(10), pp. 961–969. Available at: https://doi.org/10.1111/j.1872-034X.2008.00367.x.
176. Naldini, L., Trono, D. and Verma, I.M. (2016) 'Lentiviral vectors, two decades later', *Science*, 353(6304), pp. 1101–1102. Available at: https://doi.org/10.1126/SCIENCE.AAH6192.
177. Nasralla, D. *et al.* (2018) 'A randomized trial of normothermic preservation in liver transplantation', *Nature*, 557(7703), pp. 50–56. Available at: https://doi.org/10.1038/s41586-018-0047-9.
178. Nevens, F. and Laleman, W. (2012) 'Artificial liver support devices as treatment option for liver failure', *Best Practice and Research: Clinical Gastroenterology*, 26(1), pp. 17–26. Available at: https://doi.org/10.1016/j.bpg.2012.01.002.

179. Nguyen, D.G. *et al.* (2016) 'Bioprinted 3D Primary Liver Tissues Allow Assessment of Organ-Level Response to Clinical Drug Induced Toxicity In Vitro', *PLOS ONE*, 11(7), p. e0158674. Available at: https://doi.org/10.1371/JOURNAL.PONE.0158674.
180. Nibourg, G.A.A. *et al.* (2012) 'Liver Progenitor Cell Line HepaRG Differentiated in a Bioartificial Liver Effectively Supplies Liver Support to Rats with Acute Liver Failure', *PLOS ONE*, 7(6), p. e38778. Available at: https://doi.org/10.1371/JOURNAL.PONE.0038778.
181. Nicolas, C.T. *et al.* (2017) 'Concise Review: Liver Regenerative Medicine: From Hepatocyte Transplantation to Bioartificial Livers and Bioengineered Grafts', *Stem Cells*, 35(1), pp. 42–50. Available at: https://doi.org/10.1002/stem.2500.
182. Nitzahn, M. and Lipshutz, G.S. (2020) 'CPS1: Looking at an ancient enzyme in a modern light', *Molecular Genetics and Metabolism*, 131(3), pp. 289–298. Available at: https://doi.org/10.1016/J.YMGME.2020.10.003.
183. Norona, L.M. *et al.* (2016) 'Modeling Compound-Induced Fibrogenesis In Vitro Using Three-Dimensional Bioprinted Human Liver Tissues', *Toxicological Sciences*, 154(2), pp. 354–367. Available at: https://doi.org/10.1093/TOXSCI/KFW169.
184. Nyberg, S.L. *et al.* (1993) 'Evaluation of a hepatocyte-entrapment hollow fiber bioreactor: a potential bioartificial liver', *Biotechnology and bioengineering*, 41(2), pp. 194–203. Available at: https://doi.org/10.1002/BIT.260410205.
185. Nyberg, S.L. *et al.* (1994) 'Primary hepatocytes outperform Hep G2 cells as the source of biotransformation functions in a bioartificial liver.', *Annals of surgery*, 220(1), pp. 59–67. Available at: http://www.ncbi.nlm.nih.gov/pubmed/8024360.
186. O'Leary, M.C. *et al.* (2019) 'FDA Approval Summary: Tisagenlecleucel for Treatment of Patients with Relapsed or Refractory B-cell Precursor Acute Lymphoblastic Leukemia', *Clinical cancer research*, 25(4), pp. 1142–1146. Available at: https://doi.org/10.1158/1078-0432.CCR-18-2035.
187. Oh, S.K.W. *et al.* (2009) 'Long-term microcarrier suspension cultures of human embryonic stem cells', *Stem cell research*, 2(3), pp. 219–230. Available at: https://doi.org/10.1016/J.SCR.2009.02.005.
188. Ohara, K. *et al.* (2009) 'Prolonged exposure to ammonia increases extracellular glutamate in cultured rat astrocytes', *Neuroscience letters*, 462(2), pp. 109–112. Available at: https://doi.org/10.1016/J.NEULET.2009.06.090.
189. Orge, I.D. *et al.* (2020) 'Phenotype instability of hepatocyte-like cells produced by direct reprogramming of mesenchymal stromal cells', *Stem cell research & therapy*, 11(1), p. 154. Available at: https://doi.org/10.1186/S13287-020-01665-Z.
190. Palakkan, A.A. *et al.* (2013) 'Evaluation of Polypropylene Hollow-Fiber Prototype Bioreactor for Bioartificial Liver', *Tissue Engineering. Part A*, 19(9–10), pp. 1056–1066. Available at: https://doi.org/10.1089/TEN.TEA.2012.0332.
191. Palakkan, A.A. *et al.* (2013) 'Liver tissue engineering and cell sources: issues and challenges', *Liver International*, 33(5), pp. 666–676. Available at: https://doi.org/10.1111/liv.12134.
192. Park, K.M. *et al.* (2016) 'Decellularized Liver Extracellular Matrix as Promising Tools for Transplantable Bioengineered Liver Promotes Hepatic Lineage Commitments of Induced Pluripotent Stem Cells', *Tissue engineering. Part A*, 22(5–6), pp. 449–460. Available at: https://doi.org/10.1089/TEN.TEA.2015.0313.
193. Patzer, J.F. *et al.* (1999) 'Novel bioartificial liver support system: preclinical evaluation', *Annals of the New York Academy of Sciences*, 875, pp. 340–352. Available at: https://doi.org/10.1111/J.1749-6632.1999.TB08516.X.
194. Payne, C.M. *et al.* (2011) 'Persistence of functional hepatocyte-like cells in immune-compromised mice', *Liver international*, 31(2), pp. 254–262. Available at:

https://doi.org/10.1111/J.1478-3231.2010.02414.X.
195. Perl, K. *et al.* (2017) 'Reduced changes in protein compared to mRNA levels across non-proliferating tissues', *BMC Genomics*, 18(1), p. 305. Available at: https://doi.org/10.1186/S12864-017-3683-9/FIGURES/5.
196. Pfaffl, M.W., Horgan, G.W. and Dempfle, L. (2002) 'Relative expression software tool (REST) for group-wise comparison and statistical analysis of relative expression results in real-time PCR', *Nucleic Acids Research*, 30(9), pp. e36. Available at: https://doi.org/10.1093/nar/30.9.e36.
197. Picanço-Castro, V. *et al.* (2020) 'Establishment of a simple and efficient platform for car-t cell generation and expansion: from lentiviral production to *in vivo* studies', *Hematology, Transfusion and Cell Therapy*, 42(2), pp. 150–158. Available at: https://doi.org/10.1016/J.HTCT.2019.06.007.
198. Piechota, M. and Piechota, A. (2016) 'An Evaluation of the Usefulness of Extracorporeal Liver Support Techniques in Patients Hospitalized in the ICU for Severe Liver Dysfunction Secondary to Alcoholic Liver Disease', *Hepatitis Monthly*, 16(7), p. 34127. Available at: https://doi.org/10.5812/HEPATMON.34127.
199. Pimpin, L. *et al.* (2018) 'Burden of liver disease in Europe: epidemiology and analysis of risk factors to identify prevention policies', *Journal of Hepatology*, 69(3), p. 718-735. Available at: https://doi.org/10.1016/j.jhep.2018.05.011.
200. Pless, G. (2007) 'Artificial and bioartificial liver support', *Organogenesis*, 3(1), p. 20-24. Available at: https://doi.org/10.4161/org.3.1.3635.
201. Pluta, K. and Kacprzak, M.M. (2009) 'Use of HIV as a gene transfer vector.', *Acta biochimica Polonica*, 56(4), pp. 531–95. Available at: http://www.ncbi.nlm.nih.gov/pubmed/19936329.
202. Pluta, K.D. *et al.* (2020) 'Genetically modified C3A cells with restored urea cycle for improved bioartificial liver', *Biocybernetics and Biomedical Engineering*, 40(1), pp. 378–387. Available at: https://doi.org/10.1016/j.bbe.2019.12.006.
203. Pluta, K.D. *et al.* (2021) 'Cell-based clinical and experimental methods for assisting the function of impaired livers – Present and future of liver support systems', *Biocybernetics and Biomedical Engineering*, 41(4), pp. 1322–1346. Available at: https://doi.org/10.1016/j.bbe.2021.06.005.
204. Polidoro, M.A. *et al.* (2021) 'Experimental liver models: From cell culture techniques to microfluidic organs-on-chip', *Liver International*, 41(8), pp. 1744–1761. Available at: https://doi.org/10.1111/LIV.14942.
205. Poyck, P.P.C. *et al.* (2007) 'Functional and Morphological Comparison of Three Primary Liver Cell Types Cultured in the AMC Bioartificial Liver', *Liver Transplantation*, 13(4), pp. 589–598. Available at: https://doi.org/10.1002/lt.21090.
206. Ramboer, E. *et al.* (2015) 'Immortalized human hepatic cell lines for in vitro testing and research purposes', *Methods in molecular biology*, 1250, p. 53-76. Available at: https://doi.org/10.1007/978-1-4939-2074-7_4.
207. Ren, S. *et al.* (2015) 'Bioartificial Liver Device Based on Induced Pluripotent Stem Cell-Derived Hepatocytes', *Journal of Stem Cell Research & Therapy*, 59(2), p. 1-9. Available at: https://doi.org/10.4172/2157-7633.1000263.
208. Rezvani, M. *et al.* (2016) 'In Vivo Hepatic Reprogramming of Myofibroblasts with AAV Vectors as a Therapeutic Strategy for Liver Fibrosis', *Cell stem cell*, 18(6), pp. 809–816. Available at: https://doi.org/10.1016/J.STEM.2016.05.005.
209. Rifai, K. *et al.* (2003) 'Prometheus® - A new extracorporeal system for the treatment of liver failure', *Journal of Hepatology*, 39(6), pp. 984–990. Available at: https://doi.org/10.1016/S0168-8278(03)00468-9.
210. Ringe, H. *et al.* (2011) 'Continuous veno-venous single-pass albumin hemodiafiltration in

children with acute liver failure', *Pediatric critical care medicine*, 12(3), pp. 257–264. Available at: https://doi.org/10.1097/PCC.0B013E3181F35FA2.
211. Robertson, M.J. *et al.* (2018) 'Recellularization of rat liver: An in vitro model for assessing human drug metabolism and liver biology', *PLOS ONE*, 13(1), p. e0191892. Available at: https://doi.org/10.1371/JOURNAL.PONE.0191892.
212. Roche, M. *et al.* (2008) 'The antioxidant properties of serum albumin', *FEBS Letters*, 582(13), pp. 1783–1787. Available at: https://doi.org/10.1016/J.FEBSLET.2008.04.057.
213. Romero-Gómez, M., Montagnese, S. and Jalan, R. (2015) 'Hepatic encephalopathy in patients with acute decompensation of cirrhosis and acute-on-chronic liver failure', *Journal of hepatology*, 62(2), pp. 437–447. Available at: https://doi.org/10.1016/J.JHEP.2014.09.005.
214. Rowe, C. *et al.* (2013) 'Proteome-wide analyses of human hepatocytes during differentiation and dedifferentiation', *Hepatology*, 58(2), pp. 799–809. Available at: https://doi.org/10.1002/hep.26414.
215. Rozga, J. *et al.* (1993) 'Development of a bioartificial liver: Properties and function of a hollow-fiber module inoculated with liver cells', *Hepatology*, 17(2), pp. 258–265. Available at: https://doi.org/10.1002/hep.1840170216.
216. Rozga, J. *et al.* (1994) 'A bioartificial liver to treat severe acute liver failure.', *Annals of Surgery*, 219(5), p. 538-546. Available at: https://doi.org/10.1097/00000658-199405000-00012.
217. Rozga, J. *et al.* (2006) 'A novel plasma filtration therapy for hepatic failure: preclinical studies', *Therapeutic apheresis and dialysis*, 10(2), pp. 138–144. Available at: https://doi.org/10.1111/J.1744-9987.2006.00355.X.
218. Rozga, J. and Malkowski, P. (2010) 'Artificial liver support: Quo Vadis?', *Annals of Transplantation*, 15(4), pp. 92–101.
219. Ruoß, M. *et al.* (2020) 'Towards improved hepatocyte cultures: Progress and limitations', *Food and Chemical Toxicology*, 138, p. 111188. Available at: https://doi.org/10.1016/J.FCT.2020.111188.
220. Saito, Y. *et al.* (2021) 'Current status of hepatocyte-like cell therapy from stem cells', *Surgery Today*, 51(3), pp. 340–349. Available at: https://doi.org/10.1007/s00595-020-02092-6.
221. Saliba, F. *et al.* (2013) 'Albumin dialysis with a noncell artificial liver support device in patients with acute liver failure: a randomized, controlled trial', *Annals of internal medicine*, 159(8), pp. 522–531. Available at: https://doi.org/10.7326/0003-4819-159-8-201310150-00005.
222. Samluk, A., Zakrzewska, K.E. and Pluta, K.D. (2013) 'Generation of fluorescently labeled cell lines, C3A hepatoma cells, and human adult skin fibroblasts to study coculture models.', *Artificial organs*, 37(7), pp. E123-30. Available at: https://doi.org/10.1111/aor.12064.
223. Sauer, I.M. *et al.* (2002) 'Primary Human Liver Cells as Source for Modular Extracorporeal Liver Support - a Preliminary Report', *International Journal of Artificial Organs*, 25(10), pp. 1001–1005. Available at: https://doi.org/10.1177/039139880202501015.
224. Sauer, I.M., Kardassis, D., *et al.* (2003) 'Clinical extracorporeal hybrid liver support--phase I study with primary porcine liver cells', *Xenotransplantation*, 10(5), pp. 460–469. Available at: https://doi.org/10.1034/J.1399-3089.2003.00062.X.
225. Sauer, I.M., Zeilinger, K., *et al.* (2003) 'Extracorporeal liver support based on primary human liver cells and albumin dialysis - Treatment of a patient with primary graft non-function', *Journal of Hepatology*, 39(4), pp. 649–653. Available at: https://doi.org/10.1016/S0168-8278(03)00348-9.
226. Sauer, I.M. and Gerlach, J.C. (2002) 'Modular extracorporeal liver support', *Artificial*

organs, 26(8), pp. 703–706. Available at: https://doi.org/10.1046/J.1525-1594.2002.06931_1.X.
227. Schlegel, A. *et al.* (2023) 'Machine perfusion of the liver and bioengineering', *Journal of hepatology*, 78(6), p. 1181-1198. Available at: https://doi.org/10.1016/j.jhep.2023.02.009.
228. Schrem, H. *et al.* (2006) 'Physiological incompatibilities of porcine hepatocytes for clinical liver support', *Liver Transplantation*, 12(12), pp. 1832–1840. Available at: https://doi.org/10.1002/LT.20918.
229. Seglen, P.O. (1976) 'Preparation of isolated rat liver cells', *Methods in cell biology*, 13, pp. 29–83. Available at: https://doi.org/10.1016/S0091-679X(08)61797-5.
230. Seige, M. *et al.* (1999) 'Long term treatment of patients with acute exacerbation of chronic liver failure by albumin dialysis', *Transplantation Proceedings*, 31(1–2), pp. 1371–1375. Available at: https://doi.org/10.1016/S0041-1345(98)02033-8.
231. Sekiya, S. and Suzuki, A. (2011) 'Direct conversion of mouse fibroblasts to hepatocyte-like cells by defined factors', *Nature*, 475(7356), pp. 390–395. Available at: https://doi.org/10.1038/NATURE10263.
232. Shi, X.L. *et al.* (2016) 'Improved survival of porcine acute liver failure by a bioartificial liver device implanted with induced human functional hepatocytes', *Cell research*, 26(2), pp. 206–216. Available at: https://doi.org/10.1038/CR.2016.6.
233. Song, G. *et al.* (2016) 'Direct Reprogramming of Hepatic Myofibroblasts into Hepatocytes In Vivo Attenuates Liver Fibrosis', *Cell stem cell*, 18(6), pp. 797–808. Available at: https://doi.org/10.1016/J.STEM.2016.01.010.
234. Song, Z. *et al.* (2009) 'Efficient generation of hepatocyte-like cells from human induced pluripotent stem cells', *Cell Research*, 19(11), pp. 1233–1242. Available at: https://doi.org/10.1038/cr.2009.107.
235. Sosef, M.N. *et al.* (2002) 'Assessment of the AMC-bioartificial liver in the anhepatic pig', *Transplantation*, 73(2), pp. 204–209. Available at: https://doi.org/10.1097/00007890-200201270-00009.
236. Soto-Gutierrez, A. *et al.* (2011) 'A whole-organ regenerative medicine approach for liver replacement', *Tissue engineering. Part C, Methods*, 17(6), pp. 677–686. Available at: https://doi.org/10.1089/TEN.TEC.2010.0698.
237. Speir, E. (2000) 'Cytomegalovirus Gene Regulation by Reactive Oxygen Species: Agents in Atherosclerosis', *Annals of the New York Academy of Sciences*, 899(1), pp. 363–374. Available at: https://doi.org/10.1111/J.1749-6632.2000.TB06200.X.
238. Sponholz, C. *et al.* (2016) 'Molecular adsorbent recirculating system and single-pass albumin dialysis in liver failure--a prospective, randomised crossover study', *Critical care*, 20(1), p. 2. Available at: https://doi.org/10.1186/S13054-015-1159-3.
239. Štampar, M. *et al.* (2020) 'Characterization of In Vitro 3D Cell Model Developed from Human Hepatocellular Carcinoma (HepG2) Cell Line', *Cells*, 9(12), p. 2557. Available at: https://doi.org/10.3390/cells9122557.
240. Stange, J. *et al.* (1993) 'Dialysis against a recycled albumin solution enables the removal of albumin-bound toxins', *Artificial organs*, 17(9), pp. 809–813. Available at: https://doi.org/10.1111/J.1525-1594.1993.TB00635.X.
241. Stange, J. *et al.* (1999) 'Molecular adsorbent recycling system (MARS): clinical results of a new membrane-based blood purification system for bioartificial liver support', *Artificial organs*, 23(4), pp. 319–330. Available at: https://doi.org/10.1046/J.1525-1594.1999.06122.X.
242. Starokozhko, V. and Groothuis, G.M.M. (2018) 'Challenges on the road to a multicellular bioartificial liver', *Journal of Tissue Engineering and Regenerative Medicine*, 12(1), pp. e227–e236. Available at: https://doi.org/10.1002/term.2385.
243. Starzl, T.E. *et al.* (1968) 'Orthotopic homotransplantation of the human liver', *Annals of*

surgery, 168(3), pp. 392–415. Available at: https://doi.org/10.1097/00000658-196809000-00009.
244. Stevens, K.R. *et al.* (2014) 'Hepatic Tissue Engineering', *Principles of Tissue Engineering: Fourth Edition*, pp. 951–986. Available at: https://doi.org/10.1016/B978-0-12-398358-9.00046-X.
245. Stock, P. *et al.* (2008) 'Hepatocytes derived from adult stem cells', *Transplantation proceedings*, 40(2), pp. 620–623. Available at: https://doi.org/10.1016/J.TRANSPROCEED.2008.01.058.
246. Storm, M.P. *et al.* (2016) 'Hollow Fiber Bioreactors for In Vivo-like Mammalian Tissue Culture', *Journal of Visualized Experiments*, 2016(111), p. e53431. Available at: https://doi.org/10.3791/53431.
247. Struecker, B., Raschzok, N. and Sauer, I.M. (2014) 'Liver support strategies: Cutting-edge technologies', *Nature Reviews Gastroenterology and Hepatology*, 11(3), pp. 166–176. Available at: https://doi.org/10.1038/nrgastro.2013.204.
248. Sullivan, J.P., Gordon, J.E. and Palmer, A.F. (2006) 'Simulation of oxygen carrier mediated oxygen transport to C3A hepatoma cells housed within a hollow fiber bioreactor', *Biotechnology and Bioengineering*, 93(2), pp. 306–317. Available at: https://doi.org/10.1002/BIT.20673.
249. Sullivan, J.P., Harris, D.R. and Palmer, A.F. (2009) 'Convection and Hemoglobin-Based Oxygen Carrier Enhanced Oxygen Transport in a Hepatic Hollow Fiber Bioreactor', *Artificial cells, blood substitutes, and biotechnology*, 36(4), pp. 386–402. Available at: https://doi.org/10.1080/10731190802239065.
250. Sussman, N.L. *et al.* (1992) 'Reversal of fulminant hepatic failure using an extracorporeal liver assist device', *Hepatology*, 16(1), pp. 60–65. Available at: https://doi.org/10.1002/HEP.1840160112.
251. Sussman, N.L. *et al.* (1994) 'The Hepatix extracorporeal liver assist device: initial clinical experience', *Artificial organs*, 18(5), pp. 390–396. Available at: http://www.ncbi.nlm.nih.gov/pubmed/8037614.
252. Szyller, J. and Bil-Lula, I. (2021) 'Heat Shock Proteins in Oxidative Stress and Ischemia/Reperfusion Injury and Benefits from Physical Exercises: A Review to the Current Knowledge', *Oxidative Medicine and Cellular Longevity*, 2021, p. 6678457. Available at: https://doi.org/10.1155/2021/6678457.
253. Takebe, T. *et al.* (2013) 'Vascularized and functional human liver from an iPSC-derived organ bud transplant', *Nature*, 499(7459), pp. 481–484. Available at: https://doi.org/10.1038/nature12271.
254. Takeshita, K. *et al.* (1995) 'High Cell-Density Culture System of Hepatocytes Entrapped in a Three-Dimensional Hollow Fiber Module with Collagen Gel', *Artificial Organs*, 19(2), pp. 191–193. Available at: https://doi.org/10.1111/J.1525-1594.1995.TB02310.X.
255. Tandon, R. and Froghi, S. (2021) 'Artificial liver support systems', *Journal of Gastroenterology and Hepatology*, 36(5), pp. 1164–1179. Available at: https://doi.org/10.1111/jgh.15255.
256. Tang, N. *et al.* (2012) 'Stable overexpression of arginase I and ornithine transcarbamylase in HepG2 cells improves its ammonia detoxification', *Journal of Cellular Biochemistry*, 113(2), pp. 518–527. Available at: https://doi.org/10.1002/JCB.23375.
257. Tang, N.H. *et al.* (2008) 'Ammonia metabolism capacity of HepG2 cells with high expression of human glutamine synthetase', *Hepatobiliary and Pancreatic Diseases International*, 7(6), pp. 621–627.
258. Tanimizu, N. and Mitaka, T. (2014) 'Re-evaluation of liver stem/progenitor cells', *Organogenesis*, 10(2), pp. 208–215. Available at: https://doi.org/10.4161/ORG.27591.
259. Taverna, M. *et al.* (2013) 'Specific antioxidant properties of human serum albumin',

Annals of Intensive Care, 3(1), pp. 4. Available at: https://doi.org/10.1186/2110-5820-3-4/TABLES/1.
260. Thompson, J. *et al.* (2018) 'Extracorporeal cellular therapy (ELAD) in severe alcoholic hepatitis: A multinational, prospective, controlled, randomized trial', *Liver transplantation*, 24(3), pp. 380–393. Available at: https://doi.org/10.1002/LT.24986.
261. Tolmachov, O., Tolmachova T. and Al-Allaf F.A. (2011) 'Designing Lentiviral Gene Vectors', *Viral Gene Therapy*. Available at: https://doi.org/10.5772/17361.
262. Treyer, A. and Müsch, A. (2013) 'Hepatocyte Polarity', *Comprehensive Physiology*, 3(1), p. 243-287. Available at: https://doi.org/10.1002/CPHY.C120009.
263. Tsuchida, T. *et al.* (2020) 'Investigation of Clinical Safety of Human iPS Cell-Derived Liver Organoid Transplantation to Infantile Patients in Porcine Model', *Cell Transplantation*, 29, p. 0963689720964384. Available at: https://doi.org/10.1177/0963689720964384.
264. te Velde, A.A. *et al.* (1997) 'Immunological consequences of the use of xenogenic hepatocytes in a bioartificial liver for acute liver failure', *International Journal of Artificial Organs*, 20(4), pp. 229–233.
265. Vogel, C. and Marcotte, E.M. (2012) 'Insights into the regulation of protein abundance from proteomic and transcriptomic analyses', *Nature reviews. Genetics*, 13(4), pp. 227–232. Available at: https://doi.org/10.1038/NRG3185.
266. Walker, V. (2014) 'Ammonia metabolism and hyperammonemic disorders', *Advances in clinical chemistry*, 67, pp. 73–150. Available at: https://doi.org/10.1016/BS.ACC.2014.09.002.
267. Wallon, G. *et al.* (2022) 'Extracorporeal Albumin Dialysis in Liver Failure with MARS and SPAD: A Randomized Crossover Trial', *Blood Purification*, 51(3), pp. 243–250. Available at: https://doi.org/10.1159/000515825.
268. Wang, Q. *et al.* (2022) 'Disturbance of hepatocyte growth and metabolism in a hyperammonemia microenvironment', *Archives of biochemistry and biophysics*, 716, p. 716:109109. Available at: https://doi.org/10.1016/J.ABB.2021.109109.
269. Wang, Y. *et al.* (2017) 'Recent Advances in Decellularization and Recellularization for Tissue-Engineered Liver Grafts', *Cells, tissues, organs*, 204(3–4), pp. 125–136. Available at: https://doi.org/10.1159/000479597.
270. Wang, Y. *et al.* (2023) 'Reversal of liver failure using a bioartificial liver device implanted with clinical-grade human-induced hepatocytes', *Cell Stem Cell*, 30(5), pp. 617-631.e8. Available at: https://doi.org/10.1016/j.stem.2023.03.013.
271. Watanabe, F.D. *et al.* (1997) 'Clinical experience with a bioartificial liver in the treatment of severe liver failure. A phase I clinical trial.', *Annals of Surgery*, 225(5), p. 484-494. Available at: https://doi.org/10.1097/00000658-199705000-00005.
272. van Wenum, M. *et al.* (2016) 'Selecting Cells for Bioartificial Liver Devices and the Importance of a 3D Culture Environment: A Functional Comparison between the HepaRG and C3A Cell Lines', *International Journal of Biological Sciences*, 12(8), pp. 964–978. Available at: https://doi.org/10.7150/ijbs.15165.
273. Van Wenum, M. *et al.* (2014) 'Bioartificial livers in vitro and in vivo: tailoring biocomponents to the expanding variety of applications', *Expert opinion on biological therapy*, 14(12), pp. 1745–1760. Available at: https://doi.org/10.1517/14712598.2014.950651.
274. Wright, G. *et al.* (2011) 'Interorgan ammonia metabolism in liver failure: the basis of current and future therapies', *Liver International*, 31(2), pp. 163–175. Available at: https://doi.org/10.1111/J.1478-3231.2010.02302.X.
275. Wung, N. *et al.* (2014) 'Hollow fibre membrane bioreactors for tissue engineering applications', *Biotechnology Letters*, 36(12), pp. 2357–2366. Available at:

https://doi.org/10.1007/s10529-014-1619-x.
276. Xu, J. *et al.* (2022) Mortality in the United States, 2021, *NCHS Data Brief*, 456. Available at: https://dx.doi.org/10.15620/cdc:122516.
277. Xue, Y.-L. *et al.* (2001) 'TECA hybrid artificial liver support system in treatment of acute liver failure', *World Journal of Gastroenterology*, 7(6), p. 826-829. Available at: www.wjgnet.com.
278. Yanagi, K., Miyoshi, H. and Ohshima, N. (1998) 'Improvement of metabolic performance of hepatocytes cultured in vitro in a packed-bed reactor for use as a bioartificial liver', *ASAIO journal*, 44(5), p. M436-40. Available at: https://doi.org/10.1097/00002480-199809000-00022.
279. Yang, Q. *et al.* (2010) 'Fluidized-bed bioartificial liver assist devices (BLADs) based on microencapsulated primary porcine hepatocytes have risk of porcine endogenous retroviruses transmission', *Hepatology international*, 4(4), pp. 757–761. Available at: https://doi.org/10.1007/S12072-010-9210-6.
280. Yang, W. *et al.* (2018) 'A novel bioscaffold with naturally-occurring extracellular matrix promotes hepatocyte survival and vessel patency in mouse models of heterologous transplantation', *Biomaterials*, 177, pp. 52–66. Available at: https://doi.org/10.1016/J.BIOMATERIALS.2018.05.026.
281. Yu, Y. *et al.* (2012) 'Hepatocyte-like cells differentiated from human induced pluripotent stem cells: relevance to cellular therapies', *Stem cell research*, 9(3), pp. 196–207. Available at: https://doi.org/10.1016/J.SCR.2012.06.004.
282. Zakrzewska, K.E. *et al.* (2017) 'Liver tissue fragments obtained from males are the most promising source of human hepatocytes for cell-based therapies – Flow cytometric analysis of albumin expression', *PLOS ONE*, 12(8), p. e0182846. Available at: https://doi.org/10.1371/journal.pone.0182846.
283. Zhao, L.F., Pan, X.P. and Li, L.J. (2012) 'Key challenges to the development of extracorporeal bioartificial liver support systems', *Hepatobiliary and Pancreatic Diseases International*, 11(3), pp. 243–249. Available at: https://doi.org/10.1016/S1499-3872(12)60155-6.
284. Zhao, T. *et al.* (2011) 'Immunogenicity of induced pluripotent stem cells', *Nature*, 474(7350), pp. 212–215. Available at: https://doi.org/10.1038/NATURE10135.
285. Zhou, P. *et al.* (2016) 'Decellularization and Recellularization of Rat Livers With Hepatocytes and Endothelial Progenitor Cells', *Artificial Organs*, 40(3), pp. E25–E38. Available at: https://doi.org/10.1111/AOR.12645.
286. Zhou, W. *et al.* (2012) 'SUMOylation of HNF4α regulates protein stability and hepatocyte function', *Journal of cell science*, 125(Pt 15), pp. 3630–3635. Available at: https://doi.org/10.1242/JCS.102889.